BEHAVIOR OF CONCRETE COLUMNS UNDER VARIOUS CONFINEMENT EFFECTS

by

AHMED MOHSEN ABD EL FATTAH

B.S., Cairo University, 2000

M.S., Kansas State University, 2008

AN ABSTRACT OF A DISSERTATION

Submitted in partial fulfillment of the requirements for the degree

DOCTOR OF PHILOSOPHY

Department of Civil Engineering

College of Engineering

KANSAS STATE UNIVERSITY

Manhattan, Kansas

2012

Abstract

The analysis of concrete columns using unconfined concrete models is a well established practice. On the other hand, prediction of the actual ultimate capacity of confined concrete columns requires specialized nonlinear analysis. Modern codes and standards are introducing the need to perform extreme event analysis. There has been a number of studies that focused on the analysis and testing of concentric columns or cylinders. This case has the highest confinement utilization since the entire section is under confined compression. On the other hand, the augmentation of compressive strength and ductility due to full axial confinement is not applicable to pure bending and combined bending and axial load cases simply because the area of effective confined concrete in compression is reduced. The higher eccentricity causes smaller confined concrete region in compression yielding smaller increase in strength and ductility of concrete. Accordingly, the ultimate confined strength is gradually reduced from the fully confined value f_{cc} (at zero eccentricity) to the unconfined value f'_c (at infinite eccentricity) as a function of the compression area to total area ratio. The higher the eccentricity the smaller the confined concrete compression zone. This paradigm is used to implement adaptive eccentric model utilizing the well known Mander Model and Lam and Teng Model.

Generalization of the moment of area approach is utilized based on proportional loading, finite layer procedure and the secant stiffness approach, in an iterative incremental numerical model to achieve equilibrium points of P-ε and M-φ response up to failure. This numerical analysis is adaptod to asses the confining effect in circular cross sectional columns confined with FRP and conventional lateral steel together; concrete filled steel tube (CFST) circular columns and rectangular columns confined with conventional lateral steel. This model is validated against experimental data found in literature. The comparison shows good correlation. Finally computer

software is developed based on the non-linear numerical analysis. The software is equipped with an elegant graphics interface that assimilates input data, detail drawings, capacity diagrams and demand point mapping in a single sheet. Options for preliminary design, section and reinforcement selection are seamlessly integrated as well. The software generates 2D interaction diagrams for circular columns, 3D failure surface for rectangular columns and allows the user to determine the 2D interaction diagrams for any angle α between the x-axis and the resultant moment. Improvements to KDOT Bridge Design Manual using this software with reference to AASHTO LRFD are made. This study is limited to stub columns.

BEHAVIOR OF CONCRETE COLUMNS UNDER VARIOUS CONFINEMENT EFFECTS

by

AHMED MOHSEN ABD EL FATTAH

B.S., Cairo University, 2000

M.S., Kansas State University, 2008

A DISSERTATION

Submitted in partial fulfillment of the requirements for the degree

DOCTOR OF PHILOSOPHY

Department of Civil Engineering

College of Engineering

KANSAS STATE UNIVERSITY

Manhattan, Kansas

2012

Approved by:

Major Professor

Hayder Rasheed

Copyright

AHMED MOHSEN ABD EL FATTAH

2012

Abstract

The analysis of concrete columns using unconfined concrete models is a well established practice. On the other hand, prediction of the actual ultimate capacity of confined concrete columns requires specialized nonlinear analysis. Modern codes and standards are introducing the need to perform extreme event analysis. There has been a number of studies that focused on the analysis and testing of concentric columns or cylinders. This case has the highest confinement utilization since the entire section is under confined compression. On the other hand, the augmentation of compressive strength and ductility due to full axial confinement is not applicable to pure bending and combined bending and axial load cases simply because the area of effective confined concrete in compression is reduced. The higher eccentricity causes smaller confined concrete region in compression yielding smaller increase in strength and ductility of concrete. Accordingly, the ultimate confined strength is gradually reduced from the fully confined value f_{cc} (at zero eccentricity) to the unconfined value f'_c (at infinite eccentricity) as a function of the compression area to total area ratio. The higher the eccentricity the smaller the confined concrete compression zone. This paradigm is used to implement adaptive eccentric model utilizing the well known Mander Model and Lam and Teng Model.

Generalization of the moment of area approach is utilized based on proportional loading, finite layer procedure and the secant stiffness approach, in an iterative incremental numerical model to achieve equilibrium points of $P\text{-}\varepsilon$ and $M\text{-}\varphi$ response up to failure. This numerical analysis is adaptod to asses the confining effect in circular cross sectional columns confined with FRP and conventional lateral steel together, concrete filled steel tube (CFST) circular columns and rectangular columns confined with conventional lateral steel. This model is validated against experimental data found in literature. The comparison shows good correlation. Finally computer

software is developed based on the non-linear numerical analysis. The software is equipped with an elegant graphics interface that assimilates input data, detail drawings, capacity diagrams and demand point mapping in a single sheet. Options for preliminary design, section and reinforcement selection are seamlessly integrated as well. The software generates 2D interaction diagrams for circular columns, 3D failure surface for rectangular columns and allows the user to determine the 2D interaction diagrams for any angle α between the x-axis and the resultant moment. Improvements to KDOT Bridge Design Manual using this software with reference to AASHTO LRFD are made. This study is limited to stub columns

Table of Contents

x

List of Figures

xvi

List of Tables

Acknowledgements

All praises to Allah the lord of mankind.

The author expresses his gratitude to his supervisor, Dr. Hayder Rasheed who was abundantly helpful and offered invaluable assistance, support and guidance. Deepest gratitude are also due to the members of the supervisory committee, Dr. Asad Esmaeily, Dr Hani Melhem, Dr Sutton Stephens and Dr Brett DePaola,.

The author would also like to convey thanks to Kansas Department of transportation for providing the financial means of this research

The author wishes to express his love and gratitude to his beloved family; for their understanding & endless love, through the duration of his studies. Special thanks to his mother Dr Amany Aboellil for her support

Dedication

This work is dedicated to the memory of "the ones who couldn't make it."

Chapter 1 - Introduction

1-1 Background

Columns are considered the most critical elements in structures. The unconfined analysis for columns is well established in the literature. Structural design codes dictate reduction factors for safety. It wasn't until very recently that design specifications and codes of practice, like AASHTO LRFD, started realizing the importance of introducing extreme event load cases that necessitates accounting for advanced behavioral aspects like confinement. Confinement adds another dimension to columns analysis as it increases the column's capacity and ductility. Accordingly, confinement needs special non linear analysis to yield accurate predictions. Nevertheless the literature is still lacking specialized analysis tools that take into account confinement despite the availability of all kinds of confinement models. In addition the literature has focused on axially loaded members with less attention to eccentric loading. Although the latter is more likely to occur, at least with misalignement tolerances, the eccentricity effect is not considered in any confinement model available in the literature.

It is widely known that code Specifications involve very detailed design procedures that need to be checked for a number of limit states making the task of the designer very tedious. Accordingly, it is important to develop software that guide through the design process and facilitate the preparation of reliable analysis/design documents.

1-2 Objectives

This study is intended to determine the actual capacity of confined reinforced concrete columns subjected to eccentric loading and to generate the failure envelope at three different

levels. First, the well-known ultimate capacity analysis of unconfined concrete is developed as a benchmarking step. Secondly, the unconfined ultimate interaction diagram is scaled down based on the reduction factors of the AASHTO LRFD to the design interaction diagram. Finally, the actual confined concrete ultimate analysis is developed based on a new eccentricity model accounting for partial confinement effect under eccentric loading. The analyses are conducted for three types of columns; circular columns confined with FRP and conventional transverse steel, circular columns confined with steel tubes and rectangular columns confined with conventional transverse steel. It is important to note that the present analysis procedure will be benchmarked against a wide range of experimental and analytical studies to establish its accuracy and reliability.

It is also the objective of this study to furnish interactive software with a user-friendly interface having analysis and design features that will facilitate the preliminary design of circular columns based on the actual demand. The overall objectives behind this research are summarized in the following points:

- Introduce the eccentricity effect in the stress-strain modeling

- Implement non-linear analysis for considering the confinement effects on column's actual capacity

- Test the analysis for three types of columns; circular columns confined with FRP and conventional transverse steel, circular columns confined with steel tubes and rectangular columns confined with conventional transverse steel.

- Generate computer software that helps in designing and analyzing confined concrete columns through creating three levels of Moment-Force envelopes; unconfined curve, design curve based on AASHTO-LRFD and confined curve.

1-3 Scope

This dissertation is composed of seven chapters covering the development of material models, analysis procedures, benchmarking and practical applications.

- Chapter one introduces the objectives of the study and the content of the different chapters.

- Chapter two reviews the literature through four independent sections:

    1- Section 1: Reinforced concrete confinement models

    2- Section 2: Circular Columns Confined with FRP

    3- Section 3: Circular Concrete Filled Steel Tubes Columns (CFST)

    4- Section 4: Rectangular Columns subjected to biaxial bending and Axial Compression

- Chapter three deals with Circular columns confined with FRP and lateral steel.

- Chapter four talks about concrete filled steel tube (CFST) circular columns

- Chapter five presents rectangular columns analysis for both the unconfined and confined cases. Chapter three, four and five address the following subjects:

▪ Finite Layer Approach (Fiber Model)

▪ Present Confinement Model for Concentric Columns

▪ Present Confinement Model for Eccentric Columns

▪ Moment of Area Theorem

▪ Numerical Formulation

▪ Results and Discussion

- Chapter six introduces the software concepts and highlights the software forms and components

- Chapter seven states the conclusions and recommendations.

Chapter 2 - Literature Review

This chapter reviews four different topics; lateral steel confinement models, Circular Concrete Columns Filled Steel Tubes (CFST) and Rectangular Columns subjected to biaxial bending and Axial Compression.

2-1 Steel Confinement Models

A comprehensive review of confined models for concrete columns under concentric axial compression that are available in the literature is conducted. The models reviewed are chronologically presented then compared by a set of criteria that assess consideration of different factors in developing the models such as effectively confined area, yielding strength and ductility.

2-1-1 Chronological Review of Models

The confinement models available are presented chronologically regardless of their comparative importance first. After that, discussion and categorization of the models are carried out and conclusions are made. Common notation is used for all the equations for the sake of consistency and comparison.

2-1-1-1 Notation

$A_{s:}$ the cross sectional area of longitudinal steel reinforcement

$A_{st:}$ the cross sectional area of transverse steel reinforcement

$A_{e:}$ the area of effectively confined concrete

A_{cc}: the area of core within centerlines of perimeter spirals or hoops excluding area of longitudinal steel

b: the confined width (core) of the section

h: the confined height (core) of the section

c: center-to-center distance between longitudinal bars

d'_s: the diameter of longitudinal reinforcement

d'_{st}: the diameter of transverse reinforcement

D: the diameter of the column

d_s the core diameter of the column

f_{cc}: the maximum confined strength

f'_c: the peak unconfined strength

f_l: the lateral confined pressure

f'_l: the effective lateral confined pressure

f_{yh}: the yield strength of the transverse steel

f_s: the stress in the lateral confining steel

k_e: the effective lateral confinement coefficient

q: the effectiveness of the transverse reinforcement

s: tie spacing

s_o: the vertical spacing at which transverse reinforcement is not effective in concrete confinement

ε_{co}: the strain corresponding to the peak unconfined strength f'_c

ε_{cc}: the strain corresponding to the peak confined strength f_{cc}

ε_y: the strain at yielding for the transverse reinforcement

ε_{cu}: the ultimate strain of confined concrete

ρ_s: the volumetric ratio of lateral steel to concrete core

ρ_l: the ratio of longitudinal steel to the gross sectional area

ρ: the volumetric ratio of lateral + longitudinal steel to concrete core

Richart, Brandtzaeg and Brown (1929)

Richart *et al's*. (1929) model was the first to capture the proportional relationship between the lateral confined pressure and the ultimate compressive strength of confined concrete.

$$f_{cc} = f_c' + k_1 f_l \qquad\qquad 2\text{-}1$$

The average value for the coefficient k_1, which was derived from a series of short column specimen tests, came out to be (4.1). The strain corresponding to the peak strength ε_{cc} (see Mander *et al.* 1988) is obtained using the following function:

$$\varepsilon_{cc} = \varepsilon_{co}\left[1 + k_2\left(\frac{f_l}{f_c'}\right)\right] \qquad k_2 = 5k_1 \qquad\qquad 2\text{-}2$$

where ε_{co} is the strain corresponding to $f'c$, k_2 is the strain coefficient of the effective lateral confinement pressure. No stress-strain curve graph was proposed by Richart *et al* (1929).

Chan (1955)

A tri-linear curve describing the stress-strain relationship was suggested by Chan (1955) based on experimental work. The ratio of the volume of steel ties to concrete core volume and concrete strength were the only variables in the experimental work done. Chan assumed that OA approximates the elastic stage and ABC approximates the plastic stage, Figure (2-1). The positions of A, B and C may vary with different concrete variables. Chan assumed three different

slopes E_c, $\lambda_1 E_c$, $\lambda_2 E_c$ for lines OA, AB and BC respectively. However no information about λ_1 and λ_2 was provided.
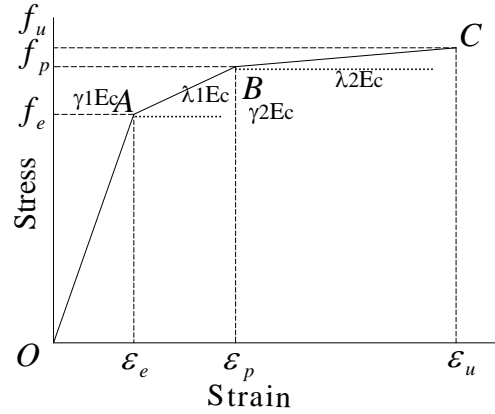
Figure 2-1: General Stress-Strain curve by Chan (1955)

Blume, Newmark and Corning (1961)

Blume *et al.* (1961) were the first to impose the effect of the yield strength for the transverse steel f_{yh} in different equations defining the model. The model generated, Figure (2-2), has ascending straight line with steep slope starting from the origin till the plain concrete peak strength f'_c and the corresponding strain ε_{co}, then a less slope straight line connect the latter point and the confined concrete peak strength f_{cc} and ε_{cc}. Then the curve flatten till ε_{cu}

$$f_{cc} = 0.85 f'_c + 4.1 \frac{A_{st} f_{yh}}{sh} \qquad \text{for rectangular columns} \qquad \text{2-3}$$

$$\varepsilon_{co} = \frac{0.22 f'_c + 400\, psi}{10^6\, psi} \qquad \text{2-4}$$

$$\varepsilon_{cc} = 5\varepsilon_y \qquad \text{2-5}$$

$$\varepsilon_{cu} = 5\varepsilon_{su} \qquad \text{2-6}$$

7
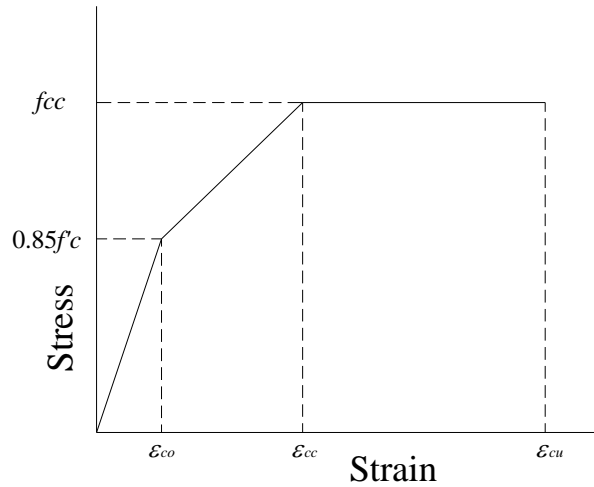
Figure 2-2: General Stress-Strain curve by Blume *et al.* (1961)

where ε_y is the strain at yielding for the transverse reinforcement, A_{st} is the cross sectional area of transverse steel reinforcement ,h is the confined cross sectional height, ε_{su} is the strain of transverse spiral reinforcement at maximum stress and ε_{cu} is the ultimate concrete strain.

Roy and Sozen (1965)

Based on their experimental results, which were controlled by two variables; ties spacing and amount of longitudinal reinforcement, Roy and Sozen (1965) concluded that there is no enhancement in the concrete capacity by using rectilinear ties. On the other hand there was significant increase in ductility. They proposed a bilinear ascending-descending stress strain curve that has a peak of the maximum strength of plain concrete f'_c and corresponding strain ε_{co} with a value of 0.002. The second line goes through the point defined by ε_{50} till it intersects with the strain axis. The strain ε_{50} was suggested to be a function of the volumetric ratio of ties to concrete core ρ_s, tie spacing s and the shorter side dimension b' (see Sheikh 1982).

8

$$\varepsilon_{50} = \frac{3\rho_s b'}{4s}$$ 2-7

Soliman and Yu (1967)

Soliman and Yu (1967) proposed another model that emerged from experimental results. The main parameters involved in the work done were tie spacing s, a new term represents the effectiveness of ties s_o, the area of ties A_{st}, and finally section geometry, which has three different variables; A_{cc} the area of confined concrete under compression, A_c the area of concrete under compression and b. The model has three different portions as shown in Figure (2-3). The ascending portion which is represented by a curve till the peak point (f'_c, ε_{ce}). The flat straight-line portion with its length varying depending on the degree of confinement. The last portion is a descending straight line passing through ($0.8\,f'_c$, ε_{cf}) then extending down till an ultimate strain.

$$q = \left(1.4\frac{A_{cc}}{A_c} - 0.45\right)\frac{A_{st}(s_o - s)}{A_{st}s + 0.0028Bs^2}$$ 2-8

$$f_{cc} = 0.9 f'_c(1 + 0.05q)$$ 2-9

$$\varepsilon_{ce} = 0.55 f_{cc} * 10^{-6}$$ 2-10

$$\varepsilon_{cs} = 0.0025(1 + q)$$ 2-11

$$\varepsilon_{cf} = 0.0045(1 + 0.85q)$$ 2-12

where q refers to the effectiveness of the transverse reinforcement , s_o is the vertical spacing at which transverse reinforcement is not effective in concrete confinement and B is the greater of b and $0.7\,h$.
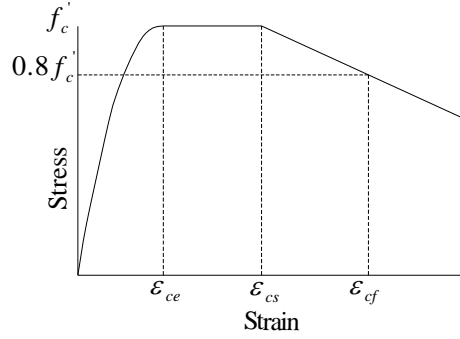
Figure 2-3: General Stress-Strain curve by Soliman and Yu (1967)

Sargin (1971)

Sargin conducted experimental work on low and medium strength concrete with no longitudinal reinforcement. The transverse steel that was used had different size and different yield and ultimate strength. The main variables affecting the results were the volumetric ratio of lateral reinforcement to concrete core ρ_s, the strength of plain concrete f'_c, the ratio of tie spacing to the width of the concrete core and the yield strength of the transverse steel f_{yh}.

$$f_c = k_3 f'_c \left[\frac{Ax + (m-1)x^2}{1 + (A-2)x + mx^2} \right]$$

2-13

where m is a constant controlling the slope of the descending branch:

$$m = 0.8 - 0.05 f'_c$$

2-14

$$x = \frac{\varepsilon_c}{\varepsilon_{cc}}$$

2-15

$$A = \frac{E_c \varepsilon_{cc}}{k_3 f'_c}$$

2-16

$$k_3 = 1 + 0.0146 \left[1 - 0.245 \frac{s}{b} \right] \frac{\rho_s f_{yh}}{\sqrt{f'_c}}$$

2-17

10

$$\varepsilon_{cc} = 0.0024 + 0.0374 \left[1 - \frac{0.734s}{b} \right] \frac{\rho_s f_{yh}}{\sqrt{f_c^{'}}}$$

2-18

$$f_{cc} = k_3 f_c^{'}$$

2-19

where k_3 is concentric loading maximum stress ratio.

Kent and Park (1971)

As Roy and Sozen (1965) did, Kent and Park (1971) assumed that the maximum strength for confined and plain concrete is the same f'_c. The suggested curve, Figure (2-4), starts from the origin then increases parabolically (Hognestad's Parabola) till the peak at f'_c and the corresponding strain ε_{co} at 0.002. Then it descends with one of two different straight lines. For the confined concrete, which is more ductile, it descends till the point (0.5 $f'c$, ε_{50c}) and continues descending to $0.2f'c$ followed by a flat plateau. For the plain concrete it descends till the point (0.5 $f'c$, ε_{50u}) and continue descending to $0.2f'_c$ as well without a flat plateau. Kent and Park assumed that confined concrete could sustain strain to infinity at a constant stress of $0.2 f'c$

$$f_c = f_c^{'} \left[\frac{2\varepsilon_c}{\varepsilon_{co}} - \left(\frac{\varepsilon_c}{\varepsilon_{co}} \right)^2 \right] \qquad \text{for ascending branch}$$

$$f_c = f_c^{'} \left[1 - Z(\varepsilon_c - \varepsilon_{co}) \right] \qquad \text{for descending branch}$$

2-20

$$\varepsilon_{50u} = \frac{3 + 0.002 f_c^{'}}{f_c^{'} - 1000}$$

2-21

$$\rho_s = \frac{2(h+b)A_{st}}{hbs}$$

2-22

$$\varepsilon_{50h} = \varepsilon_{50c} - \varepsilon_{50u}$$

2-23

$$\varepsilon_{50h} = \frac{3}{4} \rho_s \sqrt{\frac{b}{s}}$$

2-24

$$Z = \frac{0.5}{\varepsilon_{50h} + \varepsilon_{50u} - \varepsilon_{co}}$$

2-25

where ρ_s is the ratio of lateral steel to the concrete core, Z is a constant controlling the slope of descending portion.
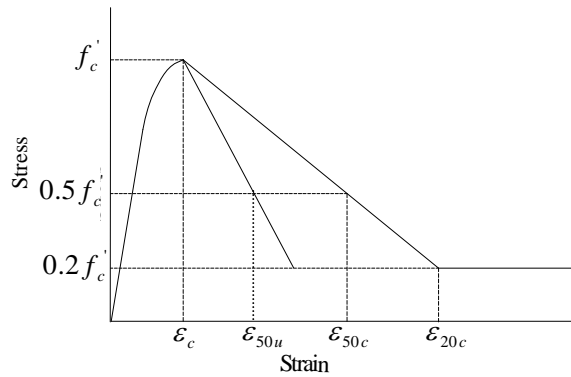
Figure 2-4: Stress-Strain curve by Kent and Park (1971).

Popovics (1973)

Popovics pointed out that the stress-strain diagram is influenced by testing conditions and concrete age. The stress equation is:

$$f_c = f_{cc} \frac{\varepsilon_c}{\varepsilon_{cc}} \frac{n}{n - 1 + \left(\dfrac{\varepsilon_c}{\varepsilon_{cc}}\right)^n}$$

2-26

$$n = 0.4 * 10^{-3} f_{cc} + 1.0$$

2-27

$$\varepsilon_{cc} = 2.7 * 10^{-4} \sqrt[4]{f_{cc}}$$

2-28

Vallenas, Bertero and Popov (1977)

12

The variables utilized in the experimental work conducted by Vallenas *et al.* (1977) were the volumetric ratio of lateral steel to concrete core ρ_s, ratio of longitudinal steel to the gross area of the section ρ_l, ties spacing s, effective width size, strength of ties and size of longitudinal bars. The model generated was similar to Kent and Park model with improvement in the peak strength for confined concrete, Figure (2-5). For the ascending branch:

$$\frac{f_c}{f_c'} = k[1 - Z\varepsilon_{cc}(x-1)] \qquad \varepsilon_{cc} \leq \varepsilon_c \leq \varepsilon_{0.3k} \tag{2-29}$$

$$\frac{f_c}{f_c'} = 0.3k \qquad \varepsilon_{0.3k} \leq \varepsilon_c \tag{2-30}$$

$$x = \frac{\varepsilon_c}{\varepsilon_{cc}} \tag{2-31}$$

$$f_{cc} = kf_c' \tag{2-32}$$

$$\frac{f_c}{f_c'} = \frac{\dfrac{E_c\varepsilon_{cc}}{f_c'}x - kx^2}{1 + \left(\dfrac{E_c\varepsilon_{cc}}{kf_c'} - 2\right)x} \qquad \varepsilon_c \leq \varepsilon_{cc} \tag{2-33}$$

For the descending branch:

$$k = 1 + 0.0091\left[1 - 0.245\frac{s}{h}\right]\frac{\left[\rho + \dfrac{d_{st}'}{d_s'}\rho_l\right]f_{yh}}{\sqrt{f_c'}} \tag{2-34}$$

$$\varepsilon_{cc} = 0.0024 + 0.005\left[1 - \frac{0.734s}{h}\right]\frac{\rho f_{yh}}{\sqrt{f_c'}} \tag{2-35}$$

$$Z = \frac{0.5}{\dfrac{3}{4}\rho_s\sqrt{\dfrac{h}{s}} + \left[\dfrac{3 + 0.002f_c'}{f_c' - 1000}\right] - 0.002} \tag{2-36}$$

where k is coefficient of confined strength ratio, Z is the slope of descending portion, d'_s and d'_{st} are the diameter of longitudinal and transverse reinforcement respectively.
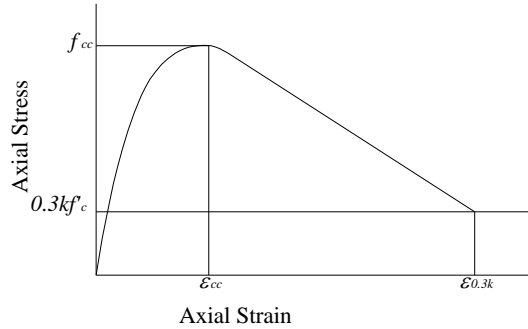
Figure 2-5: Stress-Strain curve by Vallenas *et al.* (1977).

Wang, Shah and Naaman (1978)

Wang *et al.* (1978) obtained experimentally another stress-strain curve describing the behavior of confined reinforced concrete under compression; Figure (2-6). The concrete tested was normal weight concrete ranging in strength from 3000 to 11000 psi (20.7 to 75.8 *MPa*) and light weight concrete with strength of 3000-8000 psi (20.7 to 55 *MPa*). Wang *et al.* utilized an equation, with four constants, similar to that of Sargin *et al.*

$$Y = \frac{AX + BX^2}{1 + CX + DX^2}$$

2-37

Where

$$Y = \frac{f_c}{f_{cc}}$$

2-38

$$X = \frac{\varepsilon_c}{\varepsilon_{cc}}$$

2-39

14

The four constant *A, B, C, D* were evaluated for the ascending part independently of the descending one. The four conditions used to evaluate the constants for the ascending part were

$dY/dX = E_{0.45}/E_{sec}$ at $X=0$ $E_{sec} = f_{cc}/\varepsilon_{cc}$

$Y = 0.45$ for $X = 0.45/(E_{0.45}/E_{sec})$

$Y=1$ for $X=1$

$dY/dX = 0$ at $X=1$

whereas for the descending branch:

$Y=1$ for $X=1$

$dY/dX = 0$ at $X=1$

$Y = f_i/f_{cc}$ for $X = \varepsilon_i/\varepsilon_{cc}$
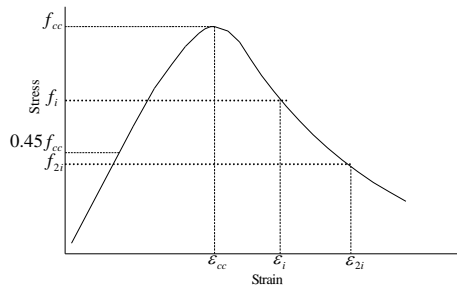
Figure 2-6: Proposed Stress-Strain curve by Wang *et al* (1978)

where f_i and ε_i are the stress and strain at the inflection point, f_{2i} and ε_{2i} refer to a point such that $\varepsilon_{2i} - \varepsilon_i = \varepsilon_i - \varepsilon_{cc}$ and $E_{0.45}$ represents the secant modulus of elasticity at 0.45 f_{cc}

$Y = f_{2i}/f_{cc}$ for $X = \varepsilon_{2i}/\varepsilon_{cc}$

Muguruma , Watanabe , Katsuta and Tanaka (1980)

15

Muguruma *et al.* (1980) obtained their stress-strain model based on experimental work conducted by the model authors, Figure (2-7). The stress-strain model is defined by three zones; Zone 1 from 0-A:

$$f_c = E_i \varepsilon_c + \frac{f_c^{'} - E_i \varepsilon_{co}}{\varepsilon_{co}^{~2}} \varepsilon_c^{~2} \qquad \text{(kgf/cm}^2\text{)} \qquad 0 \le \varepsilon_c \le \varepsilon_{co} \tag{2-40}$$

Zone 2 from A-D

$$f_c = f_{cc} + \frac{(\varepsilon_c - \varepsilon_{cc})^2}{(\varepsilon_{co} - \varepsilon_{cc})^2} (f_c^{'} - f_{cc}) \text{ (kgf/cm}^2\text{)} \qquad \varepsilon_{co} < \varepsilon_c \le \varepsilon_{cc} \tag{2-41}$$

Zone 3 from D-E

$$f_c = f_{cc} + \frac{f_u - f_{cc}}{\varepsilon_{cu} - \varepsilon_{cc}} (\varepsilon_c - \varepsilon_{cc}) \qquad \text{(kgf/cm}^2\text{)} \qquad \varepsilon_{cc} < \varepsilon_c \le \varepsilon_{cu} \tag{2-42}$$

$$f_u = \frac{2(\overline{S} - f_{cc} \varepsilon_{cc})}{\varepsilon_{cc} + \varepsilon_{cu}} \qquad \text{(kgf/cm}^2\text{)} \tag{2-43}$$

$$\varepsilon_u = 0.00413(1 - f_c^{'} / 2000) \qquad \text{(kgf/cm}^2\text{)} \tag{2-44}$$

$$Cc = \rho_s \frac{\sqrt{f_{yh}}}{f_c^{'}} \left(1 - 0.5 \frac{s}{W}\right) \tag{2-45}$$

where $\overline{S}$ is the area surrounded by the idealized stress-strain curve up to the peak stress and W is the minimum side length or diameter of confined concrete

For circular columns confined with circular hoops:

16

$$f_{cc} = (1 + 150Cc)f_c' \qquad \text{(kgf/cm}^2) \qquad\qquad\qquad 2\text{-}46$$

$$\varepsilon_{cc} = (1 + 1460Cc)\varepsilon_{co} \qquad\qquad\qquad\qquad 2\text{-}47$$

$$\varepsilon_{cu} = (1 + 990Cc)\varepsilon_u \qquad\qquad\qquad\qquad 2\text{-}48$$

Whereas for square columns confined with square hoops:

$$f_{cc} = (1 + 50Cc)f_c' \qquad \text{(kgf/cm}^2) \qquad\qquad\qquad 2\text{-}49$$

$$\varepsilon_{cc} = (1 + 450Cc)\varepsilon_{co} \qquad\qquad\qquad\qquad 2\text{-}50$$

$$\varepsilon_{cu} = (1 + 450Cc)\varepsilon_u \qquad\qquad\qquad\qquad 2\text{-}51$$
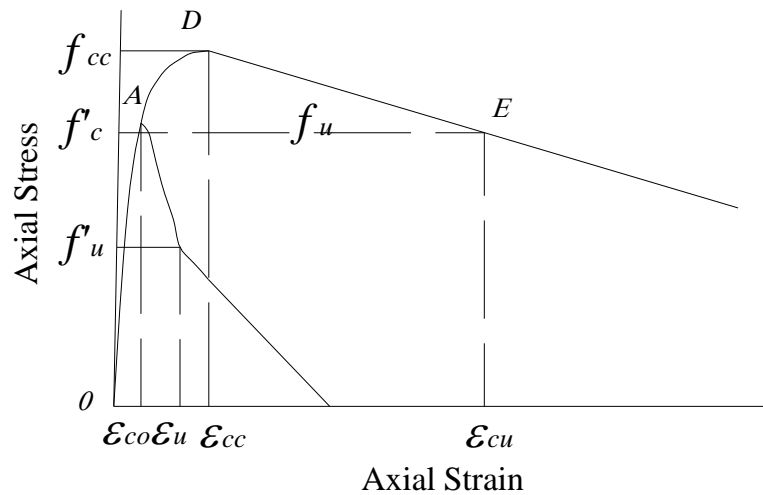
Figure 2-7: Proposed Stress-Strain curve by Muguruma *et al* (1980)

Scott, Park, Priestly (1982)

Scott *et al.* (1982) examined specimens by loading at high strain rate to correlate with the seismic loading. They presented the results including the effect of eccentric loading, strain rate, amount and distribution of longitudinal steel and amount and distribution of transverse steel. For low strain rate Kent and Park equations were modified to fit the experimental data

$$f_c = k f_c' \left[\frac{2\varepsilon_c}{0.002k} - \left(\frac{\varepsilon_c}{0.002k} \right)^2 \right] \qquad \varepsilon_c \le 0.002k \qquad \text{2-52}$$

$$f_c = k f_c' [1 - Z_m(\varepsilon_c - 0.002k)] \qquad \varepsilon_c > 0.002k \qquad \text{2-53}$$

where

$$k = 1 + \frac{\rho_s f_{yh}}{f_c'} \qquad \text{2-54}$$

$$Z_m = \frac{0.5}{\dfrac{3 + 0.29 f_c'}{145 f_c' - 1000} + \dfrac{3}{4}\rho_s\sqrt{\dfrac{b''}{s}} - 0.002k} \qquad f'_c \text{ is in } MPa \qquad \text{2-55}$$

where *b"* is the width of concrete core measured to outside of the hoops. For the high strain rate, the k and Z_m were adapted to

$$k = 1.25(1 + \frac{\rho_s f_{yh}}{f_c'}) \qquad \text{2-56}$$

$$Z_m = \frac{0.625}{\dfrac{3 + 0.29 f_c'}{145 f_c' - 1000} + \dfrac{3}{4}\rho_s\sqrt{\dfrac{b}{s}} - 0.002k} \qquad f'_c \text{ is in } MPa \qquad \text{2-57}$$

and the maximum strain was suggested to be:

$$\varepsilon_{cu} = 0.004 + 0.9\rho_s \left(\frac{f_{yh}}{300} \right)$$

2-58

It was concluded that increasing the spacing while maintaining the same ratio of lateral reinforcement by increasing the diameter of spirals, reduce the efficiency of concrete confinement. In addition, increasing the number of longitudinal bars will improve the concrete confinement due to decreasing the spacing between the longitudinal bars.

Sheikh and Uzumeri (1982)

Sheikh and Uzumeri (1982) introduced the effectively confined area as a new term in determining the maximum confined strength (Soliman and Yu (1967) had trial in effective area introduction). In addition to that they, in their experimental work, utilized the volumetric ratio of lateral steel to concrete core, longitudinal steel distribution, strength of plain concrete, and ties strength, configuration and spacing. The stress-strain curve, Figure (2-8), was presented parabolically up to (f_{cc}, ε_{cc}), then it flattens horizontally till ε_{cs}, and finally it drops linearly passing by ($0.85f_{cc}$, ε_{85}) till $0.3 f_{cc}$, In that sense, it is conceptually similar to the earlier model of Soliman and Yu (1967).

f_{cc} and ε_{cc} can be determined from the following equations:

$$f_{cc} = k_s f_{cp} \qquad f_{cp} = k_p f_c^{'} \qquad k_p = 0.85$$

2-59

$$k_s = 1 + \frac{2.73b^2}{P_{occ}} \left[\left(1 - \frac{nc^2}{5.5b^2} \right) \left(1 - \frac{s}{2b} \right)^2 \right] \sqrt{\rho_s f_{st}^{'}}$$

2-60

$$\varepsilon_{cc} = 0.55k_s f_c^{'} *10^{-6}$$

2-61

$$\varepsilon_{cs} = \varepsilon_{co}\left(1 + \frac{0.81}{c}\left(1 - 5\left(\frac{s}{b}\right)^2\right)\frac{\rho_s f_{st}'}{\sqrt{f_c'}}\right)$$ 2-62

$$\varepsilon_{85} = 0.225\rho_s\sqrt{\frac{b}{s}} + \varepsilon_{cs}$$ 2-63

$$Z = \frac{0.5}{\frac{3}{4}\rho_s\sqrt{\frac{b}{s}}}$$ 2-64

where b is the confined width of the cross section, f'_{st} is the stress in the lateral confining bar, c is center-to-center distance between longitudinal bars, ε_{s85} is the value of strain corresponding to 85% of the maximum stress on the unloading branch, n is the number of laterally supported longitudinal bars, Z is the slope for the unloading part, f_{cp} is the equivalent strength of unconfined concrete in the column, and $P_{occ} = K_p f'_c(A_{cc} - A_s)$
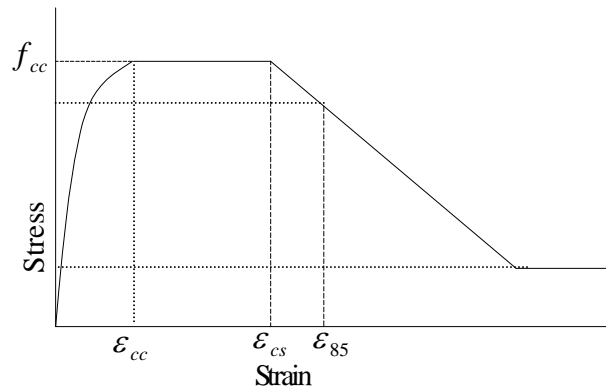
Figure 2-8: Proposed general Stress-Strain curve by Sheikh and Uzumeri (1982).

Ahmad and Shah (1982) developed a model based on the properties of hoop reinforcement and the constitutive relationship of plain concrete. Normal weight concrete and lightweight concrete were used in tests that were conducted with one rate of loading. No longitudinal reinforcement was provided and the main two parameters varied were spacing and yield strength of transverse reinforcement. Ahmed and Shah observed that the spirals become ineffective when the spacing exceeds 1.25 the diameter of the confined concrete column. They concluded also that the effectiveness of the spiral is inversely proportional with compressive strength of unconfined concrete.

Ahmad and Shah adapted Sargin model counting on the octahedral failure theory, the three stress invariants and the experimental results:

$$Y = \frac{A_i X + (D_i - 1)X^2}{1 + (A_i - 2)X + D_i X^2}$$
2-65

$$Y = \frac{f_{pcs}}{f_{pcn}}$$
2-66

$$X = \frac{\varepsilon_i}{\varepsilon_{ip}}$$
2-67

where f_{pcs} is the most principal compressive stress, f_{pcn} is the most principal compressive strength, ε_i is the strain in the i-th principal direction and ε_{ip} is the strain at the peak in the *i-th* direction.

$$A_i = \frac{E_i}{E_{ip}} \qquad\qquad E_{ip} = \frac{f_{pcn}}{\varepsilon_{ip}}$$

E_i is the initial slope of the stress strain curve, D_i is a parameter that governs the descending branch. When the axial compression is considered to be the main loading, which is typically the case in concentric confined concrete columns, Equations (2-65), (2-66) and (2-67) become:

21

$$Y = \frac{AX + (D-1)X^2}{1 + (A-2)X + DX^2}$$

2-68

$$Y = \frac{f_c}{f_{cc}}$$

2-69

$$X = \frac{\varepsilon_c}{\varepsilon_{cc}}$$

2-70

$$A = \frac{E_c}{E_{sec}}$$

2-71

Park, Priestly and Gill (1982)

Park *et al*. (1982) modified Kent and Park (1971) equations to account for the strength improvement due to confinement based on experimental work conducted for four square full scaled columns (21.7 in^2 (14 000 mm^2) cross sectional area and 10.8 ft (3292 mm) high), Figure (2-9). The proposed equations are as follow:

$$f_c = kf_c^{'} \left[\frac{2\varepsilon_c}{0.002k} - \left(\frac{\varepsilon_c}{0.002k} \right)^2 \right] \qquad \text{for ascending branch}$$

2-72

$$f_c = kf_c^{'} \left[1 - Z_m (\varepsilon_c - \varepsilon_{co}) \right] \geq 0.2kf'c \qquad \text{for descending branch}$$

2-73

$$Z_m = \frac{0.5}{\dfrac{3 + 0.29f_c^{'}}{145f_c^{'} - 1000} + \dfrac{3}{4}\rho_s\sqrt{\dfrac{b}{s}} - 0.002k}$$

2-74

$$k = 1 + \frac{\rho_s f_{yh}}{f_c^{'}}$$

2-75
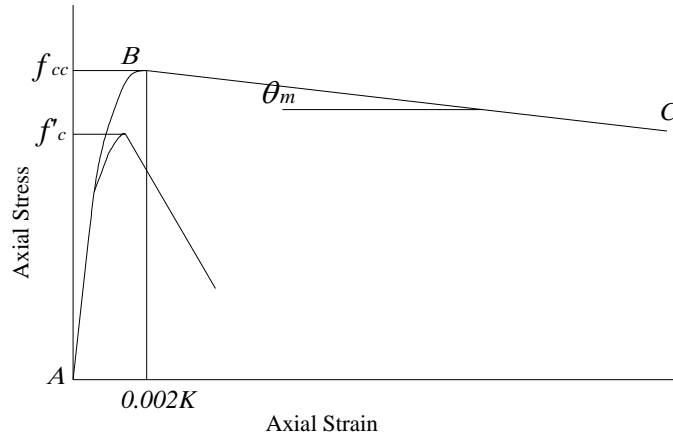
Figure 2-9: Proposed general Stress-Strain curve by Park *et al* (1982).

<u>Martinez, Nilson and Slate (1984)</u>

Experimental investigation was conducted to propose equations to define the stress strain curve for spirally reinforced high strength concrete under compressive loading. The main parameters used were compressive strength for unconfined concrete, amount of confinement and specimen size. Two types of concrete where used; normal weight concrete with strength to about 12000 *psi. (82.75 MPa)* and light weight concrete with strength to about 9000 *psi (62 MPa)*. Martinez *et al.* (1984) concluded that the design specification for low strength concrete might be unsafe if applied to high strength concrete. For normal weight concrete:

$$\left(f_{cc} - f_c^{'}\right) = 4f_l(1 - \frac{s}{d_{st}^{'}})$$

2-76

and for light weight concrete:

$$\left(f_{cc} - f_c^{'}\right) = 1.8f_l(1 - \frac{s}{d_{st}^{'}})$$

2-77

where d'_{st} is the diameter of the lateral reinforcement.

23

<u>Fafitis and Shah (1985)</u>

Fafitis and Shah (1985) assumed that the maximum capacity of confined concrete occurs when the cover starts to spall off. The experimental work was done on high strength concrete with varying the confinement pressure and the concrete strength. Two equations are proposed to express the ascending and the descending branches of the model. For the ascending branch:

$$f_c = f_{cc}\left[1-\left(1-\frac{\varepsilon_c}{\varepsilon_{cc}}\right)^A\right] \qquad 0 \le \varepsilon_c \le \varepsilon_{cc} \tag{2-78}$$

and for the descending branch:

$$f_c = f_{cc}\exp\left[-k(\varepsilon_c - \varepsilon_{cc})^{1.15}\right] \qquad \varepsilon_{cc} \le \varepsilon_c \tag{2-79}$$

The equations for the constant A and k:

$$A = \frac{E_c\varepsilon_{cc}}{f_{cc}} \tag{2-80}$$

$$k = 0.17 f_{cc}\exp(-0.01f_l) \tag{2-81}$$

f_{cc} and ε_{cc} can be found using the following equations:

$$f_{cc} = f_c^{'} + \left(1.15 + \frac{3048}{f_c^{'}}\right)f_l \tag{2-82}$$

$$\varepsilon_{cc} = 1.027*10^{-7} f_c^{'} + 0.0296\frac{f_l}{f_{cc}} + 0.00195 \tag{2-83}$$

f_l represents the confinement pressure and is given by the following equations:

$$f_l = \frac{2A_{st}f_{yh}}{sd_s} \qquad \text{for circular columns} \qquad \text{2-84}$$

$$f_l = \frac{2A_{st}f_{yh}}{d_e s} \qquad \text{for square columns} \qquad \text{2-85}$$

d_s is the core diameter of the column and d_e is the equivalent diameter.

Yong, Nour and Nawy (1988)

The model suggested by Yong *et al.* (1988) was based on experimental work done for rectangular columns with rectangular ties; Figure (2-10).

$$f_{cc} = Kf_c^{'} \qquad \text{2-86}$$

$$\varepsilon_{cc} = 0.00265 + \frac{0.0035\left(1 - \frac{0.734s}{h}\right)\left(\rho_s f_{yh}\right)^{2/3}}{\sqrt{f_c^{'}}} \qquad \text{2-87}$$

$$K = 1 + 0.0091\left(1 - \frac{0.245s}{h}\right)\left(\rho_s + \frac{nd_{st}^{'}}{8sd_s^{'}}\rho_l\right)\frac{f_{yh}}{\sqrt{f_c^{'}}} \qquad \text{2-88}$$

$$f_i = f_{cc}\left[0.25\left(\frac{f_c^{'}}{f_{cc}}\right) + 0.4\right] \qquad \text{2-89}$$

$$\varepsilon_i = K\left[1.4\left(\frac{\varepsilon_{cc}}{K}\right) + 0.0003\right] \qquad \text{2-90}$$

$$f_{2i} = f_c^{'}\left[0.025\left(\frac{f_{cc}}{1000}\right) - 0.065\right] \geq 0.3f_{cc} \qquad \text{2-91}$$
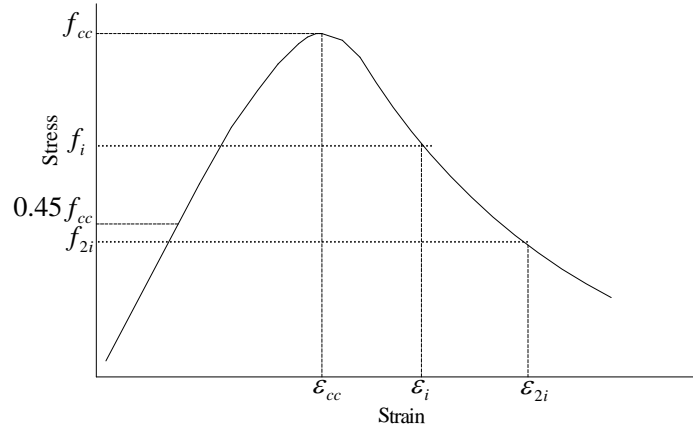
Figure 2-10: Proposed general Stress-Strain curve by Yong *et al.* (1988)

Mander, Priestly and Park (1988)

Using the same concept of effective lateral confinement pressure introduced by Sheikh and Uzumeri, Mander *et al.* (1988) developed a new confined model for circular spiral and hoops or rectangular ties; Figure (2-11). In addition Mander *et al.* (1988) was the second group after Bazant *et al.* (1972) to investigate the effect of the cyclic load side by side with monotonic one.

$$f_{cc} = f_c' \left(-1.254 + 2.254 \sqrt{1 + \frac{7.94 f_l'}{f_c'}} - 2 \frac{f_l'}{f_c'} \right)$$ 2-92

$$\varepsilon_{cc} = \varepsilon_{co} \left[1 + 5 \left(\frac{f_{cc}'}{f_c'} - 1 \right) \right]$$ 2-93

$$f_l' = \frac{1}{2} k_e \rho_s f_{yh} = k_e f_l$$ 2-94

$$f_c = \frac{f_{cc} xr}{r - 1 + x^r}$$ 2-95

26

$$r = \frac{E_c}{E_c - E_{\text{sec}}}$$

2-96

$$x = \frac{\varepsilon_c}{\varepsilon_{cc}}$$

2-97

Where k_e is the effective lateral confinement coefficient:

$$k_e = \frac{A_e}{A_{cc}}$$

2-98

A_e is the area of effectively confined concrete, $E_{sec} = f_{cc}/\varepsilon_{cc}$ and A_{cc} is area of core within centerlines of perimeter spirals or hoops excluding area of longitudinal steel.

$$k_e = \frac{\left(1 - \dfrac{s'}{2d_s}\right)^2}{1 - \rho_{cc}}$$ For Circular hoops

2-99

$$k_e = \frac{1 - \dfrac{s'}{2d_s}}{1 - \rho_{cc}}$$ For Circular spirals

2-100

$$k_e = \frac{\left(1 - \sum\limits_{i=1}^{n} \dfrac{(w_i')^2}{6b\,h}\right)\left(1 - \dfrac{s'}{2b}\right)\left(1 - \dfrac{s'}{2h}\right)}{(1 - \rho_{cc})}$$ For Rectangular ties

2-101

Where s' is the clear spacing, ρ_{cc} is the the ratio of longitudinal reinforcement to the core area $\sum w_i^2$ is the sum of the squares of all the clear spacing between adjacent longitudinal steel bars in a rectangular section. Mander *et al*. (1988) proposed calculation for the ultimate confined concrete strain ε_{cu} based on the strain energy of confined concrete.
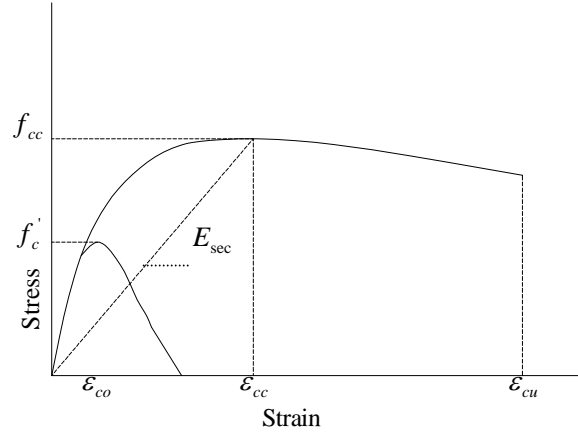
Figure 2-11: Stress- Strain Model proposed by Mander *et al* (1988)

<u>Fujii, Kobayashi, Miyagawa, Inoue and Matsumoto (1988)</u>

Fujii *et al.* (1988) developed a stress strain relation by uniaxial testing of circular and square specimen of 150 mm wide and 300 mm tall; Figure (2-12). The tested specimen did not have longitudinal bars and no cover. The proposed stress strain model has four regions;

Region 1 from 0-*A*

$$f_c = E_i \varepsilon_c + \frac{f_c^{'} - E_i \varepsilon_{co}}{\varepsilon_{co}^{2}} \varepsilon_c^{2} \qquad\qquad 0 \leq \varepsilon_c \leq \varepsilon_{co} \qquad\qquad 2\text{-}102$$

Region 2 from *A-B*

$$f_c = f_{cc} + \frac{\left(\varepsilon_c - \varepsilon_{cc}\right)^3}{\left(\varepsilon_{co} - \varepsilon_{cc}\right)^3}\left(f_c^{'} - f_{cc}\right) \qquad\qquad \varepsilon_{co} < \varepsilon_c \leq \varepsilon_{cc} \qquad\qquad 2\text{-}103$$

Region 3 from *B-C*

$$f_c = f_{cc} - \theta\left(\varepsilon_c - \varepsilon_{cc}\right) \qquad\qquad \varepsilon_{cc} < \varepsilon_c \leq \varepsilon_{c20} \qquad\qquad 2\text{-}104$$

Region 4 from *C-end*

28

$$f_c = 0.2 f_{cc} \qquad\qquad \varepsilon_{c20} < \varepsilon_c \qquad\qquad \text{2-105}$$

Fujii *et al.* (1988) defined three confinement coefficients for maximum stress C_{cf}, corresponding strain $C_{c\varepsilon u}$ and stress degradation gradient C_θ. For circular specimens, the peak strength and corresponding strain are as follow:

$$\frac{f_{cc}}{f_c^{'}} = 1.75 C_{cf} + 1.02 \qquad\qquad \text{2-106}$$

$$\frac{\varepsilon_{cc}}{\varepsilon_{co}} = 50 \, C_{c\varepsilon u} + 1.25 \qquad\qquad \text{2-107}$$

$$\theta = 417 C_\theta - 574 \qquad\qquad \text{2-108}$$

$$C_{cf} = \rho_s \left(1 - \frac{s}{0.51 d_s} \right) \frac{\sqrt{f_{yh}}}{f_c^{'}} \qquad\qquad \text{2-109}$$

$$C_{c\varepsilon u} = \rho_s \left(1 - \frac{s}{0.95 d_s} \right) \frac{\sqrt{f_{yh}}}{\left(f_c^{'} \right)^2} \qquad\qquad \text{2-110}$$

$$C_\theta = 1 / \rho_s \left(f_c^{'} \right)^2 / f_{yh} \qquad\qquad \text{2-111}$$

Whereas for square columns the values are as follow:

$$\frac{f_{cc}}{f_c^{'}} = 0.085 C_{cf} + 1.08 \qquad\qquad \text{2-112}$$

$$\frac{\varepsilon_{cc}}{\varepsilon_{co}} = 702 \, C_{c\varepsilon u} + 1.23 \qquad\qquad \text{2-113}$$

$$\theta = 1240C_\theta - 2720 \qquad\qquad\text{2-114}$$

$$C_{cf} = \rho_s\left(1 - \frac{s}{h}\right) \qquad\qquad\text{2-115}$$

$$C_{c\alpha u} = \rho_s\left(1 - \frac{s}{h}\right)\frac{\sqrt{f_{yh}}}{\left(f_c'\right)^2} \qquad\qquad\text{2-116}$$

$$C_\theta = 1/\rho_s\left(f_c'\right)^2 / f_{yh} \qquad\qquad\text{2-117}$$

They showed that the proposed model has higher accuracy than Park *et al.* (1982) model compared to the experimental work done by Fujii *et al.* (1988).
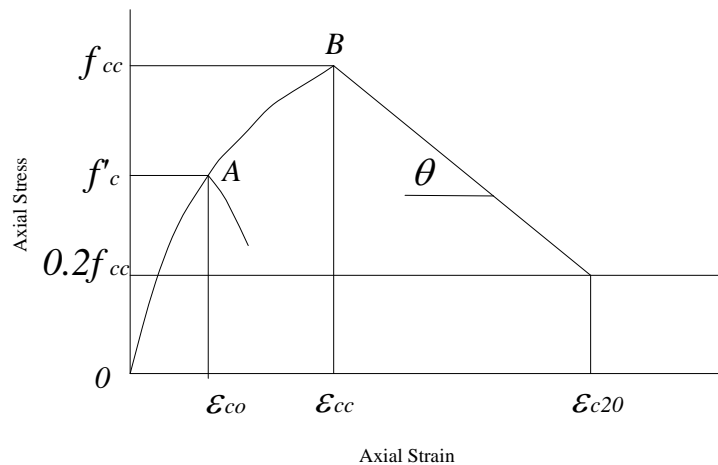
Figure 2-12: Proposed general Stress-Strain curve by Fujii *et al.* (1988)

Saatcioglu and Razvi (1992)

Saatcioglu and Razvi (1992) concluded that the passive lateral pressure generated by laterally expanding concrete and restraining transverse reinforcement is not always uniform. Based on tests on normal and high strength concrete ranging from 30 to 130 *MPa*, Saatcioglu

and Razvi proposed a new model, Figure (2-13), that has exponential relationship between the lateral confinement pressure and the peak confinement strength. They ran tests by varying volumetric ratio, spacing, yield strength, arrangement of transverse reinforcement, concrete strength and section geometry. In addition, the significance of imposing the tie arrangement as a parameter in determining the peak confined strength was highlighted

$$f_{cc} = f_c' + k_1 f_l \qquad \text{for circular cross section} \qquad \text{2-118}$$

$$k_1 = 6.7(f_l)^{-0.17} \qquad \text{2-119}$$

$$f_l = \frac{2A_s f_{yh}}{d_s s} \qquad \text{for circular cross section} \qquad \text{2-120}$$

$$f_{cc} = f_c' + k_1 f_{le} \qquad \text{for rectangular cross section} \qquad \text{2-121}$$

$$f_{le} = k_2 f_l \qquad \text{2-122}$$

$$f_l = \frac{\sum A_s f_{yh} \sin \alpha}{sh} \qquad \text{for square columns} \qquad \text{2-123}$$

$$k_2 = 0.15 \sqrt{\left(\frac{h}{s}\right)\left(\frac{h}{c}\right)\left(\frac{1}{f_l}\right)} \leq 1 \qquad \text{2-124}$$

$$f_{le} = \frac{f_{lex} b + f_{ley} h}{b + h} \qquad \text{for rectangular columns} \qquad \text{2-125}$$

$$\varepsilon_{cc} = \varepsilon_{co}\left(1 + 5\frac{k_1 f_{le}}{f_c'}\right) \qquad \text{2-126}$$

For the stress strain curve

$$\varepsilon_{85} = 260 \frac{\sum A_s}{s(b+h)} \varepsilon_{cc} + \varepsilon_{085} \qquad \text{2-127}$$

where ε_{085} is the strain at 0.85 $f'c$ for the unconfined concrete

$$f_c = f_{cc} \left[2 \left(\frac{\varepsilon_c}{\varepsilon_{cc}} \right) - \left(\frac{\varepsilon_c}{\varepsilon_{cc}} \right)^2 \right]^{1 / \left(1 + 2 \frac{k_1 f_{le}}{f_c'} \right)}$$ 2-128

where c is spacing of longitudinal reinforcement and α is the angle between the transverse reinforcement and b.
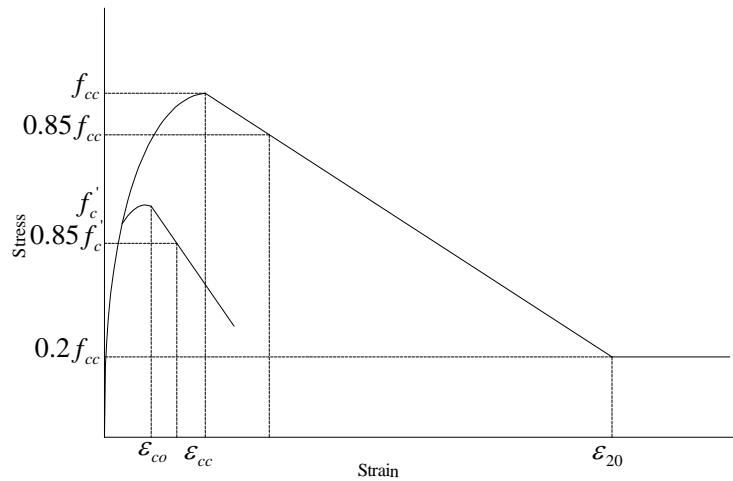
Figure 2-13: Proposed Stress-Strain curve by Saatcioglu and Razvi (1992-1999).

Sheikh and Toklucu (1993)

Sheikh and Toklucu (1993) studied the ductility and strength for confined concrete and they concluded that ductility is more sensitive, than the strength, to amount of transverse steel, and the increase in concrete strength due to confinement was observed to be between 2.1 and 4 times the lateral pressure.

Karabinis and Kiousis (1994)

32

Karabinis and Kiousis (1994) utilized the theory of plasticity in evaluating the development of lateral confinement in concrete columns. However, no stress-strain equations were proposed

Hsu and Hsu (1994)

Hsu and Hsu (1994) modified Carreira and Chu (1985) equation that was developed for unconfined concrete, to propose an empirical stress strain equations for high strength concrete. The concrete strength equation is:

$$f_c = f_{cc}\left(\frac{\xi \omega x}{\xi \omega - 1 + x^{\xi \omega}}\right) \quad \text{for} \quad 0 \le x \le x_d \qquad \text{2-129}$$

$$x = \frac{\varepsilon_c}{\varepsilon_{cc}} \qquad \text{2-130}$$

$$\omega = \frac{1}{1 - \dfrac{f_c'}{\varepsilon_{cc} E_{ic}}} \quad \text{for} \quad \omega \ge 1 \qquad \text{2-131}$$

where ω and ζ are material properties. ω depends on the shape of the stress strain curve and ζ depends on material strength and it is taken equal to 1.0 and x_d is the strain at 0.6 f'_c in the descending portion of the curve

Rasheed and Dinno (1994)

Rasheed and Dinno (1994) introduced a fourth degree polynomial to express the stress strain curve of concrete under compression.

$$f_c = a_o + a_1\varepsilon_c + a_2\varepsilon_c^2 + a_3\varepsilon_c^3 + a_4\varepsilon_c^4$$

2-132

They evaluated the constants a_o-a_4 using the boundary conditions of the stress strain curve. Similar to Kent and Park, they assumed no difference between the unconfined and confined peak strength.

$$f_{cc} = k_c f_c'$$
2-133

where

$$k_c = 1$$

They used expression taken from Kent and Park model to evaluate the slope of the descending branch starting at strain of 0.003. A flat straight line was proposed when the stress reaches $0.2\,f_{cc}$ up to $C_c\varepsilon_{cc.}$ where C_c is the ratio of maximum confined compressive strain to $\varepsilon_{cc.}$

The five boundary conditions used are:

$f_c = 0$ at $\varepsilon_c{=}0$

$d f_c /d \varepsilon_c = E_c$ at $\varepsilon_c{=}0$

$f_c = f'_c$ at $\varepsilon_c = \varepsilon_{co}$

$d f_c /d \varepsilon_c = 0$ at $\varepsilon_c = \varepsilon_{co}$

$d f_c /d \varepsilon_c = -Z f_c$ at $\varepsilon_c = 0.003$

El-Dash and Ahmad (1995)

El-Dash and Ahmad (1995) used Sargin *et al*. model to predict analytically the behavior of spirally confined normal and high strength concrete in one series of equations. They used the internal force equilibrium, properties of materials, and the geometry of the section to predict the

pressure. The parameters imposed in the analytical prediction where plain concrete strength, confining reinforcement diameter and yield strength, the volumetric ratio of lateral reinforcement to the core, the dimension of the column and spacing.

$$Y = \frac{AX + (B-1)X^2}{1 + (A-2)X + BX^2}$$

2-134

where

$$Y = \frac{f_c}{f_{cc}}$$

2-135

$$X = \frac{\varepsilon_c}{\varepsilon_{cc}}$$

2-136

$$f_{cc} = f_c' + k_1 f_l$$

2-137

$$\varepsilon_{cc} = \varepsilon_{co} + k_2 \frac{f_l}{f_c'}$$

2-138

The values of A, B, k_1, k_2 and f_l are defined by the following equations

$$A = \frac{E_c \varepsilon_{cc}}{f_{cc}} = \frac{E_c}{E_{sec}}$$

2-139

$$B = \frac{16.5}{\sqrt{f_c'}} \left(\frac{f_l}{\frac{s}{d_{st}'}} \right)^{0.33}$$

2-140

$$k_1 = 5.1 \left(\frac{f_c'}{f_{yh}} \right)^{0.5} \left(\frac{d_{st}'}{\rho_s} \right)^{0.25}$$

2-141

$$k_2 = \frac{66}{\left(\frac{s}{d_{st}'} \right) f_c'^{1.7}}$$

2-142

$$f_l = 0.5\rho_s f_{yh}(1 - \sqrt{\frac{s}{1.25d_s}})$$

2-143

where d_s is the core diameter.

<u>Cusson and Paultre (1995)</u>

Unlike all the previous work, Cusson and Paultre (1995) built their model based on the actual stress in the stirrups upon failure and they did not consider the yield strength, as the experimental work have shown that the yield strength for the transverse steel is reached in case of well confined columns. The ascending and the descending branches in the model curve are expressed by two different equations Figure (2-14). For the ascending portion:

$$f_c = f_{cc} \left(\frac{k\left(\frac{\varepsilon_c}{\varepsilon_{cc}}\right)}{k + 1 + \left(\frac{\varepsilon_c}{\varepsilon_{cc}}\right)^k} \right) \qquad \varepsilon_c \leq \varepsilon_{cc}$$

2-144

$$k = \frac{E_c}{E_c - \left(\frac{f_{cc}}{\varepsilon_{cc}}\right)}$$

2-145

For descending one:

$$f_c = f_{cc} \exp\left(k_1 \left(\varepsilon_{c50c} - \varepsilon_{cc}\right)^{k_2}\right) \qquad \varepsilon_c \geq \varepsilon_{cc}$$

2-146

$$k_1 = \frac{\ln 0.5}{\left(\varepsilon_{c50c} - \varepsilon_{cc}\right)^{k_2}}$$

2-147

$$k_2 = 0.58 + 16\left(\frac{f_l'}{f_c'}\right)^{1.4}$$

2-148

where ε_{c50c} is axial strain in confined concrete when stress drops to 0.5 fcc. It is observed that equation (2-144) proposed by Cusson and Paultre is identical to equation (2-95) suggested by Mander et al (1988).

Following the same methodology of Sheikh and Uzumeri (1982) and Mander et al. (1988) Cusson and Paultre considered the lateral confinement pressure f_l.

$$f_l = \frac{f_{hcc}}{s}\left(\frac{A_{sx} + A_{sy}}{b + h}\right)$$

2-149

where A_{sx} and A_{sy} are the lateral cross sectional area of the lateral steel perpendicular to x and y axes respectively and f_{hcc} is the stress in the transverse reinforcement at the maximum strength of confined concrete.

$$k_e = \frac{\left(1 - \frac{\sum w_i^2}{6bh}\right)\left(1 - \frac{s'}{2b}\right)\left(1 - \frac{s'}{2h}\right)}{1 - \rho_{cc}}$$

2-150

$$f_l' = k_e f_l$$

2-151

where $\sum w_i^2$ is the sum of the squares of all the clear spacing between adjacent longitudinal steel bars in a rectangular section. f_{cc} and ε_{cc} can be found by the following equations

$$f_{cc} = f_c'\left[1 + 2.1\left(\frac{f_l'}{f_c'}\right)^{0.7}\right]$$

2-152

$$\varepsilon_{cc} = \varepsilon_{co} + 0.21\left(\frac{f_l'}{f_c'}\right)^{1.7}$$

2-153

$$\varepsilon_{c50c} = 0.004 + 0.15\left(\frac{f_l'}{f_c'}\right)^{1.1}$$

2-154

37
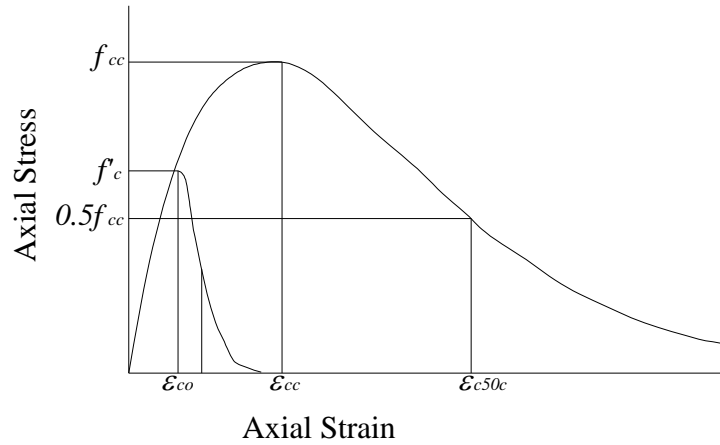
Figure 2-14: Proposed Stress-Strain curve by Cusson and Paultre (1995).

Attard and Setunge (1996)

Attard and Setunge (1996) experimentally determined full stress-strain curve for concrete with compressive strength of 60 –130 *MPa* and with confining pressure of 1-20 *MPa*, Figure (2-15). The main parameters used were peak stress; strain at peak stress, modulus of elasticity, and the stress and strain at point of inflection. Attard and Setunge followed the same equation used by Wang *et al* (1978). and Sargin (1971):

$$Y = \frac{AX + BX^2}{1 + CX + DX^2}$$

2-155

where

$$Y = \frac{f_c}{f_{cc}}$$

2-156

$$X = \frac{\varepsilon_c}{\varepsilon_{cc}}$$

2-157

For the ascending branch, the four constant are determined by setting four conditions:

38

1- at $f_c = 0$, $\dfrac{df_c}{d\varepsilon_c} = E_c$

2- at $f_c = f_{cc}$, $\dfrac{df_c}{d\varepsilon_c} = 0$

3- at $f_c = f_{cc}$, $\varepsilon_c = \varepsilon_{cc}$

4- at $f_c = 0.45 f'_c$, $\varepsilon_c = \dfrac{f_c}{E_{0.45}}$

The constants are given by:

$$A = \frac{E_c \varepsilon_{cc}}{f_{cc}} = \frac{E_c}{E_{sec}} \tag{2-158}$$

$$B = \frac{(A-1)^2}{\dfrac{E_c}{E_{0.45}}\left(1 - \dfrac{0.45 f'_c}{f_{cc}}\right)} + \frac{A^2 \left(1 - \dfrac{E_c}{E_{0.45}}\right)}{\left(\dfrac{E_c}{E_{0.45}}\right)^2 \dfrac{0.45 f'_c}{f_{cc}}\left(1 - \dfrac{0.45 f'_c}{f_{cc}}\right)} - 1 \tag{2-159}$$

$$C = A - 2 \tag{2-160}$$

$$D = B + 1 \tag{2-161}$$

while for the descending curve the four boundary conditions were

1- at $f_c = f_{cc}$, $\dfrac{df_c}{d\varepsilon_c} = 0$

2- at $f_c = f_{cc}$, $\varepsilon_c = \varepsilon_{cc}$

3- at $f_c = f_i$, $\varepsilon_c = \varepsilon_i$

4- at $f_c = f_{2i}$, $\varepsilon_c = \varepsilon_{2i}$

where f_i and ε_i refer to the coordinate of the inflection point.

The four constants for the descending curve are

$$A = \left[\frac{\varepsilon_{2i} - \varepsilon_i}{\varepsilon_{cc}} \right] \left[\frac{\varepsilon_{2i} E_i}{(f_{cc} - f_i)} - \frac{4\varepsilon_i E_{2i}}{(f_{cc} - f_{2i})} \right]$$

2-162

$$B = (\varepsilon_{2i} - \varepsilon_i) \left[\frac{E_i}{(f_{cc} - f_i)} - \frac{E_{2i}}{(f_{cc} - f_{2i})} \right]$$

2-163

$$C = A - 2$$

2-164

$$D = B + 1$$

2-165

The f_{cc} came out to be a function of the confining pressure, the compressive and tensile strength

of concrete f'_c, f_l, f_t, and a parameter k that reflects the effectiveness of confinement.

$$\frac{f_{cc}}{f'_c} = \left(\frac{f_l}{f_t} + 1 \right)^k$$

2-166

$$k = 1.25 \left[1 + 0.062 \frac{f_l}{f'_c} \right] (f'_c)^{-0.21} \qquad MPa$$

2-167

$$\frac{\varepsilon_{cc}}{\varepsilon_{co}} = 1 + (17 - 0.06 f'_c) \left(\frac{f_l}{f'_c} \right)$$

2-168

No lateral pressure equation was provided
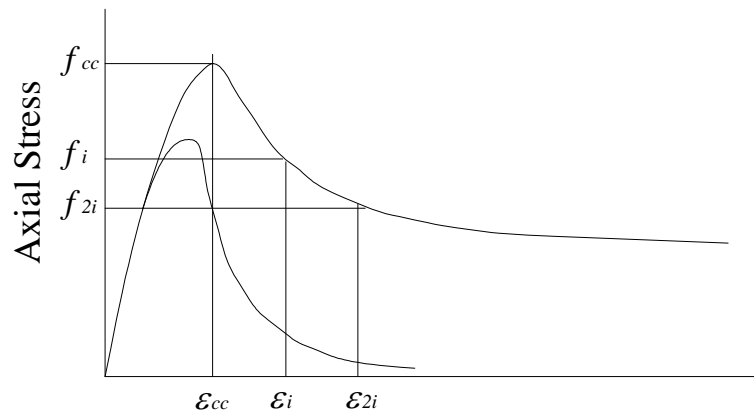
Figure 2-15: Proposed Stress-Strain curve by Attard and Setunge (1996).

<u>Mansur, Chin and Wee (1996)</u>

Mansur *et al.* (1996) introduced casting direction, if the member is cast in place(vertically) or pre-cast (horizontally), as a new term among the test parameters, for high strength concrete, which were tie diameter and spacing and concrete core area. They concluded that the vertically cast confined fiber concrete has higher strain at peak stress and higher ductility than the horizontally cast specimen. In addition, vertically cast confined non-fiber concrete has larger strain than that of horizontally cast concrete with no enhancement in ductility. Mansur *et al.* utilized the same equations found by Carreira and Chu for plain concrete with some modifications. For the ascending branch, they used the exact same equation

$$f_c = f_{cc} \left\{ \frac{\beta \left(\dfrac{\varepsilon}{\varepsilon_{cc}} \right)}{\beta - 1 + \left(\dfrac{\varepsilon}{\varepsilon_{cc}} \right)^{\beta}} \right\} \qquad \text{2-169}$$

where β is a material parameter depending on the stress strain shape diagram and can be found by :

$$\beta = \frac{1}{1 - \dfrac{f_{cc}}{\varepsilon_{cc} E_c}} \qquad \text{2-170}$$

k_1 and k_2 are two constants introduced in the equation describing the descending branch:

$$f_c = f_{cc} \left\{ \frac{k_1 \beta \left(\dfrac{\varepsilon_c}{\varepsilon_{cc}} \right)}{k_1 \beta - 1 + \left(\dfrac{\varepsilon_c}{\varepsilon_{cc}} \right)^{k_2 \beta}} \right\} \qquad \text{2-171}$$

for confined horizontally and vertically cast non-fiber concrete:

$$k_1 = 2.77\left(\frac{\rho_s f_{yh}}{f_c'}\right)$$

$$\text{2-172}$$

$$k_2 = 2.19\left(\frac{\rho_s f_{yh}}{f_c'}\right) + 0.17$$

$$\text{2-173}$$

for horizontally cast confined fiber concrete

$$k_1 = 3.33\left(\frac{\rho_s f_{yh}}{f_c'}\right) + 0.12$$

$$\text{2-174}$$

$$k_2 = 1.62\left(\frac{\rho_s f_{yh}}{f_c'}\right) + 0.35$$

$$\text{2-175}$$

and the values of f_{cc} and ε_{cc} can be obtained from the following equations:for confined non-fiber concrete:

$$\frac{f_{cc}}{f_c'} = 1 + 0.6\left(\frac{\rho_s f_{yh}}{f_c'}\right)^{1.23}$$

$$\text{2-176}$$

for confined fiber concrete:

$$\frac{f_{cc}}{f_c'} = 1 + 11.63\left(\frac{\rho_s f_{yh}}{f_c'}\right)^{1.23}$$

$$\text{2-177}$$

for vertically cast fiber concrete

$$\frac{\varepsilon_{cc}}{\varepsilon_{co}} = 1 + 62.2\left(\frac{\rho_s f_{yh}}{f_c'}\right)^2$$

$$\text{2-178}$$

for horizontally cast fiber concrete and vertically cast non-fiber concrete

$$\frac{\varepsilon_{cc}}{\varepsilon_{co}} = 1 + 2.6\left(\frac{\rho_s f_{yh}}{f_c'}\right)^{0.8}$$

$$\text{2-179}$$

and for horizontally cast non-fiber concrete

$$\frac{\varepsilon_{cc}}{\varepsilon_{co}} = 1 + 5.9 \left(\frac{\rho_s f_{yh}}{f_c'} \right)^{1.5}$$

2-180

Hoshikuma, Kawashima, Nagaya and Taylor (1997)

Hoshikuma *et al*. (1997) developed their models to satisfy bridge column section design in Japan. The model was based on series of compression loading tests of reinforced concrete column specimens that have circular, square and wall type cross sections. The variables that varied in the experimental wok were hoop volumetric ratio, spacing, configuration of the hook in the hoop reinforcement and tie arrangement.

Hoshikuma *et al*. (1997) asserted that the ascending branch represented in second degree parabola is not accurate to satisfy four boundary conditions:

1- Initial condition $f_c = 0$, $\varepsilon_c = 0$.

2- Initial stiffness condition $df_c/d\varepsilon_c = E_c$ at $\varepsilon_c = 0$.

3- Peak condition $f_c = f_{cc}$ at $\varepsilon_c = \varepsilon_{cc}$

4- Peak stiffness condition $df_c/d\varepsilon_c = 0$ at $\varepsilon_c = \varepsilon_{cc}$

The function that defines the ascending branch is:

$$f_c = E_c \varepsilon_c \left[1 - \frac{1}{\beta} \left(\frac{\varepsilon_c}{\varepsilon_{cc}} \right)^{\beta-1} \right]$$

2-181

$$\beta = \frac{E_c \varepsilon_{cc}}{E_c \varepsilon_{cc} - f_{cc}}$$

2-182

For the descending branch:

$$f_c = f_{cc} - E_{des} \left(\varepsilon_c - \varepsilon_{cc} \right)$$

2-183

where E_{des} is the deterioration rate that controls slope of the descending line and can be found using the following equation

$$E_{des} = \frac{11.2}{\dfrac{\rho_s f_{yh}}{f_c^{'2}}}$$

2-184

The peak stress and the corresponding strain for the circular section

$$\frac{f_{cc}}{f_c^{'}} = 1 + 3.83 \frac{\rho_s f_{yh}}{f_c^{'}}$$

2-185

$$\varepsilon_{cc} = 0.00218 + 0.0332 \frac{\rho_s f_{yh}}{f_c^{'}}$$

2-186

while for the square section

$$\frac{f_{cc}}{f_c^{'}} = 1 + 0.73 \frac{\rho_s f_{yh}}{f_c^{'}}$$

2-187

$$\varepsilon_{cc} = 0.00245 + 0.0122 \frac{\rho_s f_{yh}}{f_c^{'}}$$

2-188

Razvi and Saatcioglu (1999)

Razvi and Saatcioglu modified their model of Saatcioglu and Razvi (1992) to fit the high strength concrete (30 – 130 MPa). The ascending zone is defined by Popovics equation as follow:

$$f_c = \frac{f_{cc} \dfrac{\varepsilon_c}{\varepsilon_{cc}} r}{r - 1 + \left(\dfrac{\varepsilon_c}{\varepsilon_{cc}} \right)^r}$$

2-189

and for the descending branch:

$$\varepsilon_{cc} = \varepsilon_{co}(1 + 5k_3 K) \qquad \text{2-190}$$

$$\varepsilon_{85} = 260K_3 \frac{\sum A_s}{S(B+h)} \varepsilon_{cc}[1 + 0.5k_2(k_4 - 1)] + \varepsilon_{085} \qquad \text{2-191}$$

$$k_3 = \frac{40}{f_c'} \leq 1.0 \qquad k_4 = \frac{f_{yh}}{500} \geq 1.0 \qquad K = \frac{k_1 f_{le}}{f_c'} \qquad \text{2-192}$$

Razvi and Saatcioglu (1999) showed the good agreement of the model with some experimental work available in the literature.

Mendis, Pendyala and Setunge (2000)

Mendis *et al.* (2000) modified Scott *et al.* (1982) equations to fit high strength concrete. They empirically adjusted Scott *et al*. (1982) equations to the following ones:

$$f_c = kf_c' \left[\frac{2\varepsilon_c}{\varepsilon_{cc}} - \left(\frac{\varepsilon_c}{\varepsilon_{cc}}\right)^2 \right] \qquad \text{for} \qquad \varepsilon_c \leq \varepsilon_{cc} \qquad \text{2-193}$$

$$f_c = kf_c'[1 - Z_m(\varepsilon_c - \varepsilon_{cc})] \geq f_{res} \quad \text{for} \qquad \varepsilon_c > \varepsilon_{cc} \qquad \text{2-194}$$

$$f_{res} = RKf_c' \qquad \text{2-195}$$

$$K = 1 + 3\frac{f_l}{f_c'} \qquad \text{2-196}$$

$$Z_m = \frac{0.5}{\dfrac{3 + 0.29f_c'}{145f_c' - 1000} + \dfrac{3}{4}\rho_s\sqrt{\dfrac{b''}{s}} - \varepsilon_{cc}} \geq 0 \qquad f'_c \text{ in } MPa \qquad \text{2-197}$$

$$\varepsilon_{cc} = (0.24K^3 + 0.76)\varepsilon_{co} \qquad \text{2-198}$$

$$R = 0.28 - 0.0032f_c' \qquad R \geq 0 \qquad \text{2-199}$$

$$Z = 0.018f_c' + 0.55 \qquad \text{2-200}$$

f_l is calculated according to Mander equations.

<u>Assa, Nishiyama and Watanabe (2001)</u>

A new model was proposed for concrete confined by spiral reinforcement based on concrete-transverse steel interaction. The two main parameters were concrete strength and lateral stress-lateral strain relationship that represents the response characteristics of the transverse steel to the lateral expansion of concrete. Assa *et al.* (2001) modeled a confinement mechanism and limited the lateral expansion of the confined concrete with the maximum lateral expansion capacity. Assa *et al.* (2001) reached some relationships expressed in the following equations:

$$\frac{f_{cc}}{f_c'} = 1 + 3.36 \frac{f_l}{f_c'}$$
2-201

$$\frac{\varepsilon_{cc}}{\varepsilon_{co}} = 1 + 21.5 \frac{f_l}{f_c'}$$
2-202

$$\varepsilon_{lcu} = 0.0021 + 0.016 \frac{f_l}{f_c'}$$
2-203

where ε_{lcu} is the maximum lateral concrete strain. The proposed stress-strain curve has one equation:

$$f_c = f_{cc} \left(\frac{\gamma X + (\delta - 1) X^2}{1 + (\gamma - 2) X + \delta X^2} \right)$$
2-204

$$X = \frac{\varepsilon_c}{\varepsilon_{cc}}$$
2-205

where γ controls the stiffness of ascending branch and δ controls the slope of the descending branch:

$$\gamma = \frac{E_c \varepsilon_{cc}}{f_{cc}} = \frac{E_c}{E_{sec}}$$
2-206

$$\delta = \left| \frac{\left(\dfrac{\varepsilon_{80}}{\varepsilon_{cc}}\right)^2 - (0.2\gamma + 1.6)\dfrac{\varepsilon_{80}}{\varepsilon_{cc}} + 0.8}{0.2\left(\dfrac{\varepsilon_{80}}{\varepsilon_{cc}}\right)^2} \right|$$

2-207

where ε_{80} is the strain at $0.8f_{cc}$.

Lokuge, Sanjayan and Setunge (2005)

A simple stress-strain model was proposed based on shear failure. The model was based on the experimental results taken from Candappa (2000). Lokuge *et al.* (2005) proposed a relationship between axial and lateral strain:

$$\frac{\varepsilon_l}{\varepsilon_{lcc}} = v\left(\frac{\varepsilon}{\varepsilon_{cc}}\right) \qquad\qquad \varepsilon \le \varepsilon' \qquad\qquad\qquad 2\text{-}208$$

$$\frac{\varepsilon_l}{\varepsilon_{lcc}} = \left(\frac{\varepsilon}{\varepsilon_{cc}}\right)^a \qquad\qquad \varepsilon > \varepsilon' \qquad\qquad\qquad 2\text{-}209$$

where ε' is a strain at a point where axial strain and lateral strain curves deviate, v is the initial Poisson's ratio, and a is a material parameter which depends on the uniaxial concrete strength

$$v = 8 * 10^{-6}\left(f_c'\right)^2 + 0.0002 f_c' + 0.138 \qquad\qquad\qquad 2\text{-}210$$

$$a = 0.0177 f_c' + 1.2818 \qquad\qquad\qquad 2\text{-}211$$

where f'_c is in *MPa*.

Binici (2005) introduced a generalized formulas describing concrete under triaxial compression. The proposed stress strain curve is defined by elastic region then non linear curve. The axial compression is expressed using Leon-Paramono criterion as follow

$$f_c = f_c' \left(k\sqrt{c + m\phi} - (1-k)\phi^2 + \phi \right) \qquad \text{2-212}$$

$$\phi = \frac{f_l}{f_c'} \qquad\qquad m = \frac{f_c'^2 - f_t'^2}{f_c' f_t'} \qquad \text{2-213}$$

where f'_t is the uniaxial tensile strength, c is the softening parameter and is equal to one in hardening region and zero for residual strength and k is the hardening parameter and is equal to one at ultimate strength and softening region and is equal to 0.1 at the elastic limit. Binici (2005) defined three equations for determining the stress in the elastic, hardening and softening zones as follow:

For elastic zone:

$$f_c = E_c \varepsilon_c \qquad\qquad \varepsilon_c \leq \varepsilon_{1e} \qquad \text{2-214}$$

For the hardening zone:

$$f_c = f_{1e} + \left(f_{cc} - f_{1e} \right) \left(\frac{\varepsilon_c - \varepsilon_{1e}}{\varepsilon_{cc} - \varepsilon_{1e}} \right) \frac{r}{r - 1 + \left(\dfrac{\varepsilon_c - \varepsilon_{1e}}{\varepsilon_{cc} - \varepsilon_{1e}} \right)^r} \qquad \varepsilon_{1e} \leq \varepsilon_c \leq \varepsilon_{cc} \qquad \text{2-215}$$

$$r = \frac{E_c}{E_c - E_{\sec}} \qquad\qquad \varepsilon_{1e} = \frac{f_{1e}}{E_c} \qquad\qquad \varepsilon_{cc} = 5\varepsilon_{co} \left(\frac{f_{cc}}{f_c'} - 0.8 \right) \qquad \text{2-216}$$

For the softening zone:

$$\alpha = \frac{1}{\sqrt{\pi}\left(f_{cc} - f_{1r} \right)} \left(\frac{2G_{fc}}{l_c} - \frac{\left(f_{cc} - f_{1r} \right)^2}{E_c} \right) \qquad \text{2-217}$$

where l_c is the length of the specimen and G_{fc} is the compressive failure energy and is calculated as follow:

$$G_{fc} = l_c \left[\int_{\varepsilon_{cc}}^{\infty} (f_{cc} - f_{1r}) \exp\left[-\left(\frac{\varepsilon_c - \varepsilon_{cc}}{\alpha} \right)^2 \right] d\varepsilon_c + \frac{(f_{cc} - f_{1r})^2}{2E_c} \right] \qquad \text{2-218}$$

To fully define the stress strain curve for constant pressure, equation (2-212) is used to define the limit stresses. These stresses are imposed in equations (2-215, 2-217) to fully define the stress strain curve. The lateral pressure is calculated using the lateral strain ε_l found by:

$$\varepsilon_l = -\nu_s \varepsilon_c \qquad \text{2-219}$$

$$\nu_s = \nu_o \qquad \text{for} \qquad \varepsilon_c \leq \varepsilon_{1e} \qquad \text{2-220}$$

$$\nu_s = \nu_1 - (\nu_1 - \nu_o) \exp\left[-\left(\frac{\varepsilon_c - \varepsilon_{cc}}{\left(\frac{\varepsilon_{cc} - \varepsilon_{1e}}{\sqrt{-\ln \beta}} \right)} \right)^2 \right] \qquad \text{for} \qquad \varepsilon_{1e} \leq \varepsilon_c \qquad \beta = \frac{\nu_1 - \nu_p}{\nu_1 - \nu_o} \qquad \text{2-221}$$

where ν_s is the secant Poisson's ratio

$$\nu_1 = \nu_p + \frac{1}{(\phi + 0.85)^4} \qquad \varepsilon_1 \leq \varepsilon_{1e} \qquad \text{2-222}$$

whereas in case of changing lateral pressure, the lateral pressure is solved by equating the lateral strain in jacket to the lateral strain of concrete:

$$\varepsilon_1 \nu_s (f_l) - \frac{2f_l}{E_j \rho_j} = 0 \qquad \text{2-223}$$

where E_j and ρ_j is the modulus of elasticity and volumetric ratio of the jacket respectively.

2-1-2 Discussion

As stated by many research studies, like Mander *et al* (1988), Scott *et al* (1982), Sheikh and Uzumeri (1980) and Shuhaib and Mallare (1993), the spirals or circular hoops are more efficient than the rectangular hoops. The uniform pressure generated by the circular hoop is one of the reasons of circular spirals advantage.

According to Eid and Dancygier (2005), there are four main approaches for the modeling of confined concrete by lateral ties

1- The empirical approach: in which the stress-strain curve is generated based on the experimental results. Fafitis and Shah (1985) and Hoshikuma *et al*. (1997) followed that approach.

2- Physical engineering model based approach: the lateral pressure causing the confined behavior of the concrete core, is provided by the arch action between the lateral reinforcement ties. This approach was adopted by Sheikh and Uzumeri (1980), and was followed by Mander *et al*. (1988).

3- The third approach is based either on the first approach or the second one, but it does not assume the lateral ties yielding. Instead, It include computation of the steel stress at concrete peak stress, either by introducing compatibility conditions, solved by iterative process as Cusson and Paultre (1995) did, or by introducing empirical expressions as Saatcigolu and Razvi (1992) followed.

4- A plasticity model for confined concrete core introduced by Karabinis and Kiousis (1994). The shape of the confined core is based on the arching action.

Based on the reviewed models, around 50% followed the empirical approach, whereas 10% used the physical engineering approach, and the rest combined between the empirical and physical engineering approach.

According to Lokuge *et al* (2005), the stress strain models can be classified as three categories:

1- Sargin (1971) based models: Martinez *et al.* (1984), Ahmad and Shah (1982), Eldash and Ahmad (1995) Assa *et al.* (2001).

2- Kent and Park (1971) based models: Sheikh and Uzumeri (1982), Saatcigolu and Razvi (1992).

3- Popovics (1973) based models: Mander *et al.* (1988), Cusson and Paultre (1995) and Hoshikuma *et al.* (1997).

 Most of the confined models were developed by testing small specimens that did not simulate the real cases for the actual column, and small portion used real columns to verify their works such as Mander *et al.* (1988).

Table 2-1: Lateral Steel Confinement Models Comparison

	Long. steel	spacing	Lateral steel size	Lateral steel config.	Effective area	Section geometry	Lateral pressure	Lateral steel stress
Richart							*	
Chan	*							
Blume			*			*	*	*
Roy	*	*						
Soliman		*			*			

Sargin		*	*				*	*
Kent		*	*				*	
Vallenas	*	*	*				*	
Muguruma		*	*			*		
Scott	*	*	*				*	
Sheikh	*	*	*	*		*	*	
Ahmed		*						*
Park		*	*				*	
Martinez		*	*				*	
Fafitis		*	*			*	*	
Young	*	*	*				*	
Mander	*	*	*	*	*	*	*	*
Fujii		*	*			*	*	*
Saatcioglu	*	*	*	*	*	*	*	*
El-Dash		*	*				*	*
Cusson	*	*	*	*	*		*	*
Attard		*					*	*
Mansur		*					*	*
Fujii		*				*	*	*
Razvi	*	*	*	*	*	*	*	*
Mendis	*	*	*	*	*		*	*
Assa							*	*

								*	*
Binici									

Table (2-1) shows that the most successful models considering the lateral pressure determination parameters are Mander *et al*. (1988) that lies in the third group according to Lokuge et al. (2005) comparison and Saatcioglu and Razvi (1992), second group (Razvi and Saatcioglu (1999) was developed for high strength concrete). For the sake of comparing three models, one from each group, with the experimental results, El-Dash and Ahmad Model (1995) is selected from the first group as the model that considered most of the contributing factors, Table (2-1), compared to Attard and Setunge (1996), Mansur *et al.* (1997), Martinez *et al.* (1984) and Sargin (1971) models. However El-Dash and Ahmad model was developed for spirally confined concrete, hence, it was eliminated from Rectangular column comparison. The model selected from group 2 is Mander *et al*. (1988) and that chosen from group 3 is Saatcioglu and Razvi (1992) as mentioned above.

Table 2-2: Experimental cases properties

	Length (in.)	Width (in.)	Cover (in.)	Fc (ksi)	Fy (ksi)	Bars #	Bars diameter (in.)	Lateral steel diameter (in.)	Spacing (in.)	Fyh (ksi.)
Case1	19.69	Circular	0.98	4.06	42.8	12	0.63	0.47	1.61	49.3
Case2	19.69	Circular	0.98	4.2	42.8	12	0.63	0.63	3.66	44.5
Case3	17.7	17.7	0.787	3.65	57.13	8	0.945	0.394	2.83	44.8

The three models are compared with two experimental results, case 1 and case 2 for circular cross section columns, Table (2-2). All the three models are successfully capturing the ascending branch. However, Mander model is the best in expressing the descending one, Figure (2-16) and (2-17).
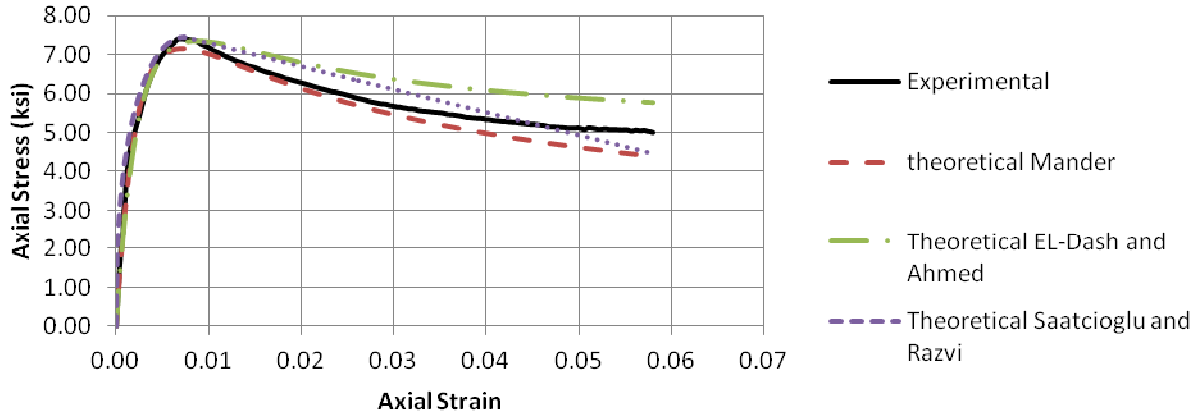
Figure 2-16: Mander et al (1988), Saatcioglu and Razvi (1992) and El-Dash and Ahmad (1995) models compared to Case 1.
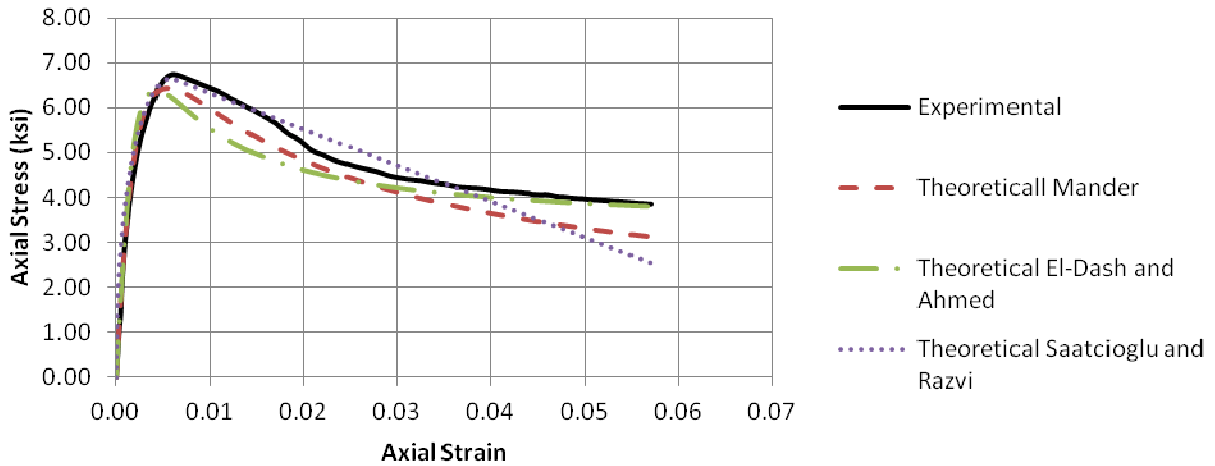
Figure 2-17: Mander et al (1988), Saatcioglu and Razvi (1992) and El-Dash and Ahmad (1995) models compared to Case 2.

For the case of rectangular column comparison, Figure (2-18), Saatcioglu and Razvi (1992) is better in capturing the ultimate compressive strength. Whereas Mander describes the softening zone better than Saatcioglu and Razvi model. Based on Table (2-1) and Figures (2-16), (2-17) and (2-18), Mander model is seen to be the best in expressing the stress strain response for circular and rectangular columns.
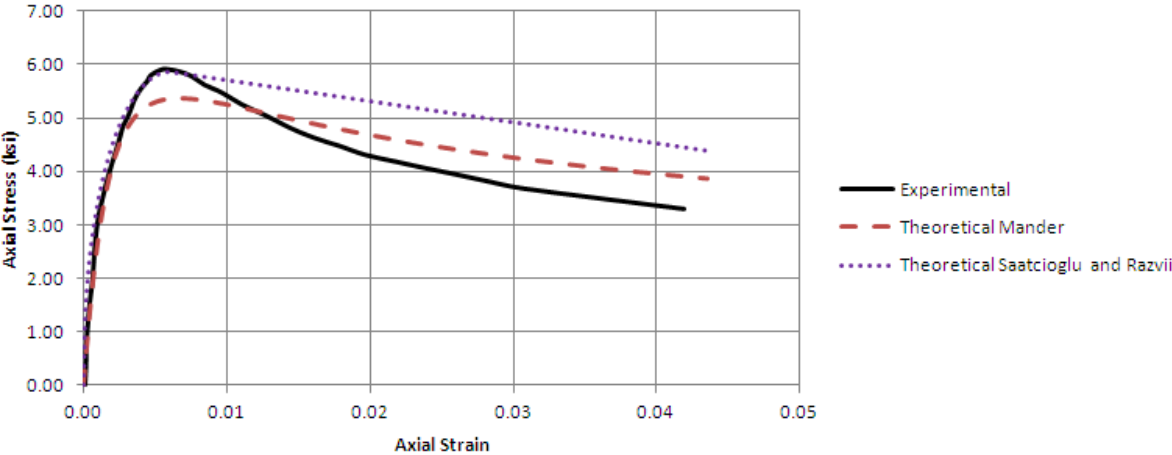
Figure 2-18: Mander et al (1988), Saatcioglu and Razvi (1992) and El-Dash and Ahmad (1995) models compared to Case 3.

2-2 Circular Columns Confined with FRP

FRP wrapping used in retrofitting concrete columns is considered one of the simplest and most efficient applications, as FRP has excellent material characteristics like high strength to weight ratio and high corrosion resistance FRP behaves elastically, and therefore its confining strength increases proportionally with increasing the force applied. The literature review in this section cares about FRP wrapping only and does not consider the effect of FRP tubes, as the mechanics is different. This section reviews the previous extensive work concerns FRP concrete columns confining chronologically. Hence, the review is classified according to its author/s.

2-2-1 Past Work Review

Fardis and Khalili (1981)

Fardis and Khalili (1981) focused on concentrically loaded short circular columns. They performed short term compression tests on 3 *6 in. and 4*8 in. cylinders and concluded that there is agreement between the strength and the axial stress suggested by Richart *et al. (*1928) and Newman and Newman equations:

$$f_c = f_c' + 4.1 f_l$$
2-224

$$f_c = f_c' + 3.7 f_l \left(\frac{f_l}{f_c'} \right)^{0.86}$$
2-225

Fardis and Khalili (1982)

Fardis and Khalili (1982) approximated the failure axial strain, using experimental results, in the following form:

$$\varepsilon_{cu} \approx 0.002 + 0.0005 \frac{E_f t}{D f_c'}$$

2-226

And the stress equation can be expressed using a simple hyperbola having initial slope of E_c:

$$f_c = \frac{E_c \varepsilon_c}{1 + \varepsilon_c \left(\dfrac{f_{cc}}{E_{cc}} - \dfrac{1}{\varepsilon_{cu}} \right)}$$

2-227

where E_{cc} is the tangent modulus at failure

Katsumata , Kobatake, Takeda (1988)

Katsumata *et al.* (1988) tested ten 7.87 * 7.87 in. rectangular specimens wound with carbon fiber. They concluded three outcomes; ultimate displacement and energy dissipation are linearly proportional to carbon fiber quantity, earthquake resistance capacities results from unbinding concrete with carbon fiber do not differ from these of wound concrete directly to carbon fiber and using equivalent quantities of carbon fiber or steel hoops, using effective strength ratio, the earthquake resistance capacity can be correlated.

Ahmed, Khaloo and Irshaid (1991)

Ahmed *et al.* (1991) tested 33 concrete cylinders confined with fiberglass wire. They concluded that the increase in confined strength decreases with increasing the unconfined concrete strength. And by decreasing the fiber wires spacing, the values of maximum strain at failure and strain at maximum stress increase. Flat or near flat post peak curves can be generated in stress-strain curves by increasing amount of confinement. Ahmed *et al.* (1991) suggested using the same equations developed for steel spirally reinforced concrete by Ahmed *et al.* (1982) by replacing f'_c and ε_{co} by f_{cc} and ε_{cc} in the stress equation:

$$f_c = f_c' \frac{A\left(\dfrac{\varepsilon_c}{\varepsilon_{co}}\right) + (B-1)\left(\dfrac{\varepsilon_c}{\varepsilon_{co}}\right)^2}{1 + (A-2)\left(\dfrac{\varepsilon_c}{\varepsilon_{co}}\right) + B\left(\dfrac{\varepsilon_c}{\varepsilon_{co}}\right)^2}$$

2-228

where

$$\frac{f_{cc}}{f_c'} = 1 + \frac{k}{4^{ns}} \qquad\qquad \frac{\varepsilon_{cc}}{\varepsilon_{co}} = 1 + \frac{k}{4^{ns}}$$

2-229

k and *n* are constants that vary based on unconfined concrete strength. Ahmed *et al.* (1991) showed the superior behavior of confining concrete with fiberglass wire that has zero spacing over the concrete confined with steel tubes. The specimen used for comparison has diameter of 76.2 mm for steel tubes confining compared to 101.6 mm for fiberglass wiring confinement.

Demers and Neale (1994)

Demers and Neale (1994) conducted experimental work on 20 circular and square columns, fourteen of which were confined with 1-3 plies of FRP, glass and carbon. The circular columns were 152 mm in diameter and 305 mm high. Whereas, the square ones were 152 mm wide and 505 mm high. The results were compared against well known proposed models that were developed for steel hoops and spirals confinement. Demers and Neale (1994) reported that all the models overestimate the ultimate strength except for Cusson *et al.* (1992). They suggested stress function as follow:

$$f_c = f_c' + \left(\varepsilon_c - \varepsilon_{co}\right) g\left(E_f t_f, 1/f_c'\right)$$

2-230

They suggested conducting more accurate analysis and further tests to generate the function $g(E_f t_f, 1/f'_c)$. They also reported that 70 % increase in strength and up to seven times strain at

58

failure can be found for wrapped columns compared to the unconfined ones. It was observed that strength improvement in squared columns is very small compared to the rounded ones.

Taniguchi, Mutsuyoshi, Kita and Machida (1993)

Taniguchi *et al*. adapted Sakai (1991) equation for concrete confined with lateral steel to fit the FRP behavior as follow:

$$f_l = \frac{0.015(\varepsilon_a - \varepsilon_a s)}{0.024^{(E_r * 6 * 10^{-5})}} * E_r \tag{2-231}$$

$$f_{cc} = \left(1 + 4\frac{f_l}{f_c^{'}}\right)^{0.5} * f_c^{'} \tag{2-232}$$

$$\varepsilon_{cc} = \left(1 + 65\frac{f_l}{f_c^{'}}\right)^{0.5} * \varepsilon_{co} \tag{2-233}$$

$$f_{cu} = \left(1 + 6\frac{f_l}{f_c^{'}}\right)^{0.5} * \varepsilon_u \tag{2-234}$$

$$\varepsilon_{cu} = 0.024^{(E_r * 6 * 10^{-5})} \tag{2-235}$$

$$E_r = \left(1 - \frac{s}{D}\right) * 2A_s E_s /(s/D) \tag{2-236}$$

where E_r is the lateral confining rigidity and ε_z is the axial strain. The past equations were developed based on experimental work done on cylinders and prisms that were confined with lateral steel and FRP. However no FRP parameters showed in the proposed equations.

Hoppel *et al*. (1994) related the hydrostatic pressure of concrete wrapped with composite to the axial stress:

$$P = \sigma(P = 0)\upsilon \frac{t_f E_f}{D E_c}$$

2-237

where *P* is the hydrostatic pressure, *σ(P=0)* is the concrete compressive failure strength at atmospheric pressure,

Saadatmantesh, Ehsani and Li (1994)

Saadatmanesh *et al.* (1994) utilized Mander *et al.* model (1988) that was originally generated for concrete confined with steel hoops or spirals, in developing a computer program that calculates the ultimate moment and curvature at failure for columns. Interaction diagrams for different cases were plotted and compared to the unconfined case from Chai *et al*. (1991). However, no evidence of the proposed procedure accuracy was conducted.

Nanni and Bradford (1995)

Nanni and Bradford (1995) tested 150 * 300 cm fifty one cylinder specimen of unconfined concrete and confined with FRP. Aramid FRP tape, glass filament winding and glass aramid pre formed shells are the three types used in confining. Nanni and Bradford (1994) reported that unconfined specimens and specimens confined with Aramid FRP tape with spacing of 50 mm had shear cone failure mode. Whereas the one with less than 50 mm spacing and glass filament wound specimens failed by shell rupture. And finally specimen confined with glass aramid pre-formed shells had joint failure. They showed that the models; Mander model (1988)

and Fardis and Khalili (1982) are correlated and accurate in predicting the ultimate strength. However, they underestimated the ultimate strain and did not represent the stress strain curves shape. They also suggested bilinear stress strain curve with a bend over point at unconfined strength and 0.003 for strain.

Howie and Karbhari (1995)

Howie and Karbhari (1995) concluded through testing study that setting plies in the hoop direction gives the largest increase in strength.

Harmon, Slattery and Ramakrishnan (1995)

Harmon *et al* (1995) developed a new model for stress-strain prediction based on linear elastic deformation and shear slip. Although the void collapse was mentioned as one of the parameter that influences the stress strain behavior, it was disregarded due to its possible small effect by having a well compacted concrete mix. Harmon *et al.* (1995) defined the confinement efficiency ratio as follow:

$$R = 4.5 + \frac{f_c' b e^z}{\sqrt{f_r + f_t}}$$
2-238

$$b = 0.6 + 0.5(k_s / 1000)^{0.25}$$
2-239

$$z = -0.2(\sigma_r + f_t)/b^2$$
2-240

where k_s is the secant stiffness f_t is the split cylinder strength and f_r is the radial stress. It was observed that stress strain curves plotted using the proposed model were having bilinear pattern.

<u>Mirmiran and Shahawy (1995)</u>

Mirmiran and Shahawy (1995) introduced a model developed specifically for concrete wrapped with FRP that considers concrete lateral expansion and the fiber composite non ductile behavior. They utilized Madas and Elnashai (1992) equation that relates the axial and radial strain to predict the radial strain. Consequently the calculated radial strain is used to find the lateral pressure as follow:

$$f_l = 2\frac{t_f}{D}E_f\varepsilon_r$$

2-241

where ε_r is the radial strain. Finally the lateral pressure f_l was used to find the equivelant stress using Mander model (1988).

<u>Hosotani , Kawashima and Hoshikuma (1997)</u>

Hosotani *et al* (1997) conducted experimental work on 10 cylinder specimens and 12 square specimen that are 600 mm high and 200 mm wide. The stress strain model proposed by idealizing the experimental stress strain curves as follow:

$$f_c = E_c\varepsilon_c - \frac{E_c\varepsilon_c}{n}\left(1-\frac{E_g}{E_c}\right)\left(\frac{\varepsilon_c}{\varepsilon_t'}\right)^{n-1} \qquad 0 \leq \varepsilon_c \leq \varepsilon_t' \qquad \text{2-242}$$

$$f_c = f_t + E_g\left(\varepsilon_c - \varepsilon_t\right) \qquad \varepsilon_t' \leq \varepsilon_c \leq \varepsilon_{ccu} \qquad \text{2-243}$$

$$n = \frac{\left(E_c - E_g\right)\varepsilon_t}{E_c\varepsilon_t - f_t} \qquad \text{2-244}$$

$$\varepsilon_t' = \frac{2f_c'}{E_c - E_2} \qquad \text{2-245}$$

$$\frac{f_t}{f_c^{'}} = 1 + 1.93 \frac{\rho_f \varepsilon_f E_f}{f_c^{'}} \qquad \text{for cylinder specimens} \qquad \text{2-246}$$

$$\frac{f_t}{f_c^{'}} = 1 + 1.53 \frac{\rho_f \varepsilon_f E_f}{f_c^{'}} \qquad \text{for square specimens} \qquad \text{2-247}$$

$$\rho_f = \frac{4nt}{D} \qquad \text{2-248}$$

$$\varepsilon_t = 0.00343 + 0.00939 \frac{\rho_f \varepsilon_f E_f}{f_c^{'}} \qquad \text{for cylinder specimens} \qquad \text{2-249}$$

$$\varepsilon_t = 0.00330 + 0.00995 \frac{\rho_f \varepsilon_f E_f}{f_c^{'}} \qquad \text{for square specimens} \qquad \text{2-250}$$

$$E_g = -7.427 \frac{f_c^{'2}}{\rho_f f_f} + 0.086 \sqrt{\rho_f} E_f \qquad \text{for cylinder specimens} \qquad \text{2-251}$$

$$E_g = -13.726 \frac{f_c^{'2}}{\rho_f f_f} + 0.023 \sqrt{\rho_f} E_f \qquad \text{for square specimens} \qquad \text{2-252}$$

where f_f is the FRP tensile strength.

$$\varepsilon_{cu} = 1.384 \sqrt{\rho_f \left(\frac{f_f}{E_{cf}} \right)} \qquad \text{for cylinder specimens} \qquad \text{2-253}$$

$$\varepsilon_{cu} = 1.212 \sqrt{\rho_f \left(\frac{f_f}{E_{cf}} \right)} \qquad \text{for square specimens} \qquad \text{2-254}$$

The proposed model compared well with the experimental work done by the same researchers. They noted that ρ_f becomes effective for values more than 1%.

Miyauchi, Nishibayashi and Inoue (1997)

Miyauchi *et al* (1997) tested cylindrical specimens (10 cm wide * 20 cm heigh and 15 cm * 30 cm heigh) wrapped with one, two and three carbon fiber sheets. They found that

compressive strength and corresponding strain improve with increasing the number of FRP sheets. The proposed ultimate compressive strength equation was adapted from Richart model as follow :

$$\frac{f_{cu}}{f_c'} = 1 + \frac{4.1 k_e f_l}{f_c'}$$

2-255

$$f_l = \frac{\rho_f f_{cf}}{2}$$

2-256

$$\rho_f = \frac{4nt}{D}$$

2-257

$$\frac{\varepsilon_{cu}}{\varepsilon_{co}} = 1.0 + 10.6 \left(\frac{f_l}{f_c'} \right)^{0.373} \qquad \text{for } 30.0 \; MPa$$

2-258

$$\frac{\varepsilon_{cu}}{\varepsilon_{co}} = 1.0 + 10.5 \left(\frac{f_l}{f_c'} \right)^{0.525} \qquad \text{for } 50.0 \; MPa$$

2-259

And the proposed stress equations are as follow:

$$f_c = f_c' \left(2 \left(\frac{\varepsilon_c}{\varepsilon_{co}} \right) - \left(\frac{\varepsilon_c}{\varepsilon_{co}} \right)^2 \right) \qquad 0 \le \varepsilon_c \le \varepsilon_t'$$

2-260

$$f_c = f_{cu} - \lambda \left(\varepsilon_{cu} - \varepsilon_c \right) \qquad \varepsilon_t' \le \varepsilon_c \le \varepsilon_{ccu}$$

2-261

$$\varepsilon_t = \varepsilon_{co} - \lambda \frac{\varepsilon_{cc}}{\varepsilon_c}$$

2-262

$$f_t' = f_c' \left(2 \left(\frac{\varepsilon_t'}{\varepsilon_{co}} \right) - \left(\frac{\varepsilon_t'}{\varepsilon_{co}} \right)^2 \right)$$

2-263

$$\lambda = \frac{\left[-2f_c^{'}(\varepsilon_{cu} - \varepsilon_c) + \left(4f_c^{'}\left(f_c^{'}\varepsilon_{cu}^2 - 2f_c^{'}\varepsilon_{cu}\varepsilon_{co} + 2f_c^{'}\varepsilon_{co}^2\right)\right)^{\frac{1}{2}} \right]}{\varepsilon_{co}^2}$$

2-264

The proposed model (Figure (2-19)) was well correlated to the experimental work done by Miyauchi *et al* (1997)
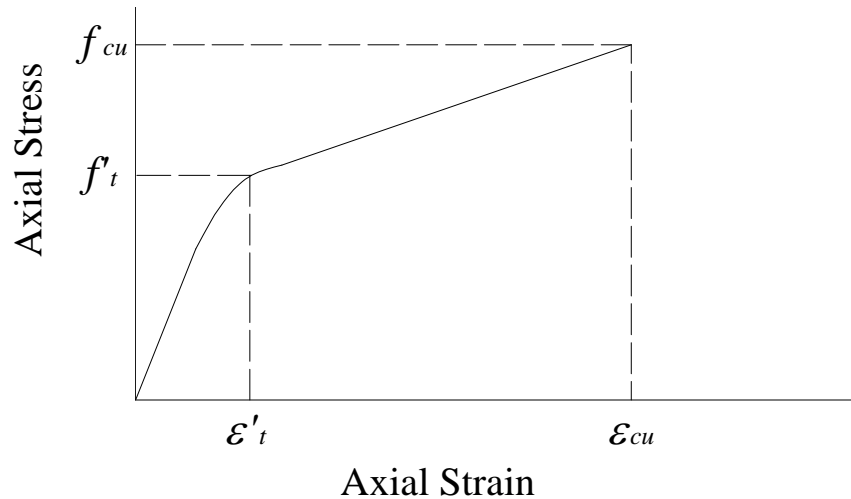
Figure 2-19: Axial Stress-Strain Curve proposed by Miyauchi *et al* (1997)

Kono , Inazumi and Kaku (1997)

Kono *et al* (1997) reported, through conducting compressive tests on 100 * 200 mm cylinder specimens wrapped with one, two or three CFRP sheets, that increasing confinement index increase compressive strength and corresponding strain linearly

Mirmiran and Shahawy (1997)

Mirmiran and Shahawy (1997) examined thirty 6*12 in. cylinder specimens, twenty four of which are concrete wrapped with FRP (6, 10 and 14plies). The rest are unconfined concrete. Failure observed was near or at the mid height of specimens due to fracture of FRP. The stress

strain response for the tested specimens is bilinear curve with no descending curve. Mirmiran and Shahawy (1997) compared different confined models in predicting the behavior of concrete wrapped with FRP. These models were Mander *et al* 1988, Ahmed and Shah 1982 and Karabinas and Kiousis 1994. They concluded that all of the compared models are overestimating the FRP behavior due to failure in imposing the dilatancy of concrete wrapped with FRP. They compared these models with Mirmiran model (1996) that was originally developed for FRP, and they showed that Mirmiran model is in best agreement with experimental work of Mirmiran and Shahawy (1997) of 14 plies.

<u>Watanabe, Nakamura, Honda, Toyoshima, Iso, Fujimaki , Kaneto and Shirai (1997)</u>

Watanabe *et al* (1997) tested cylindrical specimens (100 * 200 mm) confined with CFRP, high strength CFRP and AFRP. The number of layers varied from 1 to 4 layers. They utilized the Endochronic theory found by Bazant (1976) in a nonlinear 3D fininte element model to predict the stress-strain behavior as it was tested before for concrete confined with transverse steel by some of this study authors. They found good agreement between the model and the experimental work conducted. And they concluded that the compressive strength increase linearly with increasing the number of plies. They expressed a new term which is the C-index that is the product of lateral strain in FRP at compressive strength, young's modulus of FRP and volumetric ratio of FRP. They found that the linear relation between the ultimate strength and strain with the unconfined ultimate strength and strain can be response descriptive. They proposed the following equations:

$$f_{cc} = \alpha C + f_c'$$

<div align="right">2-265</div>

$$\varepsilon_{cc} = \beta C + \varepsilon_{co}$$

<div align="right">2-266</div>

where α and β are constants identified by the tests.

Monti and Spoelstra (1997)

Monti and Spolestra (1997) adapted the lateral pressure value in Mander model (1988) to fit the FRP elastic behavior up to failure through iterative process. The proposed process aims to iterate for the lateral pressure, based on the radial strain generated in the section, till conversion:

$$\varepsilon_{lat} = 0.5\beta \frac{E - E_{curr}}{E_{curr}}$$

<div align="right">2-267</div>

$$f_l = -0.5\rho_f E_f \varepsilon_{lat}$$

<div align="right">2-268</div>

where ε_{lat} is the lateral pressure and β is a constant depends on concrete type and it was adopted from Pantazopoulou and Mills (1995)

Then Mander model was used in the rest of the procedure of predicting stress strain behavior. The proposed model was compared successfully to experimental work done by Picher *et al* (1996)

Samaan ,Mirmiran and Shahawy (1998)

Samaan *et al*. (1998) introduced a new model, Figure (2-20), that depends mainly on the relation between the dilation rate and confining material hoop stiffness. The proposed model adapted Richard and Abbott equation (1975) as follow:

$$f_{cu} = \frac{(E_1 - E_2)\varepsilon_c}{\left[1 + \left(\dfrac{(E_1 - E_2)\varepsilon_c}{f_o}\right)^n\right]^{\frac{1}{n}}} + E_2\varepsilon_c$$

2-269

where *n* is a curve shape parameter. The ultimate strength is determined by:

$$f_{cc} = f_c^{'} + 6.0 f_l^{0.7} \quad MPa$$

2-270

$$E_2 = 245.61 f_c^{'0.2} + 1.3456 \frac{E_f t_f}{D} \quad MPa$$

2-271

$$f_o = 0.872 f_c^{'} + 0.371 f_l + 6.258 \quad MPa$$

2-272
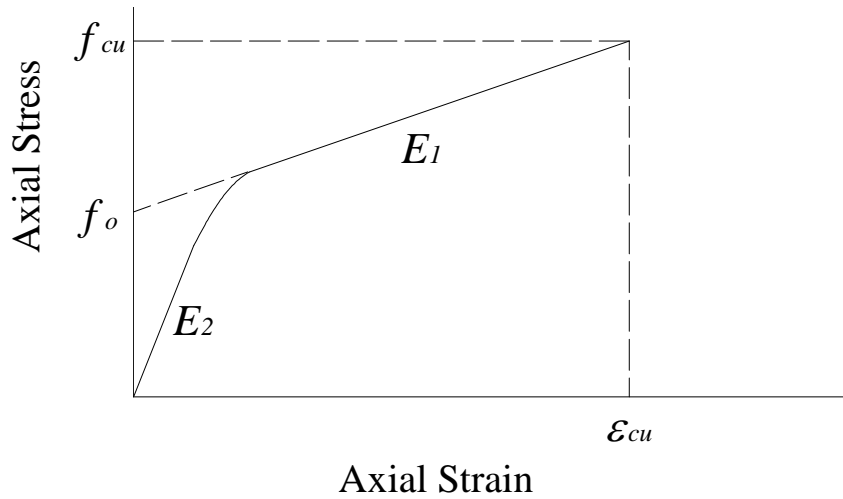
Figure 2-20: Axial Stress-Strain Curve proposed by Samaan *et al.* (1998)

And the ultimate strain:

$$\varepsilon_{cu} = \frac{f_{cu} - f_o}{E_2}$$

2-273

The proposed model was well compared with experimental work done by Picher (1995), Nanni and Bradford (1995) and Mastrapa (1997).

Mirmiran and Shahawy, Samaan ,ElEchary,Mastrapa and Pico (1998)

Mirmiran *et al*. (1998) studied the effect of shape, length and bond on FRP confined concrete on the confinement effectiveness of FRP tubes.

Harmon, Ramakrishnan and Wang (1998)

Harmon *et al* (1998) proposed two internal friction based confinement models; stress ratio model and crack path model. They assumed that total concrete strain forms from elastic strain, crack strain and void strain. The proposed models did not take into account the void strain as it is non-measurable parameter. The stress ratio equation is derived from Corona *et al*. (1995), The following equations are used iteratively with the elastic strain to generate the whole stress strain curve:

$$\varepsilon_{cu} = \frac{\sigma_a}{\sigma_r + f_l} = 4.5 + \frac{f_c' b e^z}{\sqrt{\sigma_r + f_l'}} b = 0.6 + 0.5\left(\frac{k_s}{1000}\right)^{0.25}$$

2-274

$$z = -0.2\left(\frac{\sigma_r + f_l}{b^2}\right) \qquad k_s = \frac{\sigma_r + f_l}{\varepsilon_r}$$

2-275

$$\frac{\tau}{\sigma + f_l} = \frac{\mu + \varepsilon_{,\gamma}}{1 - \mu \varepsilon_{,\gamma}}$$

2-276

where μ is the friction coefficient, $\varepsilon_{,\gamma}$ is the slope of the crack opening path, σ_a is the axial stress, σ_r is the radial stress. The crack path model is based on iterating for radial stress till converge. The internal confining stress is found from the separation strain that is calculated from crack slip strain.

Spoelstra and Monti (1999)

Spoelstra and Monti (1999) adopted the same iterative procedure from Monti and Spoelstra (1997). The procedure mainly relies on equating the lateral strain with FRP strain and uses the latter in calculating the lateral confinement. The lateral strain is calculated from a formula derived from the work done by Pantazopoulou and Mills (1995) as follow:

$$\varepsilon_l = \frac{E_c \varepsilon_c - f_c'}{2\beta f_c'}$$

2-277

$$f_l = \frac{1}{2}\rho_f E_f \varepsilon_{lat}$$

2-278

$$\phi = \frac{5700}{\sqrt{|f_c'|}} - 500 \qquad f_c'..in..MPa$$

2-279

Spoelstra and Monti (1999) showed good agreement with their procedure and the experimental work done by Picher *et al* (1996), Kawashima *et al* (1997) and Mirmiran and Shahawy (1997). They utilized Mander model stress strain curve with the secant modulus at ultimate strain to find a closed form expression for the ultimate strain. This ultimate strain is found by intersecting Mander curve with a straight line having a slope of the secant modulus at ultimate FRP strain $E_{sec,u}$:

$$E_{sec,u} = \frac{E_c}{1 + 2\beta \varepsilon_{fu}}$$

2-280

$$\varepsilon_{cu} = \varepsilon_{cc}\left(\frac{E_{sec}\left(E_c - E_{sec,u}\right)}{E_{sec,u}\left(E_c - E_{sec}\right)}\right)$$

2-281

$$f_{cu} = E_{sec,u}\varepsilon_{cu}$$

2-282

70

$$E_{\text{sec}} = \frac{f_{cc}}{\varepsilon_{cc}}$$

2-283

In addition, they proposed approximate values for the ultimate strength and strain based on regression analysis of 600 cases. The proposed equations are as follow:

$$f_{cu} = f_c' \left(0.2 + 3\sqrt{f_{lu}}\right)$$

2-284

$$\varepsilon_{cu} = \varepsilon_{co} \left(2 + 1.25 \overline{E_c} \varepsilon_{fu} \sqrt{f_{lu}}\right)$$

2-285

$$\overline{E_c} = \frac{E_c}{f_c'}$$

2-286

where f_{lu} is the lateral confinement pressure at ultimate strength

Matthys, Taerwe, and Audenaert (1999)

Mathys *et al.* (1999) conducted experimental work on cylindrical specimen (150 * 300 mm) wrapped with one layer of FRP, as well as testing full scale columns ; 8 has circular cross section (400 mm wide * 2m high) and 3 with square cross section having the same height and same cross sectional area as the circular ones. The FRP wrapping ranged from 2 to 6 layers. The experimental results are compared to Mander model (1988), CEB-FIP code model, Monti model (1997) and Samman *et al.* (1998). They concluded that the results from testing large and small scale specimens are similar. However, the circumferential strains were different. They also found that the failure load correlate well with the compared models. And the GFRP showed more ductility compared to CFRP that gave higher strength.

<u>Toutanji (1999)</u>

Toutanji (1999) tested 18 (3* 12 in) cylindrical specimen, 12 of them were wrapped with FRP and the rest were plain concrete. He reported that for the same stress level the axial strain is more than the lateral strain in the carbon fiber. Whereas, in glass fiber they are equal, he claimed that to the higher stiffness of carbon compared to glass. The proposed stress strain-model was divided into two regions, Figure (2-21). The second region when the FRP gets fully activated. Richart (1929) equation was evaluated for each experimental point in the second region to find the constant k through regression analysis. The stress and strain equations found for the second region are as follow:

$$f_c = f_c' \left(1 + 3.5 \left(\frac{f_l}{f_c'}\right)^{0.85}\right)$$

2-287

$$\varepsilon_c = \varepsilon_{co} \left(1 + (310.57\varepsilon_l + 1.9)\left(\frac{f_c}{f_c^i}\right) - 1\right)$$

2-288

The first region where the behavior is similar to unconfined concrete was evaluated based on Ahmed and Shah (1982) equation:

$$f_c = \frac{A\varepsilon_c}{1 + C\varepsilon_c + D\varepsilon_c}$$

2-289

$$A = E_{ii}$$

2-290

$$C = \frac{E_{ii}}{f_{ua}} - \frac{2}{\varepsilon_{ui}} + \frac{E_{ui}E_{ii}\varepsilon_{ui}}{f_{ua}^2}$$

2-291

$$D = \frac{1}{\varepsilon_{ui}^2} - \frac{E_{ui}E_{ii}}{f_{ua}^2}$$

2-292

$$E_{ia} = 10200\left(f_c'\right)^{\frac{1}{3}}$$

2-293

$$E_{ii} = 51000\left(f_c'\right)^{\frac{1}{3}}$$

2-294

$$\varepsilon_{ul} = 0.002$$

2-295

$$\varepsilon_{ua} = \varepsilon_{co}\left[1 + 0.0448\left(\frac{E_l}{f_c'}\right)^{0.85}\right]$$

2-296

$$f_{ua} = f_c'\left[1 + 0.0178\left(\frac{E_l}{f_c'}\right)^{0.85}\right]$$

2-297

$$E_{ul} = 7.557E_l\left(\frac{f_c'}{E_l}\right)^{0.15}$$

2-298

$$E_{ua} = 0.3075\frac{f_c'}{\varepsilon_{co}}$$

2-299

where E_{ia} is initial tangent of axial stress-strain curve, , E_{ua} is the tangent between the elastic region and plastic region of axial stress-strain curve, E_{ul} is the tangent between the elastic region and plastic region of axial stress-lateral strain curve, ε_{ul} is the strain between the elastic region and plastic region of axial stress-lateral strain curve, ε_{ua} is the strain between the elastic region and plastic region of axial stress-strain curve, and f_{ua} is the axial stress between the elastic region and plastic region , the model proposed was well compared with experimental work of Toutanji (1999), Harmon *et al* (1995), Picher et al (1996), Nanni *et al* (1994), Miyauchi *et al* (1997) and Mirmaran and Shahay (1997)
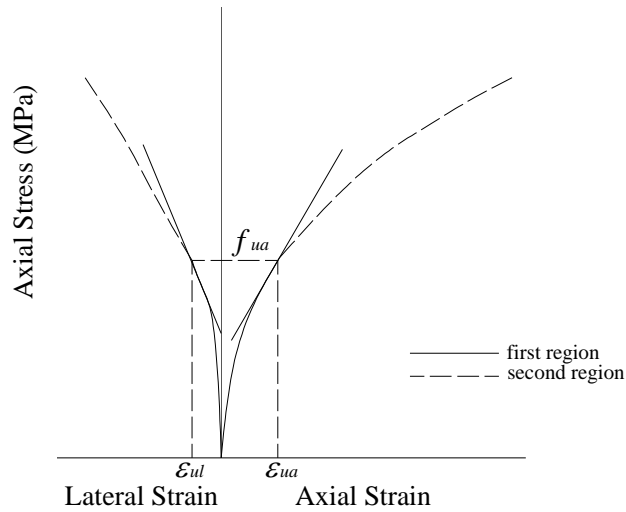
Figure 2-21: Axial Stress-(axial & lateral) Strain Curve proposed by Toutanji (1999)

<u>Xiao and Wu (2000)</u>

Xiao and Wu (2000) tested 36 cylindrical specimens 152 mm wide and 305 mm high. The concrete used was low, medium and high strength and the carbon fiber sheets ranged from 1 to 3 layers. They proposed empirical equations from experiments and from theory of elasticity equations using four parameters of confined concrete; axial stress and strain, transverse strain and confinement stress. The bilinear model describing the behavior of plain concrete confined with FRP sheets has two sets of equations; before reaching f'_c and after as follow:

Approaching f'_c:

$$f_c = E_c \varepsilon_c + 2\nu f_l \qquad\qquad 2\text{-}300$$

$$\varepsilon_l = -\frac{\nu}{1 + \dfrac{C_j}{E_c}\left(1 - \nu_c - 2\nu_c^{\,2}\right)} \varepsilon_z \qquad\qquad 2\text{-}301$$

$$f_l = -C_j \varepsilon_l \qquad\qquad 2\text{-}302$$

Whereas after reaching f'_c the equations are as follow:

$$f_c = \alpha f'_c + k f_l \qquad\qquad\qquad \text{2-303}$$

$$\varepsilon_l = \varepsilon'_{ro} - v'_c \varepsilon_z \qquad\qquad\qquad \text{2-304}$$

$$f_l = -C_j \varepsilon_r \qquad\qquad\qquad \text{2-305}$$

$$v'_c = 7 \left(\frac{f'_c}{C_j} \right)^{0.8} \qquad\qquad\qquad \text{2-306}$$

$$\varepsilon'_{ro} = 0.0005 \qquad\qquad\qquad \text{2-307}$$

$$C_j = 2 \frac{t_f}{D} E_f \qquad\qquad\qquad \text{2-308}$$

$$k = 4.1 - 0.75 \frac{f'^2_c}{C_j} \qquad\qquad\qquad \text{2-309}$$

where $\alpha = 1.1$ and v is Poisson's ratio The model proposed was well compared with Hosotani *et al*. (1996) experimental data.

Theriault and Kenneth (2000)

Theriault and Kenneth (2000) proposed empirically simple design equations for concentrically loaded short columns wrapped with FRP. They also proposed strengthening limits accounting for creep and fatigue.

Aire , Gettu and Casas (2001)

Aire *et al*. (2001) tested cylindrical specimens (150 * 300 mm) for normal and high strength concrete and they found out the following:

-The stress-strain curve behaves bilinear and the change in slope happens around the peak unconfined strength indicating that the FRP gets engaged after cracks development.

-The behavior of CFRP is better than GFRP slightly in normal concrete and is evident in high strength concrete.

-The ductility in normal concrete wrapped with CFRP is more than that of high strength concrete wrapped with CFRP as well

-Increasing the number of layers of FRP increase the slope of the stress strain curve

Pessiki, Harries, Kestner, Sause, Ricles (2001)

Pessiki *et al.* (2001) reported , by testing small and large scale circular and square specimens, that the jacket efficiency in square specimens are less than that of circular ones. They suggested using shape factor k_s in determining the lateral pressure induced by the FRP. This value was adopted from Restrepol and De Vino (1996):

$$k_s = \frac{1 - \left(\dfrac{(b-2r)^2 + (d-2r)^2}{3db} \right)}{1 - \rho_s}$$

2-310

Where b is the width of the section, d is the depth of the section, r is the radius of the corners and ρ_s is the longitudinal steel ration. Strain efficiency factor was proposed due to the premature failure of FRP as follow

$$k_e = \frac{\varepsilon_{ju}}{\varepsilon_{fr}}$$

2-311

Where ε_{ju} is the average strain in the jacket and ε_{fr} is the ultimate strain obtained from tests. Also the dilation rate can be limited by increasing the FRP strength and stiffness.

<u>Monti, Nistico and Santini (2001)</u>

Monti *et al*. (2001) proposed a procedure for determining upgrading index that relates available ductility for existing columns to target one using FRP strengthening. This procedure found an optimal thickness for FRP to enhance ductility of existing circular columns.

<u>Alsayed, Alsalloum, Almussalam and Ahmed (2001)</u>

Alsayed *et al*. (2001) showed that strength gaining from confinement decreases with size increase. They modified Satcioglou and Rasvi (1992) ultimate strength equation as follow:

$$f_{cu} = f_c' + \alpha \left[4 f_l^{'0.79} \right]$$

2-312

$f_l' = k_e f_l$ For circular columns, k_e is equal to 1 for fully wrapped columns and equals to

$$\frac{1 - \left[\dfrac{(b-2r)^2 + (h-2r)^2}{3bh} \right] - \rho_s}{1 - \rho_s} \quad \text{and} \quad \frac{1 - \left[\dfrac{(b-2r)^2 + (h-2r)^2}{3bh} \right] * \left(1 - 0.5_b^s\right)\left(1 - 0.5_h^s\right)}{1 - \rho_s} \quad \text{for continuous}$$

and separate straps respectively. α is a reduction factor and is taken equal 0.8 or 0.9. They showed that the proposed equation correlate well with the experimental work conducted by Picher *et al*. (1996), Kono *et al* (1998), Harries *et al* (1998) and Samaan *et al* (1998)

<u>Lam and Teng (2001)</u>

Lam and Teng (2001) showed from experimental work database that the strain varies with FRP types, as the GFRP and AFRP has higher ultimate strain than CFRP with the same confinement ratio. The ultimate axial strain is approximated as follow

$$\frac{\varepsilon_{cu}}{\varepsilon_{co}} = 2 + 15\frac{f_l}{f_c'}$$

2-313

But for the design use, they suggested the following equation:

$$\frac{\varepsilon_{cu}}{\varepsilon_{co}} = 1.75 + 10\frac{f_l}{f_c'}$$

2-314

It should be noted that the well know Lam and Teng model equations were first proposed in this paper. However for the sake of integrity it is mentioned in detail in Lam and Teng (2003).

Yuan, Lam, Teng and Smith (2001)

Yuan *et al*. (2001) compared the available stress strain models of FRP; Fardis and Khalilii (1982), Karbhari and Gao (1997), Samaan *et al*. (1998), Miyauchi *et al*. (1999), Saafi *et al*. (1999), Spoelstra and Monti (1999), Toutangi (1999), Xiao and Wu (2000), Lam and Teng 2001). These models showed big variation regarding the ultimate strength, ultimate strain and the ductility. Force moment interaction diagrams were plotted using the compared models. Yuan *et al*. (2001) reported that the ultimate column strength is depending mainly on concrete confining strength and is little influenced by ultimate strain.They also reported that Miyauchi *et al*. (1999), Saafi *et al*. (1999), Samaan *et al*. (1998) and Lam and Teng (2001) predicted the force moment interaction diagram similarly.

Karabinis and Rousakis (2002)

Using plasticity approach, Karabins and Rousakis (2002) modified Drucker-Prager model to capture the FRP response. The proposed model showed good agreement with the experimental work as it was compared to Samaan *et al*. (1998), Saafi *et al*. (1999), Spoelestra and Monti (1999) models. In addition they tested 22 cylinders wrapped with CFRP (200 * 320 mm).

Harries and Kharel (2002)

Harries and Kharel (2002) developed a model based on dilation relationship (relation between axial and lateral strain) and FRP stiffness. This model is utilized in an iterative model for determining the complete stress strain curve. They tested cylindrical specimens (6*12 in) confined with CFRP and E-GFRP (0-15 plies). They found out that the stress-strain response varies between descending post peak behavior for light confinement and bilinear ascending curve for heavy confinement. They reported also after certain value of strain (2 ε_{co}) the dilation ratio appeared to stop increasing. They adopted Madas and Elnashai (1992) model to develop the variably confined concrete model (VCCM) Figure (2-22). The model is defined in four quadrants as follow:

1- First quadrant: stress strain relation for concrete confined with constant pressure: they used the formula found by Popovics (1973) that was adapted later by Collins and Porasz (1992):

$$\frac{f_c}{f_{cc}} = \frac{\varepsilon_c}{\varepsilon_{cc}} \left(\frac{n}{n-1+\left(\frac{\varepsilon_c}{\varepsilon_{cc}}\right)^{nk}} \right) \qquad \text{2-315}$$

$$n = \frac{E_c}{E_c - \frac{f_{cc}}{\varepsilon_{cc}}} \qquad \text{2-316}$$

$$\varepsilon_{cc} = \frac{f_{cc}}{E_c}\left(\frac{n}{n-1}\right) \qquad \text{2-317}$$

79
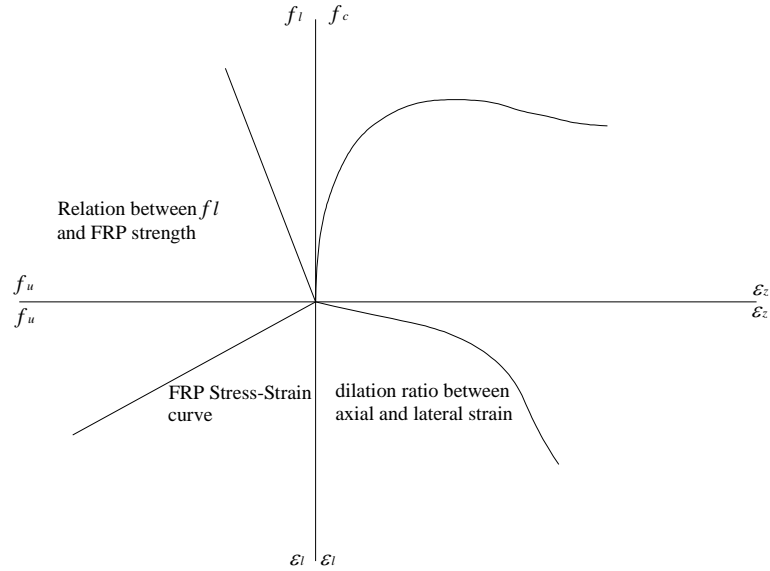
Figure 2-22: variably confined concrete model proposed by Harries and Kharel (2002)

where *k* is curve fitting factor for the descending branch. The ultimate compressive strength is taken from Mirmiran and Shahawy (1997) and the corresponding strain is adopted from Richart *et al* (1929):

$$f_{cc} = f_c^{'} + 4.269(f_l)^{0.587}$$

2-318

$$\varepsilon_{cc} = \varepsilon_c^{'}\left(5\frac{f_{cc}}{f_c^{'}} - 4\right)$$

2-319

2- Quadrant 2: finding the lateral strain from axial strain using the following equations:

$$\varepsilon_l = \eta\varepsilon_c$$

2-320

$$\eta = \eta_i \qquad \varepsilon_c \leq 0.6\varepsilon_c^{'}$$

2-321

$$\eta = \left(\frac{\eta_u - \eta_i}{1.4\varepsilon_c'} \right)\left(\varepsilon_c - 0.6\varepsilon_c' \right) + \eta_i \qquad 0.6\varepsilon_c' < \varepsilon_c < 2\varepsilon_c' \qquad \text{2-322}$$

$$\eta = \eta_u \qquad < \varepsilon_c > 2\varepsilon_c' \qquad \text{2-323}$$

$$\eta_u = -0.99\ln\left(nE_f\right) + 12 \qquad CFRP \qquad \text{2-324}$$

$$\eta_u = -0.66\ln\left(nE_f\right) + 8 \qquad E - glass \qquad \text{2-325}$$

3- Quadrent 3: determining the FRP stress from lateral strain

4- Quadrant 4: determining the lateral pressure from the FRP stress using the following equation

$$f_l = \frac{4nf_f}{D} \qquad \text{2-326}$$

The value of the lateral pressure is used in recalculating f_{cc} and ε_{cc} in equations (2-318 & 2-319) which are used in equation (2-315) to determine the stress corresponding to given strain. They showed the good agreement between the model and the experimental results.

Lam and Teng (2002)

Lam and Teng (2002) formed a database consists of 199 experimental testing cases for circular specimens wrapped with FRP with no longitudinal steel reinforcement. Based on the study conducted they concluded that the peak strength can be calculated using the following equation:

81

$$\frac{f_{cc}}{f_c'} = 1 + 2\frac{f_l}{f_c'}$$

2-327

They concluded that the confinement effectiveness of FRP depends significantly on FRP tensile strength.

Li, Lin and Sung (2002)

Li *et al*. (2002) proposed two models for concrete confined with CFRP and concrete confined with CFRP and Steel reinforcement together. The first model is found from the similarity between concrete confined with FRP and the mechanisms of the tri-axial test of the soil, according to Li *et al* (2002). The proposed equations are as follow:

For the ascending portion:

$$f_{cc} = f_c' + f_l' \tan^2\left(45^o + \phi/2\right)$$

2-328

$$f_l' = k_c \frac{2ntE_f \varepsilon_f}{D}$$

2-329

$$\phi = 36^o + 1^o\left(f_c'/35\right) \le 45^o$$

2-330

where k_c is the shape factor and ϕ is the angle of internal frication of concrete. The corresponding strain ε_{cc} is found using testing of 108 specimens:

$$\varepsilon_{cc} = \varepsilon_{co}\left[1 + \alpha \tan^2\left(45^o + \phi/2\right)\frac{f_l'}{f_c'}\right]$$

2-331

The parameter α is depending on the confinement material properties and is found equal to 2.24 using regression analysis, and the value of stress can be found using the following equation

$$f_c = f_{cc}\left[-\left(\frac{\varepsilon_c}{\varepsilon_{cc}}\right)^2 + 2\left(\frac{\varepsilon_c}{\varepsilon_{cc}}\right)\right]$$

2-332

While for the descending portion of the curve Li *et al* (2002) used Hoshikuma *et al.* (1997) straight line equation:

$$f_c = f_{cc} - E_{des}\left(\varepsilon_c - \varepsilon_{cc}\right)$$

2-333

The ultimate strain ε_{cu} is calculated from the following equation:

$$\varepsilon_{cu} = \varepsilon_{50} = \varepsilon_{cc} + \frac{f_{cc}}{2E_{des}}$$

2-334

The second proposed stress strain curve represents two types of confinement the CFRP and transverse steel. Li *et al* (2002) determined the peak strength as the summation of the unconfined strength and the strengths from steel and CFRP simultaneously. The lateral pressure from the steel action is adopted from Mander et al (1988) equation. For the ascending branch

$$f_{cc} = f_c' + \left(f_{lf}' + f_{ls}'\right)\tan^2\left(45^o + \frac{\phi}{2}\right)$$

2-335

$$\varepsilon_{cc} = \varepsilon_{co}\left[1 + 2.24\tan^2\left(45^o + \phi/2\right)\frac{f_{lf}'}{f_c'}\right]$$

2-336

$$f_c = f_{cc}\left[-\left(\frac{\varepsilon_c}{\varepsilon_{cc}}\right)^2 + 2\left(\frac{\varepsilon_c}{\varepsilon_{cc}}\right)\right]$$

2-337

For the descending portion the Hoshikuma *et al* (1997) was used. The first model was verified against 108 cylindrical specimens and the second model was verified by testing 18 cylindrical specimens (30 * 60 cm) confined with steel and CFRP.

<u>Chun and Park (2002)</u>

The proposed passive confinement model by Chun and Park (2002) is summarized in the following steps:

1- Selecting axial strain ε_c

2- Determining Poisson,s ratio v

$$v_u = -0.2305 \ln\left(\frac{f_{le}}{f_c'}\right) + 0.087$$

2-338

$$v = v_o\left[1 + 1.3763\frac{\varepsilon_c}{\varepsilon_{cc}} - 5.36\left(\frac{\varepsilon_c}{\varepsilon_{cc}}\right)^2 + 8.586\left(\frac{\varepsilon_c}{\varepsilon_{cc}}\right)^3\right]$$

2-339

$$f_{ld} = \frac{2f_{lf}t_f}{D}k_s + \frac{A_c}{A_g}f_{ls}$$

2-340

where k_s is the shape factor and A_c is the core area of concrete enclosed by hoops and v_u is the ultimate poison ratio and f_{ld} is the design confining pressure.

3- Calculating the transverse strain ε_t

$$\varepsilon_t = v\varepsilon_c$$

2-341

4- Calculating confining pressure f_l

$$f_l = \frac{2\varepsilon_{lf}E_ft_f}{D}k_s \qquad \text{for cover concrete}$$

2-342

$$f_l = \frac{2\varepsilon_{lf}E_ft_f}{D}k_s + f_{ls} \qquad \text{for core concrete}$$

2-343

5- Calculating ultimate strength and corresponding strain according to Mander Model (1988).

84

6- Calculating stress according to Mander Model (1988)

The test program was prepared for testing eccentric loading effects on the columns for 0.0 P_o , 0.25 P_o, 0.5 P_o, 0.75 P_o, and the specimen tested are 200 wide *1000 mm high, strengthened with hoops and 2 layers of FRP sheets. They concluded that using FRP sheets increases the columns strength and ductility, premature failure of FRP should be considered and the proposed model can predict reasonably the concrete wrapped with FRP behavior.

<u>Moran and Pantelides (2002) (a, b)</u>

Moran and Pantelides (2002) introduced the strain ductility ratio, which is a function of hoop stiffness and the internal damage of concrete core, in a plasticity model. The proposed plasticity model is defined by the following equations:

$$f_c = (E_s)_m \varepsilon_m \qquad \text{2-344}$$

$$(E_s)_m = \left[\frac{(E_m - E_{mp})}{\left(1 + \left|\frac{(E_m - E_{mp})\varepsilon_m}{f_{om}}\right|^{n_m}\right)^{\frac{1}{n_m}}} + E_{mp} \right] \qquad \text{2-345}$$

$$E_{cp} = \left(\frac{E_{\theta p}}{\mu_p}\right) \qquad E_{\theta p} = f_c' \omega_{je} \varphi_\theta = \frac{1}{1-\eta}\left[(\alpha_p)_i - \eta(\alpha_p)_{i-1}\right] \qquad \text{2-346}$$

$$E_\theta = \left(\frac{E_c}{\mu_o}\right) \qquad \text{2-347}$$

$$(k_o)_\theta = \frac{(f_o)_\theta}{f_c'} = 1 + \omega_{je}(\varepsilon_{\theta p})_i [(\alpha_p)_i - \varphi_\theta]$$

2-348

$$(k_o)_c = \frac{(f_o)_c}{f_c'} = (k_o)_\theta + \left(\frac{E_{\theta p}}{f_c'}\right)((\varepsilon_{\theta p})_i - \varepsilon_{co}[\mu_p + (\Delta\theta)]_i)$$

2-349

where E_{sm} is the secant modulus at ε_m (from Richard and Abbott 1975), E_{mp} is the average plastic modulus, E_m is the tangent modulus of elasticity, m_o initial Poisson's ratio for unconfined concrete, f_{om} is the reference intercept stress a, k_{om} is the normalized reference intercept stress, n_m is a curvature parameter, w_{je} is the bond dependent effective confinement index, m_p is the analytical plastic dilation rate, Δ p is the variable confinement coefficient, ε_{tp} is the plastic jacket strain, n is a factor range between 0.8 and 0.9. They compared the proposed model with Mirmiran (1997) and Xiao and Wu (2000) experimental work. The results showed good agreement

Cheng, Sotelino and Chen (2002)

Cheng *et al.* (2002) proposed the following equations:

$$f_c = \frac{(E_c - E_p)\varepsilon_c}{\left[1 + \left(\frac{(E_c - E_p)\varepsilon_c}{f_o}\right)^n\right]^{\frac{1}{n}}} + E_p\varepsilon_c$$

2-350

$$E_p = -113.3 + 42.4f_c' + 0.66\frac{E_f t_f}{D}$$

2-351

$$f_o = -1.31 + 1.15f_c' + 0.02\frac{E_f t_f}{D}$$

2-352

where n is the curve shaped parameter
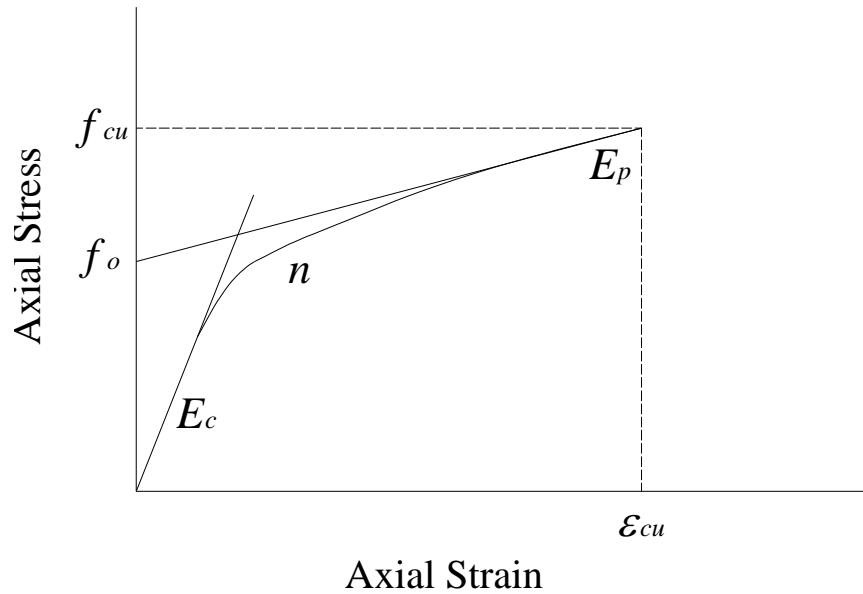
Figure 2-23: Axial Stress-Strain Model proposed by Cheng et al (2002)

Cheng showed the good agreement of the proposed model with the experimental work done by

Demers and Neale (1994), Mirmiran and Shahawy (1997) and Mastrapa (1997).

Campione and Miraglia (2003)

Campione and Miraglia (2003) suggested using Richart (1929) equation for determining

the maximum compressive strength with changing the k coefficient to be equal to 2 for concrete

wrapped with FRP

$$f_{cc} = f_c^{'} + 2f_l \qquad\qquad\qquad\qquad\qquad 2\text{-}353$$

$$f_l = \frac{2tf_u}{b_d} \qquad\qquad \text{for circular cross section} \qquad\qquad 2\text{-}354$$

$$f_l = \frac{2tf_r}{b_d} \qquad\qquad \text{square with round corners} \qquad\qquad 2\text{-}355$$

$$f_l = \frac{\sqrt{2}tf_u}{b_d}k_i \qquad\qquad \text{square cross section} \qquad\qquad 2\text{-}356$$

$$f_r = f_u \left[\left(1 - \frac{\sqrt{2}}{2} k_i \right) \frac{2r}{b_d} + k_i \frac{\sqrt{2}}{2} \right]$$

2-357

where k_i is shape reduction factor and is found experimentally to be equal to 0.2121. and f_u is the ultimate strength in FRP and b and d is the core dimension to FRP centerline.

The stress-strain equation, Figure 2-24, suggested by the authors is as follow:

$$\frac{f_c}{f_c'} = \beta \frac{\varepsilon_c}{\varepsilon_{co}} + \frac{(1-\beta)\left(\frac{\varepsilon_c}{\varepsilon_{co}}\right)}{\left[1 + \left(\frac{\varepsilon_c}{\varepsilon_{co}}\right)^R \right]^{\frac{1}{R}}}$$

2-358

$$\beta = \frac{E_h}{E_o} \qquad E_h = \frac{f_{cc} - f_c'}{\varepsilon_{cu} - \varepsilon_{co}}$$

2-359

where E_o is the initial concrete modulus of elasticity
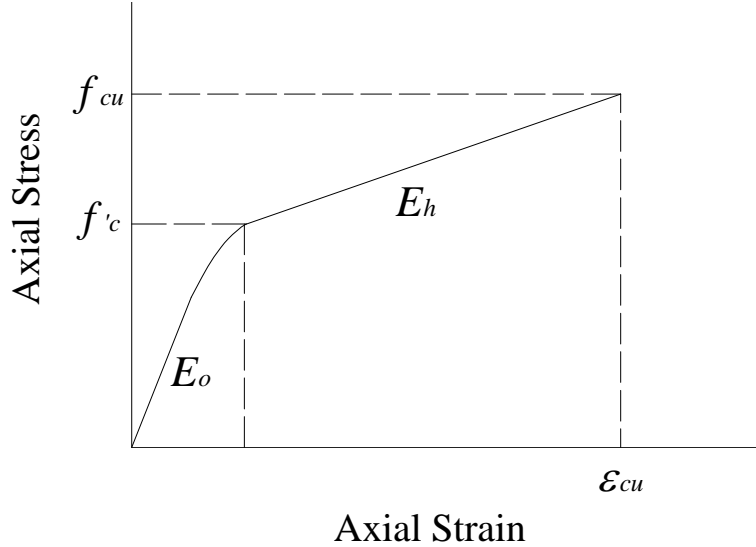
Figure 2-24: Axial Stress-Strain Model proposed by Campione and Miraglia (2003)

The ultimate strain value is calculated in a way similar to Mander ultimate strain equation using energy approach

$$\varepsilon_{cu} = \varepsilon_{co} + \Delta\varepsilon$$

2-360

They showed that the proposed model correlate well to the experimental work in the literature.

<u>Lam and Teng 2003</u>

Lam and Teng (2003) categorized the axial stress strain models into two sections; design oriented models that form closed form equations based on experimental work to predict the compressive strength and the ultimate strain, and analysis oriented models that use incremental numerical approach. This approach takes into account the equilibrium between concrete and the confining material and radial displacement compatibility considerations. They did not consider failure due to insufficient vertical lap joints. They pointed out the existence of differences between FRP ultimate strength or strain reached in material tests and those reached in specimens loading tests. This was due to two factors; premature failure of FRP Jackets due to non uniform stress distribution in cracked concrete and the curvature effect on FRP tensile strength. They determined three different cases of columns confined with FRP based on the amount of FRP; The bilinear stress strain up to failure, the ascending descending stress strain curve that has ultimate strength more than unconfined strength and the ascending descending one that has ultimate strength lower than unconfined strength. The latter is due to insufficient amount of confining material provided. Also, a certain amount of confining FRP can decrease the dilation of the concrete. They verified, as Spolestra and Monti (1999) did, that the ratio of the actual maximum confinement pressure to the unconfined strength has to be taken not less than 0.07. The proposed stress-strain model, Figure 2-25, is defined by two equations:

$$f_c = E_c \varepsilon_c - \frac{(E_c - E_2)^2}{4 f_c'} \varepsilon_c^2 \qquad 0 \le \varepsilon_c \le \varepsilon_t'$$

2-361

$$f_c = f_c' + E_2 \varepsilon_c \qquad \varepsilon_t' \le \varepsilon_c \le \varepsilon_{ccu}$$

2-362

$$E_2 = \frac{f_{cc}' - f_c'}{\varepsilon_{ccu}}$$

2-363

$$\varepsilon_t' = \frac{2 f_c'}{E_c - E_2}$$

2-364

Lam and Teng (2003) imposed the stiffness, as it varies from type to type unlike the steel, into the equation that determines the maximum axial strain:

$$\varepsilon_{cu} = \varepsilon_{co} \left(1.75 + 12 \frac{f_l}{f_c'} \left(\frac{\varepsilon_{h,rup}}{\varepsilon_{co}} \right)^{0.45} \right)$$

2-365

where $\varepsilon_{h,rup}$ is the strain at FRP rupture. And the maximum confined strength is give by:

$$f_{cu} = f_c' + 3.3 f_l$$

2-366

$$f_l = \frac{2 E_f t_f \varepsilon_{h,rup}}{D}$$

2-367
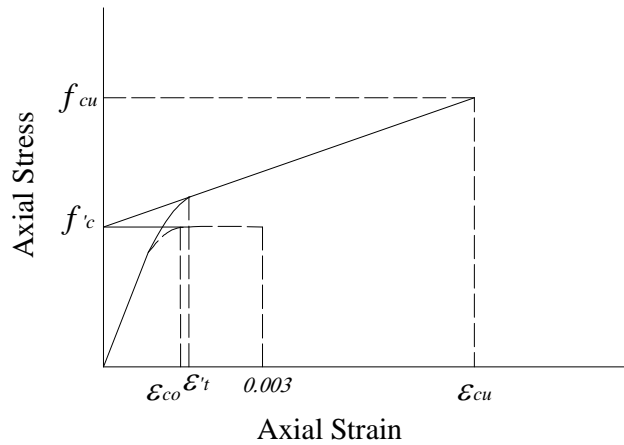
Figure 2-25: Axial Stress-Strain Model Proposed by Lam and Teng (2003)

90

The f_o that determine the linear second portion intercept with the stress axis is found by testing experimental results to range between 1.0 and 1.2 f'_c. For simplicity Lam and Teng (2003) considered $f_o = f'_c$. The efficiency factor that relates FRP premature failure strain to FRP rupture strain from coupon test is taken to be equal to 0.586

$$\varepsilon_{fe} = \kappa_\varepsilon \varepsilon_{fu}$$

2-368

<u>Ciupala, Pilakoutas and Taranu (2003)</u>

Ciupala *et al* (2003) tested cylindrical specimens wrapped with one layer of GFRP, CFRP or AFRP. The experimental stress strain curve plotted showed good agreement with Samaan *et al.* (1998) and Miyauchi et al (1999) as far as ultimate compressive strength concerns. Whereas the two models overestimated the ultimate strain. Lam and Teng model (2003) was conservative for ultimate strength while it predicted the ultimate strain closely. Finally, Spoelstra and Monti model (1999) overestimated both the ultimate strength and strain.

<u>De Lorinzis and Tepfers (2003)</u>

Lorinzis and Tepfers (2003) gathered 180 experimental data available in the literature and classified them, and by analyzing the data and the proposed models they concluded the following:

1- The FRP models derived from steel models is inaccurate in predicting the concrete confined with FRP behavior

2- Using the ultimate lateral pressure and the ultimate strain overestimate the ultimate strength and the corresponding strain found from experimental work.

91

3- None of the proposed model predict accurately the ultimate strain, accordingly they proposed an equation as follow:

$$\frac{\varepsilon_{cc}}{\varepsilon_c} = 1 + 26.2\left(\frac{f_l}{f_c'}\right)^{0.8} E_l^{-0.148}$$

2-369

where E_l is the lateral modulus.

Xiao and Wu (2003)

Xiao and Wu (2003) tested 243 concrete cylinders (152 mm * 300 mm) wrapped with CFRP and GFRP of nine types up to four layers. They found the relation between axial and lateral strain is as follow

$$\varepsilon_l = -0.00047 - 10\left(\frac{f_c' D}{2t_f E_f}\right)^{0.9} \varepsilon_c$$

2-370

They proposed a new stress strain curve relation as follow:

$$f_c = \frac{(E_1 - E_2)\varepsilon_c}{\left(1 + \left[((E_1 - E_2)\varepsilon_c)/\beta f_c'\right]^2\right)^{\frac{1}{2}}} + E_2\varepsilon_c$$

2-371

$$E_1 = E_c\left[1 + 2\nu_c\nu_o \frac{C_j}{E_c}\right]$$

2-372

$$f_{cu} = f_c' + kC_j\varepsilon_l$$

2-373

$$E_2 = 10kC_j\left(\frac{f_c' D}{2t_f E_f}\right)^{0.9}$$

2-374

$$\beta = 1 + 4.8*10^{-4} C_j^{0.85}$$

2-375

$$C_j = \frac{2t_f}{D} E_f$$

2-376

They showed that the proposed model correlate well with their experimental work.

Teng and Lam 2004

Teng and Lam (2004) studied stress-strain behavior, dilation properties and ultimate conditions. In addition to the two reasons mentioned in Lam and Teng (2003) for differences between FRP ultimate strength and strain reached in material tests and those reached in specimens loading tests, Teng and lam (2004) added the existence of overlapping zones that cause non uniform strain.

Berthet, Ferrier and Hamelin (2004)

Upon conducting experimental work on cylindrical specimens, Berthed *et al* (2004) verified the bilinear stress-strain behavior of concrete wrapped with FRP.

Theriault, Neale and Claude (2004)

Theriault *et al* (2004) studied the effect of specimens size on the experimental results. They concluded the adequacy of using cylindrical specimens size in assessing the short column behavior

Montoya, Vecchio and Sheikh (2004)

Montoya *et al.* (2004) proposed a constitutive model based on compression field modeling that considers nonlinear elasticity and plasticity. This model was incorporated in FE software to analyze columns confined with FRP or steel. The results well agreed with

experimental work done by Demers and Neale (1999), Toklucu (1992) and Sheikh and Uzumeri (1980)

Marques, Marques,Silva, and Cavalcante (2004)

Marquez *et al*. (2004) developed a numerical iterative incremental approach for predicting the stress-strain curve for rectangular and circular columns wrapped with FRP. The model iterates for area strain by changing the lateral strain then updates the axial strain according to the lateral one. The equations used in the model are as follow:

$$\varepsilon_a = \left(\frac{E_c \varepsilon_c}{\beta f_c} - \frac{1}{\beta} \right)^{\frac{1}{\psi}}$$
                                                                     2-377

$$\beta = \left(\frac{E_c \varepsilon_{co} - f_c^{'}}{f_c^{'}} \right) (\varepsilon_{co})^{-\psi}$$
                                                                     2-378

$$\psi = \frac{1}{2} \left(\frac{E_c \varepsilon_{co}}{E_c \varepsilon_{co} - f_c^{'}} \right) \frac{\varepsilon_{co} - 0.001}{\left((1 - v_c) \varepsilon_{co} - 0.001 v_c \right)}$$
                                                                     2-379

$$f_l = \frac{2t_f}{D} E_f \varepsilon_l \qquad\qquad \text{for circular cross section} \qquad\qquad 2\text{-}380$$

$$f_l = \frac{2t_f f_{lb} + 2t_f f_{lh}}{b + h} \qquad\qquad \text{for rectangular cross section} \qquad\qquad 2\text{-}381$$

where b and h are the section dimensions and f_{lb}, f_{lh} are the confining pressure acting on b and h sides respectively. The equation used to determine the axial stress from the given axial strain is Popovics (1973) equation. Marquez *et al* (2004) utilized Ravi and Saatcioglu (1999) model and Kono *et al* (1998) model to determine f_{cc} and ε_{cc} for circular and rectangular cross sections respectively as follow:

$$f_{cc} = f_c' + k_1 f_l \qquad \text{for circular cross section} \qquad \text{2-382}$$

$$\varepsilon_{cc} = \varepsilon_{co}\left(1 + 5k_1 k_3 \frac{f_l}{f_c'}\right) \qquad\qquad \text{2-383}$$

$$k_1 = 6.7_1 f_l^{-0.17} \qquad k_3 = \frac{40}{f_c'} \leq 1 \qquad\qquad \text{2-384}$$

$$f_{cc} = f_c' + 0.0572 f_l \qquad \text{for rectangular cross section} \qquad \text{2-385}$$

$$\varepsilon_{cc} = \varepsilon_{co} + 0.28 f_l \qquad\qquad \text{2-386}$$

They showed the good agreement between the model proposed and experimental work of Toutanji (1999), Saafi *et al* (1999), Rochette and Labossiere (2000) and Mirmiran (2000).

Bisby, Dent and Green (2005)

Based on analysis done on experimental results of 200 concrete wrapped cylinders available in literature, Bisby *et al.* (2005) ran comparison among the models available and they concluded that any of the available models has at least 13 % error for ultimate strength and 35 % for ultimate strain.

Berthet, Ferrier and Hamelin (2005)

Using experimental work done, Berthet *et al.* (2004) and some others experimental work, Berthet *et al.* (2005) developed a new stress-strain model for concrete wrapped with FRP. The ultimate strength and strain equation are as follow:

$$f_{cu} = f_c' + k_1 \frac{t}{r} E_f \varepsilon_{fu} \qquad\qquad \text{2-387}$$

95

$$\varepsilon_{cu} = \varepsilon_{ao} + \sqrt{2}\left(\frac{E_l}{f_c^{'2}}\right)^{\frac{2}{3}}\left(\varepsilon_{fu} - v_c \varepsilon_{ao}\right)$$

2-388

$$k_1 = 3.45 \qquad \text{for} \quad 20 \le f_c^{'} \le 50 MPa$$

2-389

$$k_1 = \frac{9.5}{\left(f_c^{'}\right)^{\frac{1}{4}}} \qquad \text{for} \quad 50 < f_c^{'} \le 200 MPa$$

2-390

where r is column radius. ε_{ao} is the maximum unconfined strain and v_c is the Poisson ratio for unconfined concrete. The stress strain curve is evaluated in two linear zones. The first one has the following equations:

$$f_c = \frac{A\varepsilon_c}{1 + B\varepsilon + C\varepsilon^2}$$

2-391

$$A = E_r$$

2-392

$$B = \frac{E_r}{f_{cp}} - \frac{2}{\varepsilon_{rp}} + \theta_r \frac{E_r \varepsilon_{rp}}{f_{cp}^{'2}} \qquad C = \frac{1}{\varepsilon_{rp}^2} - \theta_r \frac{E_r \varepsilon_{rp}}{f_{cp}^{'2}}$$

$$E_r = \frac{E_c}{v_c}\left[1 + \frac{E_l}{E_c}(1 - v_c)\right]$$

2-393

And the second zone is defined by:

$$f_c = f_{cp} + \theta_r\left[(v_c - \gamma)\varepsilon_{ao} - \varepsilon_{lp}\right] + \theta_r \gamma \varepsilon_c \qquad \varepsilon_c \ge \varepsilon_{ap} = \varepsilon_{a0} + \frac{\varepsilon_{lp} - \varepsilon_{lo}}{\gamma}$$

2-394

$$\gamma = \frac{1}{\sqrt{2}}\left(\frac{E_l}{f_c^{'2}}\right)^{\frac{-2}{3}}$$

2-395

$$f_{cp} = f_{cc} - \theta_r\left(\varepsilon_{fu} - \varepsilon_{lp}\right)$$

2-396

$$\theta_r = 2.73E_l - 163 \qquad\qquad E_l = \frac{t}{r}E_f$$

<div align="right">2-397</div>

where ε_{lp} is the transverse strain corresponding to the transition zone and is equal to 0.002 and ε_{ro} is the radial strain at ε_{ao}.

Monti and Alessandri (2005)

Monti and Alessandri (2005) proposed approximate secant approach to develop design equation for columns strengthened with FRP and exposed to axial load and bending moment. The approximate approach proposed was shown to be well compared with the exact approach.

Saenz and Pantelides (2005)

Saenz and Pantelides (2005) developed a new strain based FRP model that is based on Pantazopoulou and Mills formulas (1995). The model has three zones; linear elastic response zone, transitional zone and ultimate axial stress radial strain zone. The first zone has the same response as the elastic region for the unconfined concrete and it is limited by radial strain equal to -0.1 mm/m (Saenz 2004) (cracking strain). The proposed equations are as follow

$$\nu_c = -\frac{\varepsilon_{r,cr}}{\varepsilon_{c,cr}}$$

<div align="right">2-398</div>

$$\varepsilon_v = (1 - 2\nu_c)\varepsilon_c$$

<div align="right">2-399</div>

$$f_c = E_c\varepsilon_c$$

<div align="right">2-400</div>

$$E_c = 5700\sqrt{f_c'}$$

<div align="right">2-401</div>

The transitional zone is ranging from cracking strain to the strain were the volumetric strain becomes zero as a sign of reversing from contraction to expansion. The transitional zone equations are as follow:

$$\varepsilon_r = -v_c \varepsilon_c - \left(\frac{1-2v_c}{2}\right)\varepsilon_{c,vo}\left(\frac{\varepsilon_c - \varepsilon_{c,cr}}{\varepsilon_{c,vo} - \varepsilon_{c,cr}}\right)^c$$

2-402

$$E_{sec} = E_c \frac{1}{1+\dfrac{2\varepsilon_r}{\beta}}$$

2-403

$$f_c = E_{sec}\varepsilon_c$$

2-404

where c is the rate of unstable volumetric growth with axial strain increasing and it is equal to 2 for normal weight concrete and β is the secant modulus softening rate and is defined as follow

$$\beta = -(3.41\mu_p + 1.44)*10^{-3}$$

2-405

where μ_p is the ultimate radial to axial strain ratio and it is equal to $6.21\left(\dfrac{2t_f E_f}{Df_c'}\right)^{-0.63}$

The last region starts after expansion of volumetric strain up till ultimate radial strain. The equations are:

$$f_c = E_{r,t}\left(\varepsilon_{r,vo} - \varepsilon_\theta\right) + f_{c,vo}$$

2-406

$$E_{r,t} = \frac{f_{cu} - f_{c,vo}}{\varepsilon_{r,vo} - \varepsilon_{ru}}$$

2-407

where $\varepsilon_{c,vo} = 2.06$ mm/m (Saenz 2004). The proposed model was well compared to Saenez (2004) experimental work.

<u>Deniaud and Neale (2005)</u>

Deniaud and Neale (2005) developed elastoplastic model to assess the behavior of circular columns wrapped with FRP and compared that model to nonlinear elastic models , Ottosen (1979), Elwi and Murray (1979) , Ahmad and Shah (1982), Ahmad, Shah and Khaloo (1986). They showed the reasonability of their proposed model compared with the nonlinear elastic models against some experimental work.

<u>Binici (2005)</u>

Binici (2005) introduced a generalized formulas describing concrete under triaxial compression. The proposed stress-strain curve is defined by elastic region then non-linear curve. The axial compression is expressed using Leon-Paramono criterion as follow

$$f_c = f_c' \left(k \sqrt{c + m\phi} - (1-k)\phi^2 + \phi \right)$$

<div align="right">2-408</div>

$$\phi = \frac{f_l}{f_c'} \qquad\qquad m = \frac{f_c'^2 - f_t'^2}{f_c' f_t'}$$

<div align="right">2-409</div>

where f'_t is the uniaxial tensile strength, c is the softening parameter and is equal to one in hardening region and zero for residual strength and k is the hardening parameter and is equal to one at ultimate strength and softening region and is equal to 0.1 at the elastic limit. He defined three equation for determining the stress in the elastic , hardening and softening zones as follow:

For elastic zone:

$$f_c = E_c \varepsilon_c \qquad\qquad \varepsilon_c \le \varepsilon_{1e}$$

<div align="right">2-410</div>

For the hardening zone:

$$f_c = f_{1e} + (f_{cc} - f_{1e}) \left(\frac{\varepsilon_c - \varepsilon_{1e}}{\varepsilon_{cc} - \varepsilon_{1e}} \right) \frac{r}{r - 1 + \left(\frac{\varepsilon_c - \varepsilon_{1e}}{\varepsilon_{cc} - \varepsilon_{1e}} \right)^r} \qquad \varepsilon_{1e} \leq \varepsilon_c \leq \varepsilon_{cc} \qquad \text{2-411}$$

$$r = \frac{E_c}{E_c - E_s} \qquad\qquad \varepsilon_{1e} = \frac{f_{1e}}{E_c} \qquad\qquad \varepsilon_{cc} = 5\varepsilon_{co} \left(\frac{f_{cc}}{f_c'} - 0.8 \right) \qquad \text{2-412}$$

For the softening zone

$$f_c = f_{1r} + (f_{cc} - f_{1r}) \exp \left[-\left(\frac{\varepsilon_c - \varepsilon_{cc}}{\alpha} \right)^2 \right] \qquad\qquad \varepsilon_{cc} < \varepsilon_c \qquad\qquad \text{2-413}$$

$$\alpha = \frac{1}{\sqrt{\pi}(f_{cc} - f_{1r})} \left(\frac{2G_{fc}}{l_c} - \frac{(f_{cc} - f_{1r})^2}{E_c} \right) \qquad\qquad \text{2-414}$$

where l_c is the length of the specimen and G_{fc} is the compressive failure energy and is calculated as follow:

$$G_{fc} = l_c \left[\int_{\varepsilon_{cc}}^{\infty} (f_{cc} - f_{1r}) \exp \left[-\left(\frac{\varepsilon_c - \varepsilon_{cc}}{\alpha} \right)^2 \right] d\varepsilon_c + \frac{(f_{cc} - f_{1r})^2}{2E_c} \right] \qquad\qquad \text{2-415}$$

To fully define the stress strain curve for constant pressure, equation (2-408) is used to define the limit stresses. These stresses are imposed in equations (2-411 & 2-413) to fully define the stress strain curve. The lateral pressure is calculated using the lateral strain el found by:

$$\varepsilon_l = -v_s \varepsilon_c \qquad\qquad \text{2-416}$$

$$v_s = v_o \qquad\qquad \text{for} \qquad\qquad \varepsilon_c \leq \varepsilon_{1e} \qquad\qquad \text{2-417}$$

$$v_s = v_1 - (v_1 - v_o) \exp \left[-\left(\frac{\varepsilon_c - \varepsilon_{cc}}{\left(\frac{\varepsilon_{cc} - \varepsilon_{1e}}{\sqrt{-\ln \beta}} \right)} \right)^2 \right] \qquad \text{for} \qquad \varepsilon_{1e} \leq \varepsilon_c \qquad \beta = \frac{v_1 - v_p}{v_1 - v_o} \qquad \text{2-418}$$

100

$$v_1 = v_p + \frac{1}{(\phi + 0.85)^4} \qquad\qquad \varepsilon_1 \leq \varepsilon_{1e}$$

2-419

Whereas in case of changing lateral pressure, the lateral pressure is solved by equating the lateral

strain in jacket to the lateral strain of concrete:

$$\varepsilon_1 v_s (f_l) - \frac{2 f_l}{E_j \rho_j} = 0$$

2-420

where E_j and ρ_j is the modulus of elasticity and volumetric ratio of the jacket respectively. Bicini

(2005) verified his proposed model against experimental data for some researches including steel

hoops, steel tubes and FRP jackets.

Carey and Harries (2005)

Shawn *et al.* (2005) investigated the effect of testing large scaled columns compared to small

scaled ones and they concluded that the scale of the column does not have a significant effect on

the normalized stress strain curve behavior.

Li (2006)

After testing 24 cylindrical specimens with different amount of FRP wrapping, Li (2006)

reported that the insufficient amount of FRP determined by Spolestra and Monti (1999) cause the

concrete to behave similarly to the unconfined concrete. At the same time he supported the

bilinear behavior of concrete wrapped with sufficient amount of FRP.

Harajli (2006)

Harajli (2006) utilized Richart (1929), Scott *et al* (1982) and Toutanji (1999) equations to

generate two simple parabolas to express the stress-strain relationship for concrete confined with

FRP and transverse steel, Figure (2-26). The first ascending parabola is defined by the following equations:

$$f_c = f_{co}\left[\frac{2\varepsilon_c}{\varepsilon_{co}} - \left(\frac{\varepsilon_c}{\varepsilon_{co}}\right)^2\right] \qquad \varepsilon_c \le \varepsilon_{co} \qquad \text{2-421}$$

where f_{co} and ε_{co} are the stress and strain for the intersection point between the first and second parabolas. The equations define the second parabola are as follow:

$$f_c = \sqrt{\left(K_o^2 - K\right)} - K \qquad \text{2-422}$$

$$K_o = 0.0031k_1 E_{lf} - f_c' - \frac{1}{2}k_1 E_{ls}\varepsilon_{lo}\frac{A_{cc}}{A_g} \qquad \text{2-423}$$

$$K = f_c'^2 + k_1 f_c' E_{ls}\varepsilon_{lo}\frac{A_{cc}}{A_g} - 0.0032k_1 E_{lf} f_c'\left(\frac{\varepsilon_c}{\varepsilon_{co}} + 0.9\right) \qquad \text{2-424}$$

$$E_{lf} = k_{ef}\rho_f E_f / 2 \qquad\qquad E_{ls} = k_{es}k_e\rho_{st}E_s / 2 \qquad \text{2-425}$$

where ε_{lo} is the yield strain at hoops and is equal to 0.002. $k_1 = 4.1$ (as Richart (1929)), A_{cc} is the confined area, k_{ef} and k_{es} are the confinement coefficient in the horizontal plane, k_e is the confinement coefficient (same as Mander formula). The stress and strain at the intersection point of the two parabolas are defined by:

$$f_{co} = f_c' + k_1\varepsilon_{co}\left(\frac{k_{ef}\rho_f E_f}{2} + \frac{k_{es}k_e\rho_{st}E_s}{2}\left(\frac{A_{cc}}{A_g}\right)\right) \qquad \text{2-426}$$

$$\varepsilon_{co} = \varepsilon_{co}\left(1 + (310.57\varepsilon_{lo} + 1.9)\left(\frac{f_{co}}{f_c'} - 1\right)\right) \qquad \text{2-427}$$
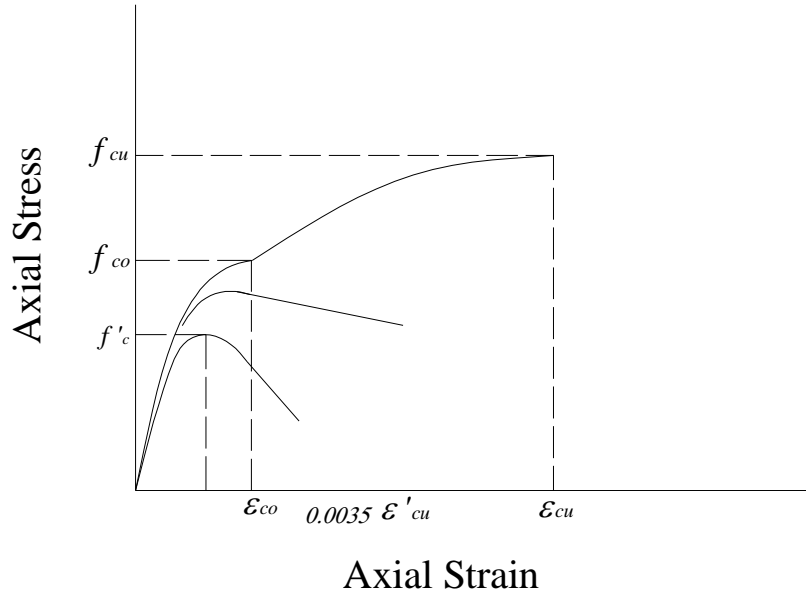
Figure 2-26: Axial Stress-Strain Model proposed by Harajli (2006)

Harajli (2006) showed the good agreement of his model with the experimental work conducted by Hantouche and Harajli (2005) for rectangular columns, Toutanji (1999), Nanni *et al* (1994), Miyauch *et al* (1997) and Teng and Lam (2002)

Braga, Gigliotti and Laterza (2006)

Braga *et al.* (2006) developed analytical model based on Elasticity theory to predict the confining pressure in stirrups and internal lateral ties for square and circular cross section columns. This model was expanded to be applied on Circular cross section columns confined with FRP. The proposed equation is as follow:

$$f_l = \frac{E_c E_f t_m (b_m / s) v}{E_c D + E_f t_f (b_m / s)(1 - v_c)(v_c \varepsilon_a + 1)} \varepsilon_z \qquad 2\text{-}428$$

where b_m is the wrapping width and s is the wrapping spacing.

103

<u>Matthys, Toutanji and Taerwe (2006)</u>

Mathys *et al* (2006) tested six large scale circular columns of 400 mm wide and 2 m heigh wrapped with CFRP, GFRP and hyprid FRP (HFRP). They adapted Toutanji (1999) equation to account for the premature failure of FRP to be as follow:

$$f_c = f_c' \left(1 + 2.3 \left(\frac{f_l}{f_c'} \right)^{0.85} \right)$$

2-429

$$f_l = \frac{2 t_f E_f \varepsilon_{fu}}{D}$$

2-430

They showed that this adaptation for Toutanji (1999) model and Spoelstra and Monti (1999) are the most accurate models compared to the experimental work. Whereas Lam and Teng (2003) model has lower stiffness for the second branch compared to higher ones for the experimental work.

<u>Rocca, Galati and Nanni (2006)</u>

Rocca *etal* (2006) concluded, by conducting testing on large size columns wrapped with FRP having different cross sectional shapes, that the size effect is negligible for sections of size aspect ratio equal to 2 or less.

<u>Youssef, Feng and Mosallam (2006)</u>

Youssef *et al* (2006) developed a bilinear stress strain relation similar to Lam and Teng (2003) model. They considered shape effect, rectangular and circular, hence the seconed linear branch was expressed by ascending or descending sloped line based on the confinement ratio and the shape geometry. For the ascending curve up to failure the proposed equation are as follow:

$$f_c = E_c \varepsilon_c \left[1 - \frac{1}{n} \left(1 - \frac{E_2}{E_c} \right) \left(\frac{\varepsilon_c}{\varepsilon_t} \right)^{n-1} \right] \qquad 0 \le \varepsilon_c \le \varepsilon_t'$$

2-431

$$n = \frac{(E_c - E_2)\varepsilon_t}{E_c \varepsilon_t - f_t}$$

2-432

$$f_c = f_t + E_2 (\varepsilon_c - \varepsilon_t)$$

2-433

Whereas for the descending branch, for the second linear curve:

$$f_c = E_c \varepsilon_c \left[1 - \frac{1}{n} \left(\frac{\varepsilon_c}{\varepsilon_t} \right)^{n-1} \right] \qquad \varepsilon_t' \le \varepsilon_c \le \varepsilon_{ccu}$$

2-434

$$n = \frac{(E_c - E_2)\varepsilon_t}{E_c \varepsilon_t - f_t}$$

2-435

$$f_c = f_t + E_2 (\varepsilon_c - \varepsilon_t)$$

2-436

The parameters used for both the ascending and descending curves are as follow:

$$f_{cu} = 1 + 2.25 \left(\frac{f_{lf}}{f_c'} \right)^{\frac{5}{4}}$$

2-437

$$\varepsilon_{cu} = 0.003368 + 0.259 \left(\frac{f_{lf}}{f_c'} \right) \left(\frac{f_f}{f_c'} \right)^{\frac{1}{2}}$$

2-438

$$f_t = 1 + 3 \left(\frac{\rho_f E_f \varepsilon_t}{f_c'} \right)^{\frac{5}{4}}$$

2-439

$$\varepsilon_t' = 0.002748 + 0.1169 \left(\frac{\rho_f E_f \varepsilon_t}{f_c'} \right)^{\frac{6}{7}} \left(\frac{f_f}{f_c'} \right)^{\frac{1}{2}}$$

2-440

Youssef *et al* (2006) showed good agreement with experimental results for rectangular (10 *15

in), square (15*15 in) and circular (16 in) specimens wrapped with FRP. They compared their

105

model with other models available in literature. It was observed the good correlation with Lam

and Teng model (2003).

<u>Debaiky, Green and Hope (2007)</u>

Debaiky *et al* (2007) developed an iterative procedure to preidct the stress strain behavior

of concrete wrapped with steel and FRP simultaneously. They divided the cross sectional area

into ; area confined with FRP only (cover coating the steel) and core area confined with steel and

FRP. The lateral pressure applied on the confined area is the summation of FRP and Steel lateral

pressure. The equations used in calculating the FRP and steel pressure are as follow:

$$f_{cc} = f_c' \left(1 + 2.1 \left(\frac{f_l}{f_c'} \right)^{0.7} \right)$$ 2-441

$$f_c = \frac{f_{cc} x r}{r - 1 + x^r}$$ 2-442

$$\varepsilon_l = \frac{E_c \varepsilon_c - f_c'}{2 \beta f_c'}$$ 2-443

$$\beta = \frac{E_c}{|f_c'|} - \frac{1}{|\varepsilon_{co}|}$$ 2-444

$$f_{lf} = \frac{2 t_f E_{frp} \varepsilon_l}{D}$$ 2-445

$$f_{ls} = \frac{2 A_s E_s \varepsilon_l}{d_s s}$$ 2-446

It is mentioned that f_{cc} equation was adopted from Cusson and Paultre (1995), stress equation

from Popovics (1973) and the lateral strain equation from Pantazapoulou and Mills (1992). The

106

proposed procedure was correlated to a 305 mm circular column tested by Lee (1998) and also with corroded columns constructed by the authors.

Teng, Huam, Lam and Ye (2007)

Teng *et al* (2007) proposed a new analysis based model for FRP-confined concrete that considers the response of concrete core and the FRP jacket. The proposed equation that relates the axial strain to lateral strain for unconfined concrete was benchmarked for its usability for confined concrete as well. The equation is:

$$\Phi\left(\frac{-\varepsilon_l}{\varepsilon_{co}}\right) = 0.85\left[\left(1+0.75\right)\left(\frac{-\varepsilon_l}{\varepsilon_{co}}\right)\right]^{0.7} - \exp\left[-7\left(\frac{-\varepsilon_l}{\varepsilon_{co}}\right)\right]$$

2-447

And the proposed equation for the ultimate strenth and strain are as follow:

$$\frac{f_{cc}}{f_c'} = 1 + 3.5\frac{f_l}{f_c'}$$

2-448

$$\frac{\varepsilon_{cc}}{e_{co}} = 1 + 17.5\frac{f_l}{f_c'}$$

2-449

The iterative procedure utilizes Popovics (1973) equation and the well know lateral pressure equation:

$$f_l = \frac{E_f t_f \varepsilon_l}{D}$$

2-450

$$f_c = \frac{f_{cc}xr}{r - 1 + x^r}$$

2-451

They showed good corelation between the proposed model and Xiao and Wu (2000) and Aire *et al* (2001).

Eid and Paultre (2007)

Eid and Paultre proposed analytical quad linear model based on the elastoplastic behavior of confined concrete columns and Druker-Brager theory. The model is charactrized by four phases; elastic phase, elasic behavior of confining materal and plastic behavior of concrete, elastic behavior of FRP and plastic behavior of concrete and steel and lastly after FRP ruptures. Eid and Paultre (2007) showed reasonable comparison between their model and experimental work done by Eid *et al* (2006) and Demers and Neale (1999)

Jiang and Teng (2007)

Jiang and Teng (2007) compared eight analysis oriented models ; Mirmiran and Shahawy(1997), Spoelstra and Monti (1999), Fam and Rizkalla (2001), Chun and Park (2002), Harries and Kharel (2002), Marquez *et al* (2004), Binici (2005), Teng *et al* (2007). And they found out that Teng *et al* (2007) model is the most accurate one to capture the stress-strain response compared to a set of 48 test cases. They also proposed a refinement equation for the ultimate strain as follow:

$$\frac{\varepsilon_{cc}}{e_{co}} = 1 + 17.5 \left(\frac{f_l}{f_c'} \right)^{1.2}$$

2-452

Eid and Paultre (2008)

Eid and Paultre (2008) pointed out the importance of having a stress-strain model accounts for the action of the transverse steel and FRP confinement together, as many structural codes dictates certain amount of steel used with FRP confinement). The effective lateral pressure due to steel and FRP action is given by:

$$f_{le} = \rho_{sey} f_{sh} + E_f \varepsilon_f - \Delta p \tag{2-453}$$

$$\rho_{sey} = \frac{K_e A_{shy}}{s d_s} \tag{2-454}$$

where f_{sh} is the lateral steel pressure, K_e is the effective confinement coefficient (Sheikh and Uzumeri (1982), A_{shy} is the total cross section area of the ties in the y direction and d_p is lateral pressure developed due to transverse steel action. The ultimate strength and strain are determined using the following equations:

$$f_{cu} = f_c' + 3.3 \left(\rho_{sey} f_{yh} + E_f \varepsilon_{fe} \right) \geq f_{cc} \tag{2-455}$$

$$\frac{\varepsilon_{cu}}{\varepsilon_{co}} = 1.56 + 12 \left(\frac{\rho_{sey} f_{yh}}{f_c'} + \frac{E_f \varepsilon_{fe}}{f_c'} \right) \left(\frac{\varepsilon_{fe}}{\varepsilon_{co}} \right)^{0.45} \tag{2-456}$$

The stress equations were proposed by modifing The Légeron and Paultre (2003) ones as follow:

$$f_{cu} = f_{cc} \exp \left(k_1 \left(\varepsilon_c - \varepsilon_{cc} \right)^{k2} + E_{cu} \left(\varepsilon_c - \varepsilon_{cc} \right) \right) \qquad \varepsilon_{cu} \geq \varepsilon_c > \varepsilon_{cc} \tag{2-457}$$

$$f_{cu} = f_{cc,s} \exp \left(k_{1,s} \left(\varepsilon_c - \varepsilon_{cc,s} \right)^{k2,s} \right) \qquad \varepsilon_c > \varepsilon_{cu} \tag{2-458}$$

$$k_1 = \frac{\ln(0.5)}{\left(\varepsilon_{cc50} - \varepsilon_{cc} \right)^{k_2}} \tag{2-459}$$

$$k_2 = 1 + 25 \left(I_{e50} \right)^2 \tag{2-460}$$

$$\frac{\varepsilon_{cc50}}{\varepsilon_{c50}} = 1 + 60 I_{e50} \tag{2-461}$$

$$I_{e50} = \frac{\rho_{sey} f_{yh}}{f_c'} + \frac{E_f \varepsilon_{fe}}{f_c'} \tag{2-462}$$

where ε_{c50} is the post peak strain corresponding to stress equal to 50% of the unconfined concrete strength and $f_{cc,s}$, $\varepsilon_{cc,s}$, $k_{1,s}$ and $k_{2,s}$ are valuse for concrete confined with steel only:

$$\frac{f_{cc,s}}{f_c'} = 1 + 2.4\left(I_e'\right)^{0.7}$$

2-463

$$\frac{\varepsilon_{cc,s}}{\varepsilon_{co}} = 1 + 35\left(I_e'\right)^{1.2}$$

2-464

$$I_e' = \frac{f_{le}}{f_c'}$$

2-465

The model was well compared with experimental work done by Eid *et al* (2006), Xiao and Wu (2000) and Demers and Neale (1999).

Benzaid, Chikh and Mesbah (2008)

Benzaid et al (2008) tested square (100 * 100 mm) and cylindrical (160 mm)high strength concrete specimens wrapped with EFRP up to 4 layers. They reported that all the stress strain response is bilinear curve with tranzition zone. Also they reported for circular specimens testing that Samaan *et al* (1998) and Saafi *et al* (1999) are more accurate than Teng *et al* (2007) model especially for concrete wrapped with 4 layers.

Rocca, Galati and Nanni (2009)

Rocca *et al* (2008) developed simplified approach for generating P-M interaction diagram through defining five points; axial compression , pure bending, three points corresponding to ultimate strain in concrete and zero strain, yield strain and 0.005 strain in tensioned steel. The ultimate strain in concrete is taken from Lam and Teng (2003) model according to ACI code

provisions. The interation diagram was ploted by connecting the five points by straight lines. And the compression controlled zone was validated against some experimental work.

<u>Teng, Jiang, Lam, and Luo (2009)</u>

This work aimed to refine the Lam and Teng (2003) model for better formulas for ultimate strength and strain. They pointed out the difficency of the former database that used in developing Lam and Teng Model in 2003 such as the uncertainty of the strain gauge location on the overlapping zone of FRP. Hence, they used additional tests that were conducted by Lam and Teng (2004), Lam *et al* (2006), Teng *et al* (2007) and Jiang and Teng (2007). Based on that new ultimate strength and strain equations were proposed as follow:

$$\frac{\varepsilon_{cu}}{\varepsilon_{co}} = 1.75 + 6.5 \left(\frac{2E_{ft_f}}{\left(f_c' \big/ \varepsilon_{co} \right) D} \right)^{0.8} \left(\frac{\varepsilon_{fu}}{\varepsilon_{co}} \right)^{1.45} \qquad\qquad\qquad 2\text{-}466$$

$$\frac{f_{cc}}{f_c'} = 1 + 3.5 \left(\left(\frac{2E_{ft_f}}{\left(f_c' \big/ \varepsilon_{co} \right) D} \right) - 0.01 \right) \left(\frac{\varepsilon_{fu}}{\varepsilon_{co}} \right) \qquad \left(\frac{2E_{ft_f}}{\left(f_c' \big/ \varepsilon_{co} \right) D} \right) \geq 0.01 \qquad 2\text{-}467$$

Farther, A new adapted model was proposed to account for concrete behavior with stress strain descending branch, Figure (2-27). The axial stress equations are as follow:

$$f_c = E_c \varepsilon_c - \frac{\left(E_c - E_2 \right)^2}{4 f_c'} \varepsilon_c^2 \qquad 0 \leq \varepsilon_c \leq \varepsilon_t' \qquad\qquad\qquad 2\text{-}468$$

111

$$f_c = f_c^{'} + E_2 \varepsilon_c \qquad \varepsilon_t^{'} \leq \varepsilon_c \leq \varepsilon_{ccu} \qquad \left(\frac{2E_{ft_f}}{\left(f_c^{'} \middle/ \varepsilon_{co} \right) D} \right) \geq 0.01 \qquad \text{2-469}$$

$$f_c = f_c^{'} - \frac{f_c^{'} - f_{cu}}{\varepsilon_{cu} - \varepsilon_{co}} \left(\varepsilon_c - \varepsilon_{co} \right) \qquad \varepsilon_t^{'} \leq \varepsilon_c \leq \varepsilon_{ccu} \qquad \left(\frac{2E_{ft_f}}{\left(f_c^{'} \middle/ \varepsilon_{co} \right) D} \right) < 0.01 \qquad \text{2-470}$$

$$f_{cu} > 0.85 f'c \qquad \left(\frac{2E_{ft_f}}{\left(f_c^{'} \middle/ \varepsilon_{co} \right) D} \right) \geq 0 \qquad \text{2-471}$$

$$f_{cu} = 0.85 f'c \qquad \left(\frac{2E_{ft_f}}{\left(f_c^{'} \middle/ \varepsilon_{co} \right) D} \right) = 0 \qquad \text{2-472}$$

This model was well compared to Lam and Teng (2004), Lam *et al* (2004), Teng *et al* (2007) and Jiang and Teng (2007) experimental work.
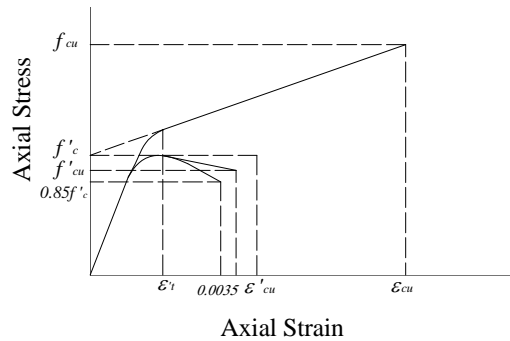
Figure 2-27: Axial Stress-Strain Model proposed by Teng *et al* (2009)

112

Csuka and Kollar (2010) built experimental database from the work done by Almusallam (2007) Al-Salloum (2007) Berthet *et al*. (2004) , De Lorenzis and Tepfers (2003), Harries and Kharel (2002), Jiang and Teng (2007), Lam and Teng (2007), Mirmiran *et al*. (2000), Shahawy *et al*. (2000), and Toutanji (1999). They reasoned the premature failure of FRP to four parameters; the vertical cracks developed in concrete that cause localized strain peak in FRP, the resistance decrease in the lateral direction due to biaxial stress on FRP, missalignement of the fiber and the variation of FRP strain in the inner and outer surface because of the curved surface. They proposed an analysis oriented model based on the concrete model found by Papaikoloau and Kappos (2007) with the introduction of the FRP stiffness. They developed an equation for the stiffness ratio as follow

$$Stiffnessratio = \frac{2E_f t}{DE_c}$$ 2-473

They pointed out the advantage of using higher stiffness FRP, that cause higher strength, over using lower stiffness ones. However using over stiffness FRP causes FRP to rupture before concrete reaches failure state. They defined the limit stiffness between high and low stiffness as follow:

$$Stiffnessratio - \lim it = 0.0195 + \frac{f_c^{'} - 40}{3100} \qquad f_c^{'} \leq 40 MPa$$ 2-474

$$Stiffnessratio - \lim it = 0.0195 + \frac{f_c^{'} - 40}{12000} \qquad f_c^{'} > 40 MPa$$ 2-475

The optimal stiffness that separates the over confined and adequately confined concrete is defined by:

$$Stiffness\,ratio - optimal = -0.1 + 0.22\left(\frac{f_{la}}{f_c'}\right)^{0.2}\left(\frac{f_c'}{20}\right)^{0.3}$$

2-476

The Lower approximation for compressive strength of confined concrete value is give by:

$$f_{cc,min} = f_{la} + \sqrt{10.16 f_{la} f_c'}$$

2-477

They also determined that the sufficient confinement ratio has to be more than 0.083. The proposed model showed good correlation with database.

<u>Wei and Wu (2011)</u>

Wei and Wu (2011) developed a unified stress-strain curve, Figure (2-28), for rectangular, square and circular columns by utilizing two ratios *h/b* and *2r/b* where r is the corner radius, and in case of circular shape, *r* represents the radius. The proposed model was built on gathering 432 specimens, 100 of which from the authors work and the rest are from literature. The model developed has the following equations:

$$f_c = E_c \varepsilon_c + \frac{f_t - E_c \varepsilon_t}{\varepsilon_t^2} \varepsilon_c^2 \qquad 0 \le \varepsilon_c \le \varepsilon_t'$$

2-478

$$f_c = f_t + E_2(\varepsilon_c - \varepsilon_t) \qquad \varepsilon_t' \le \varepsilon_c \le \varepsilon_{ccu}$$

2-479

$$\varepsilon_t = \frac{(f_t + f_{cu} + E_c \varepsilon_{cu}) - \sqrt{(f_t + f_{cu} + E_c \varepsilon_{cu})^2 - 8 f_t E_c \varepsilon_{cu}}}{2 E_c}$$

2-480

$$E_2 = \frac{f_{cu} - f_t}{\varepsilon_{cu} - \varepsilon_t}$$

2-481

$$\frac{f_{cc}}{f_c'} = 1 + 2.2\left(\frac{2r}{b}\right)^{0.72}\left(\frac{f_l}{f_c'}\right)^{0.94}\left(\frac{h}{b}\right)^{-1.9}$$

2-482

114

$$\frac{\varepsilon_{cu}}{\varepsilon_{co}} = 1.75 + 12\left(\frac{f_l}{f_c'}\right)^{0.75}\left(\frac{f_{30}}{f_c'}\right)^{0.62}\left(0.36\frac{2r}{b} + 0.64\right)\left(\frac{h}{b}\right)^{-0.3}$$

2-483

$$f_t = f_c' + 0.43\left(\frac{2r}{b}\right)^{0.68}\left(\frac{h}{b}\right)^{-1} f_l$$

2-484

where f_{30} is the concrete strength of unconfined grade *C30* concrete
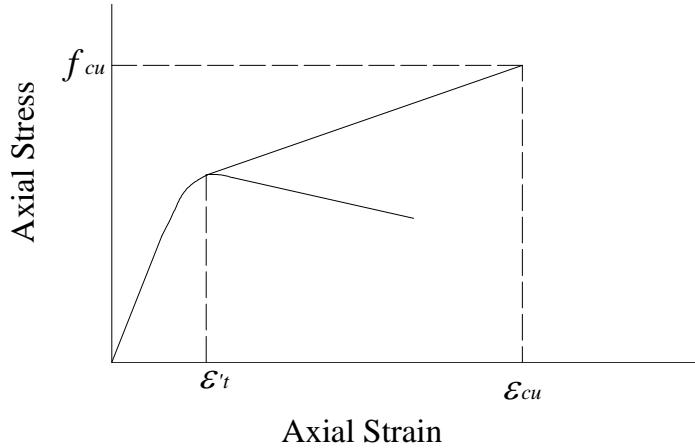
Figure 2-28: Axial Stress-Strain Model proposed by Wei and Wu (2011)

The model is well compared to the experimental work shown in the authors' database.

2-2-2 Discussion

Based on the extensive review done in the past section, some points can be concluded:

1- Most of the confinement axial stress-strain models are generated empirically from experimental work.

2- The ascending bilinear behavior up to failure of the concrete confined with FRP wrapping is confirmed by many authors such as Nanni and Bradford (1995), Harmon (1995), Miyauchi (1997), Samaan *et al* (1998), Xiao and Wu (2000), Aire *et al* (2001),

Campione and Miraglia (2003), Harries and Kharel (2002), Lam and Teng (2003), Berthed *et al* (2004), Li (2006), Youssef *et al* (2006) Benzaid *et al* (2008) and Wei and Wu (2011). In addition Lam and Teng (2003) concluded that insufficient confinement ratio yield descending second linear branch. That was confirmed by Li (2006) who stated that confined concrete with insufficient confinement behaves like unconfined one. Also Youssef *et al* (2006) reasoned the descending zone to shape geometry and confinement ratio. The first linear zone in the axial stress-strain curve is similar to the unconfined response as an evidence of inactive behavior of FRP. After unconfined strength is reached and concrete tends to dilate, FRP gets engaged in confining. Hence the modulus changes or the second line slope decreases. The linear behavior is due to the linear behavior of FRP up to Failure.

3- Specimen sizes are good representative of short confined columns and the scale effect is negligible. This was verified by Rocca *et al* (2006), Mathys *et al* (1999), Shawn *et al*. (2005) and Theriault (2004).

4- Concrete Wrapped with CFRP are higher in strength than that wrapped with same ratio of GFRP, while concrete wrapped with GFRP are more ductile. Lam and Teng (2001), Aire *et al* (2001) and Toutanji (1999) showed the advantage of CFRP and GFRP.

5- Increasing the layer numbers increase the slope of the second linear curve. Aire *et al* (2001)

6- Circular wrapping is more efficient than rectangular wrapping. Pessiki *et al* (2001)

7- The dilation rate decreases after reaching a certain strain value. MIrmiran and Shahawy (1997), Pessiki *et al* (2001), Harries and Kharel (2002) and others.

8- The shape factor is introduced in calculating the lateral confining pressure, Pessiki *et al.* (2001), Campione and Miraglia (2003), Li *et al* (2002) and Youssef (2006), especially for non-circular sections.

9- Premature failure of FRP compared to Labs Tensile strength tests was confirmed by Chun (2002), Mathys *et al.* (1999), Pessiki *et al* (2001), Chun and Park (2002), Lam and Teng (2003) and Csuka *et al* (2011). This is due to some reasons:

 - The vertical cracks developed in concrete that cause localized strain peak in FRP and non uniform stress distribution in cracked concrete

 - The curvature effect on FRP tensile strength or variation of FRP strain in the inner and outer surface because of the curved surface

 - The resistance decrease in the lateral direction due to biaxial stress on FRP

 - missalignement of the fiber and Manufacturing errors

 - Existence of overlapping zones that cause non uniform strain

10- For columns confined with lateral steel and FRP the action from both was added up to yield effective lateral pressure, Li et al (2002), Chun and Park (2002), Debaiky (2002) and Eid and Paultre (2008)

2-3 Circular Concrete Filled Steel Tube (CFST) Columns

CFST columns are not relatively new construction elements compared to lateral steel confined columns. The first to use concrete filled tubes was swelling in 1901 to resist internal rust of steel. There are some structures that used CFST columns in the early 1900s such as Almondsbury Motorway Interchange (England), Charleroi Railways (Belgium) (Shams and Saadeghvaziri (1997)). The concrete was used to stabilize the column. However extensive research on CFSTs did not start until the beginning of 1960s. And with the appearance of FRP as a cheaper and more practical material in the 1980s, CFST did not capture much attention compared to FRP. Hence, CFSTs analysis is considered a developing subject. This section reviews the previous work concerns CFST columns chronologically. Hence, the review is classified according to its author/s.

2-3-1 Past Work Review

<u>Furlong (1967)</u>

Furlong (1967) tested 22 round and 17 square CFST columns subjected to axial load and bending moment, and 8 round and 5 square CFST columns axially loaded. He proposed the following equations:

$$P_o = A_s f_y + A_c f_c' \sqrt{\frac{f_y}{0.0018 E_s}} \qquad \sqrt{\frac{f_y}{0.0018 E_s}} \le 1.00 \qquad\qquad \text{2-485}$$

$$M_o = \frac{f_y}{6}\left(D_o^3 - D_i^3\right) \qquad\qquad \text{2-486}$$

$$\left(\frac{P_u}{P_o}\right)^2 + \left(\frac{M_u}{M_o}\right)^2 \le 1 \qquad\qquad \text{2-487}$$

where P_o and M_o are the concentric ultimate load and ultimate pure bending, P_u and M_u are the ultimate force and moment capacity with given eccentricity , A_s is the steel area, A_c is the concrete area, E_s is the steel modulus of elasticity and f_y is the steel yield strength. Furlong (1967) concluded that Equation (2-487) is conservative for most of the data. He also concluded that concrete should be treated as ordinary reinforced concrete section to best predict columns strength.

Gardner and Jacobson (1967)

Gardner and Jacobson (1967) reported that CFST exposed to compression can fail under a combination of three modes; crushing, general buckling and local buckling. The internal pressure the steel is exposed to is as follow:

$$f_{st} = \frac{r}{t} f_l \hspace{4cm} \text{2-488}$$

where f_{st} is the internal force, f_l is the lateral pressure, r is the column radius and t is the steel tube thickness. The axial stress is :

$$f_c = f_c' + 4f_l \hspace{4cm} \text{2-489}$$

And the total axial load will be:

$$P = A_c f_c' + 4A_c \frac{t}{r} f_{st} + A_s f_{sl} \hspace{3cm} \text{2-490}$$

It is noted that either f_{st} or f_{sl} might reach f_y or both reach f_y. Gardner and Jacobson (1967) concluded that strong concrete core should be used to prevent local buckling

119

<u>Tomii, Yoshimara and Morishita (1977)</u>

Tomii *et al* (1977) conducted extensive study on 270 CFST concentrically loaded specimens and concluded that the ultimate strength is affected by the steel tube thickness and the cross sectional shape. He concluded three patterns in the stress-strain behavior; strain hardening, perfectly plastic and stiffness degradation.

<u>Sakino, Tomii and Watanabe (1985)</u>

Sakino *et al* (1985) tested eighteen CFST specimens with different loading conditions. They concluded that when the steel and concrete are loaded together, the steel provides no confinement till post yielding.

<u>Shams and Saadeghavaziri (1997)</u>

Shams and Saadeghavaziri (1997) presented the experimental and analytical work of the state of the art of CFST columns. They concluded the following:

- The ultimate strength is not predicted well and the confinement effect should be taken into account, as well as slenderness ratio, aspect ratio, creep and cross sectional shape.

- The effect of the bond between the steel and the concrete is not well defined

- The mechanism of local buckling should be studied as well as the effect of high strength concrete on ultimate strength and ductility.

- The importance of finding New design methods and evaluate the seismic performance of CFST columns.

Schneider tested fourteen CFST specimens, three of which were circular specimens of *D/t* equal to 47, 21.7, 21 and *L/D* equal 4.3, 4.3 and 4.4. He concluded that all the circular specimens had post peak strain hardening and they showed more ductility than the rectangular specimens. He also showed some local buckling in the tubes.

Shams and Saadeghvaziri (1999)

Shams and Saadeghvaziri (1999) developed a 3D finite element model for CFST columns simulations. This model was verified against 6 experimental cases by Tomii *et al* (1977). The steel model was the Von Mises elastic-plastic model with kinematic hardening and the concrete model was Pramano-Willimas model (fracture energy-based model). Then the 3D model was used in parametric study to evaluate the effect of the aspect ratio, length-width ratio, ultimate strength and concrete uniaxial compressive strength. Shams and Saadeghvaziri (1999) proposed the following stress-strain equations:

$$f_{cc} = f_c' \left(1 + \frac{A}{1 + \left(\frac{D/t}{B} \right)^{\alpha}} \right) \qquad \text{2-491}$$

$$\varepsilon_{cc} = \varepsilon_{co} \left(1 + \frac{3.51}{1 + \left(\frac{D/t}{60} \right)^{\alpha}} \right) \qquad \text{2-492}$$

$$A = 1.831e^{-\left(\frac{f_c'}{3.55}\right)}$$

2-493

$$B = -32.517 + \frac{510}{f_c'}$$

2-494

$$f_c = f_{cc} \left(\frac{0.0181 + 4.69430x - 5.531x^2 + 4.63689x^3 - 1.54584x^4 + 0.16773x^5}{1 + +2.12912x + 5.0808x^2 + 5.08680x^3 - 1.86773x^4 + 0.20046x^5} \right)$$

2-495

The steel tube maximum compressive stress is found as follow:

$$f_{sy} = \left(1.08 - 0.045\ln\left(\frac{D}{t}\right)\right) \left(0.59 + \frac{0.38}{1 + \left(\frac{L/D}{22.19}\right)^{3.93}}\right)$$

2-496

Where f_{cc} is the ultimate compressive strength, ε_{cc} is the strain at f_{cc}, α is equal to 1, $x = \varepsilon_{cc}/\varepsilon_{co}$ and L/D is length to width ratio. Shams and Saadeghvaziri *(1999)* concluded that

- Concrete maximum compressive strength depends on the ratio of *D/t, f'c* and cross sectional shapes

- The amount of the ratio of confinement is higher in concrete with lower unconfined compressive strength.

- Local buckling occurs at peak load for CFST that has *D/t* more than 95.

- The steel compressive strength depends on *D/t* and *L/D*

122

<u>O'shea and Bridge (2000)</u>

O'shea and Bridge (2000) tested CFST specimens having length to diameter ratio 3.5, diameter to thickness ratio ranged from 60 to 220. They loaded the specimens with with different loading conditions; axial loading of steel only, axial loaded of concrete only and axial and eccentric loading of both the steel and concrete. They adapted Mander equation for the ultimate confined strength for 50-MPa concrete as follow:

$$f_{cc} = f_c' \left(-1.228 + 2.172 \sqrt{1 + \frac{7.46 f_l'}{f_c'}} - 2\frac{f_l'}{f_c'} \right)$$

2-497

whereas they used Attard and Setunge (1996) formulas for 80-100 MPa concrete. O'shea and Bridge (2000) concluded that the highest onfinement level is provided when the concrete only is loaded, Eurocode is the best in estimating concrete strength in CFST and local buckling can't occur if there is concrete steel bonding

<u>Shanmugam and Lakshmi (2001)</u>

Shanmugam and Lakshmi (2001) conducted an extensive review of the analytical and experimental work that was done.

<u>Abdel-Salam, Abdel-Ghaffar and Zaki (2001)</u>

Abdel-Salam *et al* (2001) proposed an analytical model based on Von-mises yield criteria and plastic flow rule for steel. They derived equation for calculating the first yield axial load and the ultimate axial load and well compared these equations to experimental work done by Furlong (1967) and Sakino and Hayashi (1995).

<u>Elchalakani, Zhao and Grzebieta (2001)</u>

Elchalakani *et al* (2006) conducted experimental investigation on CFST under pure bending loading for D/t ranging from 12 to 110. They provided simplified formula to determine the CFST ultimate flexural capacity

<u>Johansson and Akesson (2002)</u>

Johansson and Akesson (2002) developed elasto-plastic model based on Drucker-Prager yield criteria. They introduced both the strength and the plastic modulus as dependence of confinement sensitivity. They developed FE program based on their model to analyze CFST.

<u>Huang, Yeh, Liu, Hu, Tsai, Weng, Wang and Wu (2002)</u>

Huang *et al* (2002) reported that the CFST is influenced by width to thickness ratio, height to width ratio, the cross sectional shape and the strength ratio of concrete to steel. Huang *et al* (2002) showed two different axial stress-strain behavior of CFST; the first is similar to elastic perfectly plastic for column ($D/t = 40$ and $f_y/f'_c = 9.79$) and the second behavior showed strain softening after reaching the peak for two columns ($D/t = 70$, 150 and $f_y/f'_c = 8.75$, 12.5 respectively). They also concluded that the CFSTs behave better than square ones in terms of strength, stiffness and ductility.

<u>Johansson and Gylltoft (2002)</u>

Johansson and Gylltoft (2002) tested 13 CFST specimens with three different concentric loading conditions. They developed a 3D FE program to verify the experimental results. They

concluded that the columns capacities was determined by steel yield and the bond between concrete and steel has no effect when the steel and concrete are loaded simultaneously.

Elremaily, Azizinamini (2002)

Elremaily, Azizinamini (2002) conducted experimental investigation of six CFST subjected to axial load and cyclic lateral load. They concluded that CFSTs have high levels of energy dissipation and ductility, AISC_LRFD are very conservative in CFST calculations and CFSTs can experience axial shortening at high level of displacements that can lead to failure.

Lakshmi and Shanmugam (2002)

Lakshmi and Shanmugam (2002) developed a finite approach to predict the moment-curvature-thrust relationship for CFST having circular or rectangular shapes. They limit the concrete ultimate strain to 0.003 and divided the cross section into finite elements. This procedure was generalized to cover the whole column to account for slenderness. Lakshmi and Shanmugam (2002) showed the accuracy of their work compared to experimental work.

Hu, Huang, Wu and Wu (2002, 2003)

Hu *et al* (2002, 2003) proposed material constitutive models for CFST columns.The steel model was Von Mises elastic-plastic model and the concrete one was modeld by elastic-plastic theory with isotropic hardening rule and based on Richart (1928) ultimate strength equations. The model was incorporated in ABAQUS and verified against experimental work done by Schneider (1998) and Huang *et al* (2002). Hu et al. concluded that good confinement can be provided especially with D/t < 40 and local buckling is not likely to occur.

Fam *et al* (2004) conducted experimental work on 10 circular CFSTs specimens. Five of which were loaded axially and the rest were loaded axially and laterally in cycles. The main objective was to evaluate the strength and ductility. They developed an analytical model to evaluate the Force-Moment diagram using the following equations (these equations are valid for axial load less or equal to *0.85f'$_c$A$_c$*):

$$M_n = K(M_c + M_s) \qquad\qquad\qquad\qquad\qquad\qquad\text{2-498}$$

$$K = 1.13 \qquad\qquad \frac{P_n}{f_c' A_c} \leq 0.1$$

$$K = 1.13 + 2.35\left[\frac{P_n}{f_c' A_c} - 0.1\right]^2 \qquad\qquad \frac{P_n}{f_c' A_c} > 0.1 \qquad\qquad\qquad\text{2-499}$$

$$M_s = f_y Z_s \qquad\qquad\qquad\qquad\qquad\qquad\qquad\text{2-500}$$

$$Z_s = \frac{\left(D_o^3 - D_i^3\right)}{6} \qquad\qquad\qquad\qquad\qquad\qquad\text{2-501}$$

$$M_c = C_c e \qquad\qquad\qquad\qquad\qquad\qquad\qquad\text{2-502}$$

where M_n is the flexural strength, M_c and M_s are the flexural strength for the concrete and steel, K is strength enhancement factor, A_c is the area of the entire cross section, Z_s is the plastic section modulus of the tube. For loads more than *0.85f'$_c$ A$_c$* linear interpolation is conducted beween the point of *0.85f'$_c$ A$_c$* force and the pure axial compression force. Fam *et al* (2004) showed the good correlation between this model and the experimental points. In addition they plotted the exact Force-Moment diagram using strain compatability, Mander Model and elastoplastic steel model with and without strain hardening that were conservative and accurate

126

without showing analysis steps. They concluded that columns subjected to axial and lateral load failed with steel fracture in the areas that had local buckling, whereas bonded columns subjected to axial load only failed by diagonal cracking and unbounded columns failed with combination of diagonal and vertical cracking. They also showed the ductility improvement of CFST columns and showed that design codes are very conservative and underestimating the columns capacity. Finally they reported that the axial strength capacity of CFST short columns at axial strain ranging from 0.009-0.012.

Inai, Mukai, Kai, Tokinoya, Fukomoto and Mori (2004)

Inai *et al* (2004) tested 33 CFST specimens with circular and square cross sections. The main variables studied were the concrete and steel strength and diameter to thickness ratio. The load pattern was axial loading and lateral cyclic load. Inai *et al* (2004) developed analytical model to express the hysteresis behavior based on Sakino *et al* (1997) and Nakahara *et al* (1998) work. They concluded ductility increasing with steel strength increase and decreasing with concrete strength increase and to utilize high strength concrete, high strength steel should be used and there is moment enhancement for circular CFST columns due to steel confinement.

Giakoumelis and Lam (2004)

Giakoumelis and Lam (2004) tested fifteen circular CFST short columns. They concluded that the shrinkage and bond effects are critical for high strength concrete and they found that the Euro code 4 give the best predicition of CFST compared to Australian Standardsand American Codes

127

Fujimoto *et al* (2004) studied the effect of higher strength on the flexural behavior and tested. They tested thirty three CFSTs specimens loaded eccentrically. They proposed a stress-strain curve based on the fiber analysis method as follow:

$$Y = \frac{VX + (W-1)X^2}{1 + (V-2)X + WX^2}$$ 2-503

$$X = \frac{\varepsilon_c}{\varepsilon_{cc}}$$ 2-504

$$Y = \frac{f_c}{f_{cc}}$$ 2-505

$$V = \frac{E_c \varepsilon_{cc}}{f_{cc}}$$ 2-506

$$W = 1.5 - 17.1 f_c' * 10^{-3} + 2.39\sqrt{f_{re}}$$ 2-507

$$f_{re} = \frac{4.1}{23} f_l$$ 2-508

$$\varepsilon_{cc} = 1 + 4.7(K-1) \qquad K \le 1.5$$ 2-509

$$\varepsilon_{cc} = 3.35 + 20(K-1.5) \qquad K > 1.5$$ 2-510

$$f_{cc} = f_c' + 4.1 f_l$$ 2-511

K is undefined parameter.
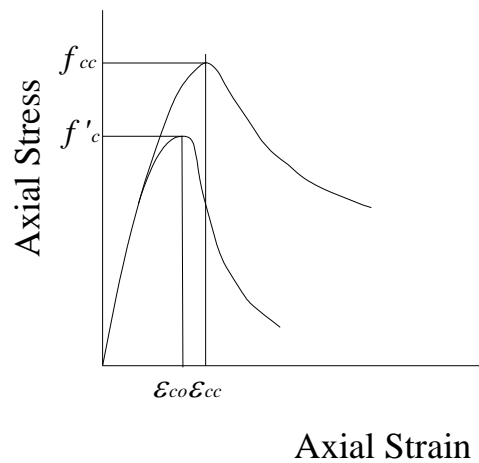
Figure 2-29: Axial stress-strain model Proposed by Fujimoto et al (2004)

Fujimoto *et al* (2004) concluded that high strength concrete cause ductility reduction but this can be improved by using high strength steel or a small diameter to thickness ratio. They also verified the two different stress-strain patterns found by Huang *et al* (2002).

Jarquio 2004

Jarquio 2004 showed analytical equation for calculating CFST's concrete force and moment. The formulas were developed for unconfined concrete by limiting the ultimate strain to 0.003.

Ellobody, Young and Lam (2005)

Ellobody *et al* (2005) conducted a study of CFST columns with concrete strength ranging from 30-110 MPa and D/t ratios from 15-80. They developed a 3D finite element model analysis. This model was verified against fourty specimens. After that a parametric study was conducted to yield the conservative approach for the desin codes.

Yu, Ding and Cai (2006)

Yu *et al* (2006) tested seventeen CFST specimens to investigate the different testing loading and parameters on the ultimate capacity of the columns. The test was conducted using self compacting concrete and normal concrete. They found out that increasing the concrete strength for either kind increases the load capacity and there was a significant confinement effect appeared after reaching certain percentage of the ultimate axial load.

Baig, Jiansheng and jianguo (2006)

Baig et al (2006) tested 16 CFST specimens and 12 hollow steel sections having different cross section shapes. The length to diameter ratio ranged from 4 to 9. They concluded that there was increase in strength for circular sections up to 60% for some cases and all the tested cases behaved in ductile manner.

Goode (2008)

Goode (2008) showed that Eurocode 4 can be used confidentally in CFST design by testing 1819 CFST specimens with circular and rectangular cross sections, and comparing the results with that code.

Yu, Tao and Wu (2008)

Yu et al (2008) tested 28 high strength self-consolidating concrete filled in thin steel tubes. The slenderness ratio ranged from 12 to 120. They reported the failure model is local outward folding for square cross section, shear failure for circular sections and overall bucking for beam-columns. They concluded that the self-consolidating concrete is less ductile than the

normal one. They also compared the results with the AISC, Euro code 4 DBJ13-51-2003 (China) and concluded that these codes give reasonable resuslts

<u>Liang and Fragomeni (2010)</u>

Liang and Fragomeni (2010) proposed a nonlinear theoretical model for the behavior of CFST stub columns under eccentric loading. They adapted mander model in the following equations:

$$f_{cc} = \gamma_c f_c' + 4.1 f_l \qquad\qquad\qquad 2\text{-}512$$

$$\varepsilon_{cc} = \varepsilon_{co}\left(1 + 20.5\frac{f_l}{\gamma_c f_c'}\right)$$

$$2\text{-}513 \quad \gamma_c = 1.85 d_s^{-0.135} \qquad\qquad 0.85 \le \gamma_c \le 1.0 \qquad\qquad 2\text{-}514$$

Where γ_c is a reduction factor that account for column size.
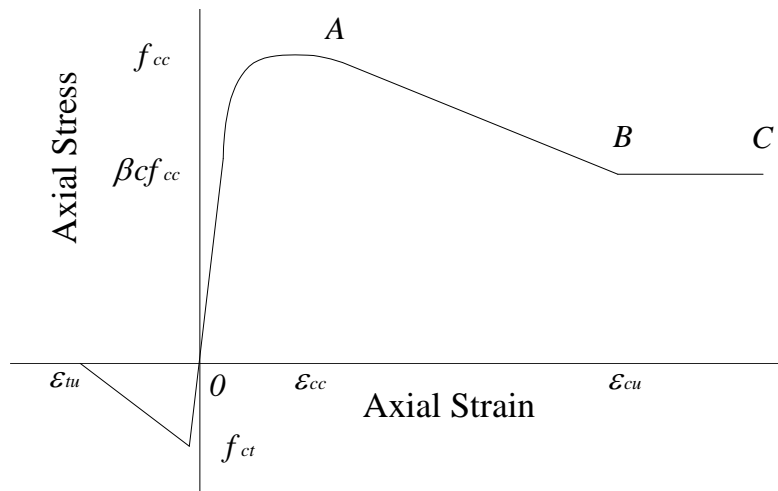
Figure 2-30: stress_strain curve for confined concrete in circular CFST columns, Liang and Fragomeni (2010)

131

$$f_l = 0.7(v_e - v_s)\frac{2t}{D-2t}f_y \qquad\qquad \frac{D}{t} \le 47 \qquad\qquad \text{2-515}$$

$$f_l = 0.7\left(0.006241 - 0.0000357\frac{D}{t}\right)f_y \qquad\qquad 47 < \frac{D}{t} \le 150 \qquad\qquad \text{2-516}$$

$$v_e = 0.2312 + 0.3582v_e' - 0.1524\left(\frac{f_c'}{f_y}\right) + 4.843v_e'\left(\frac{f_c'}{f_y}\right) - 9.169\left(\frac{f_c'}{f_y}\right) \qquad\qquad \text{2-517}$$

$$v_e' = 0.881*10^{-6}\left(\frac{D}{t}\right)^3 - 2.58*10^{-4}\left(\frac{D}{t}\right)^2 + 1.953*10^{-2}\left(\frac{D}{t}\right) + 0.4011 \qquad\qquad \text{2-518}$$

For the stress-strain curve shown in figure (2-30), part OA is expressed by Mander stress equation. Whereas part AB and BC are expressed by:

$$f_c = \beta_c f_{cc} + \left(\frac{\varepsilon_{cu} - \varepsilon_c}{\varepsilon_{cu} - \varepsilon_{cc}}\right)(f_{cc} - \beta_c f_{cc}) \qquad\qquad \varepsilon_{cc} < \varepsilon_c \le \varepsilon_{cu} \qquad\qquad \text{2-519}$$

$$f_c = \beta_c f_{cc} \qquad\qquad \varepsilon_{cu} < \varepsilon_c \qquad\qquad \text{2-520}$$

Liang and Fragomeni (2010) reported that hoops tension reduces the longitudinal yield strength due to the confinement effect as found by Neogi *et al*. (1969). The fiber element formulation was used in calculating the force and moment in the cross section. Liang and Fragomeni (2010) proposed also a formula for ultimate pure bending strength for CFST circular columns as follow:

$$M_o = \lambda_m \alpha_c \alpha_s f_y \qquad\qquad \text{2-521}$$

$$\lambda_m = 0.0087 + 12.3\left(\frac{t}{D}\right) - 36\left(\frac{t}{D}\right)^2 \qquad\qquad 10 < \frac{D}{t} \le 120 \qquad\qquad \text{2-522}$$

$$\alpha_c = 0.774\left(f_c'\right)^{0.075} \qquad\qquad 30 \le f_c' \le 120MPa \qquad\qquad \text{2-523}$$

132

$$\alpha_s = 0.883 + \left(\frac{21.147}{f_y}\right) + \left(\frac{4202}{f_y^2}\right) \qquad 250 \le f_y \le 690 MPa \qquad \text{2-524}$$

Lee, Uy, Kim, Choi and Choi (2011)

Lee et al (2011) conducted experimental work to test 11 high strength concrete circular stub CFST specimens. They utilized the concrete stress-strain model found by Hu et al (2003). They concluded that AISC and Korean building code for structures, KBCS, give good agreement with the experimental results. Whereas Eurocode 4 overestimates the eccentric testing results.

Liu , Tu and Ye (2011)

Liu et al. (2011) developed a volume-based method for calculating the value of effectively confined coefficient. They utilized Mander model for determining the lateral pressure and in stress-strain ascending relation, whereas they used Schneider (1998) formulas for the softening branch. They simulated numerical analysis for number of CFST columns using ABAQUS

Yang, Han (2011)

Yang and Han (2011) tested 28 stub CFST specimens having different cross sections. 16 specimens were subjected to partial eccentric loading and the rest were under full eccentric loading. Shape of the loading bearing plate was one of the tests variables. They showed that the partially loaded specimens have bearing capacity and ductility comparable to the fully loaded. Yang and Han (2011) constructed finite element model for the behaviour of CFST stub column under eccentric partial compression

133

2-2-2 Discussion

According to the literature review, there are some conclusions that can be drawn as follow:

- Mander Model is adopted by some researchers for CFST analysis such as Liu et al. (2011) Liang and Fragomeni (2010), O'shea and Bridge 2000 and Fam et al (2004). Hence it can be considered as a representative model for CFST.

- Failure models for CFST columns can be classified to crushing, local buckling and general buckling.

- The CFST analysis affecting parameters are width to thickness ratio, height to width ratio, the cross sectional shape and the strength ratio of concrete to steel

- Most of the research contributions are experimental work and implementation of 3D finite element models, then comparing it to the experimental outcomes.

- Bond effect and loading type affect significantly the results

- Eurocode best predicts the CFST capacity as stated by Giakoumelis and Lam (2004) Yu, *et al* (2008) and Goode (2008).

2-4 Rectangular Columns subjected to biaxial bending and Axial Compression

Rectangular reinforced concrete columns can be subjected to biaxial bending moments plus axial force. When the load acts on one of the cross section bending axes the problem becomes uniaxial bending. However when the load is applied eccentrically on a point that is not along any of the bending axes the case becomes biaxial bending. The biaxial bending case can be found in many structures nowadays. This case is visited extensively in the literature disregarding the confinement effect. The failure surface of rectangular columns is 3D surface consisted of many 2D interaction diagrams. Each of the 2D interaction diagrams represents one angle between the bending moment about x-axis and the resultant moment. Many simplifications are introduced to justify the compressive trapezoidal shape of concrete, due to the two bending axes existence. This section reviews the previous work concerns CFST columns chronologically. Hence, the review is classified according to its author/s.

2-4-1 Past Work Review

<u>A study of combined bending and axial load in reinforced concrete members (Hogenstad 1930)</u>

Hogenstad classified concrete failure subjected to flexure with or without axial load to five modes

1- Failure by excessive compressive strain in the concrete with no yield in tensioned steel (compression failure)

2- Tension failure where the tensioned steel yield cause excessive strain in the concrete

3- Balanced failure where tensioned steel yield at the same time compressive concrete fail

4- Compression failure where the tensioned steel pass the yield stress

5- Brittle failure caused by tensioned steel rupture after the cracks developed in the compressive concrete.

Hogenstad (1930) suggested designing by the ultimate failure theory in his report as opposed to the linear elastic theory (standard theory) that was widely applicable up to nearly fifty years. He discussed some of the available inelastic theories that were limited to uniaxial stress according to him. The theories discussed were E. Suenson (1912), L. Mensch (1914), H. Dyson (1922), F. Stussi (1932). C. Schreyer (1933). S. Steuermann (1933). G. Kazinczy (1933). F. Gebauer (1934) O. Baunmann (1934). E. Bittner (1935). A. Brandtzxg (1935). F. Emperger (1936). R. Saliger (1936). C. Witney (1937), USSR specifications OST 90003, (1938). V. Jensen1943. R. Chambaud (1949). Also Hognestad (1930) introduced his new theory of inelastic flexural failure. He sat equations for tension failure and compression one.

A simple analysis for eccentrically loaded concrete sections (Parker and Scanlon 1940)

Parker and Scanlon (1940) used elastic theory

$$\sigma = \frac{P}{A} \pm \frac{M_x c}{I_x} \pm \frac{M_y c}{I_y}$$

2-525

They developed a procedure by first calculating stresses at the four corners, then checking if all stresses are positive, no further steps are needed, otherwise, calculating center of gravity and recalculating moment of inertia then recalculating stress and determining the new position of the neutral axis. These steps are repeated till the internal forces converge with the applied one.

Reinforced concrete columns subjected to bending about both principal axes (Troxell 1941)

Troxell (1941) Suggested that portion of the applied axial load can be used with the bending moment about one axis to find the maximum compressive and tensile strength in the cross section. Then the remaining load along with the other bending moment about the other axis can be used the same way, using the method of superposition. The summation stresses are the stresses generated from the section. He also suggested taking equivalent steel area in each side to facilitate the calculation procedure.

Design diagram for square concrete columns eccentrically loaded in two directions (Anderesen 1941)

Andersen (1941) implemented a new procedure for determining maximum compressive and tensile stresses on cross sections without determining the location of the neutral axis. The limitation of this procedure that it is just applied on square cross sections and the steel has to be symmetric. Based on the linear elastic theory and the perpendicularity of the neutral axis to the plane of bending which was proven in a previous study, Andersen derived stresses coefficients equations basically for cross sections reinforced with four bars, and then represented them graphically. This derivation was set after classifying the problem into three different cases based on the neutral axis location

$$C = \frac{c_1 + 3np(2k - \cos\theta)\cos 2\theta}{6k\cos 2\theta} \qquad \text{2-526}$$

$$T = \left(1 - \frac{d}{D}\right)\frac{\cos\theta}{k} - 1 \qquad \text{2-527}$$

c_1 = is a coefficient that is fully determined in his paper for each case of the three cases

137

n = modular ratio

P = steel ratio

k = distance from apex of compression area to neutral axis divided by diagonal length θ

D= diagonal length

d = distance from corner to reinforcing bar

These two values can be substituted in the following equations to determine the maximum

compressive strength and tensile strength respectively

$$f_c = \frac{P}{Ca^2}$$

2-528

$$f_s = nTf_c$$

2-529

where a is the side length of cross section and P is force magnitude.
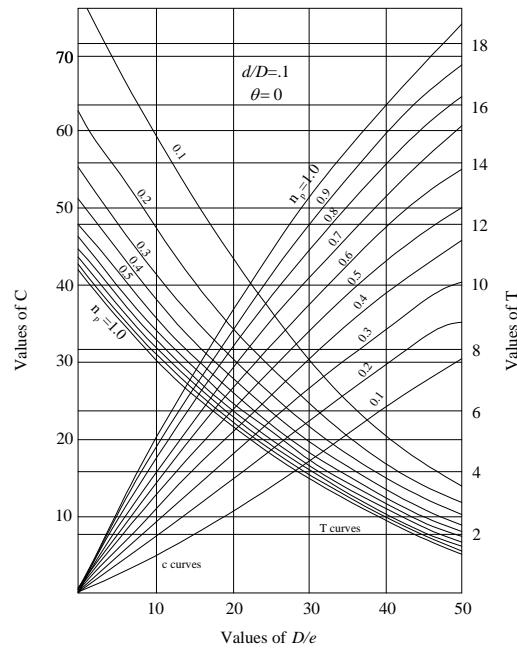
Figure 2-31: relation between T and C by Andersen (1941)

Anderesen (1941) plotted graphs relating T and C; Figure (2-31). It should be noted that the graphs differ with angle θ and the ratio *d/D* variations. Andersen adapted his procedure to fit the 8 bar reinforcement, as well as 16 bar one. That was done by finding the location of the equivalent four bars in the same cross section that yields the same internal moment and moment of inertia.

Reinforced concrete columns under combined compression and bending (Wessman 1946)

Wessman (1946) introduced algebraic method under a condition of the plane of the bending coincides with the axis of symmetry. Based on the elastic theory, Wessman (1946) found that the distance between the applied load and the neutral axis a:

$$a = \frac{I_p}{Q_p}$$
2-530

I_p = moment of inertia of the effective area with respect to the load axis

Q_p = the first moment of the effective area.

The procedure proposed has very limited applicability since it required the applied load lies on the axis of symmetry, which consider a very special case. In addition it relies on the elastic theory.

Analysis of normal stresses in reinforced concrete section under symmetrical bending (Bakhoum 1948)

Using the elastic theory and equating the internal forces and moments to the applied one, Bakhoum (1948) developed procedure in locating the neutral axis. This procedure was set for uniaxial bending. He also intensified the importance of taking the tensioned concrete into account while analyzing.

$$H' = \frac{i + \alpha_1}{s + \beta_1}$$

2-531

$$H' = \frac{H}{t}$$

2-532

$$i = \frac{nI_{ps}}{bt^3}$$

2-533

$$s = \frac{nS_{ps}}{bt^2}$$

2-534

H = distance between the load and the neutral axis

N = modular ratio

b = section width

t = section height

I_{ps} = Moment of inertia of the total reinforcement steel about the line parallel to the neutral axis through the point of application of the external force.

S_{ps} = Statical moment of the total reinforcement steel about the line parallel to the neutral axis through the point of application of the external force.

The relation between α and β is plotted graphically; Figure (2-32).
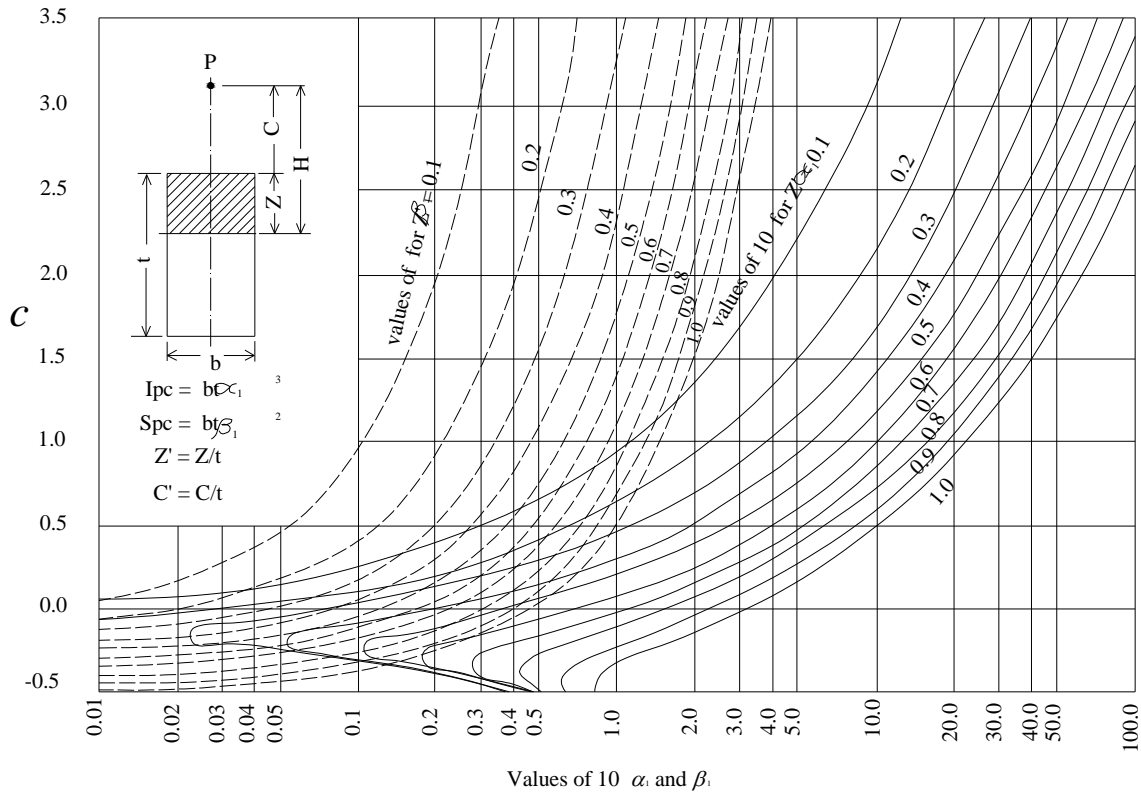
Figure 2-32: relation between c and α by Bakhoum (1948)

For the case of unsymmetrical bending, Bakhoum (1948) suggested three solutions; methods of center of action of steel and concrete, product of inertia method and method of mathematical successful trial. It is noted that the first two methods are trial and error methods, and all the three methods were built on the elastic linear theory.

Design of rectangular tied columns subjected to bending with steel in all faces (Cervin 1948)

The Portland cement association published "continuity in concrete frames" (third edition) that has an equation that relates the maximum load to the actual applied load and moment. It can be applied on a cross section:

141

$$P = N + CD\frac{M}{t}$$

2-535

P = total allowable axial load on column section

N= actual axial load on column section

M = moment

T = section height

$$C = \frac{f_a}{0.45f_c'}$$

2-536

f_a = the average allowable stress on axially loaded reinforced concrete column

$$D = \frac{t^2}{2R^2}$$

2-537

R = radius of gyration

This equation is limited to reinforcement on the end faces. Crevin (1948) redefined the term D in the equation to fit reinforcement in the four faces as follow

$$D = \frac{1+(n-1)p}{0.167+(x+yz^2)(n-1)pg^2}$$

2-538

$$n = \frac{E_s}{E_c}$$

2-539

p = reinforcement ratio

g = ratio between extremities of column steel and overall column depth

x = ratio of total column steel at one end

y = ratio of total column steel between centroid and one end

z = arm from cetroid of steel ratio y to centroid of column
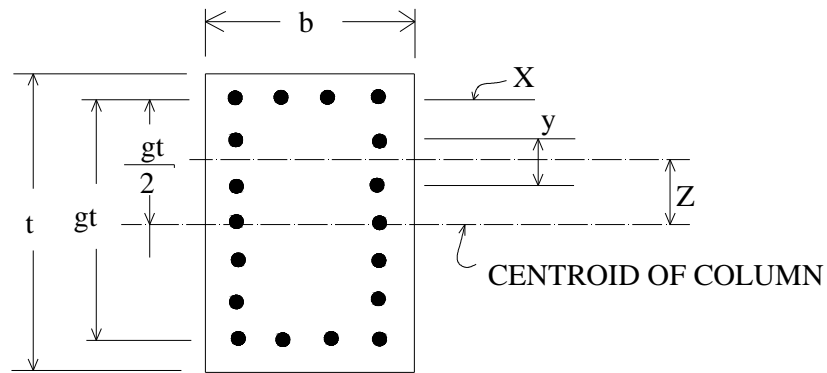
Figure 2-33: geometric dimensions in Crevin analysis (1948)

He showed that $x+yz^2$ vary from 0.25 to 0.5. The limitation of this equation applicability is that the ratio *e/t* has to be less than one.

The strength of reinforced concrete members subjected to compression and unsymmetrical bending (Mikhalkin 1952)

Mikhalkin (1952) performed studies on determination of the allowable load and ultimate load of biaxially loaded rectangular members. He developed design and analysis procedure for tension and compression failure according to ultimate theory, as he generated charts for design simplification based on the elastic theory using simple compatibility equations; Figure (2-34) and (2-35). These charts locate the concrete and steel centers of pressure with respect to the neutral axis.
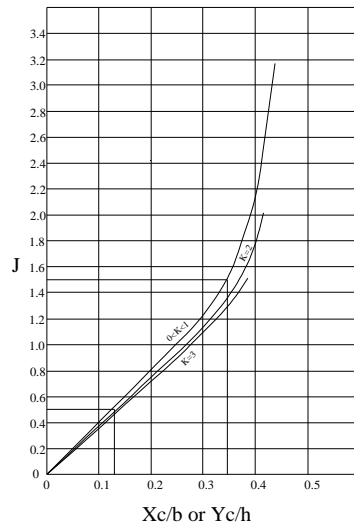
Figure 2-34: Concrete center of pressure Vs neutral axis location ,Mikhalkin 1952
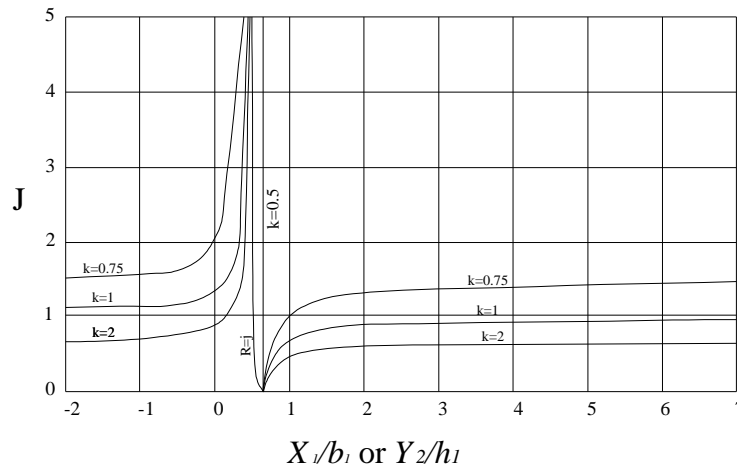
Figure 2-35: Steel center of pressure Vs neutral axis location, Mikhalkin 1952

Eccentric bending in two directions of rectangular concrete columns (Hu 1955)

Hu (1955) followed the elastic assumption in building his analysis. He showed numerically that the slope of the neutral axis for non homogeneous section can be replaced by that of homogeneous one with small error percentage. He found algebraically the equilibrium equations

144

$$\frac{N}{bdf_c} = \frac{chk}{6} - np\left(\frac{1}{2h} + \frac{1}{2k} - 1\right)$$

2-540

$$f_s = nf_c\left(1 - \frac{1-a_x}{h} - \frac{1-a_y}{k}\right)$$

2-541

$$\frac{N}{bdf_c}e_y\left(1+m^2\right) = \frac{chk}{6}\left[m\left(\frac{1}{2} - c_b\right) + \left(\frac{1}{2} - c_d\right)\right] + \frac{Qnp}{12k}$$

2-542

$$Q = \left(m^2nq_x + nq_y\right)/(np)$$

2-543

N = the normal compressive force

b = section width

d = section height

f_c = maximum concrete strength

h and k define the position of the neutral axis

c, c_b, c_d coefficients (functions of h)

A_x = cover in x direction coefficient

A_b = cover in y direction coefficient

e_x = load eccentricity from the geometric centroid (in x-direction)

e_y = load eccentricity from the geometric centroid (in y-direction)

$$n = \frac{E_s}{E_c}$$

2-544

$$p = \frac{A_s}{A_c}$$

2-545

$$q_x = \frac{I_{sx}}{I_{cx}} \qquad\qquad q_y = \frac{I_{sy}}{I_{cy}}$$

2-546

$$m = \frac{e_x}{e_y}$$

<div align="right">2-547</div>

The previous equations are plotted graphically to obtain the unkown values k, n/bdf'_c, Figure (2-36)
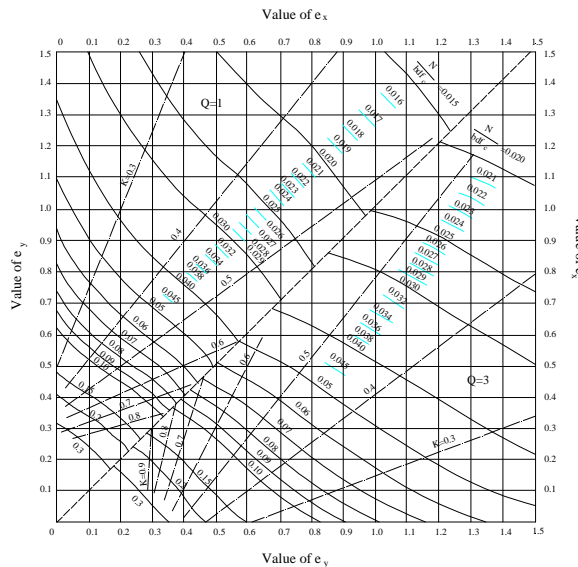
Figure 2-36: bending with normal compressive force chart $np = 0.03$, Hu (1955)

In his paper the graphs were plotted with different values of np 0.03,0.1 ,0.3.

The first obvious interest in the ultimate strength of the structural members appeared in the first half of the past century. Prior to that, there were some designations to the importance of designing with ultimate strength. While Thullies's flexural theory (1897) and Ritter's introduction of the parabolic distribution of concrete stresses (1899) were introduced prior to the straight line theory of Coignet and Tedesco (1900). The straight line theory became accepted due to its simplicity and the agreement with the tests' requirements that time. Coignet's theory grew widely till it was contradicted by some experimental work done on beams by Lyse, Slatter and Zipprodt in 1920's, and on columns by McMillan (1921), as the concrete's construction

applicability was spreading out (ACI-ASCE committee 327(1956)).. After 1950 there was a call to start working with the ultimate strength design as it was adopted in several countries in Europe and others, as the reinforced concrete design has advanced. This led the ACI-ASCE committee 327 to propose the first report on ultimate strength design in 1956 (ACI-ASCE committee 327(1956)). The committee members showed in their studies that the ultimate strength design load can be found accurately.

They defined the maximum load capacity for concentric load

$$P_o = 0.85 f_c^{'}(A_g - A_{st}) + A_{st} f_y$$

2-548

A_g = the gross area of the section.

A_{st} = steel bars area

The committee considered minimum eccentricity value to design with. For tied columns the value was 0.1 times the section's depth.

For combined axial load and bending moment

$$P_u = 0.85 f_c^{'} b d k_u k_1 + A_s^{'} f_y - A_s f_s$$

2-549

$$P_u e = 0.85 f_c^{'} b d^2 k_u k_1 \left(1 - \frac{k_2}{k_1} k_u k_1\right) + A_s^{'} f_y d \left(1 - \frac{d^{'}}{d}\right)$$

2-550

P_u = axial load on the section

e = eccentricity of the axial load measured from the centroid of tensile reinforcement.

f_s = stress in the tensile reinforcement.

dk_u = distance from extreme fiber to neutral axis, where k_u is less than one

k_1 = ratio of the average compressive stress to 0.85 $f_c^{'}$, where k_1 is not greater than 0.85 and is to be reduced at the rate of 0.5 per 1000 psi for concrete strength over 5000 psi.

k_2 = ratio of distance between extreme fiber and resultant of compressive stresses to distance between extreme fiber and the neutral axis.

$\dfrac{k_2}{k_1}$ should not be taken less than 0.5.

After ultimate strength design was released, the ACI committee 318 in their "Building code requirements for reinforced concrete (ACI 318-56)" approved the usage of the ultimate strength method for designing reinforced concrete members along with the standard method in 1956. They conditioned that:

$$\frac{f_a}{F_a} + \frac{f_{bz}}{F_b} + \frac{f_{by}}{F_b} \leq 1 \qquad \qquad \text{2-551}$$

Given that the ratio *e/t* does not exceed 2/3 where

f_{by} = the bending moment about y-axis divided by section modulus of the transformed section relative to y-axis.

f_{bz} = the bending moment about y-axis divided by section modulus of the transformed section relative to y-axis.

e = eccentricity of the load measured from the geometric centrod

t = overall depth of the column

f_a = nominal axial unit stress.

f_b = allowable bending unit stress = $0.8 * \left(0.225 f_c' + f_s p_g\right)$

p_g = steel ratio to the gross area.

f_s = nominal allowable stress in reinforcement.

Guide for ultimate strength design of reinforced concrete (Whitney and Cohen 1957)

Following this massive change in paradigm, Charles Whitney and edward cohen released their paper " guide for ultimate strength design of reinforced concrete" which served as a supplement to the ACI building code (318-56). They suggested a linear relationship between the case of the pure bending and that of concentric load in the following equation

$$\frac{M_u}{M_o} = \frac{P_o - P_u}{P_o}$$
2-552

M_u = total moment of the plastic centroid of the section.

P_o = ultimate direct load capacity for a concentrically loaded short column.

P_u = ultimate direct load capacity for an eccentrically loaded short column.

M_o = the moment capacity without thrust as controlled by compressin assuming enough tensile steel to develop it in full and it is equal to

$$M_o = 0.333bd^2 f_c' + A_s' f_y' (d - d')$$
2-553

They limited the maximum moment allowed for design to M_u using the following equation

$$\frac{M_u}{bd^2} = 0.306 f_c' + p' f_y' \left(1 - \frac{d'}{d}\right)$$
2-554

$$f_y' = f_y - 0.85 f_c'$$
2-555

$$p' = A_s' / bd$$
2-556

A_s' = compressive steel area.

d = distance from extreme compressive fiber to centroid of tension force in tensile reinforcement.

d' = distance from extreme compressive fiber to centroid of tension force in compressive reinforcement.

b = column width.
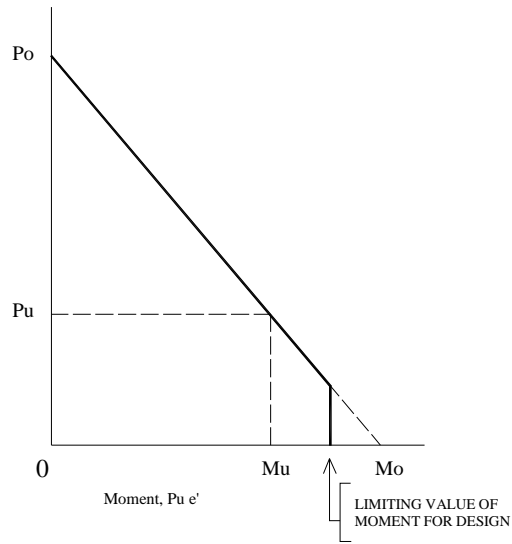
Figure 2-37: Linear relationship between axial load and moment for compression failure

Whitney and Cohen 1957

Ultimate strength design of rectangular concrete members subjected to unsymmetrical bending (Au 1958)

Au (1958) generated Charts to calculate the equivalent compressive depth of the stress block based on assumed values of section's dimensions and bars arrangements. The design equations were created complying with the ACI-ASCE assumptions.

He showed that when a member is subjected to compressive force as well as bending, the section can be controlled either by tension or compression failure depending on the magnitude of eccentricities.

His procedure is to first approximate the location of the neutral axis that can be made by observing that the applied load, the resultant of the tensile force in steel and the resultant of the

150

compressive forces in compressive steel and concrete must all lie in the same plane. This classifies the problem as one of the three cases:

1- Neutral axis intersects with two opposite sides

2- Neutral axis intersects with two adjacent sides forming a compression zone bigger than half of the cross sectional area

3- Neutral axis intersects with two adjacent sides forming a compression zone smaller than half of the cross sectional area

Equilibrium equations plus compatibility equations are needed when the section is controlled by compression (concrete crush). Whereas, equilibrium equations are sufficient in tension controlled cases. Tung specified two conditions based on ACI-ASCE report, that are the average stress f_s is assigned to each tensioned bar and the resultant tensile force is considered the tensile bar group centroid. Based on that, the bars close to the neutral axis are ignored in computations. Having equilibrium equations, Tung denoted six dimensionless variables, two for each case of the three cases mentioned above and plotted charts relating each two associated variables Figures (2-38, 2-39 & 2-40). The charts generated have an output of determining the neutral axis position. The dimensionless variables utilized are:

$$c_1 = \left(\frac{t}{d_y}\right)^2 \left[-p'm'\left(\frac{d_y}{t} - \frac{d'_y}{t}\right) + \frac{P_u}{0.85 f_c bt}\left(\frac{r_y}{t} + \frac{e'_y}{t}\right)\right]$$

2-557

$$c_2 = \left(\frac{t}{d_y}\right)\left[-p'm'\left(\frac{d_x}{b} - \frac{d'_x}{b}\right) + \frac{P_u}{0.85 f_c bt}\left(\frac{r_x}{b} + \frac{e'_x}{b}\right)\right]$$

2-558

$$Q_1 = \left(\frac{2bt^2}{d_x d_y^2}\right)\left[p'm'\left(\frac{d_y}{t} - \frac{d'_y}{t}\right) - \frac{P_u}{0.85 f_c bt}\left(\frac{r_y}{t} + \frac{e'_y}{t}\right)\right]$$

2-559

$$Q_2 = \left(\frac{2b^2 t}{d_x^2 d_y}\right)\left[p'm'\left(\frac{d_x}{b} - \frac{d'_x}{b}\right) - \frac{P_u}{0.85 f_c bt}\left(\frac{r_x}{b} + \frac{e'_x}{b}\right)\right]$$

2-560

$$U_1 = \frac{r_y}{t} - p'm'\left(\frac{d_y}{t} - \frac{d'_y}{t}\right) + \frac{P_u}{0.85 f_c bt}\left(\frac{r_y}{t} + \frac{e'_y}{t}\right)$$

2-561

$$U_2 = \frac{r_x}{b} - p'm'\left(\frac{d_x}{b} - \frac{d'_x}{b}\right) + \frac{P_u}{0.85 f_c bt}\left(\frac{r_x}{b} + \frac{e'_x}{b}\right)$$

2-562
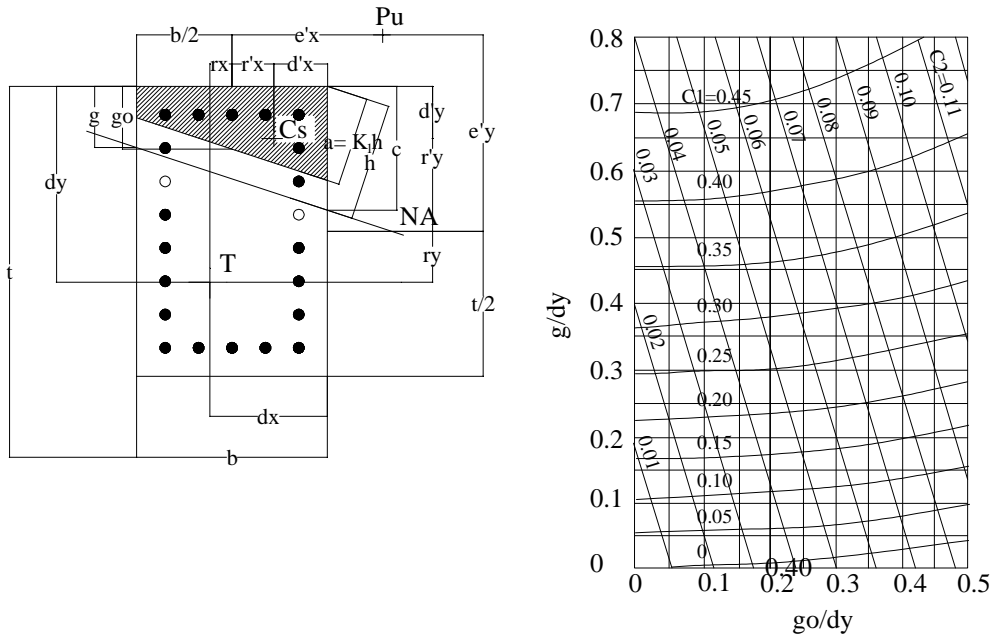
Figure 2-38: section and design chart for case 1(rx/b = 0.005), Au (1958)

152
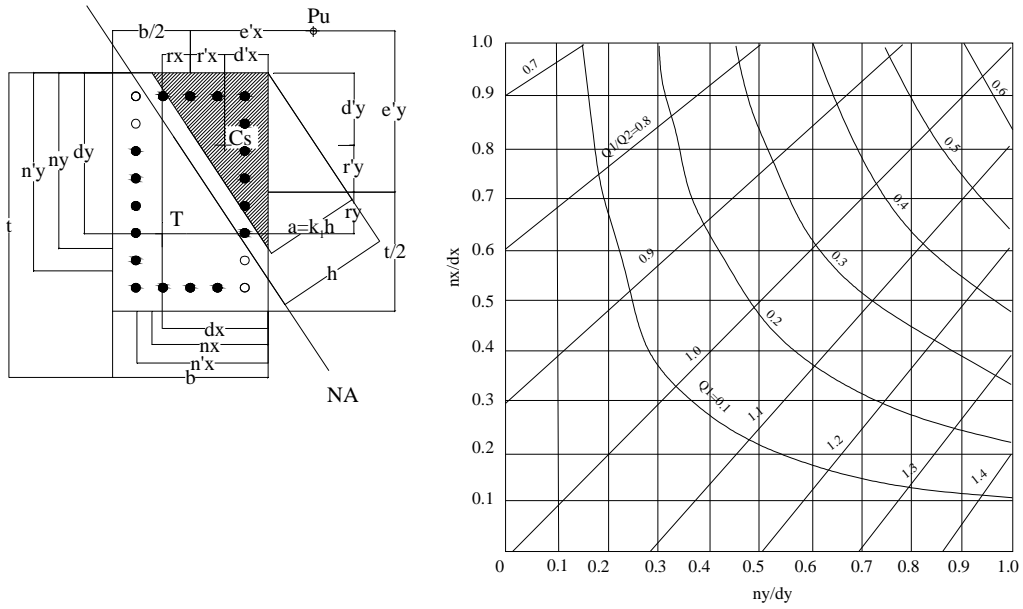
Figure 2-39: section and design chart for case 2, Au (1958)
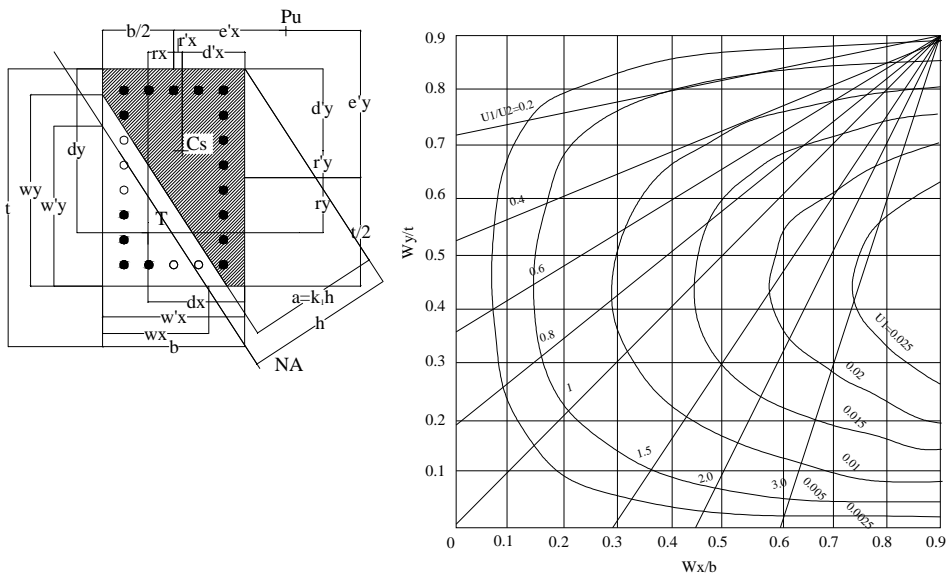
Figure 2-40: section and design chart for case 3($d_x/b = 0.7$, $d_y/t = 0.7$), Au (1958)

153

t = total depth of rectangular section

d_y = distance from extreme compressive corner to centroid of tensile reinforcement measured in the direction of y-axis

$p' = A'_s/bt$

b = width of rectangular section

$m' = m-1$, $m = f_y/0.85f'_c$

d'_y = distance from extreme compressive corner to centroid of compressive reinforcement measured in the direction of y-axis.

P_u = ultimate direct load capacity for the member subject to bending in two directions

r_y = distance from centroid of tensile reinforcement to x'-axis.

r_x = distance from centroid of tensile reinforcement to y'-axis.

e'_y = eccentricity of ultimate direct load measured from centroid of rectangular section in the direction of y-axis

d'_x = distance from extreme compressive corner to centroid of compressive reinforcement measured in the direction of x-axis

d_x = distance from extreme compressive corner to centroid of tensile reinforcement measured in the direction of x-axis

e'_x = eccentricity of ultimate direct load measured from centroid of rectangular section in the direction of x-axis.

<u>Design of symmetrical columns with small eccentricities in one or two directions (Wiesinger 1958)</u>

Using the section moment of inertia and the section modulus, Wiesinger (1957) introduced a new designing equation for the gross sectional area required by design for columns

subjected to small eccentricities in one direction or two. Wiesinger (1957) proposed gross section equation:

$$A_g = \frac{N}{Q\left[0.225f_c' + f_s p_g\right]} + \frac{Ne'/t}{F_b\left[\alpha_g + \alpha_s(n-1)g^2 p_g\right]}$$

2-563

and the capacity of a given column is calculated using the following equation

$$N = \frac{1}{\dfrac{1}{Q\left[0.225f_c' + f_s p_g\right]} + \dfrac{e'/t}{F_b\left[\alpha_g + \alpha_s(n-1)g^2 p_g\right]}}$$

2-564

$$\alpha_g = \frac{2I_g}{t^2 A_g}$$

2-565

$$\alpha_s = \frac{2I_s}{(gt)^2 A_s}$$

2-566

A_g = gross area

A_s = Steel area

t = column length in the direction of bending

I_g = gross moment of inertia in the bending direction

I_s = moment of inertia of steel in the bending direction

e' = eccentricity of the resultant load measured to center of gravity

N = applied axial load

Q = reduction factor = 0.8 for short tied column

$p_g = A_s/A_g$

F_b = allowable bending unit stress that is permitted if bending stress existed = $0.45 f'_c$

G = center to center steel in the direction of bending divided by column length in the direction of bending

<u>Biaxially loaded reinforced concrete columns (Chu and Pabarcius 1958)</u>

In 1958 Chu and Pabarcuis introduced a new numerical procedure to determine the actual stresses for a give section. Their procedure was based on the inelastic theory showed earlier by Hogenstad. Initially, they assumed the cross section is in the elastic range, and assumed a location for the neutral axis. Then used the following formula that was found by Hardy Cross (1930), to solve for stresses

$$f = \frac{P''}{A_E} + \frac{M''_{oy} - M''_{ox}\dfrac{I_{oxy}}{I_{ox}}}{I_{oy} - \dfrac{I^2_{oxy}}{I_{ox}}} X + \frac{M''_{ox} - M''_{oy}\dfrac{I_{oxy}}{I_{ox}}}{I_{ox} - \dfrac{I^2_{oxy}}{I_{oy}}} Y \qquad \text{2-567}$$

f = stress

A_e = Area of the elastic portion.

I_{ox} = moment of inertia about x-axis

I_{oy} = moment of inertia about y axis

I_{oxy} = product of inertia

M''_{oy} =moment of the elastic portion about the y axis

M''_{ox} =moment of the elastic portion about the x axis

P'' = axial force taken by the elastic portion.

If the concrete and steel stresses lie in the elastic range, the above equation was used to locate a new position for the neutral axis, and comparing it with the assumed one. The whole process is repeated till the position of the calculated neutral axis coincides with the assumed one. On the other hand if any of the concrete or steel are beyond the elastic range, the plastic load and

156

moments are calculating, then deducted from the total load and moments. The reminder is used, as the elastic portion of the load, to locate the neutral axis.

Design criteria for reinforced columns under axial load and biaxial bending (Bresler 1960)

Bresler (1960) proposed a new approach of approximations of the failure surface in two different forms. He showed the magnitude of the failure load is a function of primary factors; column dimensions, steel reinforcement, stress-strain curves and secondary factors; concrete cover, lateral ties arrangement. He introduced two different methods. The first method named reciprocal load method

$$\frac{1}{P_i} = \frac{1}{P_x} + \frac{1}{P_y} - \frac{1}{P_o}$$

2-568

P_i =approximation of P_u

P_x = load carrying capacity in compression with uniaxial eccentricity x.

P_y = load carrying capacity in compression with uniaxial eccentricity y.

P_u = load carrying capacity under pure axial compression

The second method is the load contour

$$\left(\frac{M_x}{M_{xo}}\right)^\alpha + \left(\frac{M_y}{M_{yo}}\right)^\beta = 1$$

2-569

and this can be simplified to

$$\left(\frac{y}{y_o}\right)^\alpha + \left(\frac{x}{x_o}\right)^\beta = 1$$

2-570

By equating α and β for more simplification the interaction diagram can be plotted as shown in Figure (2-43)

157

Bresler (1960) well correlated equation (2-570) to experimental studies formed from eight columns, and analytically showed the strength criteria can be approximated by

$$\left(\frac{y}{y_o}\right)^{\alpha} + \left(\frac{x}{x_o}\right)^{\alpha} = 1$$

2-571
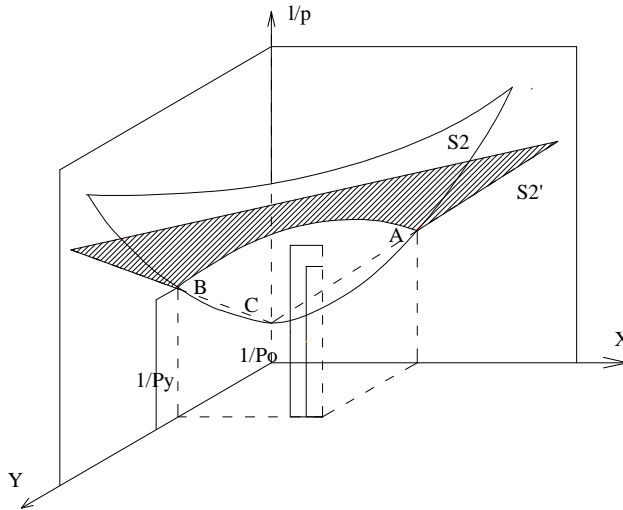
Figure 2-41: Graphical representation of Method one by Bresler (1960)
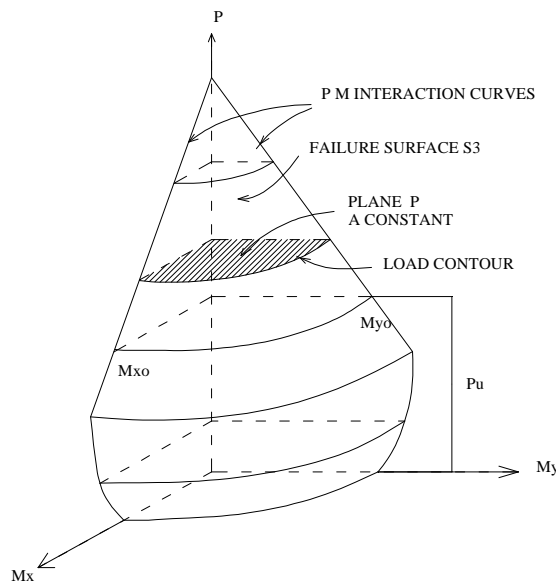
Figure 2-42: Graphical representation of Method two by Bresler (1960)

158
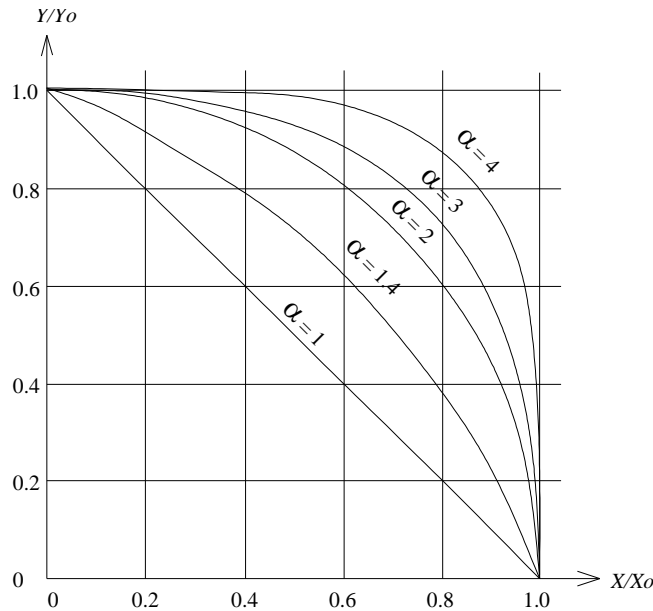
Figure 2-43: Interaction curves generated from equating α and by Bresler *(1960)*

Rectangular concrete stress distribution in ultimate strength design (Mattock and Kritz 1961)

Mattock and Kritz (1961) determined five cases for the position of the neutral axis with respect to the rectangular cross section; when the neutral axis cut through two adjacent sides with small and big compression zone, the neutral axis intersect with the section length or width and when it lies outside the cross section.

They implemented formulas for calculating the position of the neutral axis based on the load and moment equilibrium and the geometry of the compression zone.

Square columns with double eccentricities solved by numerical methods (Ang 1961)

Ang (1961) introduced a numerical method to solve the problem. He proposed iterative process to find equilibrium between internal forces and applied ones, by assuming a position for the neutral axis. The location of the neutral axis kept changing till equilibrium. However, he

159

calculated stresses based on Bernoulli's plane theorem which was built upon straight line theory (elastic theory). The stress of the extreme compression fiber was approximately calculated according to the specification of AASHTO 1957 "Standard specifications for highway bridges".

Ultimate strength of square columns under biaxially eccentric load (Furlong 1961)

Furlong (1961) analyzed square columns that have equal reinforcement in the four sides and reinforcement in two sides only, to visualize the behavior of rectangular columns that has unsymmetrical bending axis. He used a series of parallel neutral axis with the crushing ultimate strain of 0.003 at one of the section corners to develop a full interaction diagram at one angle. And by using different angles and locations of the neutral axis a full 3D interaction surface can be developed. He was the first to introduce this procedure.

Furlong (1961) concluded that the minimum capacity of a square column, having equal amount of steel in all sides, exists when the load causes bending about an axis of 45 degree from a major axis. He also concluded that

$$\left(\frac{m_x}{M_x}\right)^2 + \left(\frac{m_y}{M_y}\right)^2 < 1$$

2-572

M_x = moment component in direction of major axis.

M_y = moment component in direction of minor axis.

M_x = moment capacity when the load acts along the major axis.

M_y= moment capacity when the load acts along the minor axis.

<u>Tie requirements for reinforced concrete columns (Bresler and Gilbert 1961)</u>

Bresler (1961) introduced the importance of the tie confinement in columns as objects to hold the longitudinal bars in place and prevent them from buckling after the cover spalling off. No concrete strength improvement was discussed.

<u>Analytical approach to biaxial eccentricity (Czerniak 1962)</u>

Czerniak (1962) proved that the slope of the neutral axis is depending on the relative magnitude of moment about the X axis to the moment about the Y axis and the geometry of the sections and it is independent of the magnitude of bending moment and the applied force for the elastic range. According to the effective compressive concrete, Czerniak (1962) determined five cases based on the location of the neutral axis, Figure (2-44).

(a)　　　　(b)　　　　(c)　　　　(d)　　　　(e)
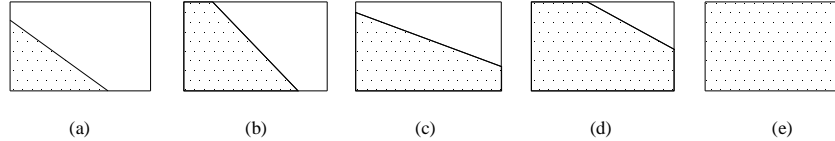
Figure 2-44: five cases for the compression zone based on the neutral axis location Czerniak (1962)

He developed an iterative procedure for locating the neutral axis position for a given cross section, by using equations (2-557 and 2-558) to determine the initial position of the neutral axis

$$a = \frac{\left(I_{xy} - Y_p Q_{oy}\right)\left(I_{xy} - X_p Q_{ox}\right) - \left(I_{ox} - Y_p Q_{ox}\right)\left(I_{oy} - X_p Q_{oy}\right)}{\left(Q_{ox} - Y_p A\right)\left(I_{xy} - X_p Q_{ox}\right) - \left(Q_{oy} - X_p A\right)\left(I_{ox} - Y_p Q_{ox}\right)}$$

2-573

$$b = \frac{\left(I_{xy} - Y_p Q_{oy}\right)\left(I_{xy} - X_p Q_{ox}\right) - \left(I_{ox} - Y_p Q_{ox}\right)\left(I_{oy} - X_p Q_{oy}\right)}{\left(Q_{ox} - X_p A\right)\left(I_{xy} - Y_p Q_{oy}\right) - \left(Q_{ox} - Y_p A\right)\left(I_{oy} - X_p Q_{oy}\right)}$$

2-574

161

a = x-intercept of the neutral axis line

b = y-intercept of the neutral axis line

I_{xy} = elastic product of inertia of the area about the origin

I_{ox} = elastic moment of inertia of the area about the x-axis

I_{oy} = elastic moment of inertia of the area about the y-axis

Q_{ox} = moment area about x-axis (within elastic region)

Q_{oy} = moment area about y-axis (within elastic region)

A = area of transformed section (within elastic regions)

Y_p = y-coordinate of the applied eccentric load

X_p = x-coordinate of the applied eccentric load

then calculating the new section properties, effective concrete and transformed steel, and finding

the new values of X_p and Y_p.

$$Y_p = \frac{\left(\overline{y} - \dfrac{r_{xy}^2}{a} - \dfrac{r_{ox}^2}{b} \right)}{\left(1 - \dfrac{\overline{x}}{a} - \dfrac{\overline{y}}{b} \right)} \qquad\qquad 2\text{-}575$$

$$X_p = \frac{\left(\overline{x} - \dfrac{r_{oy}^2}{a} - \dfrac{r_{xy}^2}{b} \right)}{\left(1 - \dfrac{\overline{x}}{a} - \dfrac{\overline{y}}{b} \right)} \qquad\qquad 2\text{-}576$$

and solving for a, b again and repeat the procedure up till convergence.

162

As for ultimate strength design, Czerniak (1962) proved with some simplification that the neutral axis is parallel to concrete plastic compression line and steel plastic tension and compression line, so they can be found by multiplying the location of the neutral axis by some values. The ultimate eccentric load and its moment about x and y axis can be found from:

$$P_u = f_o\left[A_u' - \frac{Q_{oy}}{a} - \frac{Q_{ox}}{b}\right]$$

2-577

$$M_{ux} = f_o\left[Q_{ux}' - \frac{I_{xy}}{a} - \frac{I_{ox}}{b}\right] = P_u Y_p$$

2-578

$$M_{uy} = f_o\left[Q_{uy}' - \frac{I_{oy}}{a} - \frac{I_{xy}}{b}\right] = P_u X_p$$

2-579

$$Q_{ux}' = Q_{ox} + \alpha\left[Q_{xc} + (m-1)Q_{xs}' - mQ_{xs}\right]$$

2-580

$$Q_{uy}' = Q_{oy} + \alpha\left[Q_{yc} + (m-1)Q_{ys}' - mQ_{ys}\right]$$

2-581

f_o = stress intensity at the origin

and the x-axis and y-axis intercept of the neutral axis are found:

$$a = \frac{\left(I_{xy} - Y_p Q_{oy}\right)\left(I_{xy} - X_p Q_{ox}\right) - \left(I_{ox} - Y_p Q_{ox}\right)\left(I_{oy} - X_p Q_{oy}\right)}{\left(Q_{ux}' - Y_p A_u'\right)\left(I_{xy} - X_p P_{ox}\right) - \left(Q_{uy}' - X_p A_u'\right)\left(I_{ox} - Y_p Q_{ox}\right)}$$

2-582

$$b = \frac{\left(I_{xy} - Y_p Q_{oy}\right)\left(I_{xy} - X_p Q_{ox}\right) - \left(I_{ox} - Y_p Q_{ox}\right)\left(I_{oy} - X_p Q_{oy}\right)}{\left(Q_{uy}' - X_p A_u\right)\left(I_{xy} - Y_p Q_{oy}\right) - \left(Q_{ux}' - Y_p A_u'\right)\left(I_{oy} - X_p Q_{oy}\right)}$$

2-583

where

$$A_u^{'} = A + \frac{f_c^{"}}{f_o}\left[A_{uc} + (m-1)A_{us}^{'} - mA_{us}\right]$$

2-584

$$Q_{ux}^{'} = Q_{ox} + \frac{f_c^{"}}{f_o}\left[Q_{xc} + (m-1)Q_{xs}^{'} - mQ_{xs}\right]$$

2-585

$$Q_{uy}^{'} = Q_{oy} + \frac{f_c^{"}}{f_o}\left[Q_{yc} + (m-1)Q_{ys}^{'} - mQ_{ys}\right]$$

2-586

Q_{xc} = moment of area about x-axis of the plastic portion of the concrete effective section

Q_{yc} = moment of area about y-axis of the plastic portion of the concrete effective section

Q_{xs} = moment of area about x-axis of the plastic portion of the yielded tensile reinforcement

Q_{ys} = moment of area about y-axis of the plastic portion of the yielded tensile reinforcement

$Q_{xs}^{'}$ = moment of area about x-axis of the plastic portion of the yielded compressive reinforcement

$Q_{ys}^{'}$ = moment of area about y-axis of the plastic portion of the yielded compressive reinforcement

$A_u^{'}$ = equivalent plastic transformed area.

A_{uc} = area of concrete under plastic compression

A_{us} = area of yielded tensile reinforcement

$A_{us}^{'}$ = area of yielded compressive reinforcement.

P_u = ultimate strength of eccentrically loaded cross section

M_{ux} = moment of the ultimate load about x-Axis

M_{uy} = moment of the ultimate load about y-Axis

$f_c^{"}$ = maximum concrete stress at ultimate loads (assumed as 0.85 f'_c)

$$m = \frac{f_y}{f_c^{"}}$$

Failure surfaces for members in compression and biaxial bending (Pannell 1963)

Pannell implemented a relation between the failure moment about y-axis for a given load and the *y* component of radial moment with the same load. The formula was found based on deviation study between the actual load contour curve and an imaginary curve found from the revolution of the failure point about y axis, with the same load, about the z axis. The equation found for sections that have equal steel in each face:

$$M_{fy} = \frac{M_y}{1 - N \sin^2 2\theta} \tag{2-587}$$

$$N = 1 - \frac{M_d}{M_{fy}} \tag{2-588}$$

M_{fy} = failure moment for some load in plane y

θ = angle between y and the transformed failure plane

He showed that his formula is more accurate and conservative than that of Bresler. He also developed a chart for N for unequal steel distribution; Figure (2-43).
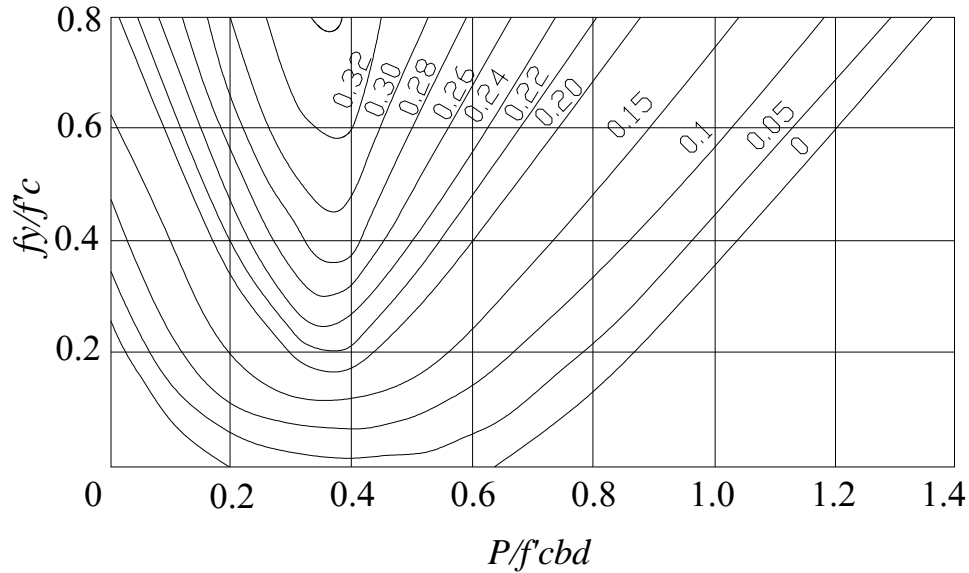
Figure 2-45: Values for N for unequal steel distribution by Pannell (1963)

Ultimate strength of column with biaxially eccentric load (Meek 1963)

Meek (1963) assumed constant ratio of moment about the x-axis and the y-axis. Consequently, increasing the force will increase the moment proportionally.

$$\frac{M_y}{M_x} = \frac{e_x}{e_y} = \alpha = const.$$

2-589

Using the above relation a location of the neutral axis is selected. Then this location is adjusted until the following relation is satisfied

$$P_u = \sum A_c f_c + \sum A_{sc} f_{sc} - \sum A_{st} f_{st}$$

2-590

He also showed set of experimental points correlated well to the theoritical interaction diagram developed.

Biaxial eccentricities in ultimate load design (Aas-Jakobsen 1964)

To comply with local design code, Aas-jakbosen (1964) replaced biaxially eccentric load acts on a regtangular cross section with an equivelant load acts on the main axis of symmetry with an equivelant moment. He showed , using moment and force equilibrium, that the eqivelant moment M_e:

$$M_e = (Pe_x + cM_1)m$$

2-591

$$c = \frac{e_y t_x}{e_x t_y}$$

2-592

$$m = \sqrt{1 + c^2}$$

2-593

The moment M_1 is small additional moment depends on failure mode and some other factors. And in most cases it is equal to zero.

Design of columns subjected to biaxial bending (Fleming and Werner 1965)

Fleming and Werner (1965) utilized the formulas found by Mattock (1961) for locating the neutral axis in the different cases of the compression zone shape along with Furlong (1961) method, by varying the location and inclination angle of the neutral axis, to plot the interaction diagram. Fleming and Werner (1965) plotted dimensionless interaction diagram for a square cross section for fourteen cases using parameters that is commonly used.
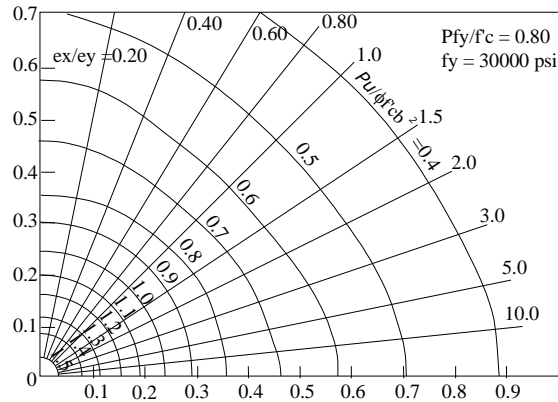
Figure 2-46: design curve by Fleming *et al* (1961)

<u>Investigation of the ultimate strength of square and rectangular column under biaxially eccentric loads (Ramamurthy 1966)</u>

Ramamurthy (1966) proposed a new method for defining the load contour for sections having eight or more bars distributed evenly. He mentioned that the available methods of design of biaxially loaded column are trial and error procedure and determination of ultimate load from failure surface. He showed that columns containing four bars behave differently than those containing eight or more bars with the same reinforcement ratio. He found theoretically for square columns that the neutral axis inclination angle and the angle formed between the load ray and y-axis are almost equal. And the relation between the moment and the moment about x-axis in any load contour level is equal to

$$M_{ux} = M_{uxo}\left(1 - \sin^3 \theta\right)$$

2-594

M_{ux} =ultimate moment about x-Axis

M_{uxo} = uniaxial moment on the same load contour of M_{ux}

θ = inclination of the neutral axis to x-axis angle

Equation (2-594) can be simplified to

168

$$M_u = M_{uxo}(1 - \sin^3 \alpha)\sec\alpha$$

2-595

M_u =ultimate radial load about z axis

and with plotting the previous equation against some actual load contour he found the following relation is more accurate especially for small angle (α)

$$M_u = M_{uxo}\left(1 - 0.1\frac{\alpha}{45}\right)$$

2-596

Similarly for rectangular columns, by finding the transformed shape of the rectangular interaction diagram to the square ones using some similar triangles calculations

$$M_u = M_{uxo}\left(1 - 0.1\frac{\beta}{45}\right)\sqrt{\cos^2 \beta + \frac{\sin^2 \beta}{K^2}}$$

2-597

β = transformed equivalent angle of α

K = transformation factor equal to $= \dfrac{M_{uxo}}{M_{uyo}}$

Also he showed that the upper equation is in good comparison with experimental actual load contour. He plotted the relation between θ and α for different ratios of length to width for rectangular columns.
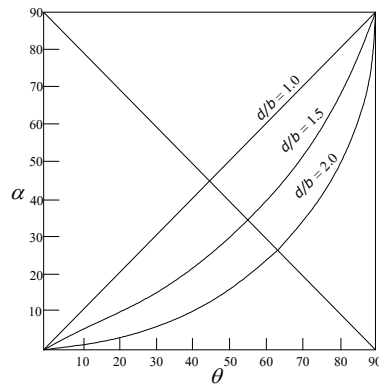
Figure 2-47: relation between α and θ by Ramamurthy (1966)

Capacity of reinforced rectangular columns subjected to biaxial bending (Parme, Nieves, and Gouwens 1966)

Parme *et.al* (1966). suggested relating the biaxial bending to the uniaxial resistance. They restated Bresler equation

$$\left(\frac{M_x}{M_{ux}}\right)^{\frac{\log 0.5}{\log \beta}} + \left(\frac{M_y}{M_{uy}}\right)^{\frac{\log 0.5}{\log \beta}} = 1 \qquad\qquad 2\text{-}598$$

$M_x =$ uniaxial ultimate moment capacity about x-axis

$M_{uy} =$ uniaxial ultimate moment capacity about y-axis

$M_x =$ biaxial bending capacity component about x-axis.

$M_y =$ biaxial bending capacity component about y-axis.

β is a function of reinforcement position, column dimension and the materialistic properties of steel and concrete. Parme *et.al* (1966) used a computer program to obtain values for β. Then β was represented graphically in four charts, Figure (2-49, 2-40, 2-51, 2-52).
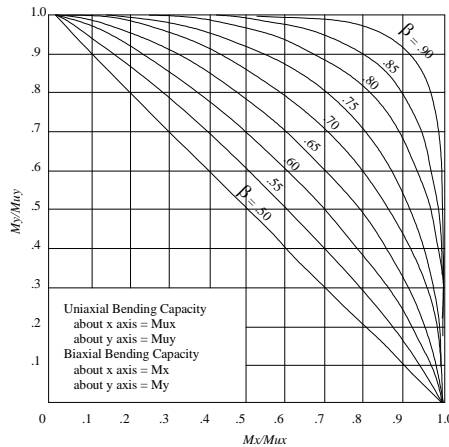
Figure 2-48: biaxial moment relationship by Parme *et al. (1966)*

170
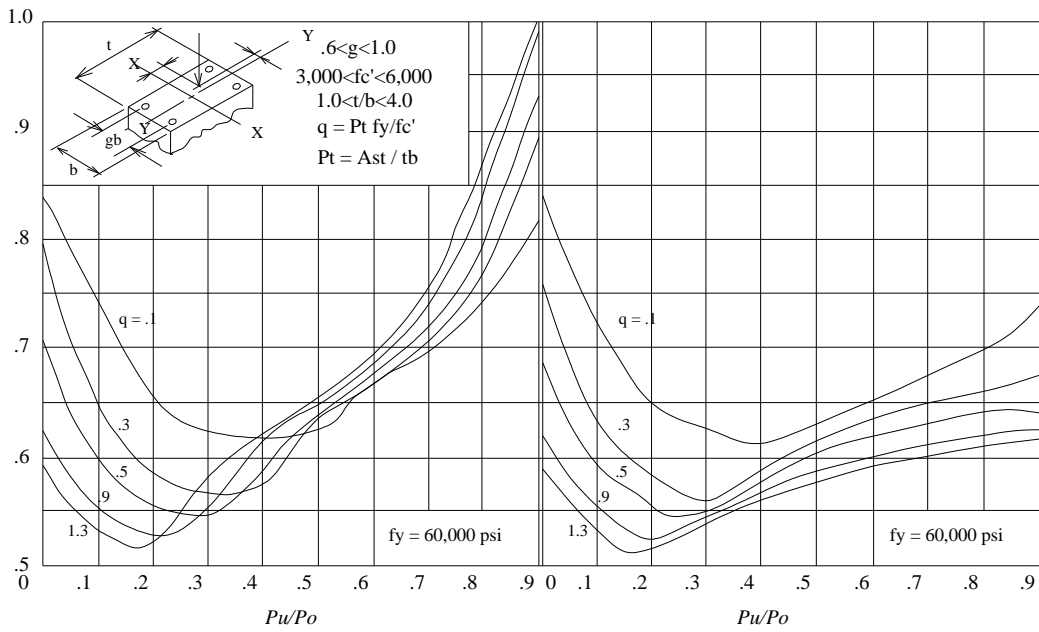
Figure 2-49: Biaxial bending design constant (four bars arrangement) by Parme *et al. (1966)*
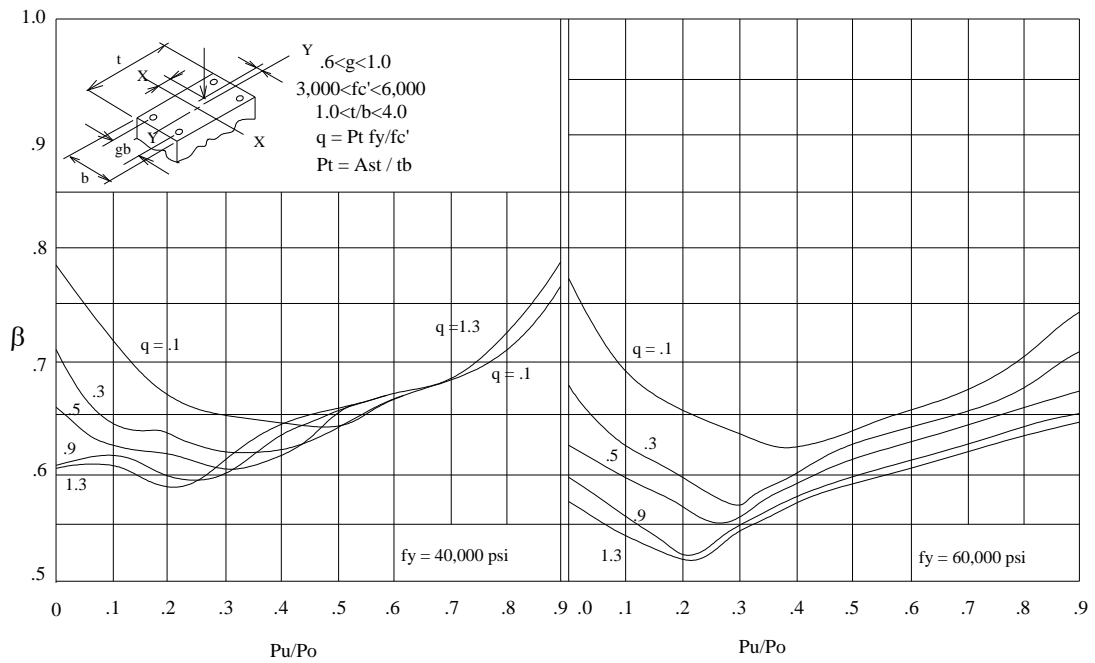
Figure 2-50: Biaxial bending design constant (eight bars arrangement) by Parme *et al. (1966)*

171
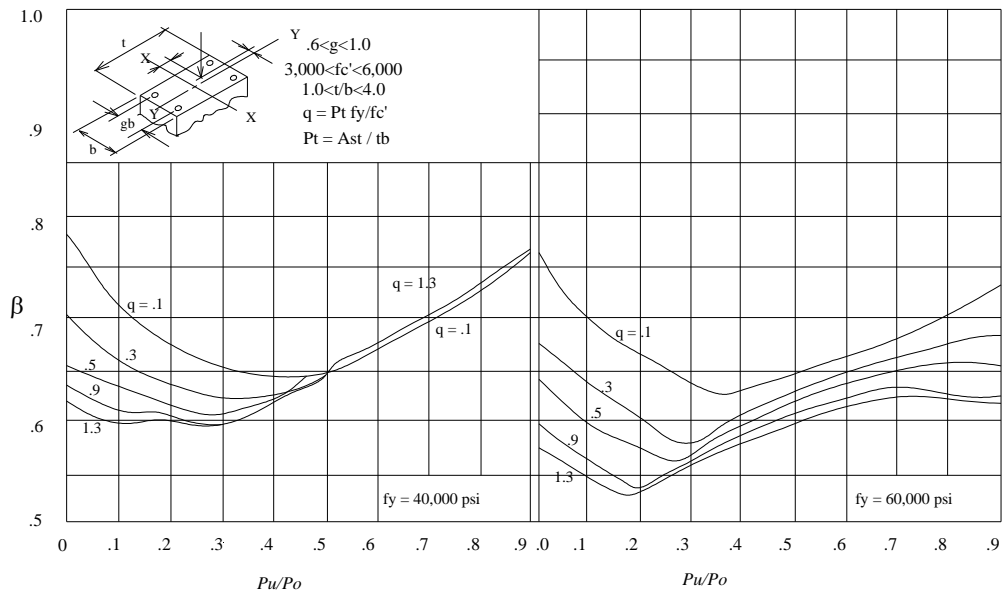
Figure 2-51: Biaxial bending design constant (twelve bars arrangement) by Parme *et al. (1966)*
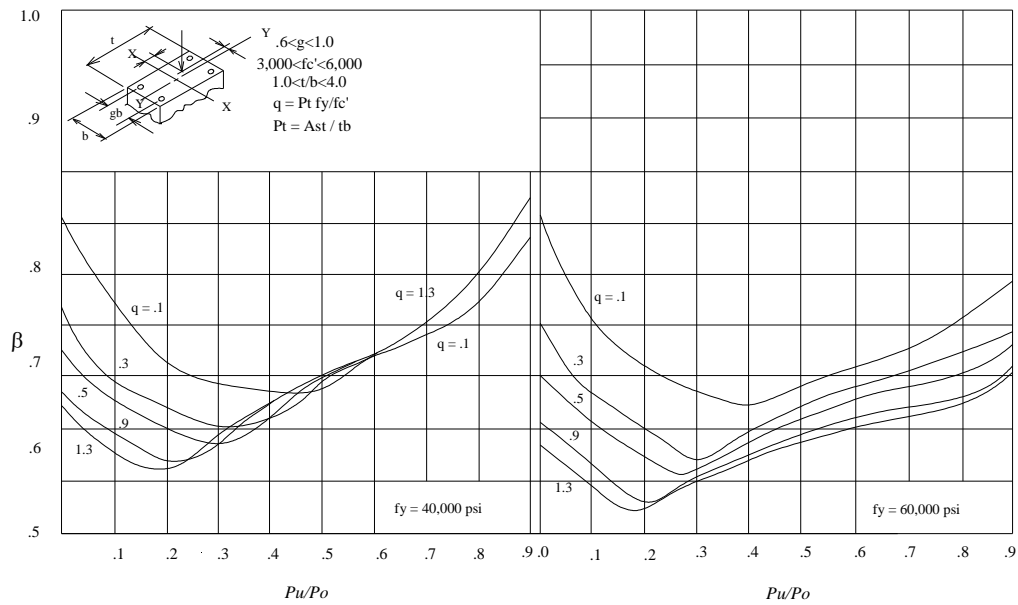
Figure 2-52: Biaxial bending design constant (6-8-10 bars arrangement) by Parme *et al. (1966)*

Parme *et al* (1966) showed agreement between the suggested equations (2-598) and the theoretical one calculated with equilibrium equations. Furthermore, they simplified the

172

exponential representation of the upper equation by introducing two equations for two straight

line starting from My/M_{uy} =1 and $M_x/$ M_{ux} =1 intersecting at the point of equal relative moment

(Figure 2-52). The equations of the two straight lines are as follow:

$$M_y + M_x \frac{M_{uy}}{M_{ux}} \frac{(1-\beta)}{\beta} = M_{uy}$$

2-599

$$M_x + M_y \frac{M_{ux}}{M_{uy}} \frac{(1-\beta)}{\beta} = M_{ux}$$

2-600
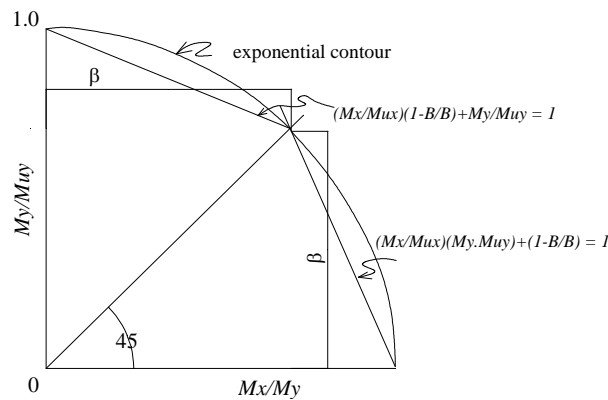
Figure 2-53: Simplified interaction curve by Parme *et al.* *(1966)*

Ultimate strength design charts for columns with biaxial bending (Weber1966)

Based on Furlong conclusion that the most critical bending axes is the 45 degree ones

after the major and minor axes in the case of biaxial bending. Weber (1966) generated sixteen

chart for the 45 degree interaction diagrams for square columns . the columns are having

symmetrical reinforcement with different amount of steel bars. Design aids in the 1970 ACI SP-

17A Handbookl2 and the 1972 CRSI Handbookl3 were based on interaction diagrams developed

be Weber (1966).

Working stress column design using interaction diagrams (Mylonas 1967)

Mylonas (1967) adapted the interaction diagrams charts generated in the ACI Design

handbook (1965), that were mainly for columns subjected to axial load and uniaxial bending and

the steel is distributed on two faces parallel to the bending axis, to fit cases of biaxial bending

and steel distributed along the four faces. Two reduction factors were introduced , one for each

zone (Figure 2-54).
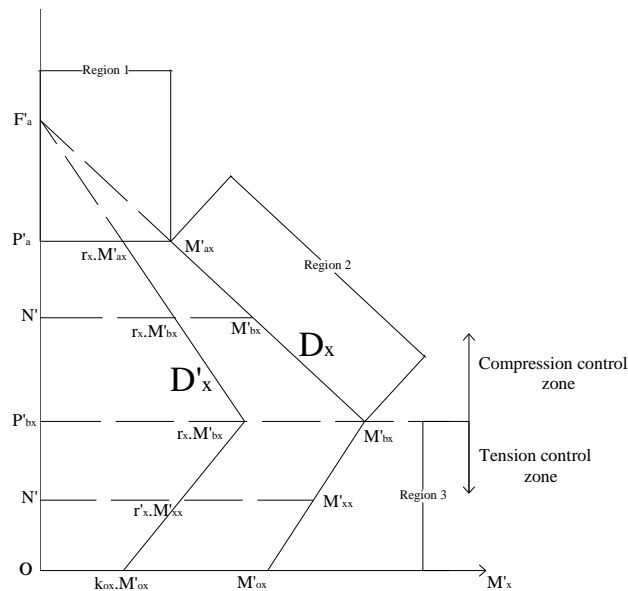
Figure 2-54: Working stress interaction diagram for bending about x-axis by Mylonas (1967)

for zone 2:

$$r_x = \frac{1 + k_x w_x}{1 + w_x}$$

2-601

174

k_x is the momet of the steel distributed on two faces and is equal to

$$k_x = \frac{\sum a_s \lambda_x^2}{\sum a_s (0.5)^2}$$

2-602

$$w_x = 3(2n-1)g_x^2 p_g$$

2-603

g_x =bars center

p_g = steel ratio

a_s = section area of arbitrary bar

λ_x = bar distance from x-axis divided by gx t(section height)

For zone 3

$$r_x' = k_{ox} + \frac{N'}{P_{bx}'}(r_x - k_{ox})$$

2-604

K_{ox} is the moment reduction factor for pure bending about x-axis

$$k_{ox} = \frac{\sum a_s \lambda_x}{\sum a_s (0.5)}$$

2-605

P'_{bx} = load at balance failure

N' = normalized axial load

Mylonas (1967) also suggested that the applied bending moment should be compared to the reduced moment capacity, the moment capacity found from uniaxial bending interaction chart, of the section in form

$$\frac{M'_x}{r_x M'_{xx}} + \frac{M'_y}{r_y M'_{yy}} \leq 1 \qquad\qquad\qquad 2\text{-}606$$

M'_x , M'_y are the applied moment

M'_{xx} , M'_{yy} moment capacity

Comparison of experimental results with ultimate strength theory for reinforced concrete columns in biaxial bending (Brettle and Taylor 1968)

Brettle and Taylor (1968) suggested partitioning the cross section into small size area, and using the limiting strain and the neutral axis position in calculating stresses in each filament using curvilinear stress distribution or rectangular stress distribution or trapezoidal stress distribution for concrete. They generated ultimate strength design charts relating P_u/P_o to e_r/b for different t/b ratios and different inclination angle beween the line conecting the load to the centroid and the x-axis.
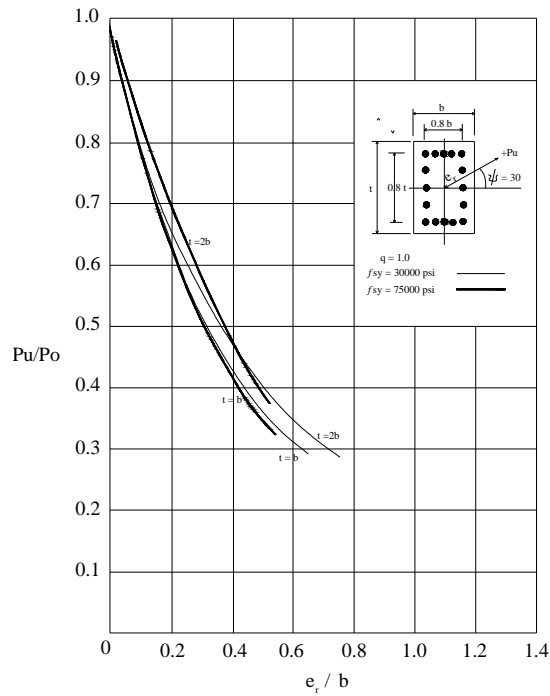
Figure 2-55: Comparison of steel stress variation for biaxial bending when $\psi = 30$ & q = 1.0

Brettle and Taylor (1968)

e_r = resultant eccentricityed

t = section height

b = section width

P_o = theoritical ultimate load with no eccentricities

Pu= theoritical ultimate load with eccentricities

177

Biaxial Flexure and Axial Load Interaction in Short Rectangular Reinforced Concrete Columns (Row and Paulay 1973)

Row and Paulay (1974) introduced six charts relating the m_ϕ to P_u/f'_cbh to facilitate the design process. However these charts are applicable to limited cases only based on the material properties required for design

$$m_\theta = \frac{M_{ux}\sqrt{1+k^2}}{f'_cbh^2}$$
                                                                        2-607

$$k = \frac{M_y}{M_x}$$
                                                                        2-608

Biaxial bending simplified (Gouwens 1975)

Gouwens (1975) proposed simplified analytical equations for design column subjected to biaxial bending. He utilized Parme *et al* (1966) simplified moment equations (2-599 & 2-600). He found that β approaches 1 for $0.25 f'_c$ bh by examining 67 column cases. Based on that he proposed β equations as follow:

For $P \geq 0.25 C_c$

$$\beta = \beta_{25} + 0.2\frac{P/C_c - 0.25}{0.85 + C_s/C_c}$$
                                                                        2-609

For $P < 0.25 C_c$

$$\beta = \beta_{25} + 0.2\left(0.25 - P/C_c\right)^2\left(0.85 + C_s/2C_c\right)$$
                                                                        2-610

$$C_c = f'_cbh \qquad C_s = A_sf_y$$
                                                                        2-611

178

$$\beta_{25} = 0.485 + 0.03\frac{C_c}{C_s} \qquad\qquad \frac{C_c}{C_s} \geq 0.5 \qquad\qquad 2\text{-}612$$

$$\beta_{25} = 0.545 + 0.35\left(0.5 - \frac{C_c}{C_s}\right)^2 \qquad\qquad \frac{C_c}{C_s} < 0.5 \qquad\qquad 2\text{-}613$$

Analysis of Short Rectangular Reinforced Concrete Columns Subjected to Biaxial Moments (Sallah 1983)

Sallah (1983) evaluated the Parameter β, found by Parme *et al* (1966) and found that it was most affected by f_y, f'_c, r, P_u/P_{uo} and less affected by the number of bars. Sallah (1983) introduced number of charts similar to Parme *et al's* (1966) for finding β

Design contour charts for biaxial bending of rectangular reinforced concrete columns using bresler method (Taylor and Ho 1984)

Taylor and Ho (1984) developed a computer program to generate the two main interaction diagrams (with uniaxial bending-one for each axis). These two charts were used to generate the whole biaxial failure surface (and the failure contours)using Bresler equations. Different positions of parallel neutral axis and crushing strain of concrete were used to generate strain profile. The stresses were generated by stress block or other accepted formulas. And forces and moments were calculated. They plotted chart showing the load tracing on the cross section
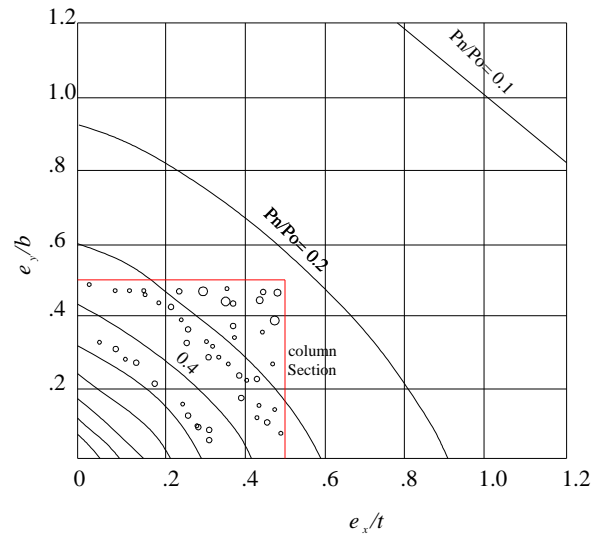
Figure 2-56: Non dimensional biaxial contour on quarter column by Taylor and Ho (1984).

Radial contour method of biaxial short column design (Hartley 1985)

Hartley (1985) proposed two design procedure, one for finding the cross sectional length and the other to calculate the steel reinforcement, given all other desin parametes. He showed an optimum point to exist on the *3 D.* interaction diagram that relates to the smallest area of the cross section. Initially, he showed the relation between the load and eccentricity in the form:

$$\ln\left(\frac{P_u}{P_o}\right) = C\left(\frac{e}{b}\right)$$

2-614

where *c* is a curve constant, *b* is section length and *e* is force eccentricity the initial value of the cross section length can be found by

$$3.58b^2 - \left[3.26 + \ln\left(\frac{P_u}{P_o/A_g} * \frac{b}{t}\right)\right]b + c\left(\frac{M_x}{P_u}\right) = 0$$

2-615

180

Hartley (1985), using computer program, plotted graphically the relation between the cross sectional area and the ratio of P_u/P_o. These charts can be used to determine the suitable length in design
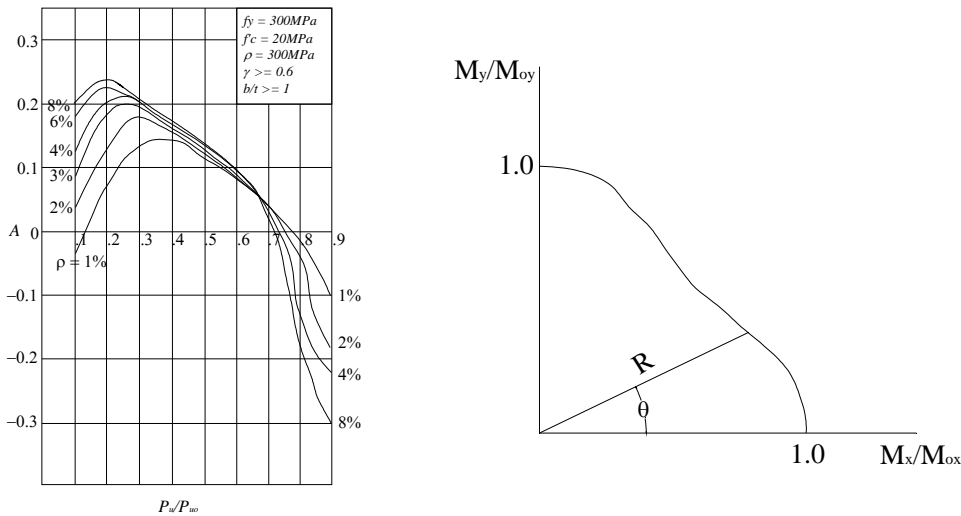
Figure 2-57: P_u/P_{uo} to A relation for 4bars arrangement by Hartley (1985) (left) non dimensional load contour (right)

Hartley (1985) also showed the relation between the R and θ in the load contour by

$$R = 1 - A \sin^n 2\theta$$

2-616

Where R and θ are showen in Figure 2-57 (right).

Expert interactive design of R/C columns under biaxial bending (Sacks snd Buyukozturk 1986)

Sacks and Buyukozturk (1986) developed computer software EIDOCC (Expert interactive design of concrete columns) to analyse and design columns subjected to biaxial bending. The procedure as follow

181

1- Finding the neutral axis location, according to Ramamurthy procedure, such that

$$\tan\left(\frac{e_{uy}}{e_{ux}}\right) = \tan\left(\frac{e_y}{e_x}\right)$$ 2-617

e_{ux} = ultimate eccentricity measured parallel to x-axis

e_{uy} = ultimate eccentricity measured parallel to y-axis

e_x = eccentricity measured parallel to x-axis

e_y = eccentricity measured parallel to y-axis

2- Using the neutral axis depth,c, for the balanced failure as initial value

3- Calculating P_u and iterating for c using modified secant numerical method till the load is very close to P_u

4- Calculating e_{uy}, e_{ux} and comparing them to e_y, e_x to check section adequacy.

<u>Interactive design of reinforced concrete columns with biaxial bending (Ross and Yen 1986)</u>

Ross and Yen (1986) developed a computer program to analyze and design rectangular columns subjected to biaxial bending. The procedure is to change the inclination angle of the neutral axis to find adequate relation between M_{nx}, M_{ny}, and then change the position of the neutral axis to solve for the axial load. The section capacity is calculated using a predifined postion of the neutral axis and crushing strain equal to 0.003

182

for concrete. They suggested using four bars initially in the design process and keep

increasing according to the applied loads with limiting the number of bars as stated by

ACI code.

Design of columns subjected to biaxial bending (Horowitz 1989)

Horowitz (1989) developed a computer program for columns with any cross section

subjected to biaxial bending. He relied on finding the least possible location of steel bars that

make the section capacity more than the applied load.

Strength of reinforced concrete column in biaxial bending (Amirthandan 1991)

Amirthandan *et.al (1991)* showed good corelation between the experimental work done

before and the method propsed in the austrailian standard for concrete structures AS 3600 for

short columns. The load contour in the standard is approximated by bresler equation. They

adopted the beta value from the british standard

$$\beta = 0.7 + 1.7(N / 0.6 Nuo)$$
<div align="right">2-618</div>

N = design axial force

N_{uo} = ultimate axial load.

Computer analysis of reinforced concrete sections under biaxial bending and longitudinal

load (Zak 1993)

Zak (1993) proposed solving the equilibrium equation with the modification of the secant modulus method. The ultimate strain was not determined. However, it was found using maximization method.

Analysis and Design of Square and Rectangular Column by Equation of Failure Surface Hsu (1994)

Hsu (1994) proposed equation that covers columns subjected to biaxial bending and axial compression or tension. The proposed equation is as follow:

$$\left(\frac{P_n - P_{nb}}{P_o - P_{nb}}\right) + \left(\frac{M_{nx}}{M_{nbx}}\right)^{1.5} + \left(\frac{M_{ny}}{M_{nby}}\right)^{1.5} = 1.0 \qquad \text{2-619}$$

P_n = nominal axial compression or tension

M_{nx}, M_{ny} = nominal bending moments about x and y axis

P_o = maximum nominal axial compression or axial tension

P_{nb} = nominal axial compression at balanced strain condition

M_{nbx}, M_{nby} = nominal bending moments about x and y axis at balanced strain condition.

Biaxial Interaction Diagrams For short RC columns of any cross section (Rodriguez and Ochoa (1999)

Rodriguez and Ochoa (1999) proposed a general method for analyzing any cross section subjected to biaxial bending. They developed closed form solution for nominal total axial force

184

strength and nominal bending moment strengths about the global X and Y-axes. Quasi-Newton's

method was used to solve these coupled nonlinear equations to locate the neutral axis position.

$$P_n = \sum_{i=1}^{m} P_{ci} + \sum_{i=1}^{n} A_{bi} f_{si} - \sum_{i=1}^{n_{bc}} A_{bi} f_{si} \qquad \text{2-620}$$

$$M_{nx} = \sin\alpha \sum_{i=1}^{n_t} M_{ciy} + \cos\alpha \sum_{i=1}^{n_t} M_{cix} + Y_a \sum_{i=1}^{n_t} P_{ci} + \sum_{i=1}^{n_t} A_{bi} f_{si} Y_{bi} - \sum_{i=1}^{n_{bc}} A_{bi} f_{ci} Y_{bi} \qquad \text{2-621}$$

$$M_{ny} = \cos\alpha \sum_{i=1}^{n_t} M_{ciy} - \sin\alpha \sum_{i=1}^{n_t} M_{cix} + X_a \sum_{i=1}^{n_t} P_{ci} + \sum_{i=1}^{n_t} A_{bi} f_{si} X_{bi} - \sum_{i=1}^{n_{bc}} A_{bi} f_{ci} X_{bi} \qquad \text{2-622}$$

P_n= Nominal axial force strength.

M_{nx} = nominal bending moment strength about x axis

M_{ny} = nominal bending moment strength about x axis

X_a, Y_a = coordinates of origin with respect to global x, xaxes

α = angle of inclination of neutral axis with respect to Xaxis;

n = number of reinforcement bars;

n_{bc} = number of rebars located on compression side of cross section;

n_t = number of trapezoids used to approximate concrete under compression;

A_{bi} = area of steel rebar i;

f_{ci} = concrete stress at reinforcement bar i

f_{si} = steel stress at reinforcement bar i

P_{ci} = force for each trapazoid.

M_{ciy} = Moment of each trapazoid about y axis.

M_{cix} = Moment of each trapazoid about x axis.

Short reinforced concrete column capacity under biaxial bending and axial load (Hong 2000)

Hong (2000) did not assume any crushing strain limit. He proposed two equation from equating forces and moments

$$\frac{M_y}{P_n} - e_{xL} = 0 \qquad\qquad\qquad\qquad 2\text{-}623$$

$$\frac{M_x}{P_n} - e_{yL} = 0 \qquad\qquad\qquad\qquad 2\text{-}624$$

where e_{xl}, e_{yl} is the load eccentricity to x and y axes respectively. The two equations has three unknows; the curvature, neutral axis inclination angle and the neutral axis intercipt with the y-axis. Hong (2000) used the sequential quadratic programming method to solve the case as a nonlinearly constrained optimization problem.

Reliability of Reinforced Concrete Columns under Axial Load and Biaxial Bending (Wang and Hong 2002)

Wang and Hong (2002) evaluated the parameter β (Parme *et al* (1966)) and fount that it is insensitive to the reinforced ratio, it is more sensitive to biaxial bending than uniaxial bending, it increases withload and concncrete compressive strength

Analysis and design of concrete columns for biaxial bending –overview-(Furlong , Hsu and Mirza 2004)

Furlong *et al* (2004) reviewed many of the proposed formulas for analysis. These formulas were compared to experimental work. They concluded that the equations of Bresler (1960), although simple, are not very conservative, while Hsu equation is much more conservative. As Hsu equation can be used in biaxial bending and tension as well. However, both Hsu equation and Bresler reciprocal load equation can not be used in selecting cross section, unlike Bresler load contour equation.

New Method to Evaluate the Biaxial Interaction Exponent for RC Columns (Bajaj and Mendis 2005)

Bajaj and Mendis (2005) suggested new equations to evaluate the biaxial interaction exponenet a found by Bresler (1960). The proposed equations are as follow

$$\beta = \frac{\dfrac{M_{nx}}{M_{nox}} + \dfrac{M_{ny}}{M_{noy}}}{2}$$

2-625

$$\alpha = K \frac{\log 0.5}{\log \beta}$$

2-626

Bajaj and Mendis (2005) benchmarked their equastion by comparing the results with experimental work done on 8 (150* 150 mm) columns.

Analysis of Reinforced Concrete Columns Subjected to Biaxial Loads (Demagh, Chabil and Hamzaoui 2005)

Demagh *et al* (2005) suggested solving for the three equations of equilibrium to find the nominal force P_n, the inclination angle of the neutral axis α and the depth of the neutral axis b. The three equation are:

$$P_n = \sum P_{ci} + \sum (f_{si} - f_{ci}) A_{si}$$

2-627

$$M_{nx} = P_n e_y = \sin \alpha \sum M_{ci} y + \cos \alpha \sum M_{ci} x + Y \sum P_{ci} + \sum (f_{si} - f_{ci}) A_{si} y_{si}$$

2-628

$$M_{ny} = P_n e_x = \cos \alpha \sum M_{ci} y + \sin \alpha \sum M_{ci} x + X \sum P_{ci} + \sum (f_{si} - f_{ci}) A_{si} y_{si}$$

2-629

Where the subscript *i* refers to a concrete layer or steel bar element.

Analytical approach to failure surfaces in reinforced concrete sections subjected to axial loads and biaxial bending (Bonet, Miguel, Fernandez and Romero 2006)

Bonet *et al* (2006) developed a new method for the surface failure based on numerical simulation. The numerical simulation was generated using a computer program capable of analysing moment-curvature diagram for given axial load and moment ratio. The maximum value was used as a failure point for the given loads. The failure surface is defined by two

188

directrix curves and generatrix curves. The directrix curves are the curve corresponds to zero axial force and the one corresponds to balance failure.the generatix curves are defined in Muy/Mux plane, the first curve connects the pure tension axial load to balnce failure load. Whearas the second curve connects the balnce failure load to the pure compression load. The equations for the four curves are as follow

Directrix 1

$$\left[\frac{M_{d1}.\cos\beta}{M_{d1,x}}\right]^{\gamma 1} + \left[\frac{M_{d1}.\sin\beta}{M_{d1,y}}\right]^{\gamma 2} = 1$$

2-630

Directrix 2

$$\left[\frac{M_{d2}.\cos\beta}{M_{d2,x}}\right]^{\eta 1} + \left[\frac{M_{d2}.\sin\beta}{M_{d2,y}}\right]^{\eta 2} = 1$$

2-631

generatix 1

$$\left(\frac{M_u - M_{d1}\left(1-\frac{N_u}{n_{ut}}\right)}{M_{d2} - M_{d1}\left(1-\frac{N_{d2}}{N_{ut}}\right)}\right) - \left(\frac{N_u - N_{ut}}{N_{d2} - N_{ut}}\right) * \left(\frac{N_u}{N_{d2}}\right) = 0$$

2-632

generatix 2

$$\left(\frac{M_u - M_{d1}\left(1-\frac{N_u}{n_{ut}}\right)}{M_{d2} - M_{d1}\left(1-\frac{N_{d2}}{N_{ut}}\right)}\right) - \left(\frac{N_u - N_u}{N_{uc} - N_{d2}}\right)^{\zeta} - \left(\frac{M_u}{M_{d2}}\right) = 0$$

2-633

M_{d1}= absolute value of the nominal bending moment of the section in simple flexure corresponding to angle beta

$Md_{1,x}$, $Md_{1,y}$= nominal bending moments of the section in simple flexure for the x and y axes, respectively.

M_{d2} = absolute value of the nominal bending moment corresponding to the maximum bending capacity

of the section for a particular angle β

$Md_{2,x}$, $Md_{2,y}$ = nominal bending moments corresponding to the maximum flexure capacity of the section for the x and the y axes, respectively.

γ, η=exponents of the directrices.

$\gamma = 1.3\omega + 2$

$\eta = -0.22\omega + 1.15$

ω = steel reinforcement

N_u = axial load applied

N_{uc} = the ultimate axial load in pure compression

N_{d2} =balance failure load.

$$\zeta = (0.8 * \omega - 0.7)\left[\frac{N_{uc} - N_u}{N_{uc} - N_{lim}}\right] + 0.95$$

2-634

N_{lim} = nominal axial compression at the balanced strain condition

Biaxial bending of concrete columns:An analytical solution (Cedolin, Cusatis, Eccheli, Roveda 2006)

Cedolin *et al* (2006) introduced analytical solution of the failure envelope of rectangular R/C cross sections subjected to biaxial bending and to an axial force by approximating the rectangle to equivalent square section. The analysis was for unconfined concrete and the solution outcome was dimensionless

Comparative study of analytical and numerical algorithms for designing reinforced concrete sections under biaxial bending (Bonet , Barros , Romero 2006)

Bonet *et al* (2006) introduced analytical and numerical methods for designing circular and rectangular cross sections subjected to bi-axial bending. The analytical method uses the heviside function (Barros *et al* 2004) to define the failure strain, then integrate the stress based on that failure. The numerical method breaks the section into multi thick layers parallel to the nuteral axis. The internal forces are found by numerical integration of each layer using Gausss-Legendre quadrature (Barros *et al* 2004). They concluded that the two method are effeicint for circular cross section's analysis and the modified thick layer integration is more efficient for the rectangular cross section's analysis.

Investigation of Biaxial Bending of Reinforced Concrete Columns Through Fiber Method Modeling (Lejano 2007)

Lejano (2007) expanded the finite element method found by Kaba and Mahin (1984). To predict the behavior of unconfined rectangular columns subjected to biaxial bending. The analysis was limited to uniform semmetric square columns. Lejano (2007) utilized Bazant's Endochronic theory for concrete and Ciampi model for steel.

Variation of ultimate concrete strain at RC Columns Subjected to Axial Loads with Bi-directional Eccentricities (Yoo and Shin 2007)

Yoo and Shin (2007) introduced the modified rectangular stress block (MRSB) to account for non-rectangular compression zone induced by bi-axial bending. They showed experimentally that the ultimate strain of concrete exposed to bi-directional eccentricities can reach up to 0.0059. Based on this finding they introduced new equation for the unconfined ultimate strain as follow:

$$\varepsilon_{cu} = 0.003 + \frac{\varepsilon_{0.45} - 0.003}{0.45}\frac{P_n}{P_o} \qquad\qquad \frac{P_n}{P_o} \le 0.45 \qquad\qquad\qquad \text{2-635}$$

$$\varepsilon_{cu} = 0.003 + \frac{\varepsilon_{0.45} - 0.003}{0.55}\left(1 - \frac{P_n}{P_o}\right) \qquad\qquad \frac{P_n}{P_o} \ge 0.45 \qquad\qquad\qquad \text{2-636}$$

$$\varepsilon_{0.45} = 0.003 + \frac{0.0025}{\tan^{-1}\left(\dfrac{h}{b}\right)}\theta \qquad\qquad 0 \le \theta \le \tan^{-1}\left(\frac{h}{b}\right) \qquad\qquad\qquad \text{2-637}$$

$$\varepsilon_{0.45} = 0.003 + \frac{0.0025}{90 - \tan^{-1}\left(\dfrac{h}{b}\right)}(90 - \theta) \qquad \tan^{-1}\left(\frac{h}{b}\right) \leq \theta \leq 90 \qquad\qquad \text{2-638}$$

No definition for θ was provided.

<u>Capacity of Rectangular Cross Sections under Biaxially Eccentric Loads (Cedolin, Cusatis, Eccheli, Roveda 2008)</u>

Cedolin *et al* (2008) utilized the work of Cedolin et al (2006) to generate more accurate moment failure contour through creating one extra points on the contour. This point correspond to the load acting on rectangle diagonlas and was approximated by using equivelant square to benefit from symmetry. The developed moment contour was used for better evaluating the parameter α found by Bresler (1960)

<u>Development of a computer program to design concrete columns for biaxial moments and normal force (Helgason 2010)</u>

Helgason 2010 developed a computer program using Matlab for designing unconfined rectangular hollow or solid columns subjected to axial force and bending moment. Helgason 2010 used the predefined strain profile to generate the interaction diagram and the equivelant stress block equal to 80 % of the compression zone depth. The outcome was compared to Eurocode

2-4-2 Discussion

According to the literature review, there are five different approaches that treated the columns under axial load and bending moment problem. These ways are summarized as follow:

1- Trial for locating the neutral axis position such as Parker and Scanlon (1941), Ang (1961) and Czerniak (1962) works.

2- Implementing closed form equations for special cases such as Andersen (1941), Wiesinger (1958), Cedolin *et al* (2006) and Yoo and Shin (2007) works.

3- Generating charts that relate two or more variable to facilitate the design process, such as Mikhalkin, Au (1958), Fleming and Werner (1965) and Brettle and Taylor (1968) works.

4- Developing simplified Interaction diagrams by using coefficients for curve defining. This method was adopted by some researchers like Whitney and Cohen (1957), Bresler (1960), Furlong (1961), Parme (1966), Mylons (1967), Bonet et al (2006).

5- Generating Sets of ready Interaction diagrams to be used directly by designers, Weber (1966) and others

   There are some conclusions that can be drawn as follow

- The finite layer approach is successful in analysis. This approach was adopted by some authors such as Brettle and Taylor (1968), Bonet et al (2006) and Lejano (2007)

- The Bresler Method is one of the most well known and successful method in predicting the unconfined interaction diagrams and load contours. This method was utilized and refined by many such as Rammamurthy (1966), Parme et al (1966), Gouwens (1975), Sallah (1983) Amirthandan (1991), Wang and Hong (2002) and

194

Bajaj and Mendis (2005). However it is very conservative for some cases as shown by Furlong *et al* (2004) and others.

- Software applications on columns spreaded and became popular in the beginning of 1980s.Taylor and Ho (1984) developed computer program based on Bresler Method. Sacks and Bugukoztruck (1986) developed their program based on iterating for neutral axis and load converge. Ross and Yen (1986) used the predefined strain profile in their software. Horowitz (1989) incremented the steel bars till the column capacity exceeded the load applied. This transition in relying on machines for facilitates calculations. Hence more accurate and precise analysis is needed to define exactly the unconfined and confined capacity of different sections.

- The predefined strain profile is seen to be one of the most effective and fast procedure foe unconfined analysis. This method was suggested by Furlong (1961) and utilized by many, such as Ross and Yan (1986)

- There is lack of confinement effect analysis on columns capacity. Nowadays, there is a need in predicting columns extreme events as stated by some structural codes like AASHTO-LRFD.

Chapter 3 - Circular Columns Confined with FRP and lateral Steel

3-1 Introduction

FRP used in retrofitting concrete columns is considered one of the simplest and most efficient application, as FRP has excellent material characteristics like high strength to weight ratio and high corrosion resistance FRP behaves elastically, and therefore its confining strength increases proportionally with increasing the force applied. On the other hand, the confining steel provides constant confining pressure after its yielding. Many empirical and theoretical models were proposed describing the FRP contribution to confinement. According to Lam and Teng (2003), the proposed models can be classified as design oriented and analysis oriented. In the design oriented approach, closed-form equations are developed to predict the stress-strain behavior based on experimental findings. Examples of such models are those of Fardis and Khalili (1982), Ahmed *et al* (1991); Saadatmanesh *et al* (1994); Karbhari and Gao (1997), Saafi *et al* (1998) and Toutanji (1999).Whereas in the second approach, an incremental numerical analysis is generated and an active confined model is utilized to determine the Stress-Strain curve. Examples of such models are those of Spolestra and Monti (1999), Xiao and Wu (2000). Several researchers realized the importance of implementing the effect of the Lateral Steel Reinforcement (LSR) and FRP combined in one model. Braga *et al*. (2006) and Eid and Paultre (2008) are two different models accounting for minimum amount of confining steel to be used in the columns when FRP wrapping is used. This chapter is proposing a new model accounting for the FRP and LSR side by side based on a direct extension of the procedure established by ACI 440.2R-08. This chapter discusses the finite layer approach used, the material models, eccentric based models, numerical formulation of the algorithm and finally the results and discussion.

3-2 Formulations

3-2-1 Finite Layer Approach (Fiber Model)

The column cross section is divided into a finite number of thin layers (Figure 3-1). The force and moment of each layer is calculated and stored. The rebars are treated as discrete objects in their actual locations. The advantage of that is to avoid inaccuracy generated from using the approximation of the stress block method, as a representative of the compression zone and to precisely calculate the internal forces induced by steel bars and concrete layers in the column cross section.
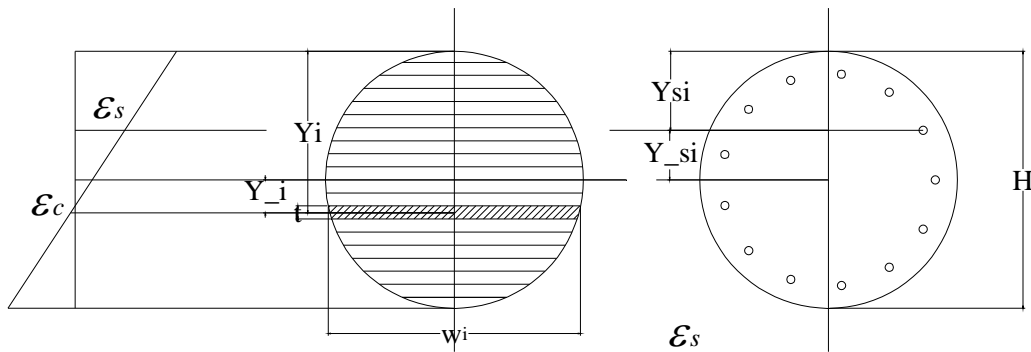
Figure 3-1: Using Finite Layer Approach in Analysis

3-2-2 Present Confinement Model for Concentric Columns

3-2-2-1 Lam and Teng Model

Lam and Teng (2003) proposed a new model for concrete wrapped with Fiber Reinforced Polymer (FRP). This model is adopted by ACI 440.2R-08 code for FRP wrapping. The stress-strain equations are as follow:

$$f_c = E_c \varepsilon_c - \frac{(E_c - E_2)^2}{4f_c^{'}} \varepsilon_c^2 \qquad 0 \leq \varepsilon_c \leq \varepsilon_t^{'}$$

3-1

$$f_c = f_c^{'} + E_2 \varepsilon_c \qquad \varepsilon_t^{'} \leq \varepsilon_c \leq \varepsilon_{ccu}$$

3-2

$$E_2 = \frac{f_{cc} - f_c^{'}}{\varepsilon_{ccu}}$$

3-3

$$\varepsilon_t^{'} = \frac{2f_c^{'}}{E_c - E_2}$$

3-4

where ε'_t is the transition strain. To find the maximum confined concrete compressive strength

$$f_{cc} = f_c^{'} + 3.3 \Psi_f \kappa_a f_l$$

3-5

$$f_l = \frac{2E_f n t_f \varepsilon_{fe}}{D}$$

3-6
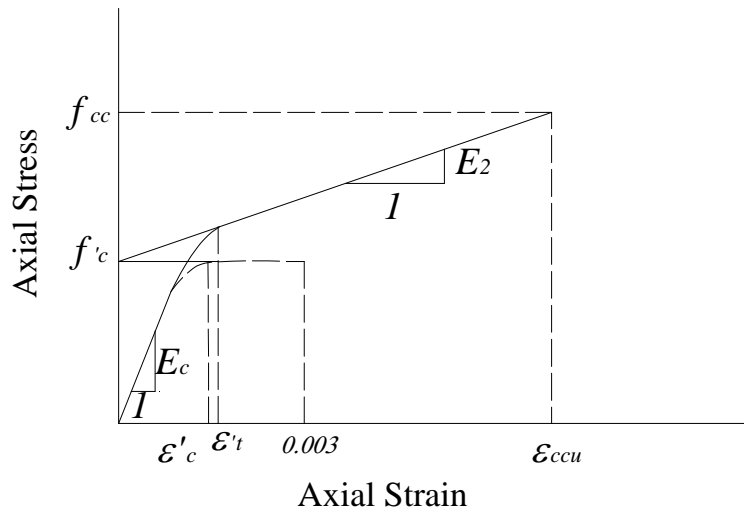
Figure 3-2:Axial Stress-Strain Model proposed by Lam and Teng (2003).

f_l is the maximum confined pressure. E_f is tensile modulus of elasticity of FRP. κ_a is the efficiency factor accounts for the geometry of the section and it is equal to 1 in case of the

198

circular cross section, n is the number of plies used, t_f is the nominal thickness of one ply, D is the cross section diameter of the column, ψ_f is a reduction factor determined by the code to be 0.95. ε_{fe} is the effective strain level at failure and it is given by:

$$\varepsilon_{fe} = \kappa_\varepsilon \varepsilon_{fu} \qquad\qquad 3\text{-}7$$

κ_ε is a reduction factor that considers the premature failure of the FRP. ACI 440.2R-08 implements an average value of $\kappa_\varepsilon = 0.586$ based on Lam and Teng (2003 a) finding. It is found experimentally to range between 0.57 and 0.61. It should be noted that the lowest level of confinement pressure (f_l) required is equal to 0.08 f'_c to avoid having a descending branch in the stress strain curve. This note is verified by Spolestra and Monti (1999). The maximum compressive strain ε_{ccu} can be found by:

$$\varepsilon_{ccu} = \varepsilon_c' \left(1.50 + 12\kappa_b \frac{f_l}{f_c'} \left(\frac{\varepsilon_{fe}}{\varepsilon_c'} \right)^{0.45} \right) \qquad\qquad 3\text{-}8$$

And to avoid excessive cracking, this strain should be limited to:

$$\varepsilon_{ccu} \le 0.01$$

where κ_b accounts for the geometry of the cross section and is equal to 1 for circular columns.

3-2-2-2 Mander Model for transversely reinforced steel

Mander model (1988) was developed based on the effective lateral confinement pressure, f'_l, and the confinement effective coefficient k_e which is the same concept found by Sheikh and Uzumeri (1982). The advantage of this procedure is its applicability to any cross section since it defines the lateral pressure based on the section geometry. Mander *et al* (1988)

showed the adaptability of their model to circular or rectangular sections, under static or dynamic loading, either monotonically or cyclically applied. In order to develop a full stress-strain curve and to assess ductility, an energy balance approach is used to predict the maximum longitudinal compressive strain in the concrete.

Mander derived the longitudinal compressive concrete stress-strain equation from Popovics model that was originally developed for unconfined concrete (1973):

$$f_c = \frac{f_{cc} x r}{r - 1 + x^r}$$
3-9

$$x = \frac{\varepsilon_c}{\varepsilon_{cc}}$$
3-10

$$r = \frac{E_c}{E_c - E_{sec}}$$
3-11

$$E_c = 4723\sqrt{f_c'} \quad in \ MPa$$
3-12

$$E_{sec} = \frac{f_{cc}}{\varepsilon_{cc}}$$
3-13

and as suggested by Richart *et al.* (1928) the strain corresponding to the peak confined compressive strength f_{cc} is:

$$\varepsilon_{cc} = \varepsilon_{co}\left[1 + 5\left(\frac{f_{cc}}{f_c'} - 1\right)\right]$$
3-14

The different parameters are defined in Figure (3-3).
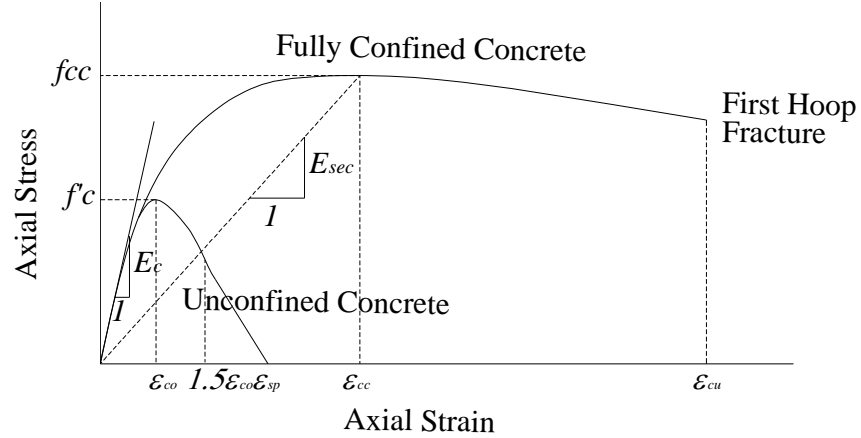
Figure 3-3: Axial Stress-Strain Model proposed by Mander *et al.* (1988) for monotonic loading

As shown in Figure 3-3: Axial Stress-Strain Model proposed by Mander et *al.* (1988) for monotonic loading, Mander *et al.* (1988) model has two curves; one for unconfined concrete (lower curve) and the other for confined concrete (upper one). The upper one refers to the behavior of confined concrete with concentric loading (no eccentricity). It is shown that it has ascending branch with varying slope starting from E_c decreasing till it reaches the peak confined strength at (f_{cc}, ε_{cc}). Then the slope becomes slightly negative in the descending branch representing ductility till the strain of ε_{cu} where first hoop fractures. The lower curve expresses the unconfined concrete behavior. It has the same ascending branch as the confined concrete curve till it peaks at (f'_c, ε_{co}). Then, the curve descends till 1.5-2ε_{co}. A straight line is assumed after that till zero strength at spalling strain ε_{sp}

Mander *et al.* (1988) utilized an approach similar to that of Sheik and Uzumeri (1982) to determine effective lateral confinement pressure. It was assumed that the area of confined

concrete is the area within the centerlines of perimeter of spiral or hoop reinforcement A_{cc} as illustrated in Figure (3- 4)

Figure 3-4: Effectively confined core for circular hoop and spiral reinforcement (Mander Model)

Figure 3-4 shows that effectively confined concrete core A_e, inbetween hoops or spirals, is smaller than the area of core within center lines of perimeter spiral or hoops excluding longitudinal steel area, A_{cc}. To satisfy that condition, the effective lateral confinement pressure, f'_l, should be a percentage of the lateral pressure f_l:

$$f_l^{'} = k_e f_l \qquad\qquad 3\text{-}15$$

and the confinement effectiveness coefficient k_e is defined as the ratio of effective confined area to the area enclosed by centerlines of spiral or hoop:

$$k_e = \frac{A_e}{A_{cc}} \qquad\qquad 3\text{-}16$$

$$A_{cc} = A_c - A_{sl} = \frac{\pi}{4}d_s^2 - A_{sl} \qquad\qquad 3\text{-}17$$

$$\frac{A_{cc}}{A_c} = 1 - \frac{A_{sl}}{A_c}$$

3-18

$$A_{cc} = A_c\left(1 - \rho_{cc}\right)$$

3-19

where A_c is the area of the section core enclosed by spirals or hoops, A_{sl} is the area of longitudinal steel and ρ_{cc} is the ratio of longitudinal steel to the area of the core.

For hoop case, the effective lateral confined core:
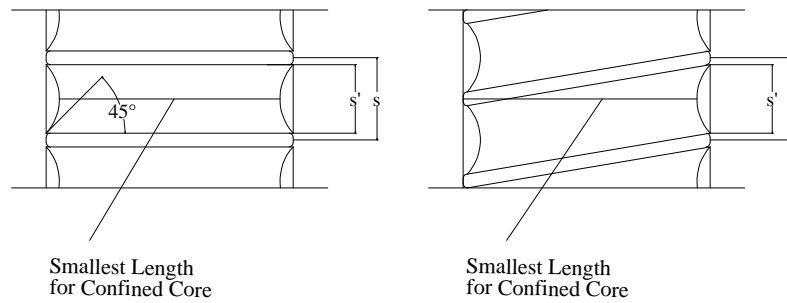
Figure 3-5: Effective lateral confined core for hoop and spiral reinforcement (Mander Model)

$$A_e = \frac{\pi}{4}d_s^2\left(1 - \frac{s'}{2d_s}\right)^2 = A_c\left(1 - \frac{s'}{2d_s}\right)^2$$

3-20

$$k_e = \frac{\left(1 - \frac{s'}{2d_s}\right)^2}{1 - \rho_{cc}}$$

3-21

where s' is the clear spacing between spiral or hoop bars and d_s is the core diameter to spirals or hoops centerline. While for spiral case it can be shown from Figure (3-5) that

$$A_e = \frac{\pi}{4}d_s^2\left(1 - \frac{s'}{4d_s}\right)^2 = \frac{\pi}{4}d_s^2\left(1 - \frac{2s'}{4d_s} + \frac{s'^2}{16d_s^2}\right)$$

3-22

and the last term can be neglected so the value of k_e is found from the following equation:

203

$$k_e = \frac{1 - \dfrac{s'}{2d_s}}{1 - \rho_{cc}}$$

3-23
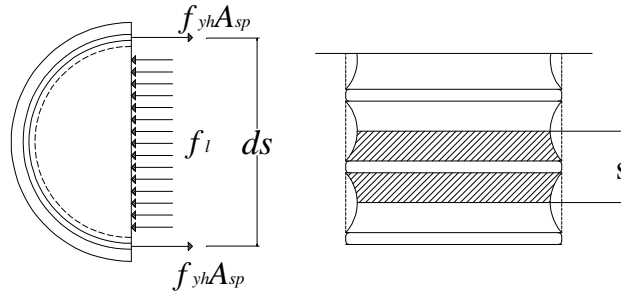
Figure 3-6: Confinement forces on concrete from circular hoop reinforcement

Figure (3-6) illustrates force equilibrium on a half turn of a circular hoop. The uniform hoop tension at yield generated in the transverse steel should be balanced by the uniform lateral stress on the concrete core:

$$2f_{yh}A_{sp} = f_l s d_s$$

3-24

$$f_l = \frac{2f_{yh}A_{sp}}{sd_s}$$

3-25

and the ratio of the volume of transverse steel to the volume of confined core area ρ_s can be expressed as

$$\rho_s = \frac{A_{sp}\pi d_s}{\dfrac{\pi}{4}sd_s^2} = \frac{4A_{sp}}{sd_s}$$

3-26

hence

$$f_l = \frac{1}{2}\rho_s f_{yh}$$

3-27

and from equation (3-15) f'_l can be found:

204

$$f_l' = \frac{1}{2} k_e \rho_s f_{yh}$$

3-28

The maximum confined compressive strength can be described as a function of the peak unconfined strength and the uniform effective lateral confinement pressure:

$$f_{cc} = f_c' \left(-1.254 + 2.254\sqrt{1 + \frac{7.94 f_l'}{f_c'}} - 2\frac{f_l'}{f_c'} \right)$$

3-29

Mander *et al*. (1988) proposed an energy balancing theory to predict the ultimate confined strain, which is determined at the first hoop fracture. They stated that the additional ductility for confined concrete results from the additional strain energy stored in the hoops U_{sh}. Therefore from equilibrium:

$$U_{sh} = U_g - U_{co}$$

3-30

where U_g is the external work done in the concrete to fracture the hoop, and U_{co} is the work done to cause failure to the unconfined concrete. U_{sh} can be represented by the area under the tension stress strain curve for the transverse steel between zero and fracture strain ε_{sf}.

$$U_{sh} = \rho_s A_{cc} \int_0^{\varepsilon_{sf}} f_s d\varepsilon$$

3-31

while Ug is equal to the area under the confined stress strain curve plus the area under the longitudinal steel stress strain curve:

$$U_g = \int_0^{\varepsilon_{scu}} f_c A_{cc} d\varepsilon + \int_0^{\varepsilon_{scu}} f_s A_{sl} d\varepsilon$$

3-32

Similarly, it was proven experimentally that U_{co} is equal to:

205

$$U_{co} = A_{cc} \int_{0}^{\varepsilon_{spall}} f_c d\varepsilon = A_{cc} 0.017 \sqrt{f_c'} \text{ in } MPa \qquad \text{3-33}$$

and

$$U_{sh} = \rho_s A_{cc} \int_{0}^{\varepsilon_{sf}} f_s d\varepsilon = 110 \rho_s A_{cc} \qquad \text{3-34}$$

Substituting equations (3-32), (3-33) and (3-34) into equation (3-30):

$$110\rho_s = \int_{0}^{\varepsilon_{cu}} f_c d\varepsilon + \int_{0}^{\varepsilon_{cu}} f_{sl} d\varepsilon - 0.017 \sqrt{f_c'} \qquad \text{3-35}$$

where f_{sl} is the stress in the longitudinal steel. Equation (3-35) can be solved numerically for ε_{cu}

The above equations (3-30) to (3-35) are develoed using the SI units

3-2-3Present Confinement Model for Eccentric Columns

Unlike concentric loading, the eccentric loading generates bending moment in addition to axial loading. Columns subjected to eccentric loading behave differently from those concentrically loaded, as the shape of the stress strain curve for fully confined reinforced concrete (concentric loading) shows higher peak strength and more ductility than the unconfined one (infinite eccentricity). Most of the previous studies were based on the uniform distribution of compressive strain across the column section.
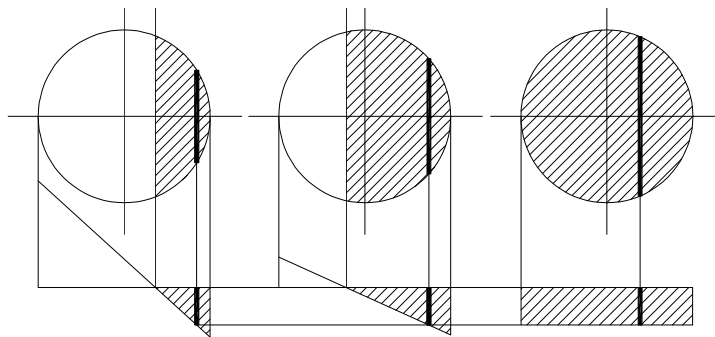
Figure 3-7: Effect of compression zone depth on concrete strength

Figure (3-7) illustrates three different sections under concentric load, combination of axial load and bending moment and pure bending moment, the highlighted fiber in the three cases has the same strain. Any current confinement model yields the same stress for these three fibers. So the depth or size of compression zone does not have any role in predicting the stress. Hence, it is more realistic to relate the strength and ductility in a new model to the level of confinement utilization and compression zone.
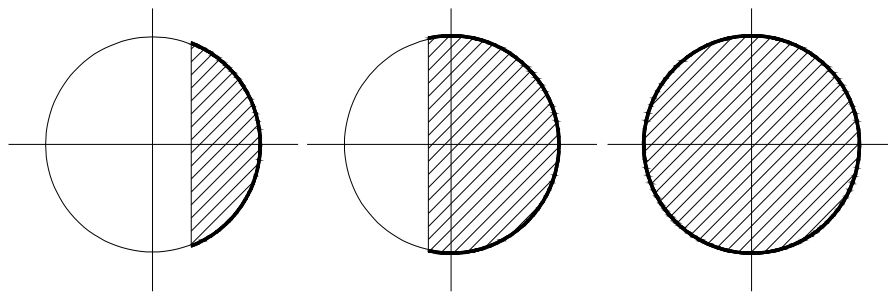
Figure 3-8: Amount of confinement gets engaged in different cases

By definition, confinement gets engaged only when member is subjected to compression. Compressed members tend to expand in lateral direction, and if confined, confinement will prevent this expansion to different levels based on the degree of compressive force and confinement strength as well. For fully compressed members (Figure 3-8 c), confinement becomes effective 100% as it all acts to prevent the lateral expansion. Whereas members subjected to compression and tension, when the neutral axis lies inside the section perimeter, only adjacent confinement to the compression zone gets engaged. Accordingly, members become partially confined.

In FRP wrapped columns literature, various models were implemented to assess the ultimate confined capacity of columns under concentric axial load. On the other hand the effect of partial confinement in case of eccentric load (combined axial load and bending moments) is

not investigated in any proposed model. Therefore, it is pertinent to relate the strength and ductility of reinforced concrete to the degree of confinement utilization in a new model.

The two curves of fully confined and unconfined concrete in any proposed model are used in the eccentricity-based model as upper and lower bounds. The upper curve refers to concentrically loaded confined concrete (zero eccentricity), while the lower one refers to pure bending applied on concrete (infinite eccentricity). In between the two boundaries, infinite numbers of stress-strain curves can be generated based on the eccentricity which is found to directly relate to the size of compression zone, Figure (3-9). The higher the eccentricity the smaller the confined concrete region in compression. Accordingly, the ultimate confined strength is gradually reduced from the fully confined value f_{cc} to the unconfined value f'_c as a function of eccentricity to diameter ratio. In addition the Ultimate strain is reduced linearly from the ultimate strain ε_{cu} for confined concrete to the ultimate strain for unconfined concrete $1.5\varepsilon_{co}$ or 0.003
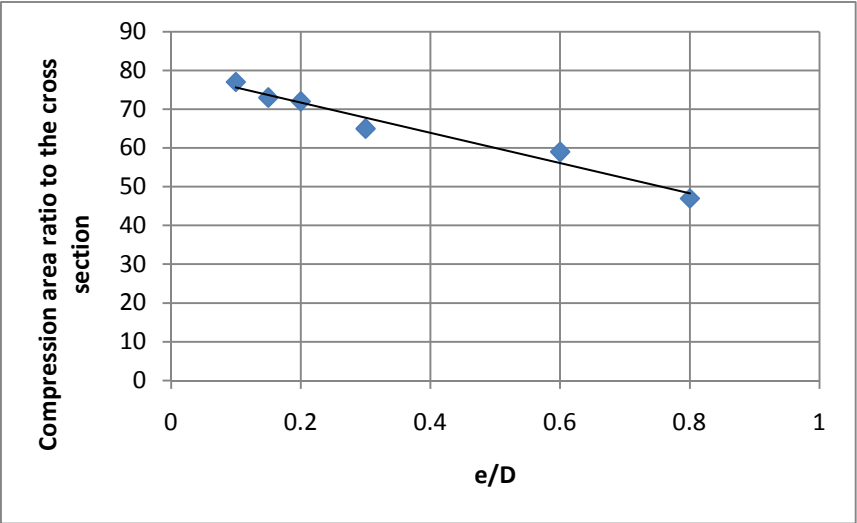
Figure 3-9: Relation between the compression area ratio to the normalized eccentricity

Figure (3-9) shows that the compression area to the total area decreases linearly with the increase in normalized eccentricity. This relation is almost linear as it is depicted by the solid line. Hence,

the eccentricity can be related simply to the compression zone area as explained in the following section.

3-2-3-1 Eccentric Model Based on Lam and Teng Equations

The ultimate eccentric or partially confined strength $\overline{f_{cc}'}$ is determined from the following equation:

$$\overline{f_{cc}'} = \frac{1}{1+\dfrac{e}{D}} \overline{f_{cc}} + \frac{1}{1+\dfrac{D}{e}} f_c' \qquad\qquad 3\text{-}36$$

where e is the eccentricity, D is the column diameter and $\overline{f_{cc}}$ is the eccentric peak strength at the eccentricity (e).

The strain $\overline{\varepsilon_{cu}}$ corresponding to the peak partially confined strength $\overline{f_{cc}}$, which corresponds to the ultimate point on the curve, Figure (3-10), is given by linear interpolation between the two extreme bounds of strain:

$$\overline{\varepsilon_{cu}} = \frac{\overline{f_{cc}} - f_c'}{f_{cc} - f_c'}\left(\varepsilon_{ccu} - 0.003\right) + 0.003 \qquad\qquad 3\text{-}37$$

Any point on the generated eccentric curves can be calculated using the following equations:

$$f_c = E_c \varepsilon_c - \frac{\left(E_c - \overline{E_2}\right)^2}{4 f_c'}\varepsilon_c^2 \qquad\qquad 0 \le \varepsilon_c \le \overline{\varepsilon_t'} \qquad\qquad 3\text{-}38$$

$$f_c = f_c' + \overline{E_2}\varepsilon_c \qquad\qquad \overline{\varepsilon_t'} \le \varepsilon_c \le \overline{\varepsilon_{cu}} \qquad\qquad 3\text{-}39$$

$$\overline{E_2} = \frac{\overline{f_{cc}} - f_c'}{\overline{\varepsilon_{cu}}} \qquad\qquad 3\text{-}40$$

$$\overline{\varepsilon_t'} = \frac{2 f_c'}{E_c - \overline{E_2}} \qquad\qquad 3\text{-}41$$

209
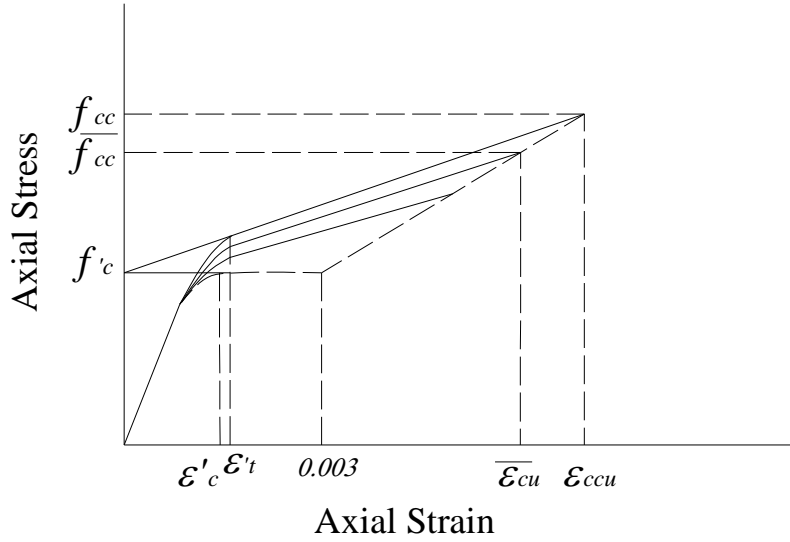
Figure 3-10: Eccentricity Based Confined -Lam and Teng Model-

3-2-3-2 Eccentric Model based on Mander Equations

The equation that defines the eccentric peak strength according to the eccentricity is simply a

mixture rule: $\overline{f_{cc}} = \dfrac{1}{1+\dfrac{e}{D}} f_{cc} + \dfrac{1}{1+\dfrac{D}{e}} f_c^{'}$ 3-42

where e is the eccentricity, D is the column diameter and $\overline{f_{cc}}$ is the eccentric peak strength at the

eccentricity (e). The corresponding strain $\overline{\varepsilon_{cc}}$ is given by

$$\overline{\varepsilon_{cc}} = \varepsilon_{co}\left[1+5\left(\dfrac{\overline{f_{cc}}}{f_c^{'}}-1\right)\right]$$ 3-43

and the maximum strain corresponding to the required eccentricity will be a linear function of

the stress corresponding to maximum strain for fully confined concrete f_{cu} and the stress at the

maximum unconfined train f_{cuo} at $\varepsilon_{cuo} = 0.003$.

210

$$\overline{\varepsilon_{cu}} = \overline{\varepsilon_{cc}} \left[\frac{\dfrac{\overline{E_{sec}}}{E_{sec,u}}\overline{r}}{\dfrac{c}{\overline{\varepsilon_{cu}}}+1} - \overline{r} + 1 \right]^{\frac{1}{r}} \qquad\qquad E_{sec,u} = \frac{\overline{f_{cu}} - f_{cuo}}{\varepsilon_{cu} - 0.003} \qquad\qquad \text{3-44}$$

$$c = \frac{\overline{f_{cu}} - E_{sec,u} * 0.003}{E_{sec,u}}$$

$$\overline{E_{sec}} = \frac{\overline{f_{cc}}}{\overline{\varepsilon_{cc}}} \qquad\qquad \overline{r} = \frac{E_c}{E_c - \overline{E_{sec}}}$$

In order to verify the accuracy of the model at the extreme cases, the eccentricity is first set to be zero. The coefficient of f'_c will be zero and equation (3-42), (3-43) and (3-44) will reduce to be:

$$\overline{f_{cc}} = f_{cc} \qquad\qquad\qquad \text{3-45}$$

$$\overline{\varepsilon_{cc}} = \varepsilon_{cc} \qquad\qquad\qquad \text{3-46}$$

$$\overline{\varepsilon_{cu}} = \varepsilon_{cu} \qquad\qquad\qquad \text{3-47}$$

On the other hand, if the eccentricity is set to be infinity the other coefficient of f_{cc} will be zero, and the strength, corresponding strain and ductility equations will be:

$$\overline{f_{cc}} = f_{cc}' \qquad\qquad\qquad \text{3-48}$$

$$\overline{\varepsilon_{cc}} = \varepsilon_{co} \qquad\qquad\qquad \text{3-49}$$

$$\overline{\varepsilon_{cu}} = 0.003 \qquad\qquad\qquad \text{3-50}$$
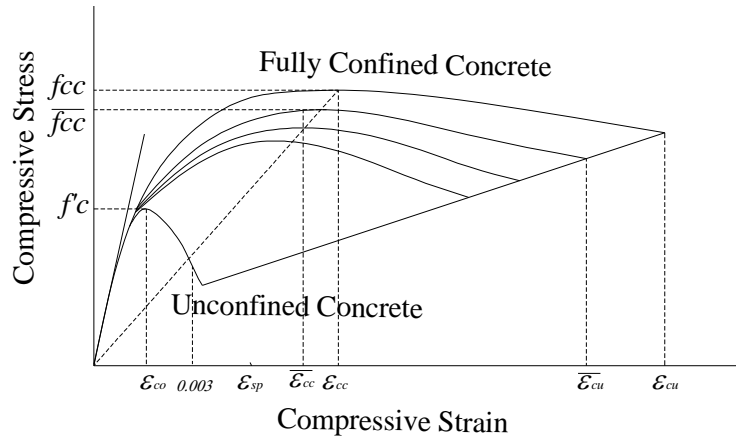
Figure 3-11: Eccentricity Based Confined -Mander Model -

Any point on the generated eccentric curves can be calculated using the following equation:

$$f_c = \frac{\overline{f_{cc}}\,\overline{x}\,\overline{r}}{\overline{r}-1+\overline{x}^{\overline{r}}}$$

3-51

where:

$$\overline{x} = \frac{\overline{\varepsilon_c}}{\overline{\overline{\varepsilon_{cc}}}}$$

3-52

$$\overline{r} = \frac{E_c}{E_c - \overline{\overline{E_{sec}}}}$$

3-53

$$\overline{E_{sec}} = \frac{\overline{f_{cc}}}{\overline{\overline{\varepsilon_{cc}}}}$$

3-54

3-2-4 Moment of Area Theorem

The very general axial stress equation in a symmetrical section subjected to axial force *P* and uniaxial bending M_x (Hardy Cross 1930):

$$\sigma_z = \frac{P}{A} + \frac{M_x}{I_x} y \qquad\qquad\qquad 3\text{-}55$$

σ_z = normal stress at any point (a) in cross section

P = applied load.

A = cross sectional area.

M_x = bending moment about x-axis

y = distance between the point (a) and the centroidal x-axis

I_x = moment of inertia about the centroidal x-axis

Rewriting Equation (3-55) to determine the strain at any point in the cross section:

$$\varepsilon_z = \frac{P}{EA} + \frac{M_x}{EI_x} y \qquad\qquad\qquad 3\text{-}56$$

In case of linear elastic analysis, E in EA or EI expressions is constant ($E=E_c$). However, if the section has variable strain and stress profile, it will amount to variable E profile (per layer) in nonlinear analysis. Accordingly, the section parameters must include $\sum_i E_i A_i$, $\sum_i E_i I_i$ for a more generalized theory (Rasheed and Dinno 1994). Note that the linear strain profile of the section from Equation (3-56) yields a distinct constant curvature:

$$\phi_x = \frac{M_x}{EI_x} \qquad\qquad\qquad\qquad 3\text{-}57$$

$$M_x = \phi_x EI_x \qquad\qquad\qquad\qquad 3\text{-}58$$

where ϕ_x = x- curvature

Rewriting equation (3-56) in terms of ϕ_x

$$\varepsilon_z = \frac{P}{EA} + \phi_x y \qquad\qquad\qquad 3\text{-}59$$

Finding ε_z at the centroid, since $y = 0$.

$$\varepsilon_o = \frac{P}{EA}$$

<div align="right">3-60</div>

Finding ez at the geometric centroid, $y = \bar{y}$

$$\bar{\varepsilon_o} = \frac{P}{EA} + \phi_x \bar{y}$$

Solving for P at the geometric centroid;

$$P = EA\bar{\varepsilon_o} - EA\bar{y}\phi_x$$

<div align="right">3-61</div>

$\bar{\varepsilon_o}$ is the axial strain at the geometric centroid

But

$$EAM_x = EA\bar{y} \qquad\qquad \bar{y} = Y_G - Y_c$$

Y_G is the vertical distance to the geometric centroid measured from bottom extreme fiber and Y_c is the vertical distance to the inelastic centroid measured from the bottom extreme fiber, Figure (3-12)

The general formula of the moments about the geometric x-axis is derived as follows: when the moment is transferred from the centroid to the geometric centroid , Figure (3-12)

$$\bar{M_x} = M_x - P\bar{y}$$

<div align="right">3-62</div>

Substituting equation (3-58) and (3-61) in (3-62) yields:

$$\bar{M_x} = -EAM_x \bar{\varepsilon_o} + \left(EI_x + EAM_x \bar{y}\right)\phi_x$$

<div align="right">3-63</div>
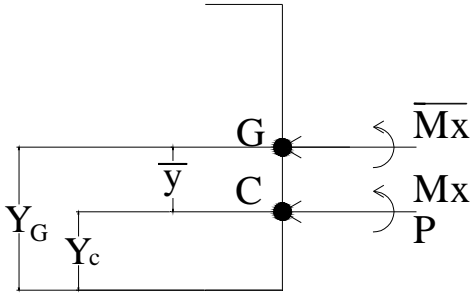
Figure 3-12: Transfering moment from centroid to the geometric centroid

The term $EI_x + EAM_x\bar{y}$ represents the $\overline{EI_x}$ about the geometric centroid using the parallel axis theorem. Using equations (3-61) and (3-63) yields the Moment of Area equation:

$$\begin{bmatrix} P \\ \overline{M_x} \end{bmatrix} = \begin{bmatrix} EA & -EAM_x \\ -EAM_x & \overline{EI_x} \end{bmatrix} \cdot \begin{bmatrix} \overline{\varepsilon_o} \\ \phi_x \end{bmatrix}$$

3-64

Since the moment of area about the actual centroid vanishes (Rasheed and Dinno 1994), Equation (3-64) reduces to an uncoupled set when it is applied back at the actual centroid since EAM_x vanish about the centroid.

$$\begin{bmatrix} P \\ M_x \end{bmatrix} = \begin{bmatrix} EA & 0 \\ 0 & EI_x \end{bmatrix} \cdot \begin{bmatrix} \varepsilon_o \\ \phi_x \end{bmatrix}$$

3-65

which is simply equations (3-58) and (3-60).

215

3-3 Numerical Formulation

3-3-1 Model Formulation
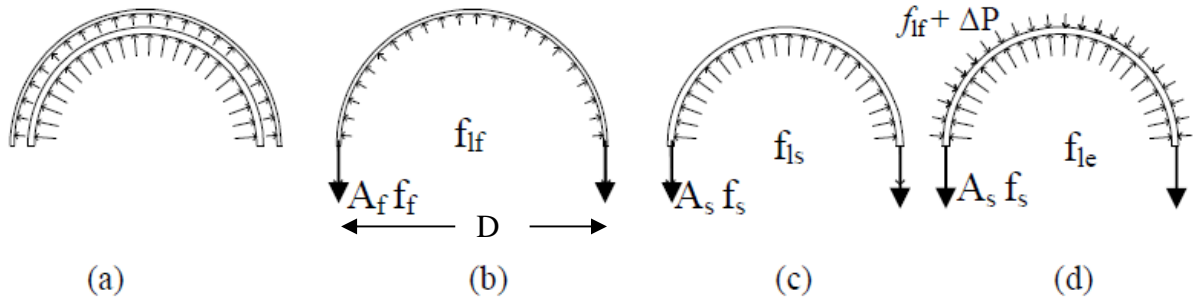
Figure 3-13: Equilibrium between Lateral Confining Stress, LSR and FRP Forces

It is demanded to integrate the effect of lateral Steel reinforcement (LSR) and Fiber Reinforced Polymer (FRP) simultaneously in one model to accurately express the whole column confinement behavior. As shown in Fig (3-12 d) and considering equilibrium:

$$f_{le} = \left(f_{lf}' + \Delta p \right) + f_{ls}'$$

3-66

f_{le} = effective lateral confinement due to LSR and FRP together

f'_{lf} = effective lateral confinement due to FRP only

f'_{ls} = effective lateral confinement due to LSR only.

Δp = lateral pressure difference developed due to transferring the f'_{lf} from the FRP position to the LSR position.

It is noted that Δp is negligible especially for proportionally small cover compared to core diameter of cross section (Eid and Paultre 2008). Accordingly Δp may be neglected from the previous equation that can be simplified to:

$$f_{le} = f'_{lf} + f'_{ls}$$

3-67

Using equilibrium in the free body diagram in Figure (3-13 b), the valure of f'_{lf} is:

$$f'_{lf} = k_e f_{lf}$$

3-68

And for fully wrapped columns k_e is equal to 1, hence:

$$f'_{lf} = f_{lf}$$

3-69

By using force equilibrium in the y- direction:

$$f_{lf} ds = 2 f_f A_f = 2 E_f \varepsilon_f t_f sn$$

3-70

d = column diameter

E_f = FRP modulus of Elasticity

t = FRP layer thickness

n = number of FRP layers

ε_f = FRP strain.

s = column length

Accordingly:

$$f_{lf} = \frac{2 E_f \varepsilon_f t_f n}{D}$$

3-71

Similarly to find f'_{ls}, equilibrium of forces in Figure (3-13 c) in the vertical direction are summed:

$$f'_{ls} = k_e f_{js}$$

3-72

$$f'_{ls} d_s s = 2 k_e A_s f_s$$

3-73

It can be assumed that spiral steel yields at ultimate strength, so f_s is replaced by f_{yh}

$$f'_{ls} = \frac{2k_e A_s f_{yh}}{d_s s}$$

3-74

k_e = lateral Steel confinement coefficient and it is equal to $\dfrac{1 - \dfrac{s'}{2d_s}}{1 - \rho_{ss}}$

A_s = Lateral Steel area

f_{yh} = Lateral Steel yield strength

d_s = core diameter

s = spiral spacing

By subistituting equations (3-71) and (3-74) into (3-67)

$$f_{le} = \frac{2E_f \varepsilon_f t_f n}{D} + \frac{2k_e A_s f_{yh}}{d_s s}$$

3-75

Lam and Teng (2003) stated that the ratio of f_{lf}/f'_c has not to be taken less than 0.07 to furnish minimum sufficient ratio of FRP and to ensure that the stress-strain curve is ascending beyond f'_c up to failure. But ACI 440 guidelines adopted 0.08 as a minimum for this ratio. This note is verified by Spolestra and Monti (1999). Based on the previous statement, the f_{lf}/f'_c ratio is calculated and if it is more than 0.08, Lam and Teng equations are used according to ACI 440. Otherwise Mander model is used since it generates a stress-strain curve with a descending branch, Figure (3-14). The reason for that is the limited FRP confinement ratio is considered minor and the FRP characteristics are not dominant. Hence, the cross section behavior is governed by lateral steel.
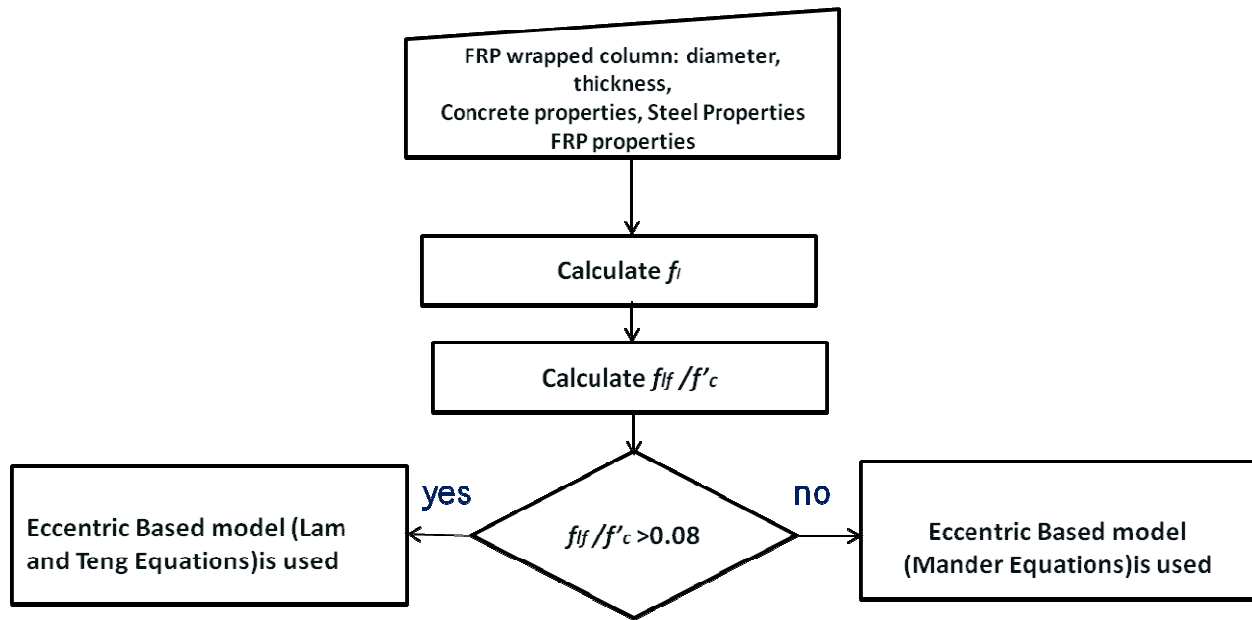
Figure 3-14: FRP and LSR Model Implementation

3-3-2 Numerical Analysis

The cross section analyzed is loaded incrementally by maintaining a certain eccentricity between the axial force P and the resultant moment M_R. Since increasing the load and resultant moment causes the neutral axis and centroid to vary nonlinearly, the generalized moment of area theorem is devised.

The method is developed using incremental iterative analysis algorithm, secant stiffness approach and proportional or radial loading. It is explained in the following steps (Figure 3-18):

   1- Calculating the initial section properties:

- Elastic axial rigidity *EA*:

$$EA = \sum_i E_c w_i t_i + \sum_i (E_s - E_c) A_{si}$$
3-76

E_c = initial modulus of elasticity of the concrete

219

E_s = initial modulus of elasticity of the steel rebar

The depth of the elastic centroid position from the bottom fiber of the section Y_c

$$Y_c = \frac{\sum_i E_c w_i t_i (H - Y_i) + \sum_i (E_s - E_c) A_{si} (H - Y_{si})}{EA}$$

3-77

- Elastic flexural rigidity about the elastic centroid *EI*:

$$EI_x = \sum_i E_c w_i t_i (H - Y_i - Y_c)^2 + \sum_i (E_s - E_c) A_{si} (H - Y_{si} - Y_c)^2$$

3-78

Typically Yc = *H/2*.

- The depth of the geometric section centroid position from the bottom and left fibers of the section Y_G:

$$Y_G = \frac{H}{2}$$

3-79
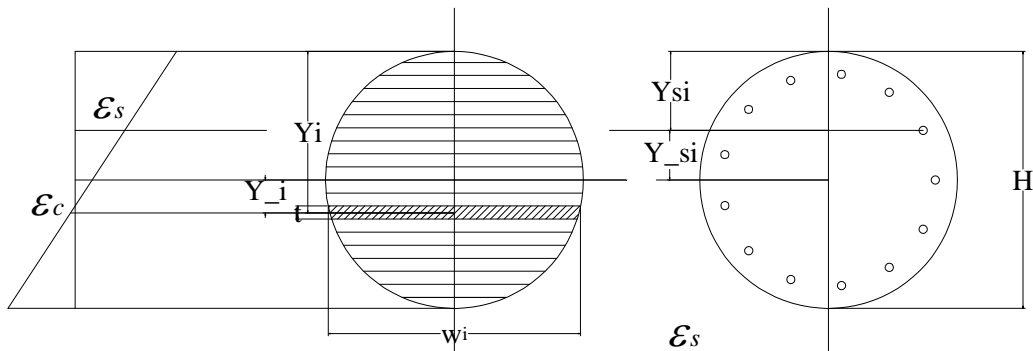
Figure 3-15: Geometric properties of concrete layers and steel rebars

2- Calculating f_{lf}/f'_c and check the ratio to decide which model is used (Eccentric model based on Lam and Teng Equations or Eccentric model based on Mander Equations) Figure (3-14).

220

3- Defining eccentricity *e*, which specifies the radial path of loading on the interaction diagram.
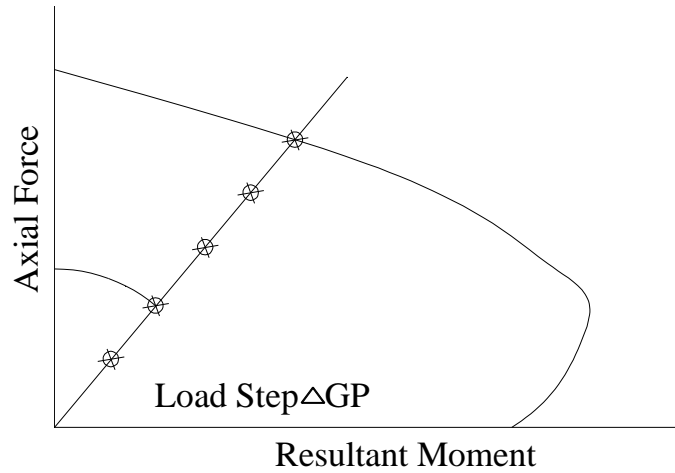
Figure 3-16: Radial loading concept

4- Defining loading step ΔGP as small portion of the maximum load, and computing the axial force at the geometric centroid.

$$GP_{new} = GP_{old} + \Delta GP \qquad \text{3-80}$$

5- Calculating moment *GM* about the geometric centroid.

$$e = \frac{GM_x}{GP} \qquad\qquad GM_x = e * GP \qquad \text{3-81}$$

6- Transferring moment to the updated inelastic centroid and calculating the new transferred moment TM_X :

$$TM_X = GM_x + GP(Y_G - Y_c) \qquad \text{3-82}$$

The advantage of transferring the moment to the position of the inelastic centroid is to eliminate the coupling effect between the force and moment, since $EAM_x = 0$ about the inelastic centroid

221

$$\begin{bmatrix} P \\ TM_x \end{bmatrix} = \begin{bmatrix} EA & 0 \\ 0 & EI_x \end{bmatrix} \begin{bmatrix} \varepsilon_o \\ \phi_x \end{bmatrix}$$

3-83
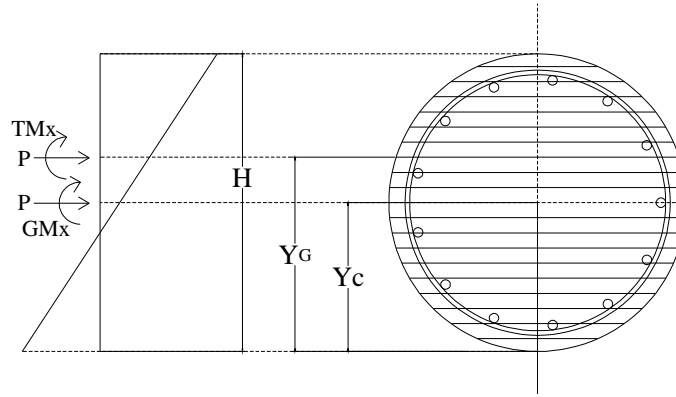
Figure 3-17: Transfering Moment from geometric centroid to inelastic centroid

7- Finding: Curvatures ϕ

$$\phi_x = \frac{TM_x}{EI_x}$$

3-84

Strain at the inelastic centroid ε_o, the extreme compression fiber strain ε_{ec}, and strain at the extreme level of steel in tension ε_{es} are found as follow:

$$\varepsilon_o = \frac{GP}{EA}$$

3-85

$$\varepsilon_{ec} = \varepsilon_o + \phi_x(H - Y_c)$$

3-86

$$\varepsilon_{es} = \varepsilon_o - \phi_x(Y_c - Cover)$$

3-87

where cover is up to center of bars

8- Calculating strain ε_{ci} and corresponding stress f_{ci} in each layer of concrete section by using selected model from step 2.

$$\varepsilon_{ci} = \varepsilon_{ec} - \phi Y_i$$

3-88

9- Calculating strain ε_{si} and corresponding stress f_{si} in each bar in the given section by using the steel model (Elastic up to yield strength and then perfectly plastic)

$$\varepsilon_{si} = \varepsilon_{ec} - \phi Y_{si}$$

$$3\text{-}89$$

10- Calculating the new section properties: axial rigidity EA, flexural rigidities about the inelastic centroid EI_x, moment of axial rigidity about inelastic centroid EAM_x, internal axial force F_z, internal bending moments about the inelastic centroid M_{ox},

$$EA = \sum_i E_{ci} w_i t_i + \sum_i (E_{si} - E_{ci}) A_{si}$$

$$3\text{-}90$$

$$EAM_x = \sum_i E_{ci} w_i t_i (H - Y_c - Y_i) + \sum_i (E_{si} - E_{ci}) A_{si} (H - Y_c - Y_{si})$$

$$3\text{-}91$$

$$F_z = \sum f_{ci} w_i t_i + \sum (f_{si} - f_{ci}) A_{si}$$

$$3\text{-}92$$

$$EI_x = \sum_i E_{ci} w_i t_i (H - Y_c - Y_i)^2 + \sum_i (E_{si} - E_{ci}) A_{si} (H - Y_c - Y_{si})^2$$

$$3\text{-}93$$

$$M_{ox} = \sum f_{ci} w_i t_i (H - Y_c - Y_i) + \sum (f_{si} - f_{ci}) A_{si} (H - Y_c - Y_{si})$$

$$3\text{-}94$$

where E_{ci} = secant modulus of elasticity of the concrete layer.

E_{si} = secant modulus of elasticity of the steel bar.

11- Transferring back the internal moment about the geometric centroid

$$GM_{ox} = M_{ox} - GP(Y_G - Y_c)$$

$$3\text{-}95$$

12- Checking the convergence of the inelastic centroid

$$TOL_x = EAM_x / EA / Y_c$$

$$3\text{-}96$$

13- Comparing the internal force to applied force, internal moments to applied moments, and assuring that the moments are calculated about the geometric centroid :

$$\left| GP - F_z \right| \leq 1 * 10^{-5}$$

$$3\text{-}97$$

223

$$\left|GM_x - GM_{ox}\right| \leq 1 * 10^{-5}$$

$$\left|Tol_x\right| \leq 1 * 10^{-5}$$

If Equations (3-97), (3-98) and (3-99) are not satisfied, the location of the inelastic centroid is updated by EAM_x/EA and steps 5 to 11 are repeated till Equations (3-97), (3-98) and (3-99) are satisfied.

$$Y_{c_{new}} = Y_{c_{old}} + \frac{EAM_x}{EA}$$

Once equilibrium is reached, the algorithm checks for ultimate strain in concrete ε_{ec} and steel ε_{es} not to exceed $\overline{\varepsilon_{cc}}$ (or $\overline{\varepsilon_{cu}}$ based on the selected model) and 0.05 respectively, then it increases the loading by ΔGP and runs the analysis for the new load level using the latest section properties. Otherwise, if ε_{ec} equals $\overline{\varepsilon_{cc}}$ (or $\overline{\varepsilon_{cu}}$ based on the selected model) or ε_{es} equals 0.05, the target force and resultant moment are reached as a point on the failure surface for the amount of eccentricity used.

Figure 3-18: Flowchart of FRP wrapped columns analysis

3-4 Results and Discussion

First the stress-strain curves are compared with some experimental work found in the literature. Then, Interaction diagrams generated by KDOT Column Expert Software are plotted and compared to the corresponding experimental work as well. Interaction diagrams are generated using the numerical formulation described in section 3-3

3-4-1 Stress-Strain Curve Comparisons with Experimental Work

To validate the concentrically confined model, a set of experimental data are compared to this model. The cross section properties of the columns are shown in Table 3-1

Table 3-1: Experimental data used to verify the ultimate strength and strain for the confined model (Eid *et a*l. 2006)

					FRP		LSR		
case	D	cover	f'_c	ε'_c	t	E_f	f_{yh}	S	Φ
	mm	mm	MPa		mm	GPa	MPa	mm	mm
1	253	0	36	0.002	0.762	78	456	65	11.3
2	303	25	31.7	0.002	1.524	78	456	100	11.3
3	303	25	31.7	0.002	0.762	78	456	65	11.3
4	303	25	50.8	0.002	1.524	78	456	65	11.3

ε_{fu} for all cases is 0.0134

As shown in Fig. 3-18 there is an excellent correlation between the experimental point and the stress strain curve developed theoretically, since the theoretical ultimate peak strength and strain are 9.35 ksi (64.5 MPa) and 0.0142, whereas the experimental point is at 9.5 ksi (65.5 MPa) in strength with a strain of 0.0155. The percentage errors are about 3% for strength and 8% for strain. From Table 3-1, the cross section has no cover which means the LSR and the FRP act

on the same position. The ratio of f_{lf}/f'_c is 0.1 which is bigger than 0.08, hence, the stress-strain curve is generated based on Lam and Teng model. Also, the lateral pressure due to FRP is equal to 0.535 ksi that contributes to 40% of the total effective lateral confinement which has a value of 1.32 ksi. So the amount of confinement provided by the FRP is significantly high.
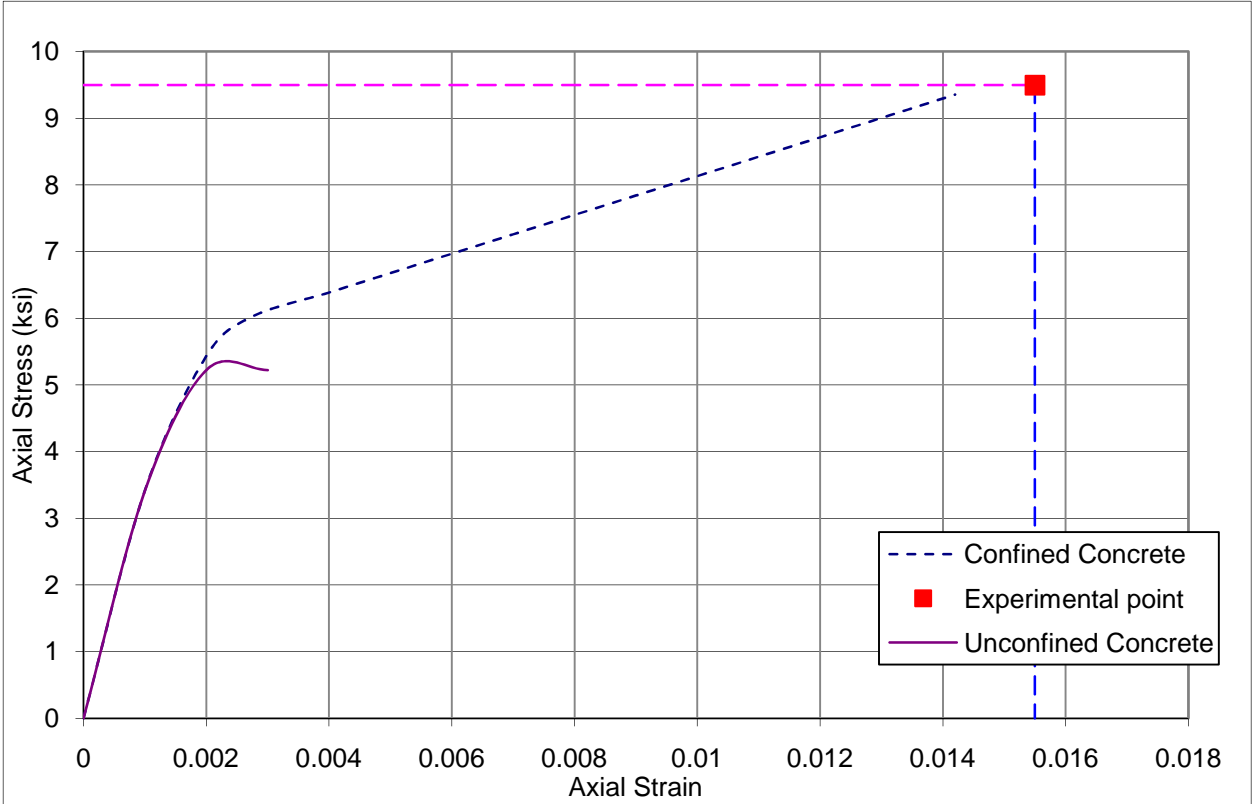
Figure 3-19: Case 1 Stress-Strain Curve Compared to Experimental Ultimate Point
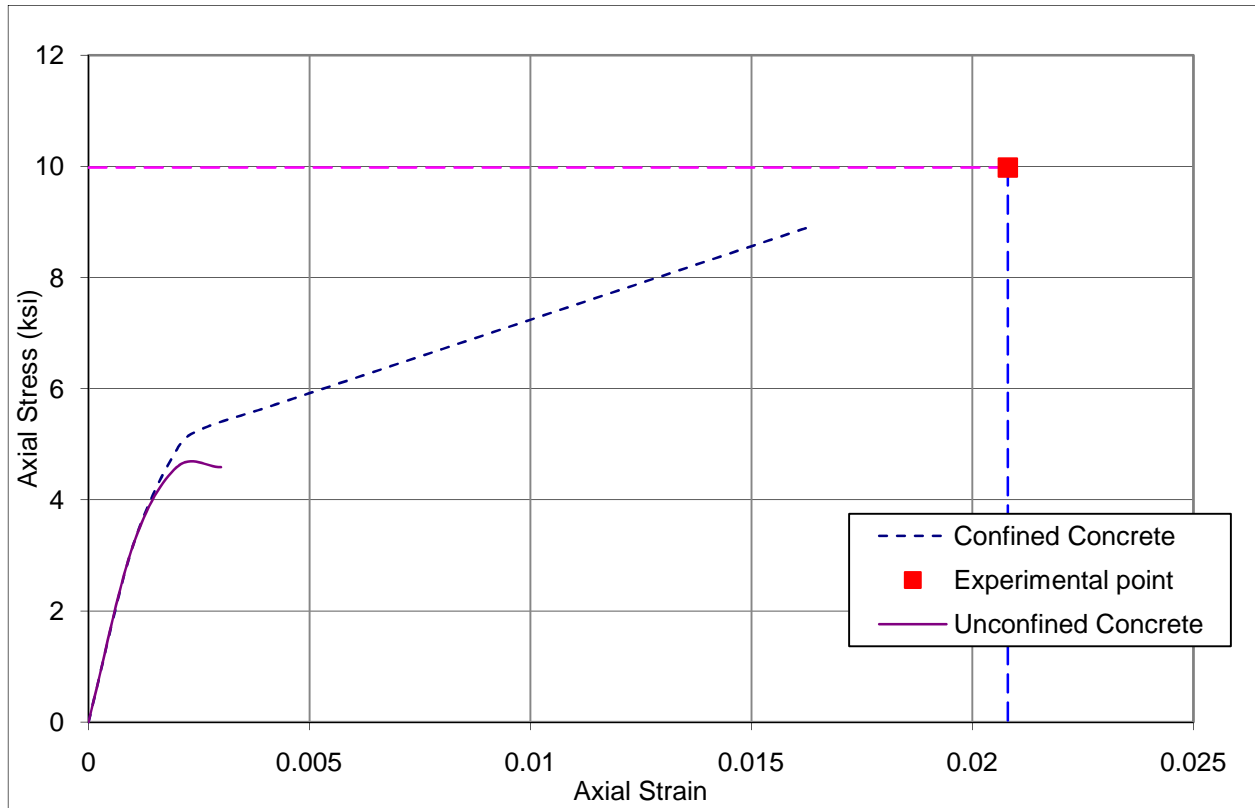
Figure 3-20: Case 2 Stress-Strain Curve Compared to Experimental Ultimate Point

The cross section in case 2 has a 25 mm cover representing 16.5 % of the full diameter. At the same time the FRP contribution to the overall lateral pressure is around 65% (0.89 ksi to 1.37 ksi). The curve is underestimating the actual experimental data by 9% for strength and 21% for the strain. The theoretical strength is 8.9 ksi (61.36 MPa) and the ultimate strain is 0.016 compared to 9.98 ksi (68.8 MPa) and 0.0208 from the experiment. This might be attributed to the fact of neglecting the Δp action, since the FRP pressure is more than 50% of the total confining pressure and at the same time the cover is not small compared to the full diameter. Dependently, the effective lateral confining pressure was under estimated so it did not push the curve further closer to the experimental point. Yet, if the second line is extended it will perfectly intersect the experimental point. This is a sign of the conservative ultimate strain prediction.
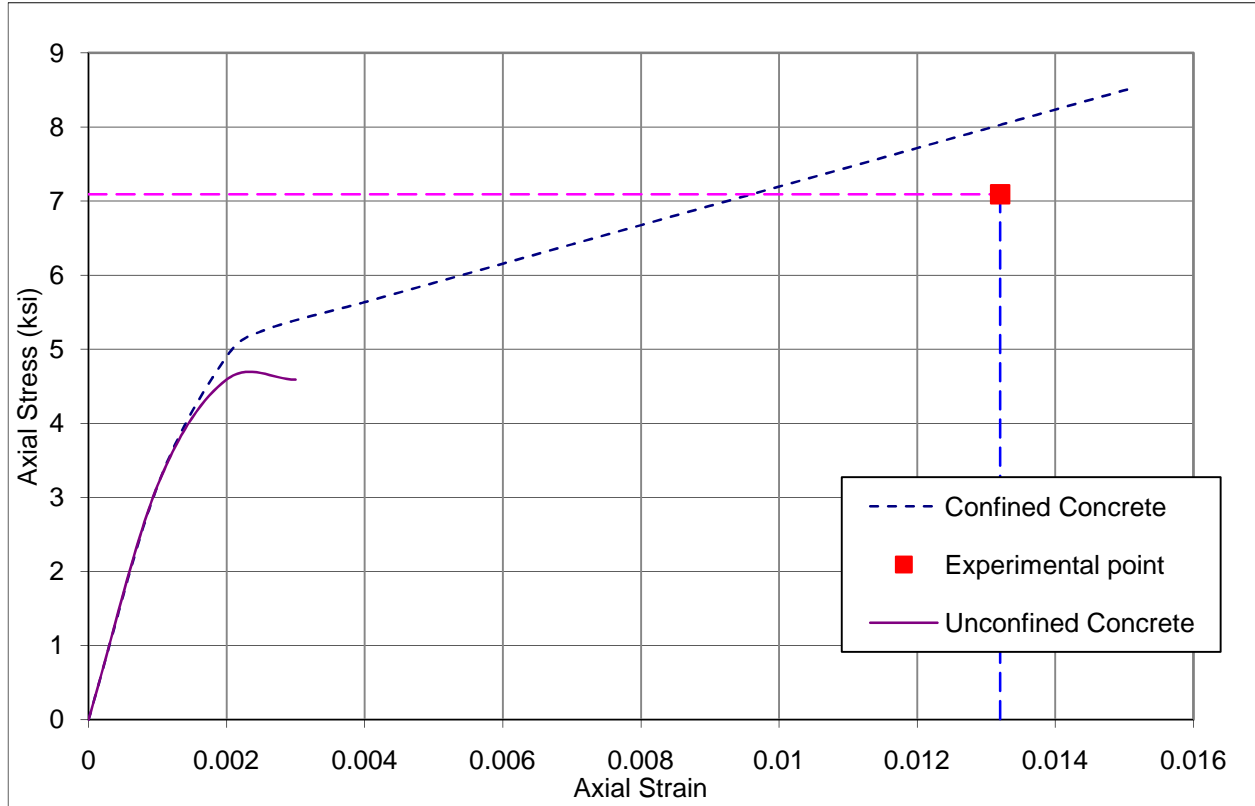
Figure 3-21: Case 3 Stress-Strain Curve Compared to Experimental Ultimate Point

The cross section parameters in case 3 are exactly the same as case 2 with two important variations. FRP thickness is half that of case 2 (0.762 mm) and the LSR spacing is 65 mm as opposed to 100 mm for case 2. These differences contribute to increase the LSR lateral pressure and decrease the FRP lateral pressure. However, the overall effective lateral pressure is close to that of case 2 (1.26 ksi compared to 1.37 ksi for case 2 or 8% difference). The peak ultimate theoretical strength and strain are 8.55 ksi and 0.015 while the peak ultimate experimental strength and strain are 7.1 ksi and 0.0132. The error percentages are 14% and 12% for strength and strain respectively. The ultimate theoretical point is close to the previous case. This is due to the fact that the decrease in the FRP lateral confinement is balanced out by the increase in LSR lateral confinement. The ratio of $f_{lf}/f'c$ is 0.097 which is still above but close to the ACI 440.2R-

08 ratio and the contribution of the FRP is about 35% of the total confinement. Those two ratios are way less than those of the previous case. Even if this case appears not to be conservative, the experimental peak point is close to that of the theoretical peak point.
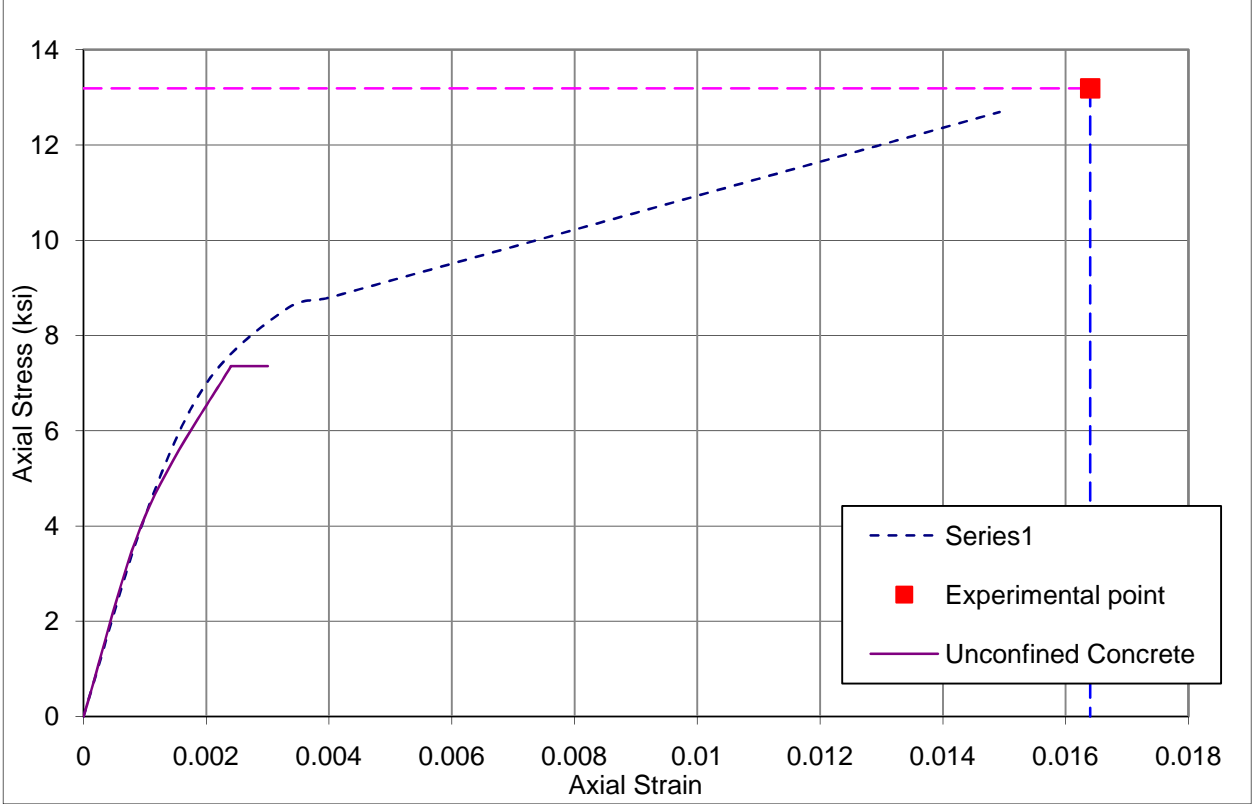
Figure 3-22: Case 4 Stress-Strain Curve Compared to Experimental Ultimate Point

Case 4 is similar to case 2 but with 50.8 *ksi* for *f'c* and LSR spacing of 65 mm. The contribution of the FRP and LSR are almost the same in this case (51% and 49% for FRP and LSR respectively). There is an obvious enhancement in effective confinement pressure compared to case 2 (1.7 ksi compared to 1.37 ksi) due to the increase in the peak unconfined strength and the decrease in LSR spacing. Also there is a noticeable increase in the ultimate strength and decrease in the ultimate strain (13.2 ksi and .0164). It is also noticed that the ratio of *flf /f'c* decreased to 0.12 as opposed to 0.19 for case 2. The reason of the decrease in ultimate strain is due to the

increase of $f'c$ since they are inversely proportional. However $f'c$ increases the ultimate strength because of the proportional relation between the two values.

In conclusion all the four cases were generated theoretically according to Lam and Teng model since the ratio of f_{lf}/f'_c exceeded 0.08. The reason of wrapping the section with FRP is to increase its ultimate strength and strain, so having a value of f_{lf}/f'_c less than 0.08 in experimental work or even practically will be very rare. Also, the confining pressure provided by the FRP was at least 30% of the total effective lateral pressure. In general the proposed model successfully compared to the experimental data with acceptable tolerance.

Furthermore, the proposed model is compared to the full stress-strain curves from experimental work and another analytical modeling. The experimental work cases are shown in Table (3-2).

Table 3-2: Experimental data used to verify the fully confined model

				FRP			TSR		
	D	c	f'c	t	E_f	ε_{fu}	f_{yh}	S	bar #
	(in)	(in)	(ksi)	(mm)	MPa		(ksi)	(in)	
1	303	25	31.7	0.762	78000	0.013	456	65	11.3
2	303	25	31.7	0.762	78000	0.013	456	100	11.3
3	253	0	36	0.762	78000	0.013	456	5	11.3
4	303	25	31.7	0.762	78000	0.013	602	70	9.5
5	303	25	0.8	1.524	78000	0.013	456	65	11.3
6	303	25	50.8	0.762	78000	0.013	456	65	11.3
7	300	20	23.9	0.9	84000	0.015	400	150	11.3
8	300	20	43.7	0.9	84000	0.015	400	300	6.4
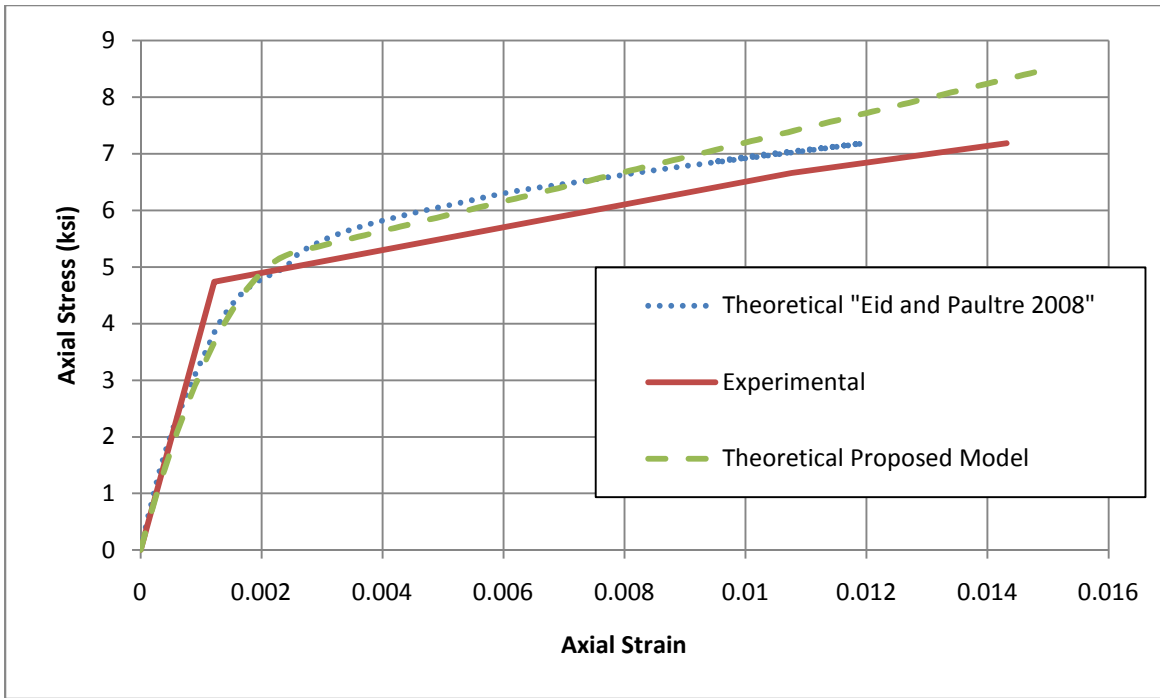
Figure 3-23: Case 1 Proposed Stress-Strain Curve Compared to Experimental and Eid and

Paultre (2008) theoretical ones
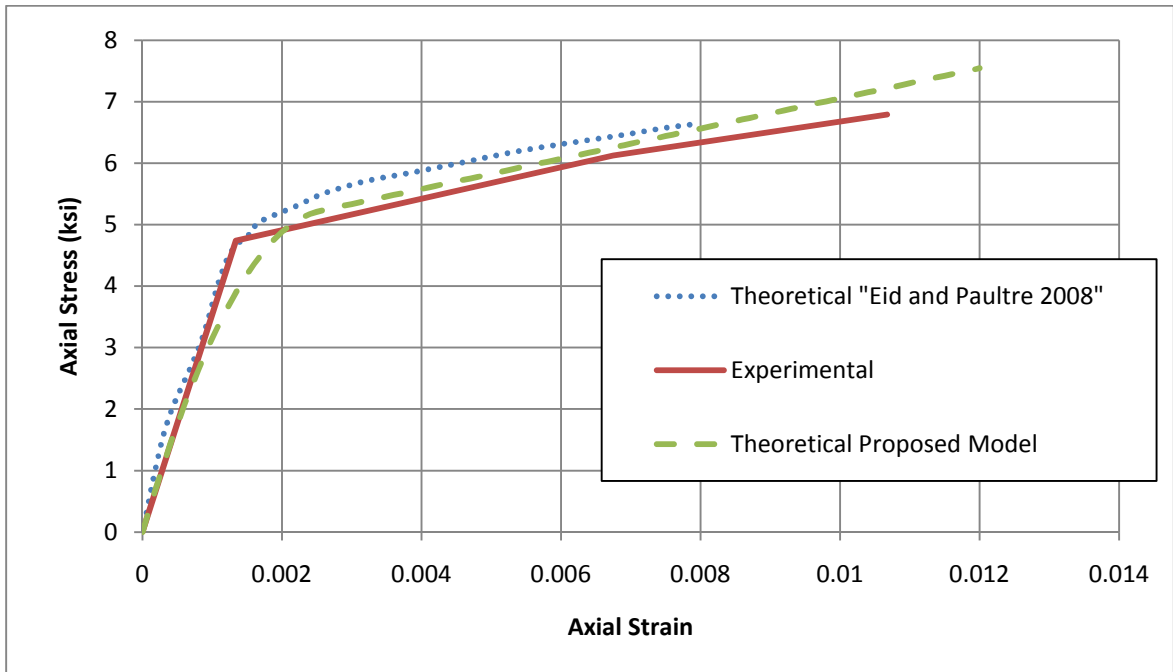
Figure 3-24: Case 2 Proposed Stress-Strain Curve Compared to Experimental and Eid and

Paultre (2008) theoretical ones
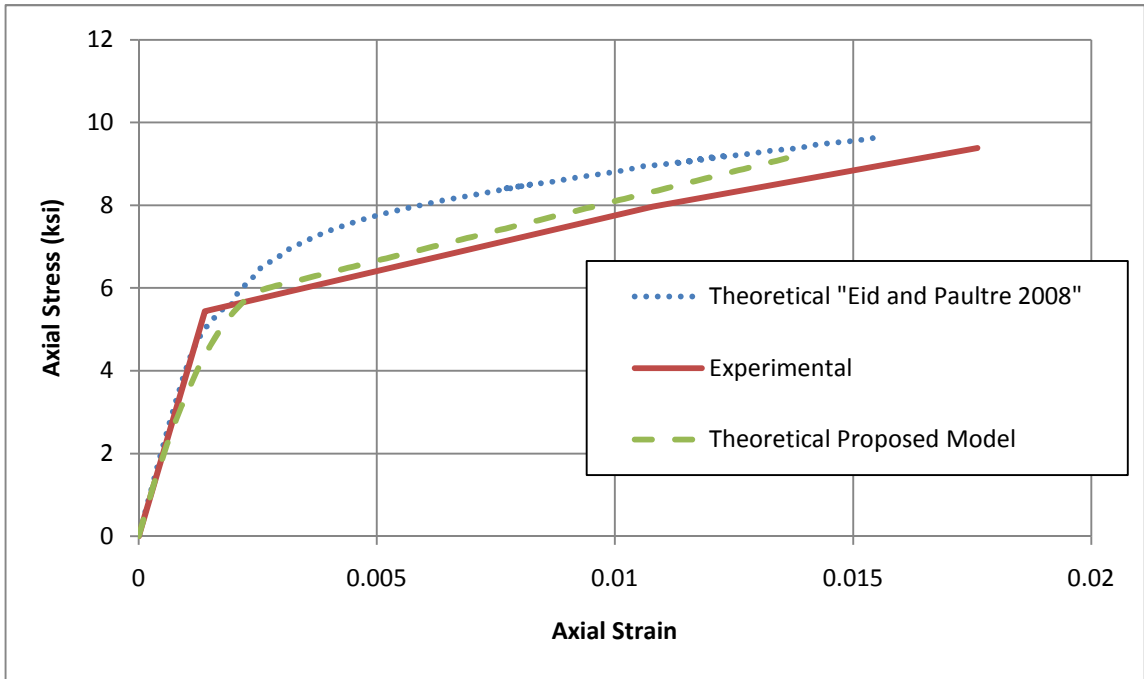
Figure 3-25: Case 3 Proposed Stress-Strain Curve Compared to Experimental and Eid and

Paultre (2008) theoretical ones
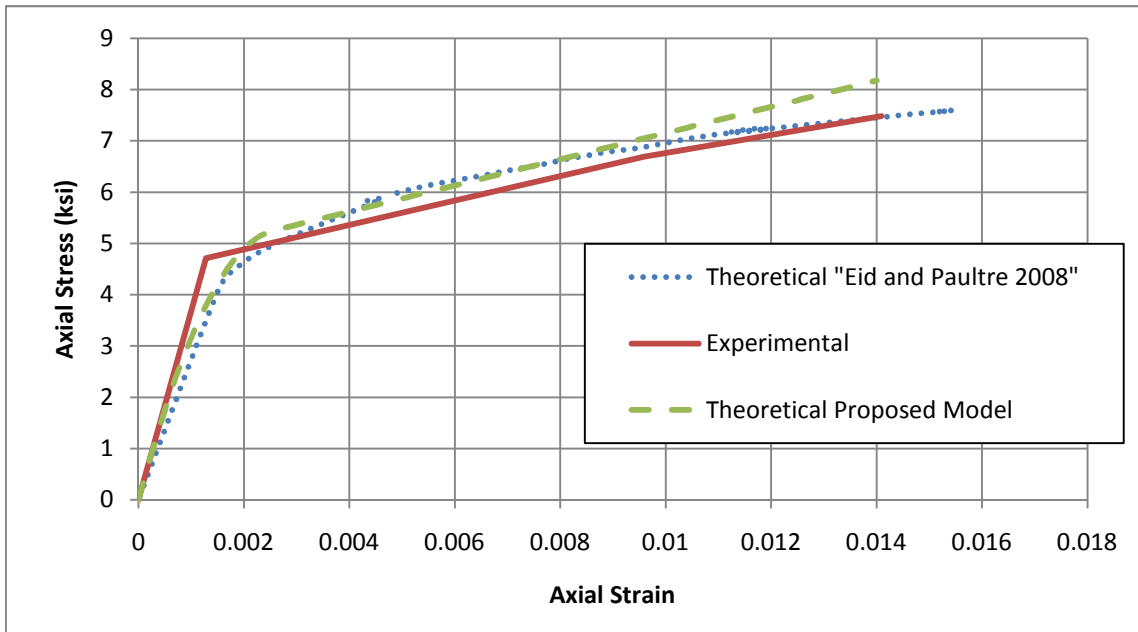
Figure 3-26: Case 4 Proposed Stress-Strain Curve Compared to Experimental and Eid and

Paultre (2008) theoretical ones
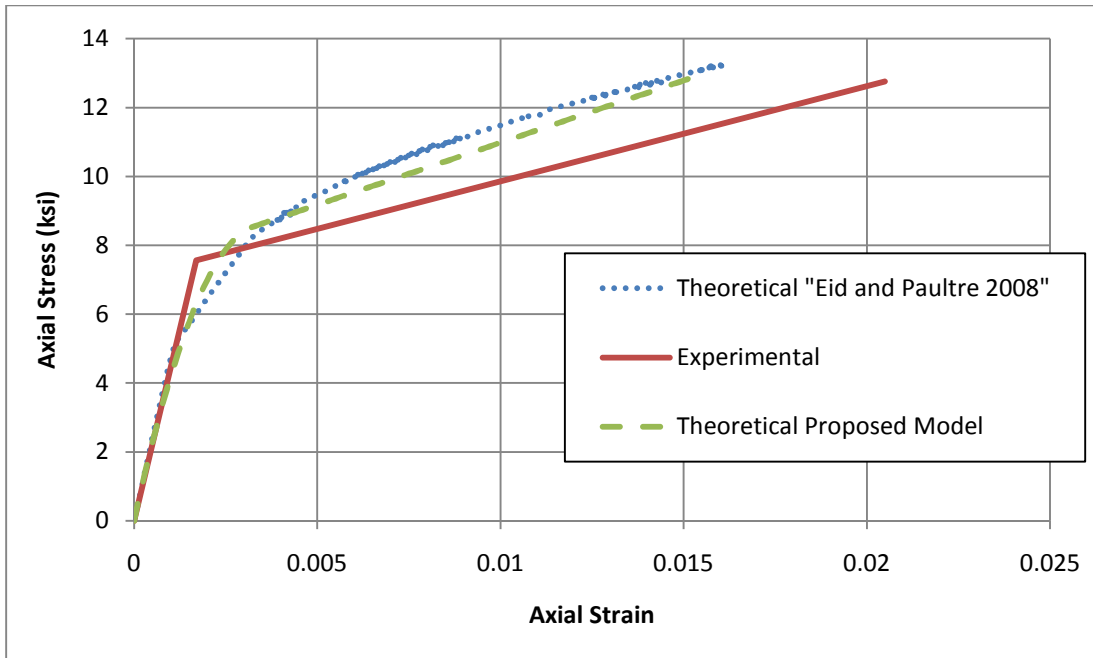
Figure 3-27: Case 5 Proposed Stress-Strain Curve Compared to Experimental and Eid and

Paultre (2008) theoretical ones
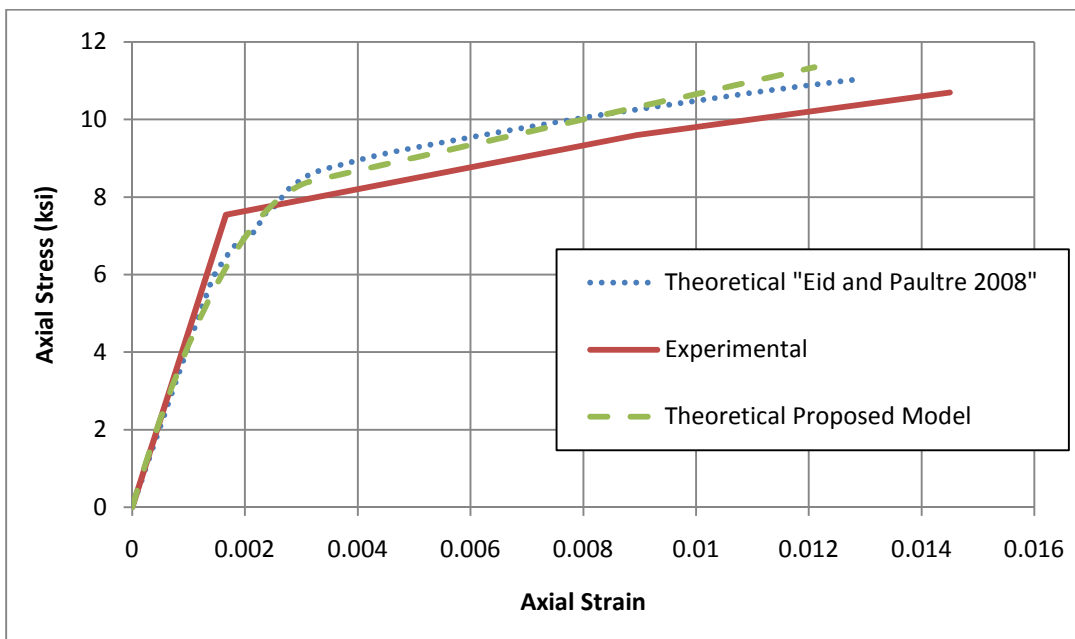
Figure 3-28: Case 6 Proposed Stress-Strain Curve Compared to Experimental and Eid and

Paultre (2008) theoretical ones
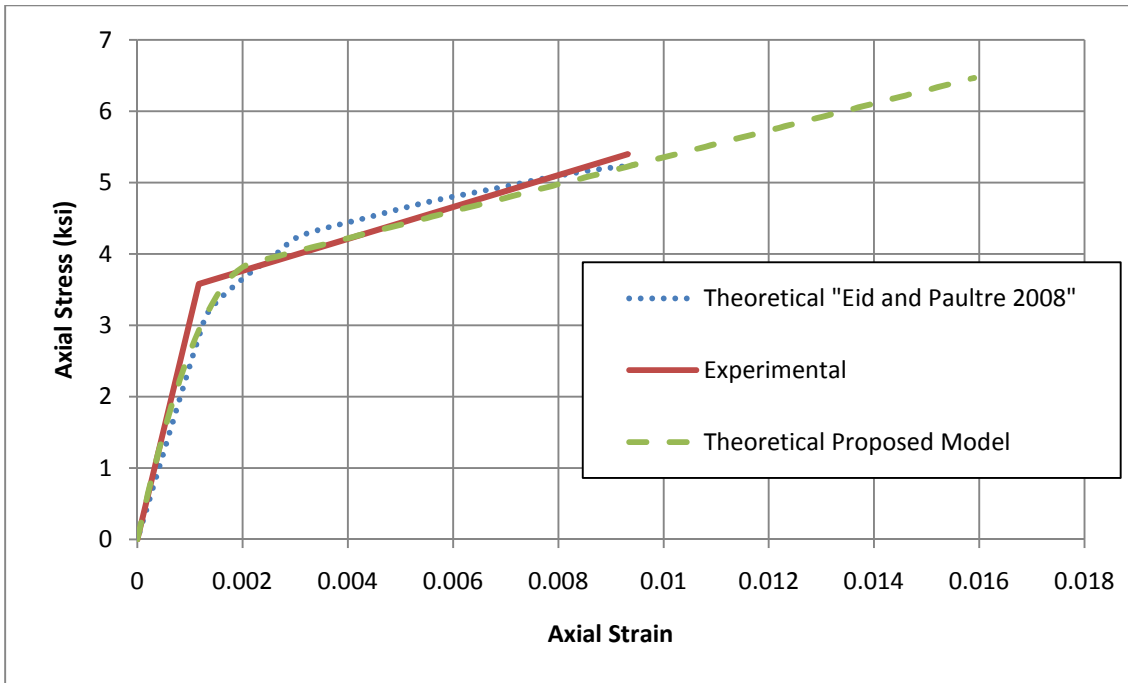
Figure 3-29: Case 7 Proposed Stress-Strain Curve Compared to Experimental and Eid and

Paultre (2008) theoretical ones
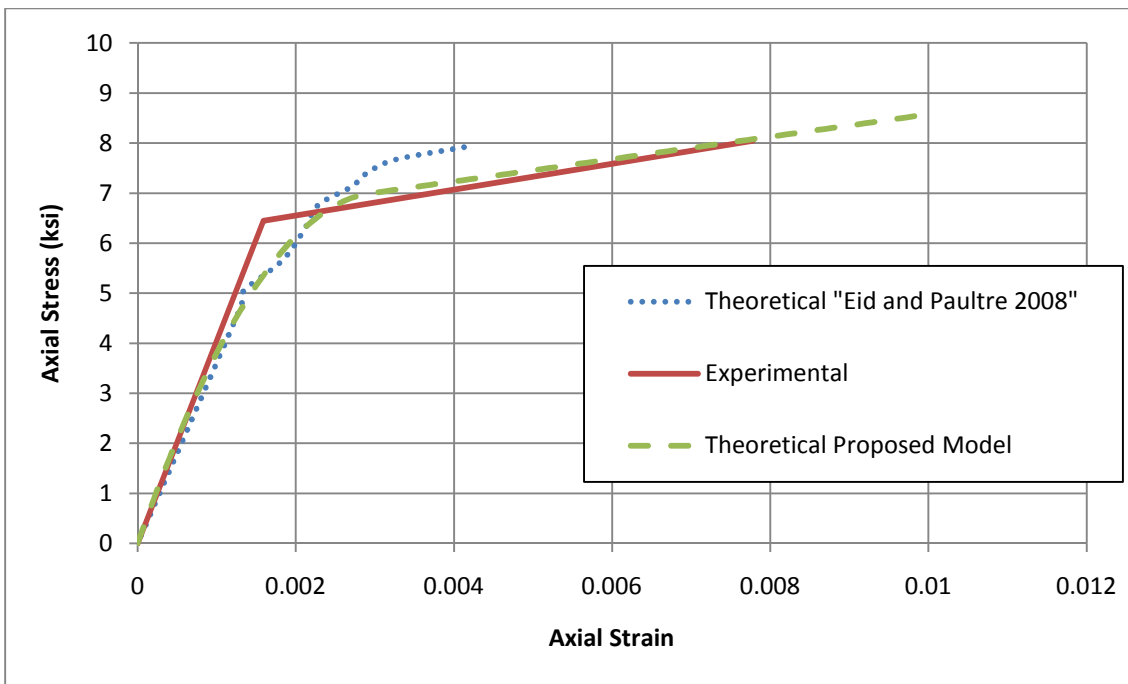
Figure 3-30: Case 8 Proposed Stress-Strain Curve Compared to Experimental and Eid and

Paultre (2008) theoretical ones

Figure (3-23) to (3-30) show the accuracy of the proposed model compared to experimental work and the plasticity model proposed by Eid and Paultre (2008). The eight cases in table 3-2 are taken from Eid and Paultre (2008) paper.

3-4-2 Interaction Diagram Comparisons with Experimental Work

To illustrate the results of the eccentricity based model, the interaction diagram is plotted using the eccentricity model and compared to experimental points.

Table 3-3: Experimental data used to verify the interaction diagrams.

				FR			TSR			Long. Steel	
	D	c	f'c	t	E_f	ε_{fu}	f_{yh}	s	#	#	fy
	mm	mm	MPa	mm			MPa	mm			MPa
1	303	25	31.7	2*0.381	78000	0.013	456	100	#3	6#5	423
2	303	25	36	2*0.381	78000	0.013	456	100	#3	6#5	423
3	303	25	31.7	4*0.381	78000	0.013	456	100	#3	6#5	423
4	303	25	31.7	2*0.381	78000	0.013	456	100	#3	6#5	550
5	303	25	50.7	2*0.381	78000	0.013	456	100	#3	6#5	423
6	303	25	31.7	2*0.381	78000	0.013	456	65	#3	6#5	423
7	303	25	36	2*0.381	78000	0.013	456	65	#3	6#5	423
8	303	25	36	4*0.381	78000	0.013	456	65	#3	6#5	423
9	303	25	50.7	2*0.381	78000	0.013	456	65	#3	6#5	423
10	303	25	50.7	4*0.381	78000	0.013	456	65	#3	6#5	430

11	305	25	34.5	6*0.762	18600	0.029	89	3.5	#3	14#4	65
12	355	25	40.3	1.245	25533	0.02	500	300	#3	6#8	500
13	355	25	44.8	0.99	75000	0.013	500	300	#3	6#8	500
14	355	25	40.3	0.5	75000	0.013	500	300	#3	6#8	500

The first ten cases are taken from Eid *et al* (2006), case number 11 is taken from Saadatmanesh *et al* (1996) and the last three cases are taken from Sheikh and Yau (2002)
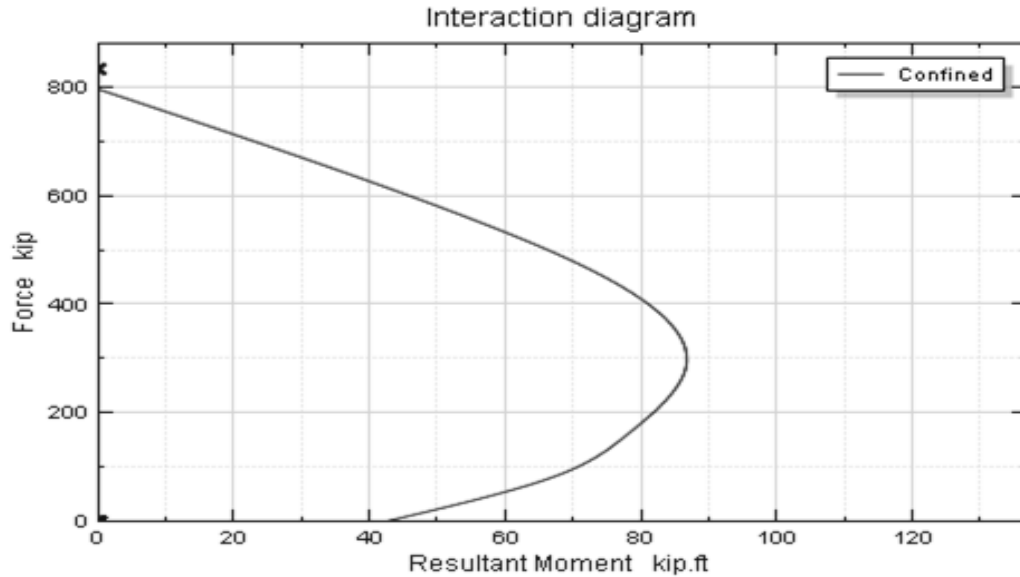
Figure 3-31: Case 1 Proposed Interaction Diagram compared to Experimental point from Eid *et al* (2006)
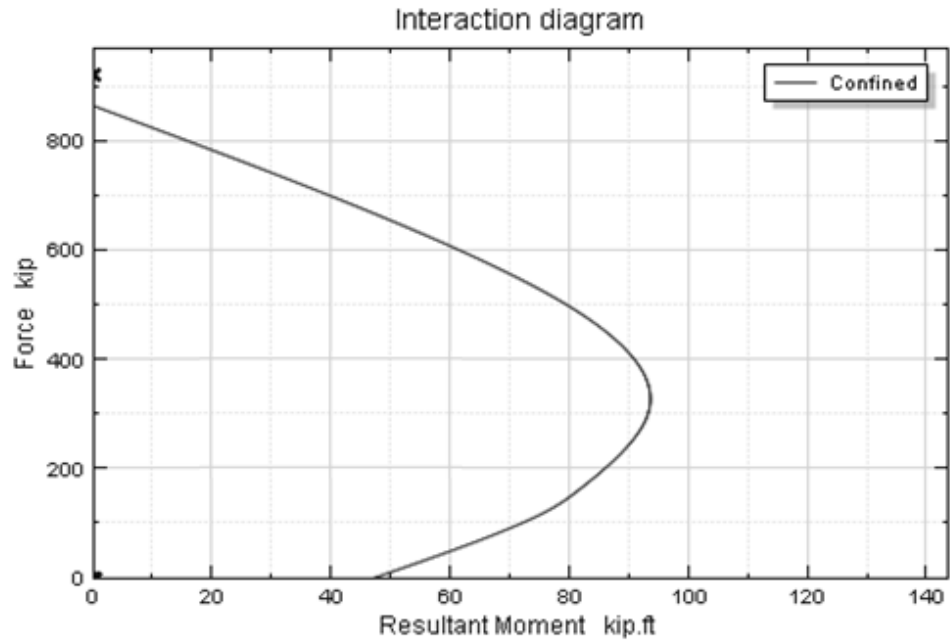
Figure 3-32: Case 2 Proposed Interaction Diagram compared to Experimental point from Eid *et*
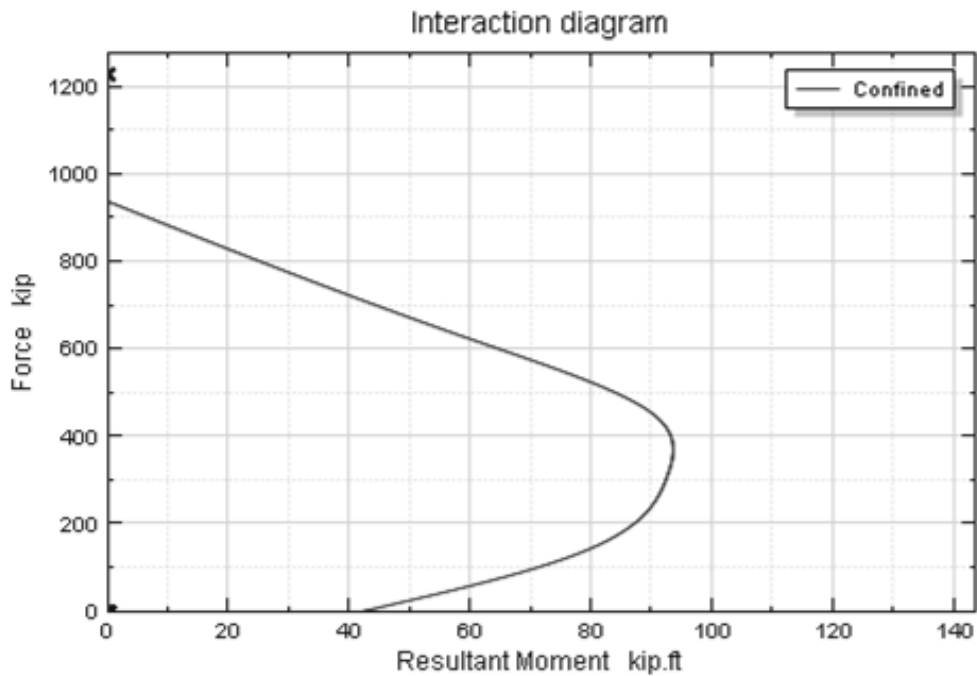
al (2006)

Figure 3-33: Case 3 Proposed Interaction Diagram compared to Experimental point from Eid *et*
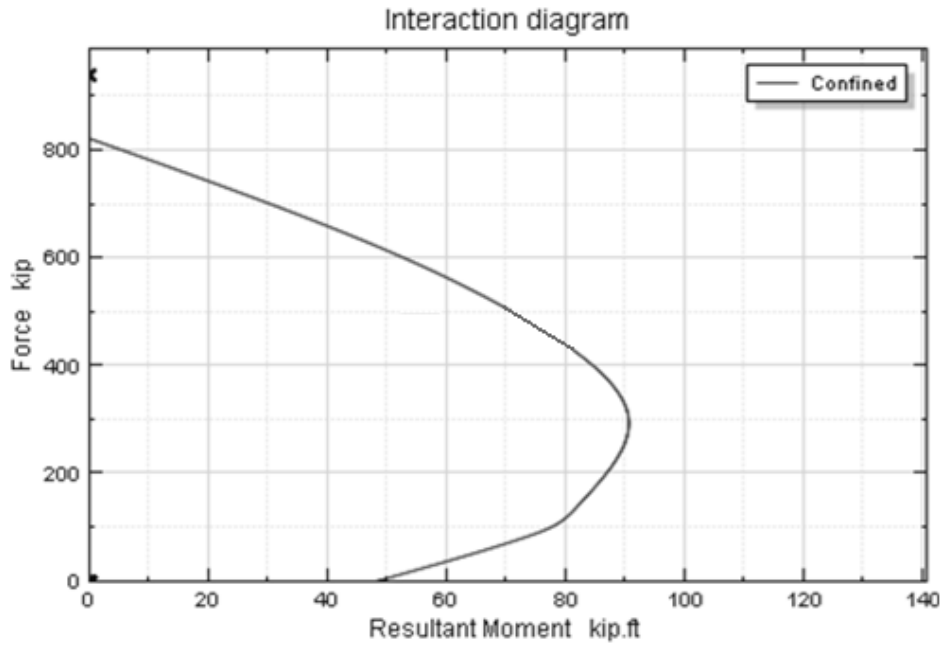
al (2006)

Figure 3-34: Case 4 Proposed Interaction Diagram compared to Experimental point from Eid *et al* (2006)
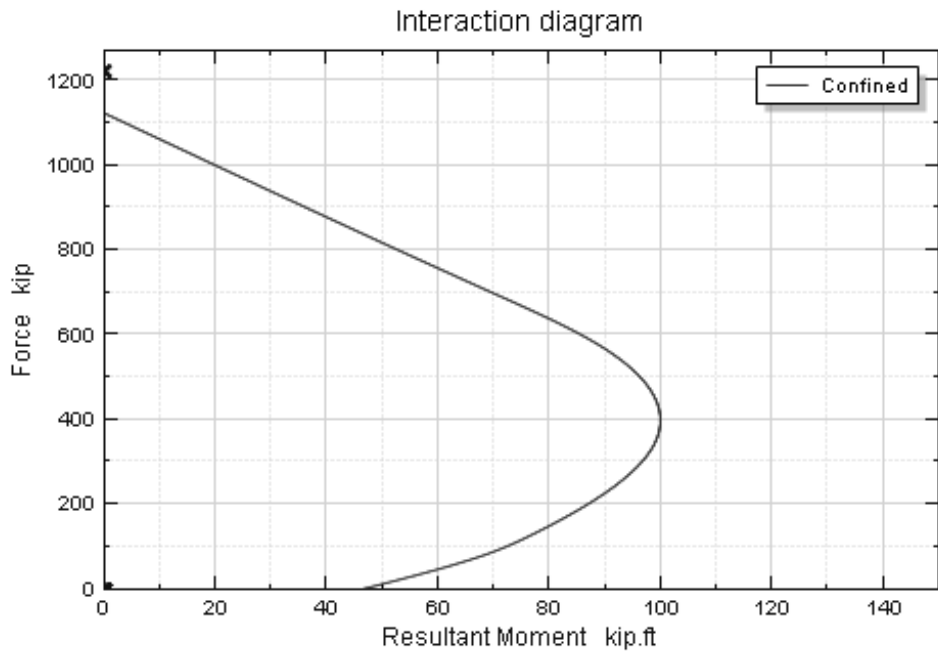
Figure 3-35: Case 5 Proposed Interaction Diagram compared to Experimental point from Eid *et al* (2006)
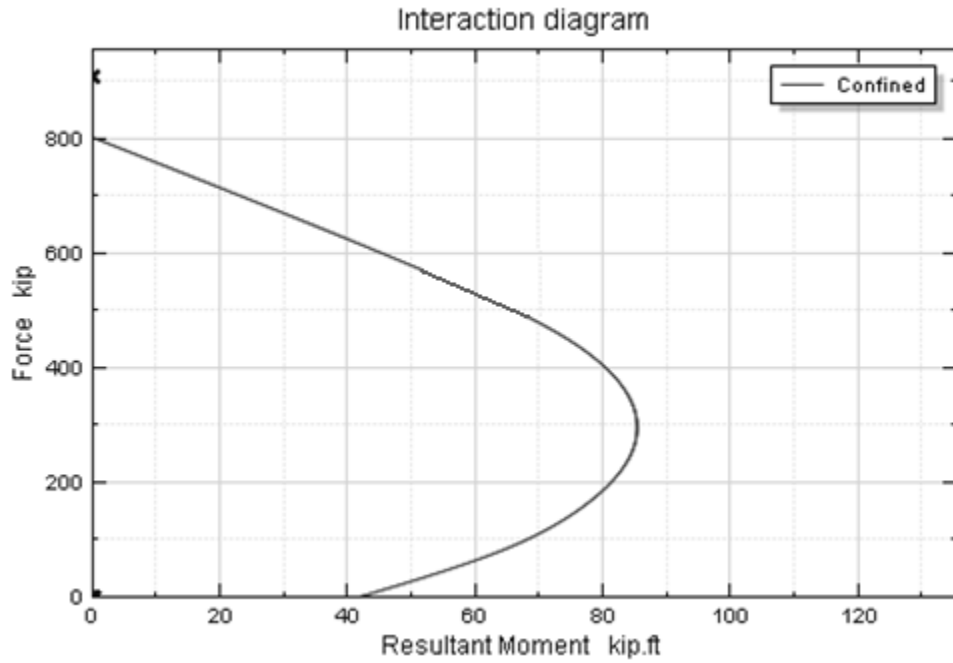
Figure 3-36: Case 6 Proposed Interaction Diagram compared to Experimental point from Eid *et al* (2006)
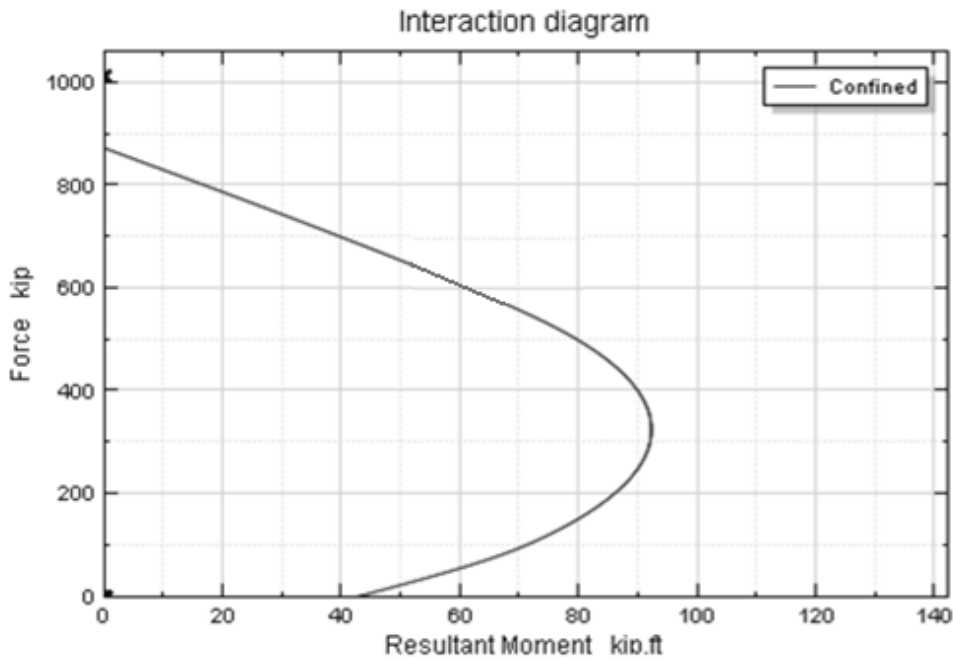
Figure 3-37: Case 7 Proposed Interaction Diagram compared to Experimental point from Eid *et al* (2006)

240
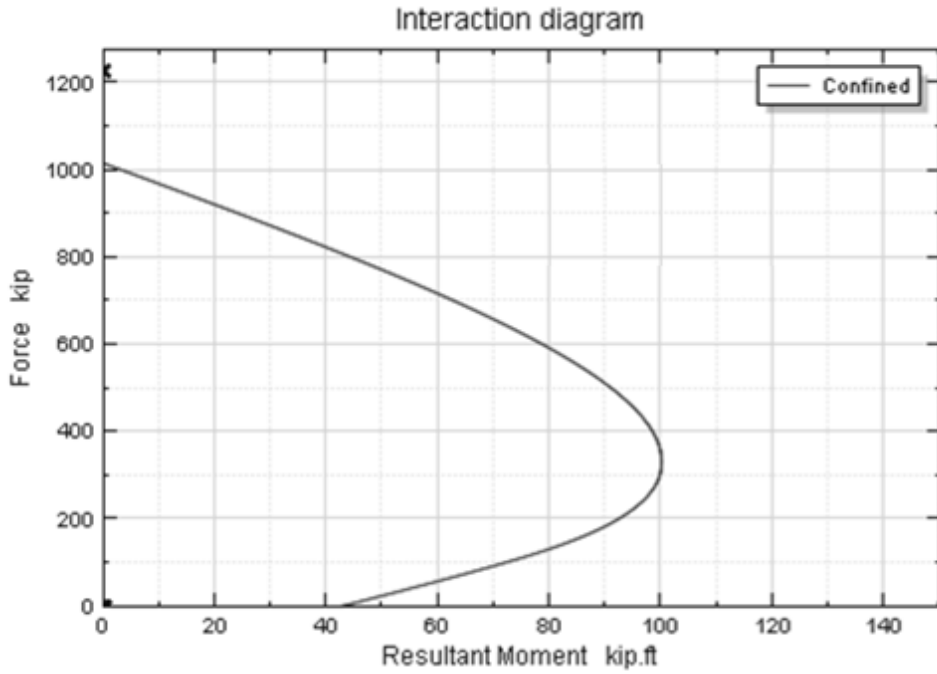
Figure 3-38: Case 8 Proposed Interaction Diagram compared to Experimental point from Eid *et al* (2006)
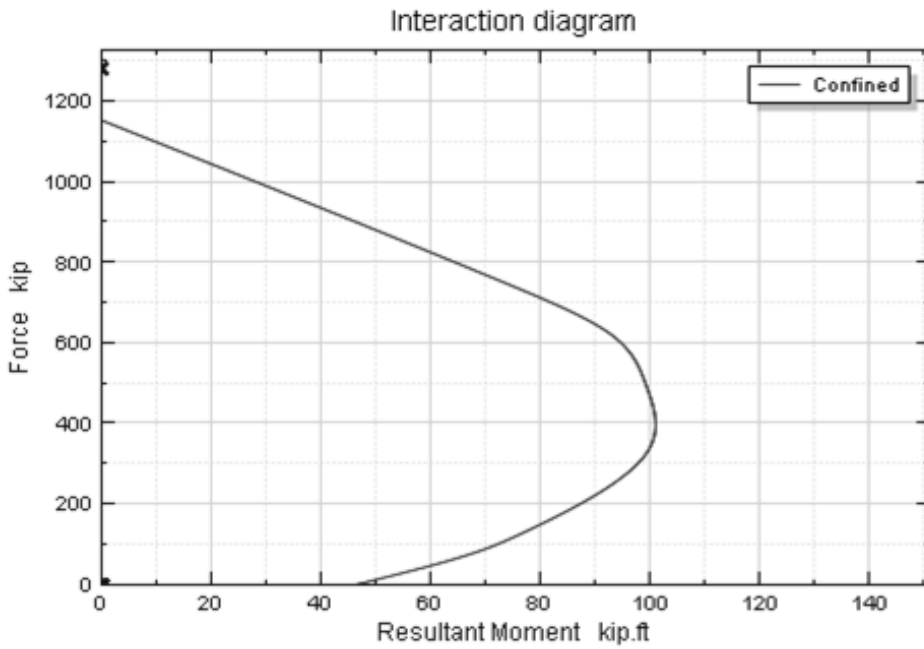
Figure 3-39: Case 9 Proposed Interaction Diagram compared to Experimental point from Eid *et al* (2006)
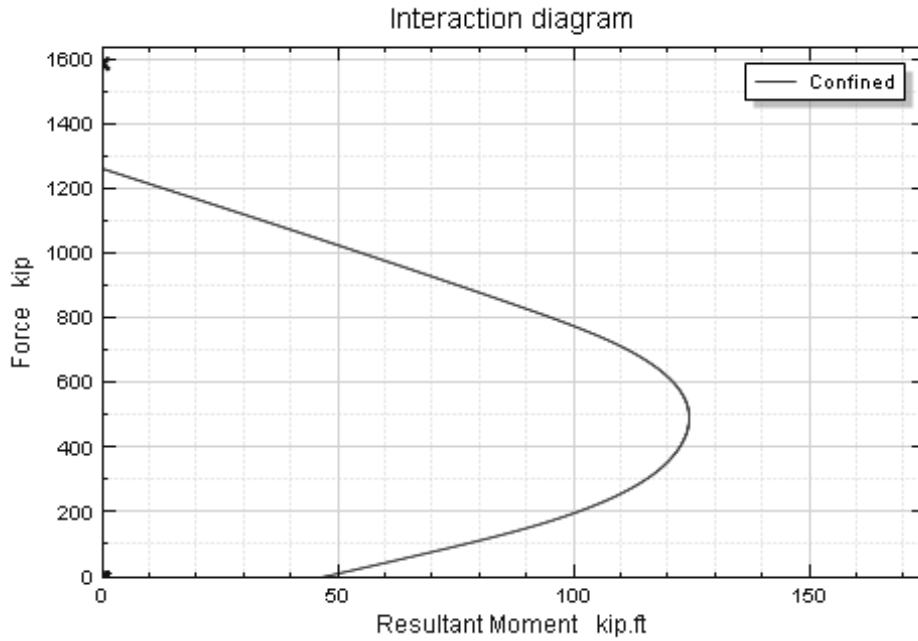
Figure 3-40: Case 10 Proposed Interaction Diagram compared to Experimental point from Eid *et al* (2006)
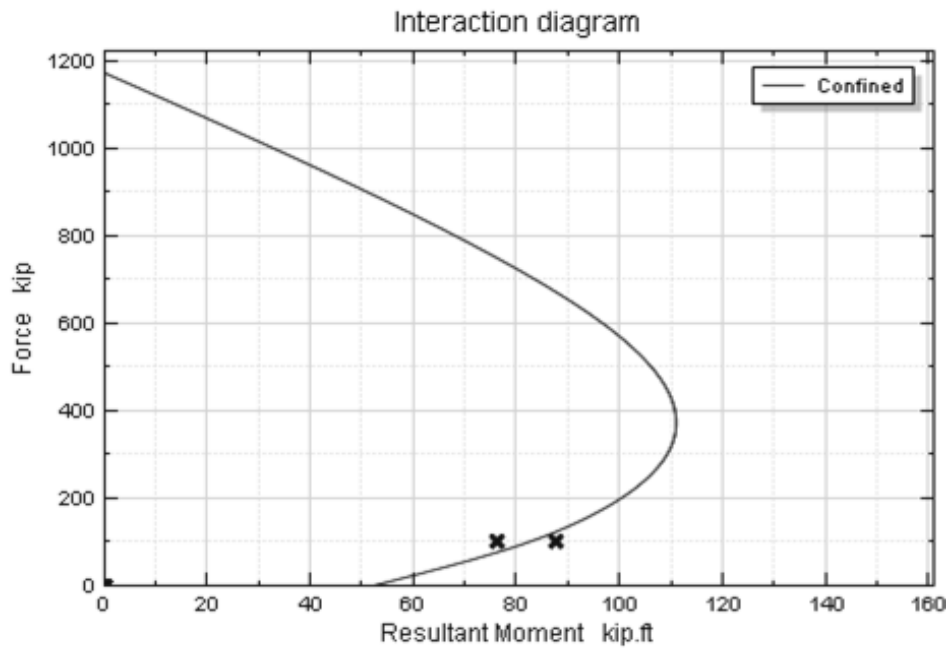
Figure 3-41: Case 11 Proposed Interaction Diagram compared to Experimental point from Saadatmanesh *et al* (1996)

242
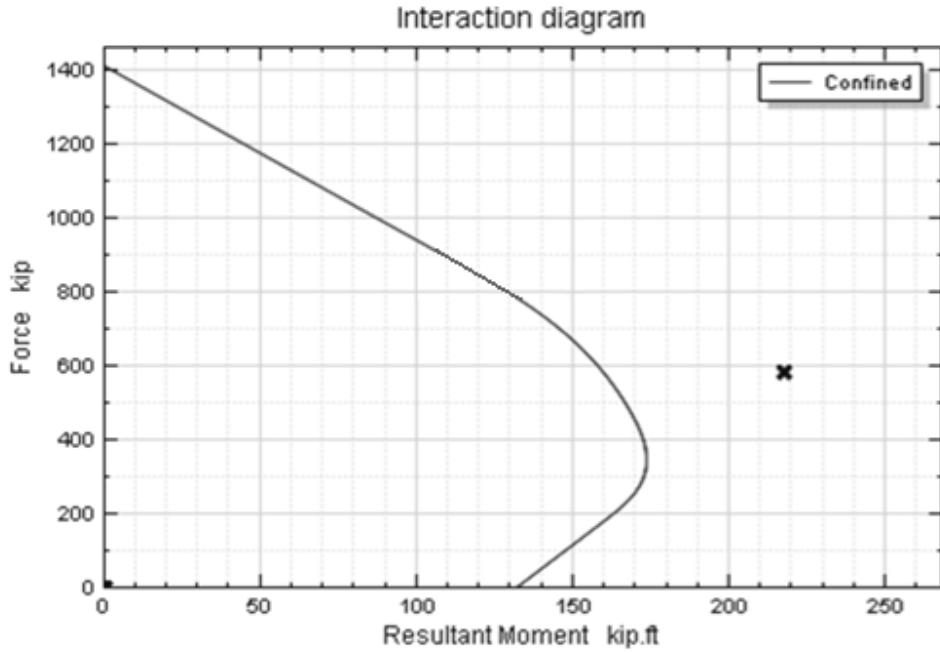
Figure 3-42: Case 12 Proposed Interaction Diagram compared to Experimental point from
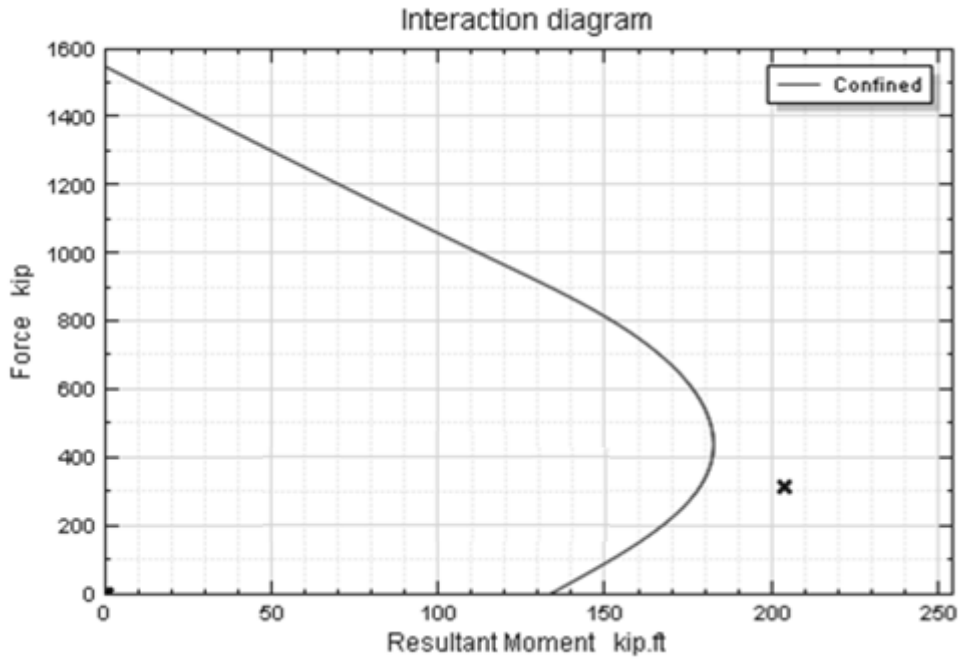
Sheikh and Yau (2002)

Figure 3-43: Case 13 Proposed Interaction Diagram compared to Experimental point from

Sheikh and Yau (2002)

243
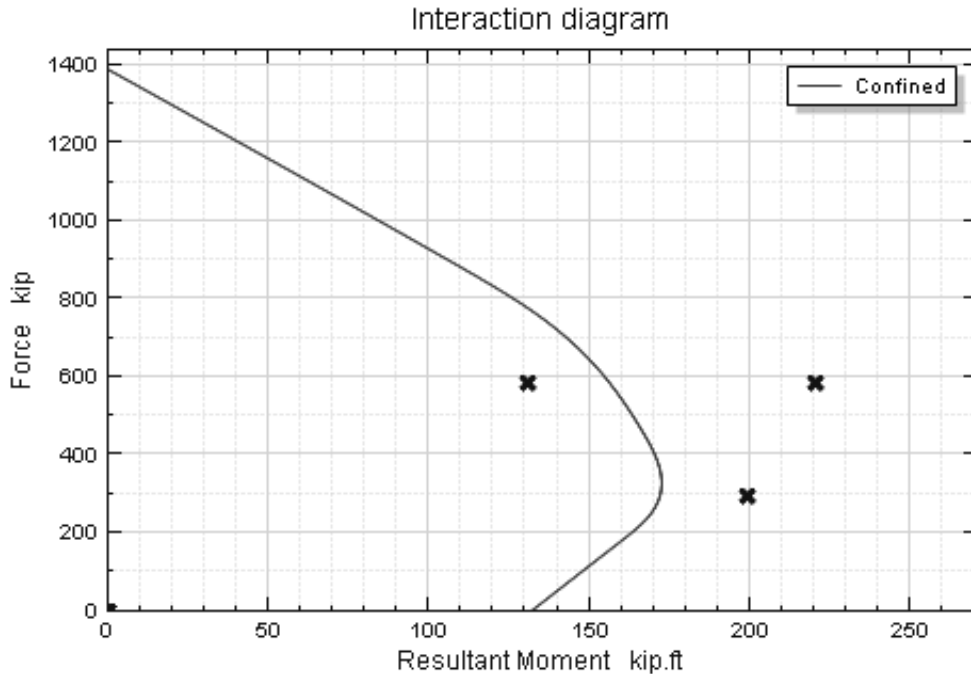
Figure 3-44: Case 14 Proposed Interaction Diagram compared to Experimental point from

Sheikh and Yau (2002)

The upper fourteen cases, Figure (3-31) to Figure (3-44) show the accuracy of the interaction diagrams generated by the proposed numerical analysis and the eccentric based stress-strain model. For most of the cases the experimental points lie outside the interaction diagram expressing conservative approach used through analysis. Figure (3-44) shows two experimental points having the same load level and significantly different moment values which is theoretically not feasible, since the moment has to be relatively proportional to the load applied. This justifies that the load and moment values of the inner experimental point might not be accurate.

Chapter 4 - Circular Concrete Filled Steel Tube Columns (CFST)

4-1 Introduction

CFST columns are not a relatively new construction approach compared to lateral steel confined columns. There are some structures that used CFST columns in the early 1900s such as Almondsbury Motorway Interchange (England), Charleroi Railways (Belgium) (Shams and Saadeghvaziri 1997). The concrete was used to stabilize the steel column against buckling. However extensive research on CFST columns did not start until the beginning of 1960s. With the appearance of FRP as a more durable material in the 1980s, CFST did not capture much attention compared to FRP. Hence, CFST column analysis is still considered a developing subject. Research was focused on CFST axially loaded columns and formulas were derived to predict their ultimate capacity. In addition there is some work that focuses on eccentric loading. However, there is still need for analysis of CFST columns under combined force and moment as the literature is lacking formulas and analysis procedure in this direction. The CFST columns are superior to conventional reinforced concrete and steel members as they provide more stiffness, ductility and energy absorption. The steel tube serves as construction formwork so there is no need for temporary formwork. The steel tube also confines the concrete and shares the axial load. The concrete, besides taking axial load, prevent the steel inward buckling. Studies showed that the behavior of CFST columns are influenced by width or diameter to thickness ratio, height to width or diameter ratio, cross sectional shapes and concrete to steel strength ratio. This study focuses only on circular stub columns so the shape and height to diameter ratio are insignificant. Poisson's ratio is a very important factor in evaluating the loading behavior. During the initial loading of CFST section, concrete has lower Poisson's ratio compared to steel. Hence it expands

laterally with no engagement from the steel. As cracks develop and concrete behaves inelastically, concrete Poisson's ratio becomes greater than steel's one and steel starts to confine concrete. Accordingly, concrete becomes under triaxial state of stress while steel is under biaxial stress state.

To develop a realistic estimation of the value of ultimate confined strength f_{cc} under pure axial compression, the Mander and Richart models are adapted to the case of concrete filled steel tubes and their predictions are compared to experimental data of normal and high strength concrete. Accordingly, a modified Richart equation is developed and used to obtain predictions for f_{cc}. Once the augmented strength f_{cc} is computed, the eccentricity model is incorporated in a numerical procedure that combines radial loading, finite layer method, secant stiffness procedure and moment of area concept to incrementally-iteratively generate the moment-curvature response of the column up to failure using a spectrum of eccentricities that yield the confined column interaction diagram. This has not been studied earlier. This procedure is benchmarked by comparing its results to some experimenetl data in the literature

4-2 Formulations

4-2-1 Finite Layer Approach (Fiber Model)

The column cross section is divided into a finite number of thin layers (Figure 4-1). The force and moment of each layer is calculated and stored. The steel tube is divided also into small radial segments. The advantage of that is to avoid inaccuracy generated from using the approximation of the stress block method, as a representative of the compression zone and to

precisely calculate the internal forces induced by steel tube segments and concrete layers in the column cross section.
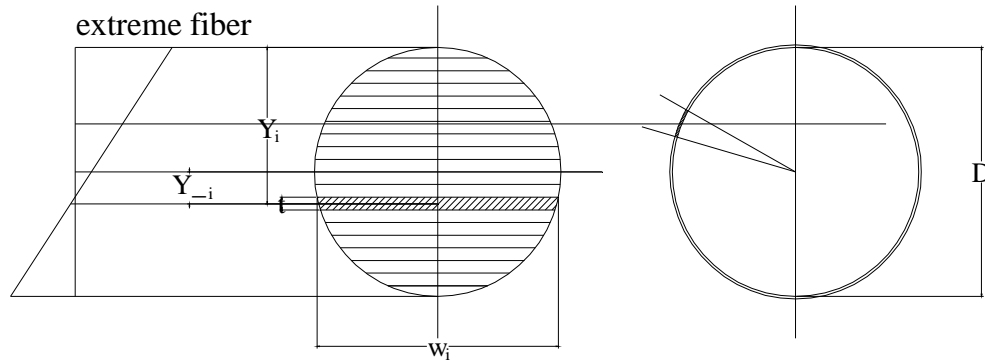
Figure 4-1: Using Finite Layer approach in analysis (CFST section)

4-2-2 Present Confinement Model for Concentric Columns

4-2-2-1 Mander Model for transversely reinforced steel

Mander model (1988) was developed based on the effective lateral confinement pressure (f'_l) and the confinement effective coefficient (k_e) which is the same concept found by Sheikh and Uzumeri (1982). The advantage of this procedure is its applicability to any cross section since it defines the lateral pressure based on the section geometry. Mander *et al.* (1988) showed the adaptability of their model to circular or rectangular sections, under static or dynamic loading, either monotonically or cyclically applied. In order to develop a full stress-strain curve and to assess ductility, an energy balance approach is used to predict the maximum longitudinal compressive strain in the concrete.

Mander derived the longitudinal compressive concrete stress-strain equation from Popovics model that was originally developed for unconfined concrete (1973):

247

$$f_c = \frac{f_{cc} x r}{r - 1 + x^r}$$

4-1

$$x = \frac{\varepsilon_c}{\varepsilon_{cc}}$$

4-2

$$r = \frac{E_c}{E_c - E_{sec}}$$

4-3

$$E_c = 4723\sqrt{f_c'} \quad in \ MPa$$

4-4

$$E_{sec} = \frac{f_{cc}}{\varepsilon_{cc}}$$

4-5

and as suggested by Richart *et al*. (1928) the strain corresponding to the peak confined compressive strength (f_{cc}):

$$\varepsilon_{cc} = \varepsilon_{co}\left[1 + 5\left(\frac{f_{cc}}{f_c'} - 1\right)\right]$$

4-6

The different parameters of this model are defined in Figure (4-2).
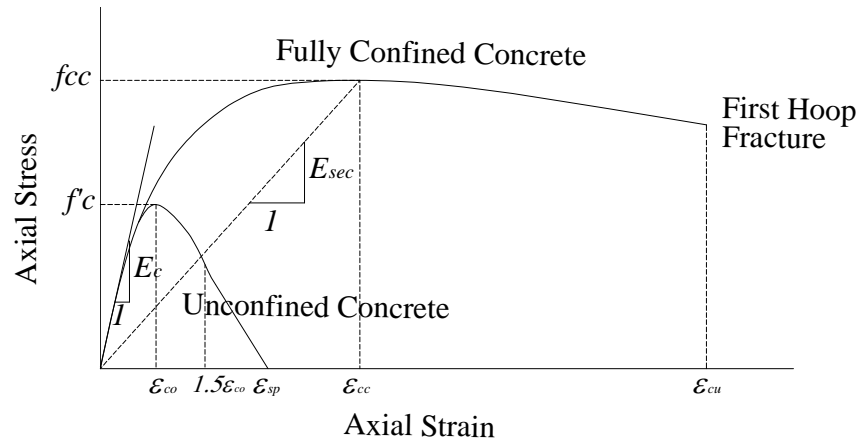
Figure 4-2: Axial Stress-Strain Model proposed by Mander *et al*. (1988) for monotonic loading

As shown in Figure (4-2) Mander *et al*. (1988) model has two curves; one for unconfined concrete (lower curve) and the other for confined concrete (upper one). The upper one refers to

248

the behavior of confined concrete with concentric loading (no eccentricity). It is shown that it has

ascending branch with varying slope starting from E_c decreasing till it reaches the peak confined

strength at (f_{cc}, ε_{cc}). Then the slope becomes slightly negative in the descending branch

representing ductility till the strain of ε_{cu} where first hoop fractures. The lower curve expresses

the unconfined concrete behavior. It has the same ascending branch as the confined concrete

curve till it peaks at (f'_c, ε_{co}). Then, the curve descends till 1.5-2$\varepsilon_{co.}$ A straight line is assumed

after that till zero strength at spalling strain ε_{sp}

The rest of this section discusses the spiral and hoops effectiveness as they were originally

explained in Mander *et al* (1988). However the adaptability of this model to fit the CFST

columns is explaind in section 3.4.1.

Mander *et al.* (1988) utilized an approach similar to that of Sheik and Uzumeri (1982) to

determine effective lateral confinement pressure. It was assumed that the area of confined

concrete is the area within the centerlines of perimeter of spiral or hoop reinforcement A_{cc} as

illustrated in Figure (4-3).
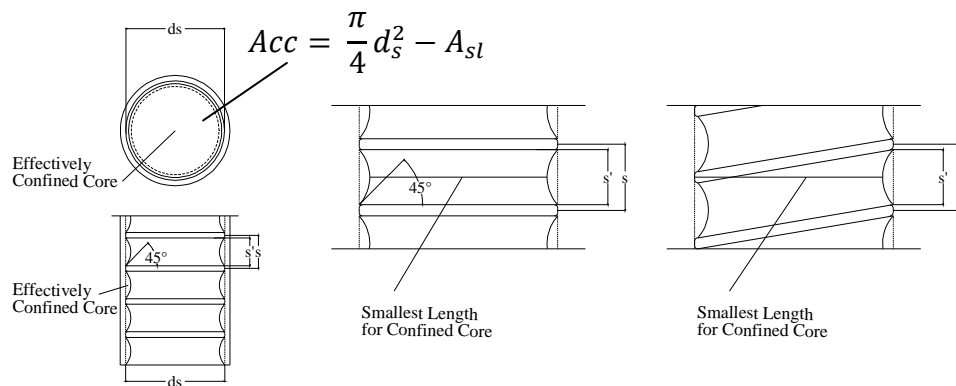
Figure 4-3: Effectively confined core for circular hoop and spiral reinforcement (Mander Model)

Figure (4-3) shows that effectively confined concrete core A_e, in between hoops or spirals, is smaller than the area of core within center lines of perimeter spiral or hoops excluding longitudinal steel area, A_{cc}. To satisfy that condition, the effective lateral confinement pressure f'_l, should be a percentage of the lateral pressure f_l:

$$f'_l = k_e f_l \qquad\qquad 4\text{-}7$$

and the confinement effectiveness coefficient k_e is defined as the ratio of effective confined area, A_e, to the area enclosed by centerlines of spiral or hoop, A_{cc}:

$$k_e = \frac{A_e}{A_{cc}} \qquad\qquad 4\text{-}8$$

$$A_{cc} = A_c - A_{sl} = \frac{\pi}{4} d_s^2 - A_{sl} \qquad\qquad 4\text{-}9$$

$$\frac{A_{cc}}{A_c} = 1 - \frac{A_{sl}}{A_c} \qquad\qquad 4\text{-}10$$

$$A_{cc} = A_c \left(1 - \rho_{cc}\right) \qquad\qquad 4\text{-}11$$

where A_c is the area of the section core enclosed by spirals or hoops, A_{sl} is the area of longitudinal steel and ρ_{cc} is the ratio of longitudinal steel to the area of the core.

For hoop case, the effective lateral confined core:
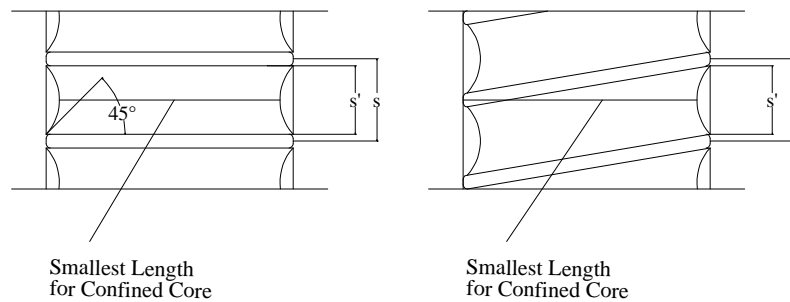
Figure 4-4: Effective lateral confined core for hoop and spiral reinforcement (Mander Model)

$$A_e = \frac{\pi}{4} d_s^2 \left(1 - \frac{s'}{2d_s}\right)^2 = A_c \left(1 - \frac{s'}{2d_s}\right)^2 \qquad \text{4-12}$$

$$k_e = \frac{\left(1 - \frac{s'}{2d_s}\right)^2}{1 - \rho_{cc}} \qquad \text{4-13}$$

where *s'* is the clear spacing between spiral or hoop bars and d_s is the core diameter tospiral or hoops centerline. While for spiral case it can be shown from Figure 4-4) that:

$$A_e = \frac{\pi}{4} d_s^2 \left(1 - \frac{s'}{4d_s}\right)^2 = \frac{\pi}{4} d_s^2 \left(1 - \frac{2s'}{4d_s} + \frac{s'^2}{16d_s^2}\right) \qquad \text{4-14}$$

and the last term can be neglected so the value of k_e is found from the following equation:

$$k_e = \frac{1 - \frac{s'}{2d_s}}{1 - \rho_{cc}} \qquad \text{4-15}$$
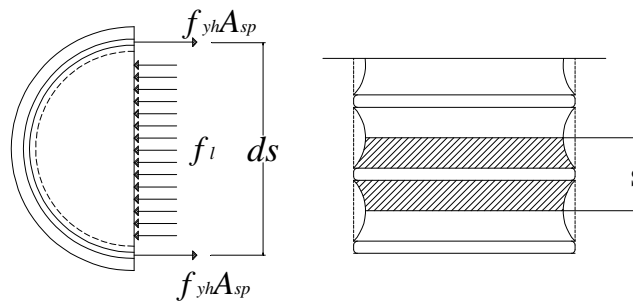
Figure 4-5: Confinement forces on concrete from circular hoop reinforcement

Figure (4-5) illustrates force equilibrium on a half turn of a circular hoop. The uniform hoop tension at yield generated in the transverse steel should be balanced by the uniform lateral stress on the concrete core:

251

$$2f_{yh}A_{sp} = f_l s d_s \qquad \text{4-16}$$

$$f_l = \frac{2f_{yh}A_{sp}}{s d_s} \qquad \text{4-17}$$

and the ratio of the volume of transverse steel to the volume of confined core area ρ_s can be expressed as

$$\rho_s = \frac{A_{sp}\pi d_s}{\frac{\pi}{4}s d_s^2} = \frac{4A_{sp}}{s d_s} \qquad \text{4-18}$$

hence

$$f_l = \frac{1}{2}\rho_s f_{yh} \qquad \text{4-19}$$

and from Equation (4-7) f'_l can be found:

$$f'_l = \frac{1}{2}k_e \rho_s f_{yh} \qquad \text{4-20}$$

The maximum confined compressive strength can be described as a function of the peak unconfined strength and the uniform effective lateral confinement pressure:

$$f_{cc} = f'_c\left(-1.254 + 2.254\sqrt{1+\frac{7.94f'_l}{f'_c}} - 2\frac{f'_l}{f'_c}\right) \qquad \text{4-21}$$

Mander *et al.* (1988) proposed an energy balancing theory to predict the ultimate confined strain, which is determined at the first hoop fracture. They stated that the additional ductility for confined concrete results from the additional strain energy stored in the hoops U_{sh}. Therefore from equilibrium:

$$U_{sh} = U_g - U_{co} \qquad \text{4-22}$$

252

where U_g is the external work done in the concrete to fracture the hoop, and U_{co} is the work done to cause failure to the unconfined concrete. U_{sh} can be represented by the area under the tension stress strain curve for the transverse steel between zero and fracture strain ε_{sf}.

$$U_{sh} = \rho_s A_{cc} \int_0^{\varepsilon_{sf}} f_s d\varepsilon \qquad \text{4-23}$$

while Ug is equal to the area under the confined stress strain curve plus the area under the longitudinal steel stress strain curve:

$$U_g = \int_0^{\varepsilon_{scu}} f_c A_{cc} d\varepsilon + \int_0^{\varepsilon_{scu}} f_s A_{sl} d\varepsilon \qquad \text{4-24}$$

similarly, it was proven experimentally that U_{co} is equal to:

$$U_{co} = A_{cc} \int_0^{\varepsilon_{spall}} f_c d\varepsilon = A_{cc} 0.017\sqrt{f_c'} \quad \text{in } MPa \qquad \text{4-25}$$

and

$$U_{sh} = \rho_s A_{cc} \int_0^{\varepsilon_{sf}} f_s d\varepsilon = 110 \rho_s A_{cc} \qquad \text{4-26}$$

Substituting Equations (4-23), (4-24) and (4-25) into Equation (4-27)

$$110\rho_s = \int_0^{\varepsilon_{cu}} f_c d\varepsilon + \int_0^{\varepsilon_{cu}} f_{sl} d\varepsilon - 0.017\sqrt{f_c'} \qquad \text{4-27}$$

where f_{sl} is the stress in the longitudinal steel. Equation (4-27) can be solved numerically for $\varepsilon_{cu.}$

The above equations (4-22) to (4-27) are developed using SI units

4-2-2-2 Lam and Teng Model

Lam and Teng (2003) proposed a new model for concrete wrapped with Fiber Reinforced Polymer (FRP). This model is adopted by ACI 440.2R-08 code for FRP wrapping. The stress-strain equations are as follow:

$$f_c = E_c \varepsilon_c - \frac{\left(E_c - E_2\right)^2}{4 f_c^{'}} \varepsilon_c^2 \qquad 0 \leq \varepsilon_c \leq \varepsilon_t^{'} \qquad \text{4-28}$$

$$f_c = f_c^{'} + E_2 \varepsilon_c \qquad \varepsilon_t^{'} \leq \varepsilon_c \leq \varepsilon_{ccu} \qquad \text{4-29}$$

$$E_2 = \frac{f_{cc} - f_c^{'}}{\varepsilon_{ccu}} \qquad \text{4-30}$$

$$\varepsilon_t^{'} = \frac{2 f_c^{'}}{E_c - E_2} \qquad \text{4-31}$$

where ε'_t is the transition strain. To find the maximum confined concrete compressive strength

$$f_{cc} = f_c^{'} + 3.3 \Psi_f \kappa_a f_l \qquad \text{4-32}$$

$$f_l = \frac{2 E_f n t_f \varepsilon_{fe}}{D} \qquad \text{4-33}$$
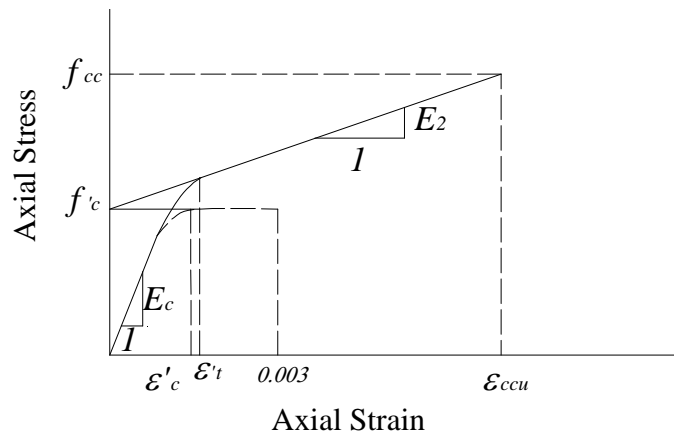
Figure 4-6:Axial Stress-Strain Model proposed by Lam and Teng (2003).

254

f_l is the maximum confined pressure. E_f is tensile modulus of elasticity of FRP. κ_a is the efficiency factor accounts for the geometry of the section and it is equal to 1 in case of the circular cross section, n is the number of plies used, t_f is the nominal thickness of one ply, D is the cross section diameter of the column, ψ_f is a reduction factor determined by the code to be 0.95. ε_{fe} is the effective strain level at failure and it is given by:

$$\varepsilon_{fe} = \kappa_\varepsilon \varepsilon_{fu}$$ 4-34

κ_ε is a reduction factor that considers the premature failure of the FRP.ACI 440.2R-08 implements an average value of $\kappa_\varepsilon = 0.586$ based on Lam and Teng (2003 a) finding. It is found experimentally to range between 0.57 and 0.61. It should be noted that the lowest level of confinement pressure (f_l) required is equal to $0.08 f'_c$ to avoid having a descending branch in the stress strain curve. This note is verified by Spolestra and Monti (1999). The maximum compressive strain ε_{ccu} can be found by:

$$\varepsilon_{ccu} = \varepsilon_c' \left(1.50 + 12\kappa_b \frac{f_l}{f_c'} \left(\frac{\varepsilon_{fe}}{\varepsilon_c'} \right)^{0.45} \right)$$ 4-35

And to avoid excessive cracking, this strain should be limited to:

$$\varepsilon_{ccu} \leq 0.01$$

where κ_b accounts for the geometry of the cross section and is equal to 1 for circular columns.

4-2-3 Present Confinement Model for Eccentric Columns

Unlike concentric loading, the eccentric loading generates bending moment in addition to axial loading. Columns subjected to eccentric loading behave differently from those concentrically loaded, as the shape of the stress strain curve for fully confined reinforced

255

concrete (concentric loading) shows higher peak strength and more ductility than the unconfined one (infinite eccentricity). Most of the previous studies were based on the uniform distribution of compressive strain across the column section.
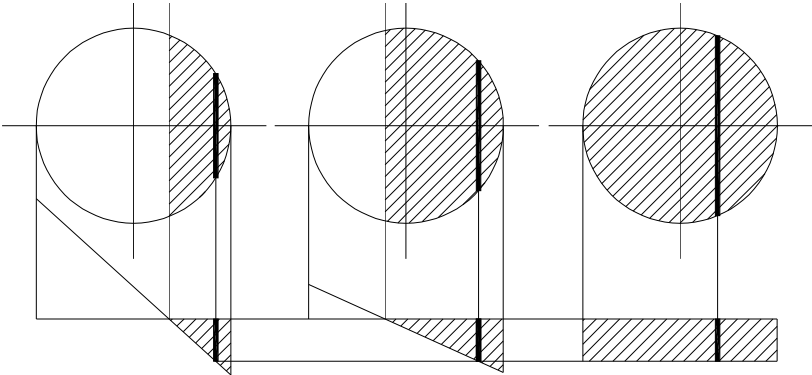
Figure 4-7: Effect of compression zone depth on concrete strength

Figure (4-7) illustrates three different sections under concentric load, combination of axial load and bending moment and pure bending moment, the highlighted fiber in the three cases has the same strain. Any current confinement model yields the same stress for these three fibers. So the depth or size of compression zone does not have any role in predicting the stress. Hence, it is more realistic to relate the strength and ductility in a new model to the level of confinement utilization and compression zone.
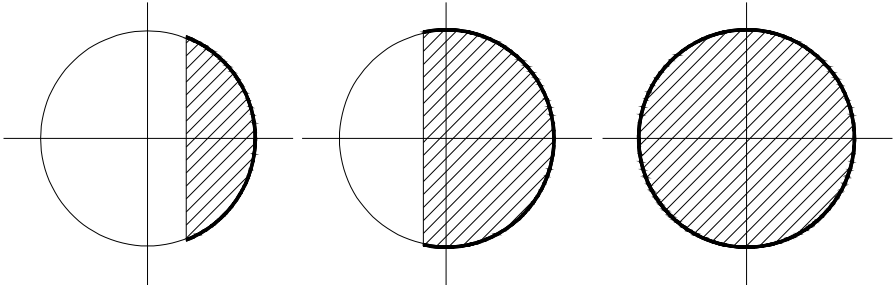
Figure 4-8: Amount of confinement gets engaged in different cases

By definition, confinement gets engaged only when member is subjected to compression. Compressed members tend to expand in lateral direction, and if confined, confinement will prevent this expansion to different levels based on the degree of compressive force and confinement strength as well. For fully compressed members (Figure 4-8 c), confinement becomes effective 100% as it all acts to prevent the lateral expansion. Whereas members subjected to compression and tension, when the neutral axis lies inside the section perimeter, only adjacent confinement to the compression zone gets engaged. Accordingly, members become partially confined.

In CFST literature, various models were implemented to assess the ultimate confined capacity of columns under concentric axial load. On the other hand the effect of partial confinement in case of eccentric load (combined axial load and bending moments) is not investigated in any proposed model. Therefore, it is pertinent to relate the strength and ductility of reinforced concrete to the degree of confinement utilization in a new model.

The two curves of fully confined and unconfined concrete in any proposed model are used in the eccentricity-based model as upper and lower bounds. The upper curve refers to concentrically loaded confined concrete (zero eccentricity), while the lower one refers to pure bending applied on concrete (infinite eccentricity). In between the two boundaries, infinite numbers of stress-strain curves can be generated based on the eccentricity, which is found to directly relate to the size of compression zone, Figure (4-9). The higher the eccentricity the smaller the confined concrete region in compression. Accordingly, the ultimate confined strength is gradually reduced from the fully confined value f_{cc} to the unconfined value f'_c as a function of eccentricity to diameter ratio. In addition the ultimate strain is reduced linearly from the ultimate strain ε_{cu} for confined concrete to the ultimate strain for unconfined concrete $1.5\varepsilon_{co}$ or 0.003.

257
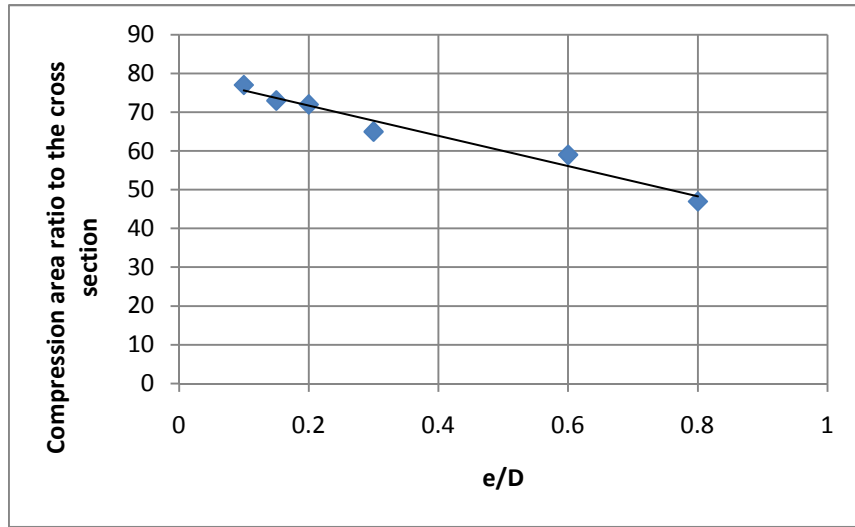
Figure 4-9: Relation between the compression area ratio to the normalized eccentricity

Figure (4-9) shows that the compression area to the total area decreases linearly with the increase in normalized eccentricity. This relation is almost linear as it is depicted by the solid line. Hence, the eccentricity can be related simply to the compression zone area as explained in the following section.

4-2-3-1 Eccentric Model based on Mander Equations

The equation that defines the eccentric peak strength $\overline{f_{cc}}$ according to the eccentricity is simply

a mixture rule: $\overline{f_{cc}} = \dfrac{1}{1+\dfrac{e}{D}} f_{cc} + \dfrac{1}{1+\dfrac{D}{e}} f_c'$ $\qquad$ 4-36

where e is the eccentricity, D is the column diameter and $\overline{f_{cc}}$ is the eccentric peak strength at the eccentricity (e). The corresponding strain $\overline{\varepsilon_{cc}}$ is given by

$\overline{\varepsilon_{cc}} = \varepsilon_{co}\left[1 + 5\left(\dfrac{\overline{f_{cc}}}{f_c'} - 1\right)\right]$ $\qquad$ 4-37

and the maximum strain corresponding to the required eccentricity will be a linear function of the stress corresponding to maximum strain for fully confined concrete f_{cu} and the stress at the maximum unconfined strain f_{cuo} at $\varepsilon_{cuo} = 0.003$

$$\overline{\varepsilon_{cu}} = \overline{\varepsilon_{cc}} \left[\frac{\dfrac{\overline{E_{sec}}}{E_{sec,u}}\overline{r}}{\dfrac{c}{\overline{\varepsilon_{cu}}}+1} - \overline{r}+1 \right]^{\frac{1}{\overline{r}}} \qquad\qquad E_{sec,u} = \frac{f_{cu} - f_{cuo}}{\overline{\varepsilon_{cu}} - 0.003} \qquad\qquad \text{4-38}$$

$$c = \frac{f_{cu} - E_{sec,u} * 0.003}{E_{sec,u}}$$

$$\overline{E_{sec}} = \frac{\overline{f_{cc}}}{\overline{\varepsilon_{cc}}} \qquad\qquad \overline{r} = \frac{E_c}{E_c - \overline{E_{sec}}}$$

In order to verify the accuracy of the model at the extreme cases, the eccentricity is first set to be zero. The coefficient of f'_c will be zero and equation (4-36), (4-37) and (4-38) will reduce to be:

$$\overline{f_{cc}} = f_{cc} \qquad\qquad\qquad \text{4-39}$$

$$\overline{\varepsilon_{cc}} = \varepsilon_{cc} \qquad\qquad\qquad \text{4-40}$$

$$\overline{\varepsilon_{cu}} = \varepsilon_{cu} \qquad\qquad\qquad \text{4-41}$$

On the other hand, if the eccentricity is set to be infinity the other coefficient of f_{cc} will be zero, and the strength, corresponding strain and ductility equations will be:

$$\overline{f_{cc}} = f'_c \qquad\qquad\qquad \text{4-42}$$

$$\overline{\varepsilon_{cc}} = \varepsilon_{co} \qquad\qquad\qquad \text{4-43}$$

$$\overline{\varepsilon_{cu}} = 0.003 \qquad\qquad\qquad \text{4-44}$$
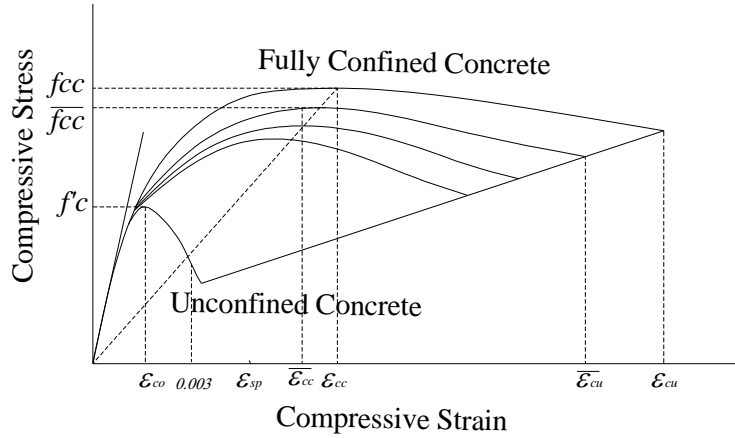
Figure 4-10: Eccentricity Based Confined -Mander Model -

Any point on the generated eccentric curves can be calculated using the following equation:

$$f_c = \frac{\overline{\overline{f_{cc}}}\,\overline{x}\,\overline{r}}{\overline{r}-1+\overline{x}^{\overline{r}}}$$

4-45

where:

$$\overline{x} = \frac{\varepsilon_c}{\overline{\overline{\varepsilon_{cc}}}}$$

4-46

$$\overline{r} = \frac{E_c}{E_c - \overline{\overline{E_{sec}}}}$$

4-47

$$\overline{E_{sec}} = \frac{\overline{\overline{f_{cc}}}}{\overline{\overline{\varepsilon_{cc}}}}$$

4-48

4-2-3-2 Eccentric Model Based on Lam and Teng Equations

The ultimate eccentric or partially confined strength $\overline{f_{cc}}$ is determined from the following equation:

$$\overline{f_{cc}} = \frac{1}{1+\dfrac{e}{D}}f_{cc} + \frac{1}{1+\dfrac{D}{e}}f_c'$$

4-49

260

where e is the eccentricity, D is the column diameter and $\overline{f_{cc}}$ is the eccentric peak strength at the eccentricity (e).

The strain $\overline{\varepsilon_{cu}}$ corresponding to the peak partially confined strength $\overline{f_{cc}}$, which corresponds to the ultimate point on the curve, Figure (4-11), is given by linear interpolation between the two extreme bounds of strain:

$$\overline{\varepsilon_{cu}} = \frac{\overline{f_{cc}} - f_c'}{f_{cc} - f_c'}\left(\varepsilon_{ccu} - 0.003\right) + 0.003 \qquad\qquad 4\text{-}50$$

Any point on the generated eccentric curves can be calculated using the following equations:

$$f_c = E_c\varepsilon_c - \frac{\left(E_c - \overline{E_2}\right)^2}{4f_c'}\varepsilon_c^2 \qquad\qquad 0 \le \varepsilon_c \le \overline{\varepsilon_t'} \qquad\qquad 4\text{-}51$$

$$f_c = f_c' + \overline{E_2}\varepsilon_c \qquad\qquad \overline{\varepsilon_t'} \le \varepsilon_c \le \overline{\varepsilon_{cu}} \qquad\qquad 4\text{-}52$$

$$\overline{E_2} = \frac{\overline{f_{cc}} - f_c'}{\overline{\varepsilon_{cu}}} \qquad\qquad 4\text{-}53$$

$$\overline{\varepsilon_t'} = \frac{2f_c'}{E_c - \overline{E_2}} \qquad\qquad 4\text{-}54$$
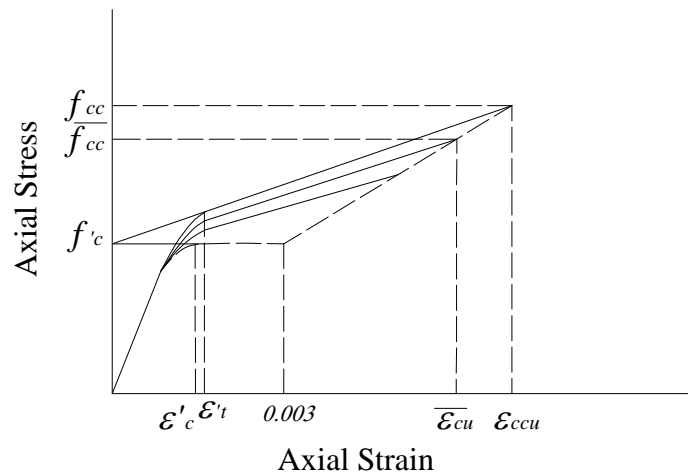
Figure 4-11: Eccentricity Based Confined -Lam and Teng Model-

261

4-2-4 Moment of Area Theorem

The very general axial stress equation in a symmetrical section subjected to axial force P and uniaxial bending M_x (Hardy Cross 1930):

$$\sigma_z = \frac{P}{A} + \frac{M_x}{I_x} y \qquad\qquad 4\text{-}55$$

σ_z = normal stress at any point (a) in cross section

P = applied load.

A = cross sectional area.

M_x = bending moment about x-axis

y = distance between the point (a) and the centroidal x-axis

I_x = moment of inertia about the centroidal x-axis

Rewriting Equation (4-55) to determine the strain at any point in the cross section:

$$\varepsilon_z = \frac{P}{EA} + \frac{M_x}{EI_x} y \qquad\qquad 4\text{-}56$$

In case of linear elastic analysis, E in EA or EI expressions is constant ($E=E_c$). However, if the section has variable strain and stress profile, it will amount to variable E profile (per layer) in nonlinear analysis. Accordingly, the section parameters must include $\sum_i E_i A_i$, $\sum_i E_i I_i$ for a more generalized theory (Rasheed and Dinno 1994). Note that the linear strain profile of the section from Equation (4-56) yields a distinct constant curvature:

$$\phi_x = \frac{M_x}{EI_x} \qquad\qquad 4\text{-}57$$

$$M_x = \phi_x EI_x \qquad\qquad 4\text{-}58$$

262

where ϕ_x = x- curvature

Rewriting equation (4-56) in terms of ϕ_x

$$\varepsilon_z = \frac{P}{EA} + \phi_x y \qquad\qquad 4\text{-}59$$

Finding ε_z at the centroid, since $y = 0$.

$$\varepsilon_o = \frac{P}{EA} \qquad\qquad 4\text{-}60$$

Finding ε_z at the geometric centroid, $y = \bar{y}$

$$\bar{\varepsilon}_o = \frac{P}{EA} + \phi_x \bar{y}$$

Solving for P at the geometric centroid;

$$P = EA\bar{\varepsilon}_o - EA\bar{y}\phi_x \qquad\qquad 4\text{-}61$$

$\bar{\varepsilon}_o$ is the axial strain at the geometric centroid

But

$$EAM_x = EA\bar{y} \qquad\qquad \bar{y} = Y_G - Y_c$$

Y_G is the vertical distance to the geometric centroid measured from bottom extreme fiber and Y_c is the vertical distance to the inelastic centroid measured from the bottom extreme fiber, Figure (4-12)

The general formula of the moments about the geometric x-axis is derived as follows: when the moment is transferred from the centroid to the geometric centroid ,Figure (4-12)

$$\bar{M}_x = M_x - P\bar{y} \qquad\qquad 4\text{-}62$$

Substituting equation (4-58) and (4-61) in (4-62) yields:

$$\overline{M}_x = -EAM_x \overline{\varepsilon}_o + \left(EI_x + EAM_x \overline{y}\right)\phi_x$$

<div align="right">4-63</div>
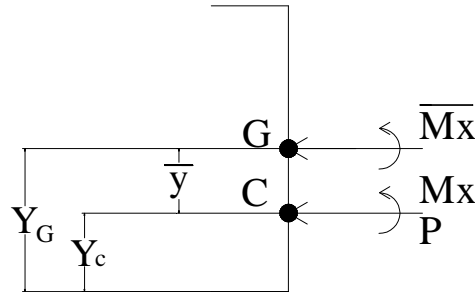
Figure 4-12: Transfering moment from centroid to the geometric centroid

The term $EI_x + EAM_x \overline{y}$ represents the $\overline{EI}_x$ about the geometric centroid using the parallel axis theorem. Using equations (4-61) and (4-63) yields the Moment of Area equation:

$$\begin{bmatrix} P \\ \overline{M}_x \end{bmatrix} = \begin{bmatrix} EA & -EAM_x \\ -EAM_x & \overline{EI}_x \end{bmatrix} \cdot \begin{bmatrix} \overline{\varepsilon}_o \\ \phi_x \end{bmatrix}$$

<div align="right">4-64</div>

Since the moment of area about the actual centroid vanishes (Rasheed and Dinno 1994), Equation (4-64) reduces to an uncoupled set when it is applied back at the actual centroid since EAM_x vanish about the centroid.

$$\begin{bmatrix} P \\ M_x \end{bmatrix} = \begin{bmatrix} EA & 0 \\ 0 & EI_x \end{bmatrix} \cdot \begin{bmatrix} \varepsilon_o \\ \phi_x \end{bmatrix}$$

<div align="right">4-65</div>

which is simply equations (4-58) and (4-60)

4-3 Numerical Model Formulation

4-3-1 Model Formulation
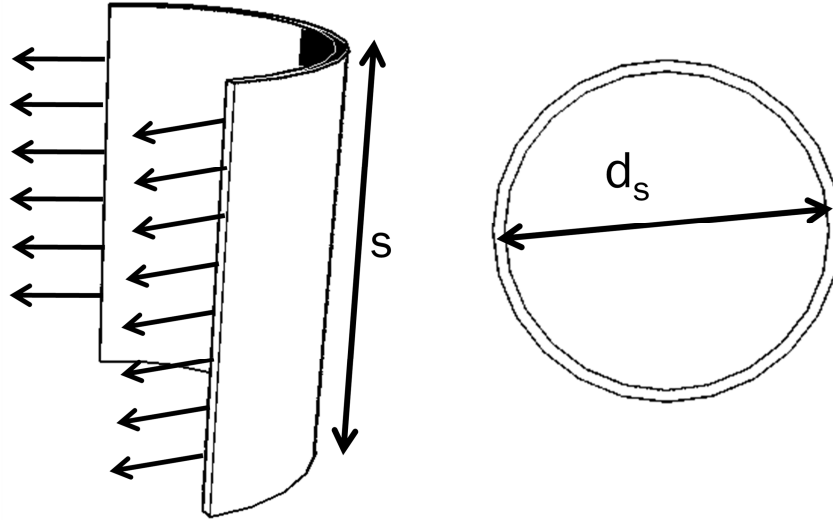
Figure 4-13: 3D Sectional elevation and plan for CFST column.

Using equilibrium in the free body diagram in Figure (4-13):

$$2f_{yh}ts = sd_s f_l$$

4-66

Rearranging equation (4-66) by solving for f_l:

$$f_l = \frac{2f_{yh}t}{d_s}$$

4-67

Since the confinement coefficient k_e is equal to 1 for steel tube confinement case:

$$f_l' = f_l$$

4-68

Equation (4-68) means that the whole cross section is effectively confined, hence:

$$f'_l = \frac{2f_{yh}t}{d_s}$$

4-69

Equation (4-69) represents the effective lateral pressure induced by the steel. To evaluate the peak ultimate concrete confined strength, two well know equations are adapted. These equations are Mander and Richart equations and they have the following formulas:

$$f'_{cc} = f'_c\left(-1.254 + 2.254\sqrt{1 + 7.94\frac{f'_l}{f'_c}} - 2\frac{f'_l}{f'_c}\right) \qquad \text{(Mander)}$$

4-70

$$f'_{cc} = f'_c\left(1 + 4.1\frac{f'_l}{f'_c}\right) \qquad \text{(Richart)}$$

4-71

The literature showed that Mander equation is utilized in several studies to represent CFST confined cases. In addition, Richart formula is used in other studies with coefficient adaption to best fit experimental results. These two equations are adopted herein, plotted and compared against the experimental results shown in Table (4-1). This experimental data is taken from several references as detailed below

Table 4-1: CFST Experimental data

case	t	f_y	D	f'_c	f_l	f_l/f'_c	D/t
	$in.$(mm)	ksi (MPa)	in. (mm)	ksi (MPa)	ksi (MPa)		
1	0.26(6.5)	45.4(313)	5.5(140)	3.45(23.8)	4.65(32.04)	1.35	21.54
2	0.2(5)	38.5(265.8)	7.87(200)	3.94(27.15)	2.03(14)	0.52	40
3	0.12(3)	37.4(285)	5.5(140)	4.1(28.18)	1.85(12.76)	0.45	46.67
4	0.16(4)	39.5(272.6)	11(280)	4.52(31.15)	1.16(8.02)	0.26	70
5	0.12(3)	33.6(232)	11.8(300)	4.00(27.23)	0.7(4.73)	0.17	100

6	0.08(2)	49.6(341.7)	11.8(300)	4.00(27.23)	0.67(4.62)	0.17	150
7	0.11(2.82)	52.7(363.3)	6.5(165)	7.00(48.3)	1.83(12.63)	0.26	58.5
8	0.08(1.94)	37.2(256.4)	7.5(190)	6.00(41)	0.77(5.29)	0.13	97.9
9	0.06(1.52)	44.4(306.1)	7.5(190)	7.00(48.3)	0.72(4.94)	0.1	125
10	0.04(1.13)	26.9(185.7)	7.5(190)	6.00(41)	0.32(2.2)	0.05	168.1
11	0.03(0.86)	30.6(210.7)	7.5(190)	6.00(41)	0.28(1.92)	0.05	220.9
12	0.11(2.82)	52.7(363.3)	6.5(165)	11.6(80.2)	1.83(12.6)	0.18	58.51
13	0.08(1.94)	37.2(256.4)	7.5(190)	10.8(74.7)	0.77(5.29)	0.07	97.94
14	0.06(1.52)	44.4(306.1)	7.5(190)	11.6(80.2)	0.72(4.94)	0.06	125
15	0.04(1.13)	26.9(185.7)	7.5(190)	11.6(80.2)	0.32(2.2)	0.028	168.1
16	0.03(0.86)	30.6(210.7)	7.5(190)	11.6(80.2)	0.28(1.92)	0.03	220.9
17	0.11(2.82)	52.7(363.3)	6.5(165)	15.7(108)	1.83(12.6)	0.12	58.51
18	0.08(1.94)	37.2(256.4)	7.5(190)	15.7(108)	0.77(5.29)	0.05	97.94
19	0.06(1.52)	44.4(306.1)	7.5(190)	15.7(108)	0.72(4.94)	0.05	125
20	0.04(1.13)	26.9(185.7)	7.5(190)	15.7(108)	0.32(2.2)	0.02	168.1
21	0.03(0.86)	30.6(210.7)	7.5(190)	15.7(108)	0.28(1.92)	0.02	220.9

Cases 1, 3 and 5 are from Schneider's work (1998). Cases 2, 4 and 6 are taken from Huang *et al's* work (2002). The rest of the cases are from O'shea and Bridge's work (2000). The experimental data is classified according to the concrete strength to normal and high strength concrete and is analyzed separately. The ultimate compressive confined strength (f_{cc}) is plotted against unconfined strength (f'_c) in Figure (4-14), for normal strength concrete, and (4-15), for high strength concrete.
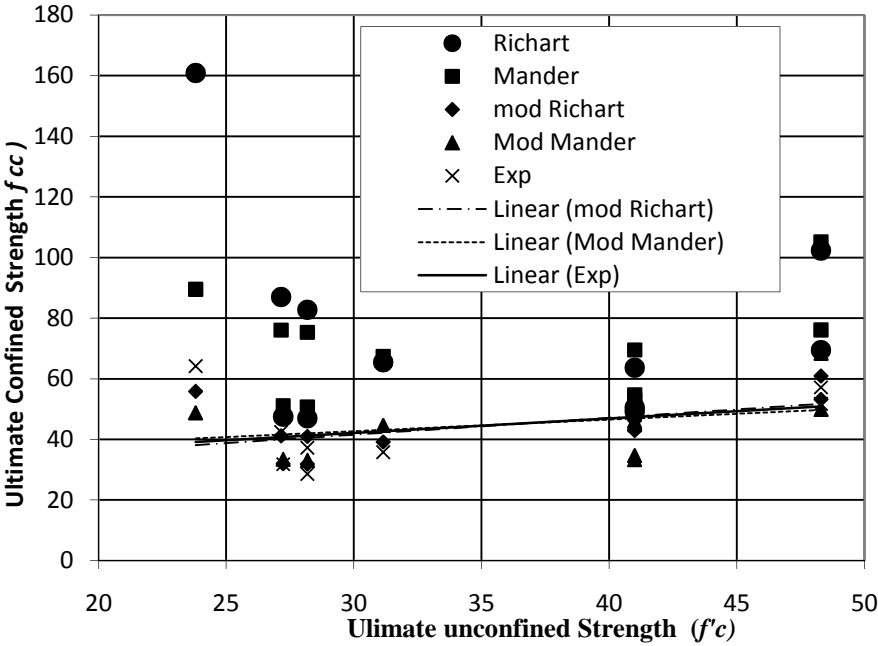
Figure 4-14: f_{cc} vs f'_c for normal strength concrete
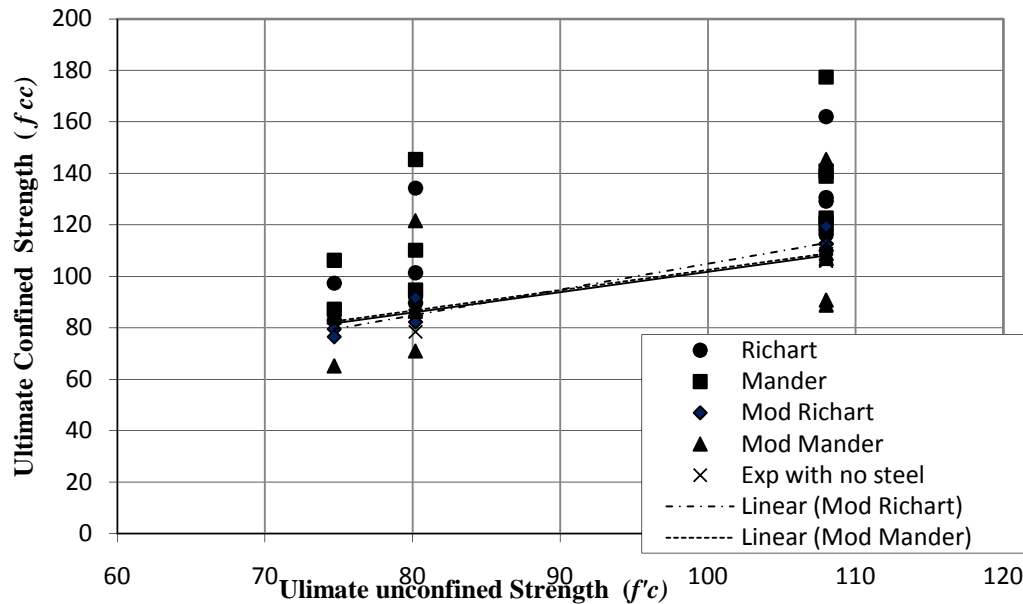
Figure 4-15: f_{cc} vs f'_c for high strength concrete

The best equations fitting the best fit line of experimental data are those of the modified Richart as follows:

For normal strength concrete

$$f'_{cc} = f'_c \left(1 + 1\frac{f'_l}{f'_c} \right)$$

4-72

For high strength concrete

$$f'_{cc} = f'_c \left(1 + 0.9\frac{f'_l}{f'_c} \right)$$

4-73

It is observed from the literature that there are two different patterns for the stress-strain curves as shown in Figure (4-16). Pattern1; ascending up to failure (case 1 and 2 from Table 4-1). Pattern 2; ascending then softening after peak (case 4 and 5 from Table 4-1)
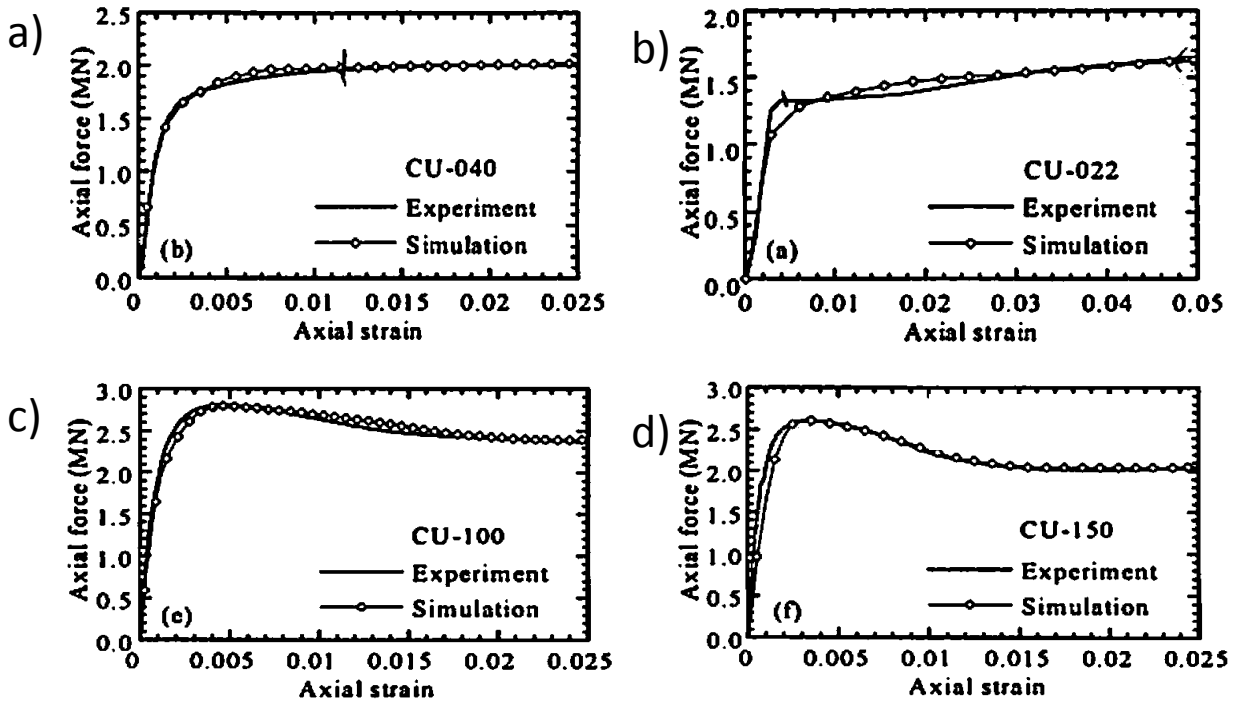
Figure 4-16: CFST Stress-strain Curve for different cases from Table 4-1

a)   case 1   b) case 2   c) case 4   d) case 5

It can be seen from Table 4-1 that the cut off value of f_l/f'_c that determines the sterss-strain pattern is 0.4. The reason of selecting this parameter is to impose the impact of the most influencing parameter that affect the CFST behavior. According to equation (4-69), f'_l is a function of steel yield strength, tube thickness and column diameter. Hence; the value f_l/f'_c is a good representitve measure of all column parameters.

Case 1,2 and 3 from Table (4-1) are plotted using Lam and Teng Model that describes the same behavior of CFST pattern 1 and compared to the experimental stress-strain curves. It is evident from Figure (4-17), (4-18) and (4-19) that Lam and Teng Equations are well correlating

270

to the experimental curves. Hence, Lam and Teng Equations can be used to express pattern 1. Besides that, Mander model is used to express pattern 2.
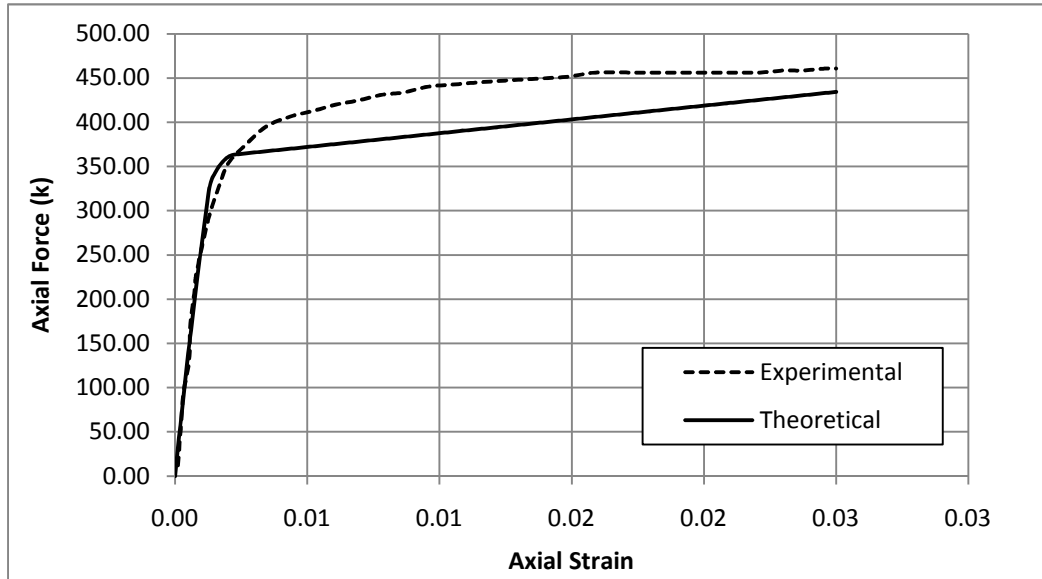
Figure 4-17: Case 1 Stress-Strain curve using Lam and Teng equations compared to Experimetal curve.
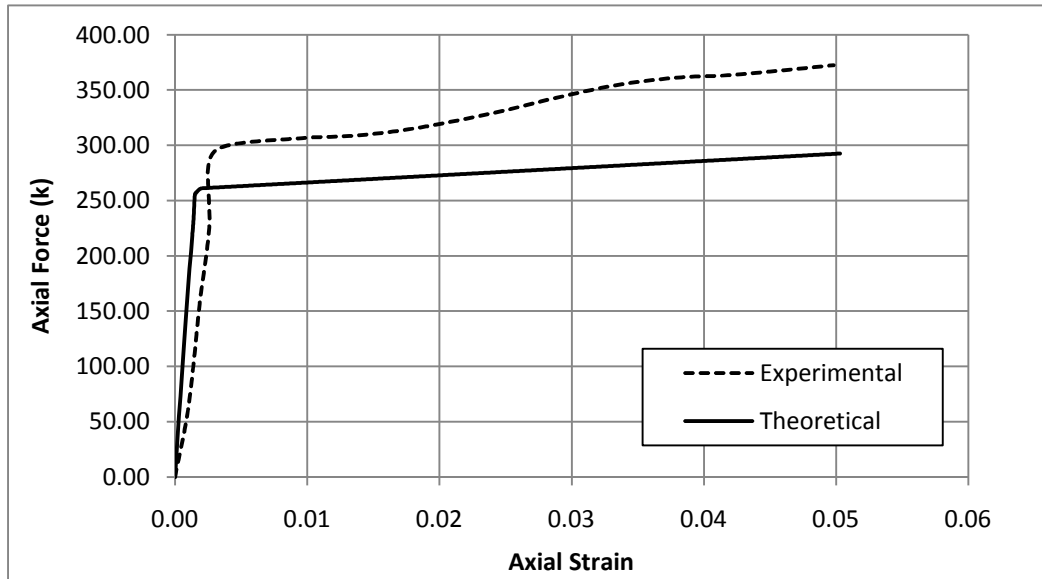
Figure 4-18: Case 2 Stress-Strain curve using Lam and Teng equations compared to Experimetal curve.

271
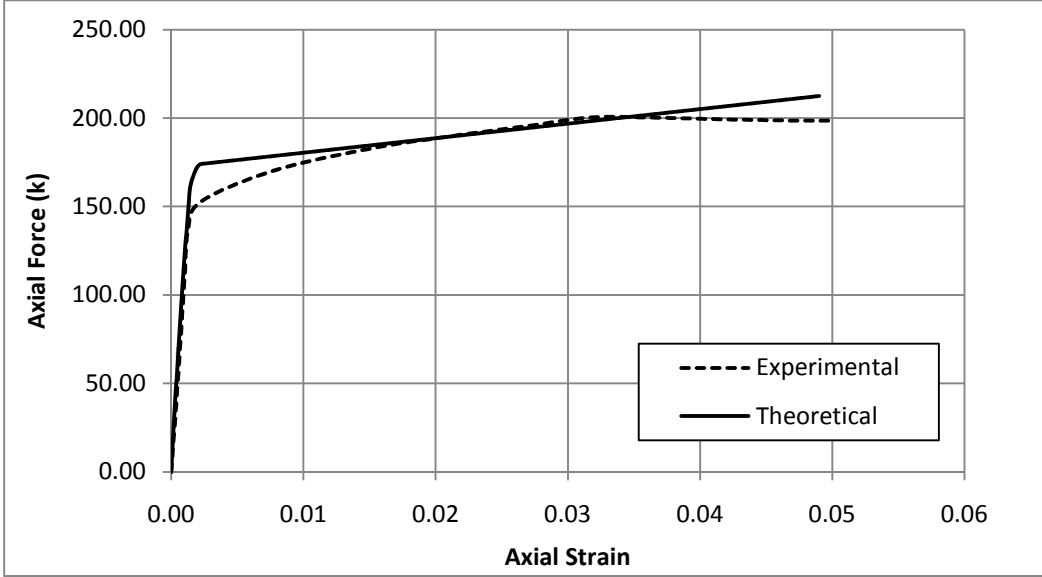
Figure 4-19: Case 3 Stress-Strain curve using Lam and Teng equations compared to Experimetal

curve.
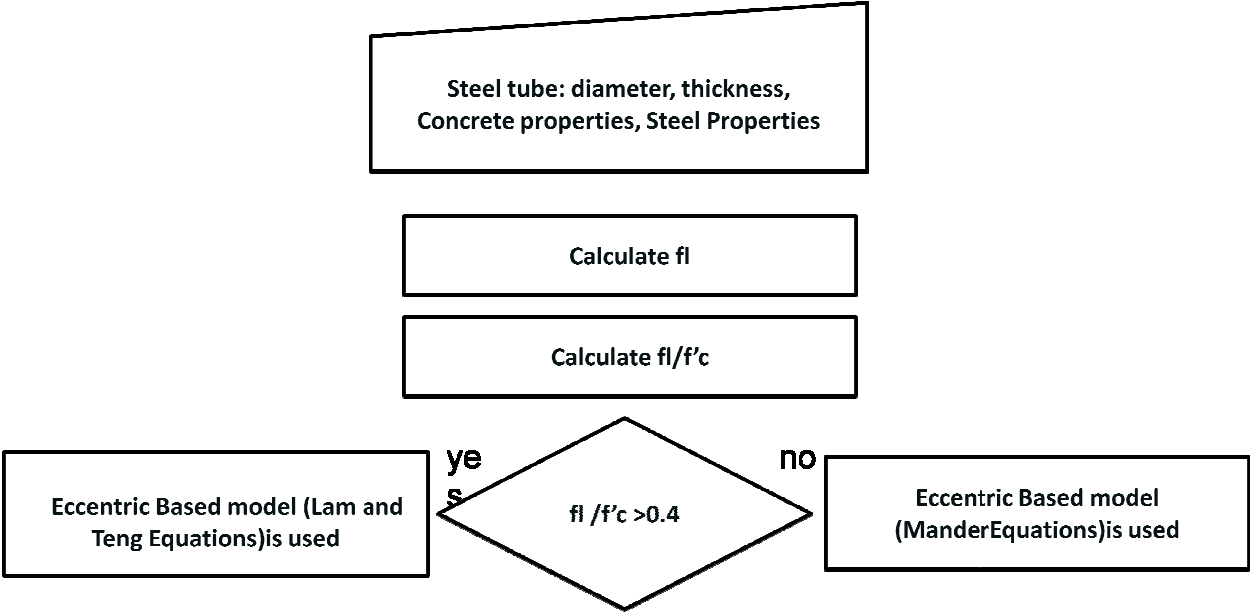
Figure 4-20: CFST Model Flowchart

4-3-2 Numerical Analysis

The cross section analyzed is loaded incrementally by maintaining a certain eccentricity between the axial force *P* and the resultant moment M_R. Since increasing the load and resultant moment causes the neutral axis and centroid to vary nonlinearly, the generalized moment of area theorem is devised.

The method is developed using incremental iterative analysis algorithm, secant stiffness approach and proportional or radial loading. It is explained in the following steps (Figure 4-24):

1- Calculating the initial section properties:

- Elastic axial rigidity *EA*:

$$EA = \sum_i E_c w_i t_i + \sum_i E_s A_{si}$$
<div align="right">4-74</div>

E_c = initial modulus of elasticity of the concrete

E_s = initial modulus of elasticity of the steel rebar

The depth of the elastic centroid position from the bottom fiber of the section Y_c

$$Y_c = \frac{\sum_i E_c w_i t_i (H - Y_i) + \sum_i E_s A_{si}(H - Y_{si})}{EA}$$
<div align="right">4-75</div>

- Elastic flexural rigidity about the elastic centroid *EI*:

$$EI_x = \sum_i E_c w_i t_i (H - Y_i - Y_c)^2 + \sum_i E_s A_{si}(H - Y_{si} - Y_c)^2$$
<div align="right">4-76</div>

Typically Yc = *H/2*.

- The depth of the geometric section centroid position from the bottom fiber of the section Y_G:

$$Y_G = \frac{H}{2}$$
<div align="right">4-77</div>
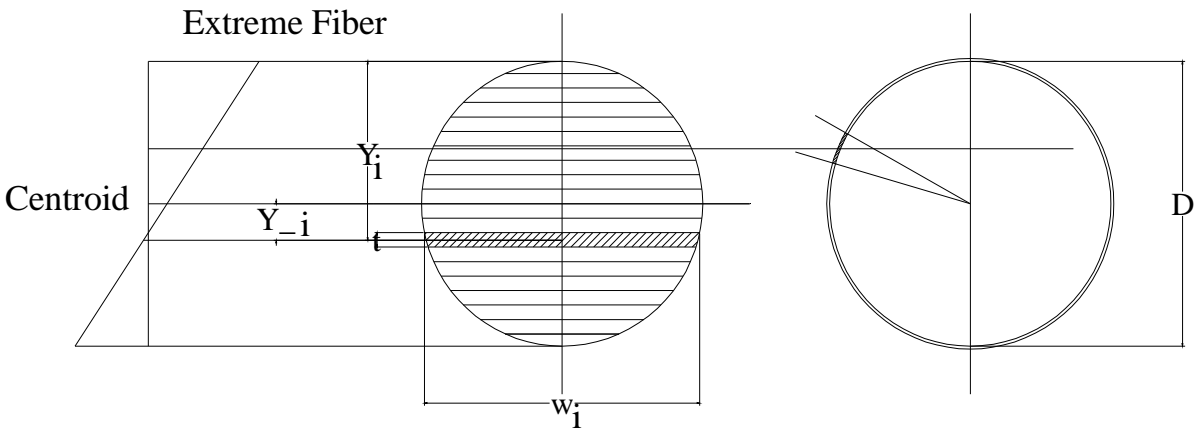
Figure 4-21: Geometric properties of concrete layers and steel tube

2- Calculating f_l / f'_c and check the ratio against 0.4 to decide which model is used (Eccentric model based on Lam and Teng Equations or Eccentric model based on Mander Equations), Figure (4-20).

3- Defining eccentricity e, which specifies the radial path of loading on the interaction diagram.
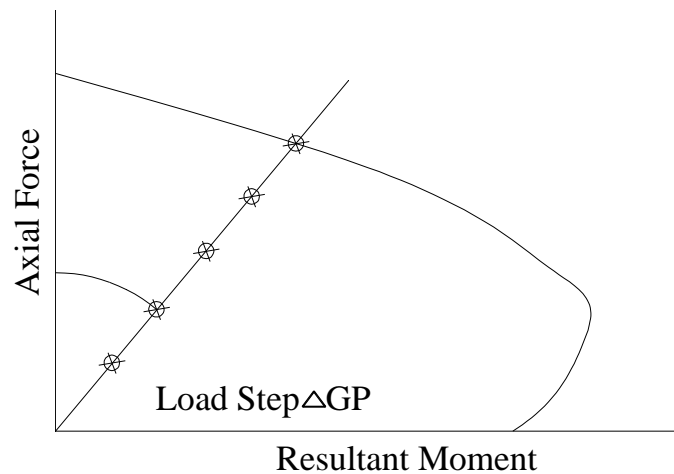
Figure 4-22: Radial loading concept

4- Defining loading step ΔGP as small portion of the maximum load, and computing the axial force at the geometric centroid.

$$GP_{new} = GP_{old} + \Delta GP \qquad 4\text{-}78$$

274

5- Calculating moment *GM* about the geometric centroid.

$$e = \frac{GM_x}{GP} \qquad\qquad GM_x = e * GP$$

6- Transferring moment to the updated inelastic centroid and calculating the new transferred moment TM_X :

$$TM_X = GM_x + GP(Y_G - Y_c)$$

The advantage of transferring the moment to the position of the inelastic centroid is to eliminate

the coupling effect between the force and moment, since $EAM_x = 0$ about the inelastic centroid

$$\begin{bmatrix} P \\ TM_x \end{bmatrix} = \begin{bmatrix} EA & 0 \\ 0 & EI_x \end{bmatrix} \begin{bmatrix} \varepsilon_o \\ \phi_x \end{bmatrix}$$

Figure 4-23: Moment transferring from geometric centroid to inelastic centroid

7- Finding the Curvature ϕ_X

$$\phi_x = \frac{TM_x}{EI_{x-current}}$$

Strain at the inelastic centroid ε_o, the extreme compression fiber strain ε_{ec}, and strain at the

extreme level of steel in tension ε_{es} are found as follow:

$$\varepsilon_o = \frac{GP}{EA_{current}}$$

$$\text{4-83}$$

$$\varepsilon_{ec} = \varepsilon_o + \phi_x (H - Y_c)$$

$$\text{4-84}$$

$$\varepsilon_{es} = \varepsilon_o - \phi_x Y_c$$

$$\text{4-85}$$

where cover is up to center of bars

8- Calculating strain ε_{ci} and corresponding stress f_{ci} in each layer of concrete section by using selected model from step 2.

$$\varepsilon_{ci} = \varepsilon_{ec} - \phi_x Y_i$$

$$\text{4-86}$$

9- Calculating strain ε_{si} and corresponding stress f_{si} in each steel tube segment in the given section by using the steel model (Elastic up to yield strength and then perfectly plastic)

$$\varepsilon_{si} = \varepsilon_{ec} - \phi_x Y_{si}$$

$$\text{4-87}$$

10- Calculating the new section properties: axial rigidity EA, flexural rigidity about the inelastic centroid EI_x , moment of axial rigidity about inelastic centroid EAM_x, internal axial force F_z, internal bending moments about the inelastic centroid M_{ox} ,

$$EA = \sum_i E_{ci} w_i t_i + \sum_i E_{si} A_{si}$$

$$\text{4-88}$$

$$EAM_x = \sum_i E_{ci} w_i t_i (H - Y_c - Y_i) + \sum_i E_{si} A_{si} (H - Y_c - Y_{si})$$

$$\text{4-89}$$

$$F_z = \sum f_{ci} w_i t_i + \sum f_{si} A_{si}$$

$$\text{4-90}$$

$$EI_x = \sum_i E_{ci} w_i t_i (H - Y_c - Y_i)^2 + \sum_i E_{si} A_{si} (H - Y_c - Y_{si})^2$$

$$\text{4-91}$$

$$M_{ox} = \sum_i f_{ci} w_i t_i (H - Y_c - Y_i) + \sum_i f_{si} (H - Y_c - Y_{si})$$

$$\text{4-92}$$

where E_{ci} = secant modulus of elasticity of the concrete layer.

276

E_{si} = secant modulus of elasticity of the steel tube segment.

11- Transferring back the internal moment about the geometric centroid

$$GM_{ox} = M_{ox} - GP(Y_G - Y_c)$$

<div align="right">4-93</div>

12- Checking the convergence of the inelastic centroid

$$TOL_x = EAM_x / EA / Y_c$$

<div align="right">4-94</div>

13- Comparing the internal force to applied force, internal moments to applied moments, and making sure that the moments are calculated about the geometric centroid :

$$GP - F_z \leq 1*10^{-5}$$

<div align="right">4-95</div>

$$GM_x - GM_{ox} \leq 1*10^{-5}$$

<div align="right">4-96</div>

$$Tol_x \leq 1*10^{-5}$$

<div align="right">4-97</div>

If Equations (4-95), (4-96) and (4-97) are not satisfied, the location of the inelastic centroid is updated by EAM_x/EA and steps 6 to 11 are repeated untill Equations (4-95), (4-96) and (4-97) are satisfied.

$$Y_{c_{new}} = Y_{c_{old}} + \frac{EAM_x}{EA}$$

<div align="right">4-98</div>

Once equilibrium is reached, the algorithm checks for ultimate strain in concrete ε_{ec} and steel ε_{es} not to exceed $\overline{\varepsilon_{cc}}$ (or $\overline{\varepsilon_{cu}}$ based on the selected model) and 0.05 respectively. Then, it increases the loading by ΔGP and runs the analysis for the new load level using the latest section properties. Otherwise, if ε_{ec} equals $\overline{\varepsilon_{cc}}$ (or $\overline{\varepsilon_{cu}}$ based on the selected model) or ε_{es} equals 0.05, the target force and resultant moment are reached as a point on the interaction diagram is attained for the amount of eccentricity used.

Start

Calculate initial
section properties
$EA, EI_x, \ Y_c, Y_G,$

Input
e & P

Transfer moment
to inelastic centroid
$TM_x = GM_x + P(Y_G - Y_c)$

Calculate
$\emptyset_x, \varepsilon_o, \varepsilon_{ec}, \varepsilon_{es}$

Calculate
$\varepsilon_{ci}, \varepsilon_{si}, f_{ci}, f_{si}$

Calculate new
section properties
$EA, EI_x, \ EAM_x.$

Calculate internal
force and moments
F_z, M_{ox}

Transfer moment
back to G.C.
$GM_{ox} = M_{ox} - P(Y_G - Y_c)$

No convergance
achieved. stop

$P \mathrel{+}= \varDelta P$

$\dfrac{EAMx}{EA*Yc} < 10^{-5}$

yes

$|GP - F_z| < 10^{-5}$
$|GM_x - GM_{ox}| < 10^{-5}$

yes

$\varepsilon_{ec} > \overline{\varepsilon}_{cc} \, \text{or} \, \varepsilon_{ec} > \overline{\varepsilon}_{cu}$
$\varepsilon_{es} > 0.05$

no

no

no

yes

$Y_c \mathrel{+}= EAMx/EA$

New eccintricity

P & M achieved

yes

no

End

Figure 4-24: Flowchart of CFST columns analysis

4-4 Results and Discussion

4-4-1 Comparisons with Experimental Work

The proposed numerical algorithm explained in section (4-3-2) is compared with experimental data shown in Table (4-2)

Table 4-2: Experimental data for CFST

case	D in.(mm)	t in.(mm)	f_y ksi (MPa)	$f'c$ ksi (MPa)	L/D	D/t	f_l ksi (MPa)	f'_c/f_y	f_l/f_y	f_l/f_c
1	6.5 (165)	0.11 (2.82)	52.7 (363.3)	7 (48.3)	3.5	58.5	1.83 (12.6)	0.133	0.035	0.26
2	6.5 (165)	0.11 (2.82)	52.7 (363.3)	11.63 (80.2)	3.5	58.5	1.83 (12.6)	0.22	0.035	0.16
3	6.5 (165)	0.11 (2.82)	52.7 (363.3)	15.7 (108)	3.5	58.5	1.83 (12.6)	0.3	0.035	0.12
4	7.48 (190)	.076 (1.94)	37.19 (256.4)	5.95 (41)	3.48	97.9	0.77 (5.29)	0.16	0.02	0.13
5	7.48 (190)	.076 (1.94)	37.19 (256.4)	10.83 (74.7)	3.49	97.9	0.77 (5.29)	0.29	0.02	0.07
6	7.48 (190)	.076 (1.94)	37.19 (256.4)	15.66 (108)	3.49	97.9	0.77 (5.29)	0.42	0.02	0.05
7	7.48 (190)	.076 (1.94)	44.39 (306)	7 (48.3)	3.49	125	0.72 (4.94)	0.16	0.016	0.1

279

8	7.48 (190)	.076 (1.94)	44.39 (306)	11.6 (80.2)	3.49	125	0.72 (4.94)	0.26	0.016	0.06
9	7.48 (190)	.076 (1.94)	44.39 (306)	16.34 (112.7)	3.49	125	0.72 (4.94)	0.35	0.016	0.045
10	7.48 (190)	.044 (1.13)	26.9 (185.7)	5.95 (41)	3.49	168	0.32 (2.22)	0.22	0.012	0.054
11	7.48 (190)	.044 (1.13)	26.9 (185.7)	11.63 (80.2)	3.5	168	0.32 (2.22)	0.43	0.012	0.028
12	7.48 (190)	.044 (1.13)	30.55 (210.7)	5.95 (41)	3.49	168	0.32 (2.22)	0.58	0.012	0.02
13	7.48 (190)	.034 (0.86)	30.56 (210.57)	10.83 (74.7)	3.49	221	0.28 (1.92)	0.19	0.009	0.047
14	5.5 (140)	0.26 (6.5)	45.4 (313)	3.45 (23.8)	4.3	22	4.65 (32.04)	0.08	0.097	1.35
15	7.87 (200)	0.2 (5)	38.5 (265.8)	3.94 (27.15)	4.2	40	2.03 (14)	0.1	0.053	0.52
16	5.5 (140)	0.12 (3)	37.4 (285)	4.52 (31.15)	4.3	47	1.85 (12.76)	0.1	0.043	0.45
17	11 (280)	0.16 (4)	39.5 (272.6)	4.5 (31.2)	3	70	1.16 (8.02)	0.1	0.029	0.26
18	11.8 (300)	0.12 (3)	33.65 (232)	4 (27.23)	3	100	0.68 (4.62)	0.1	0.02	0.17
19	11.8	0.08	49.6	4	2.8	150	0.67	0.08	0.013	0.16

(300)	(2)	(341.7)	(27.23)			(4.62)			

Table 4-3 shows nineteen experimental data cases collected from the literature. The first thirteen cases are from O'shea and Bridge (2000) paper. Cases 14, 16 and 18 are from Schneider (1998) paper. Cases 15, 17 and 19 are taken from Huang *et al* (2002) paper
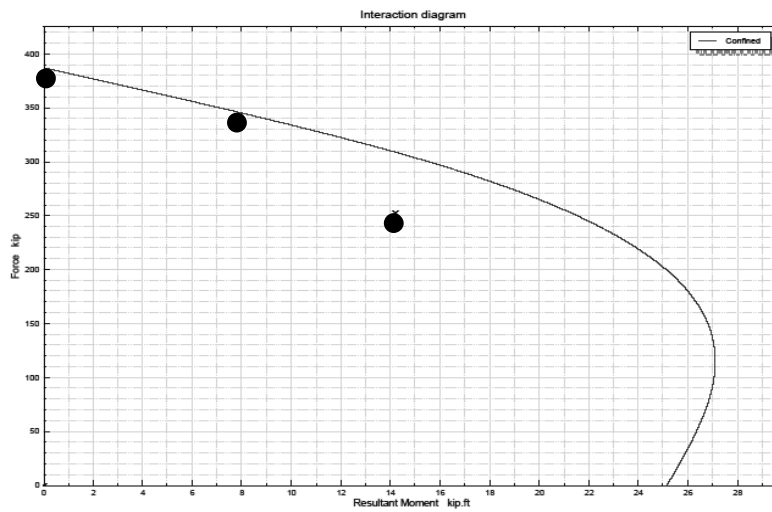
Figure 4-25: KDOT Column Expert Comparison with CFST case 1:
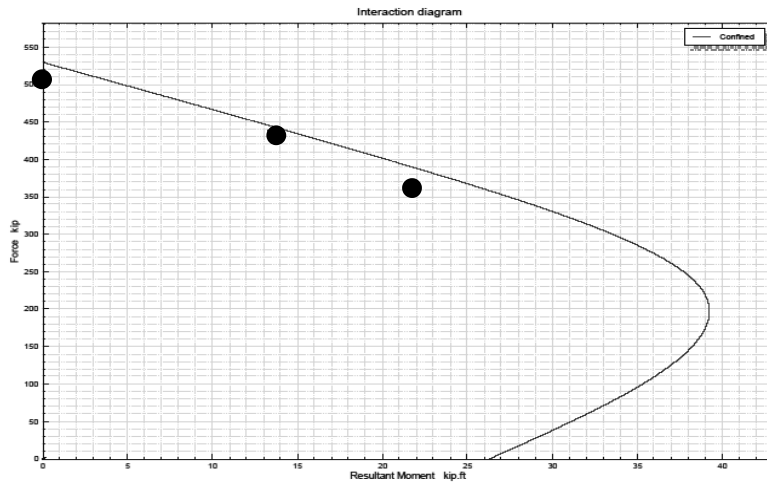
Figure 4-26: KDOT Column Expert Comparison with CFST case 2
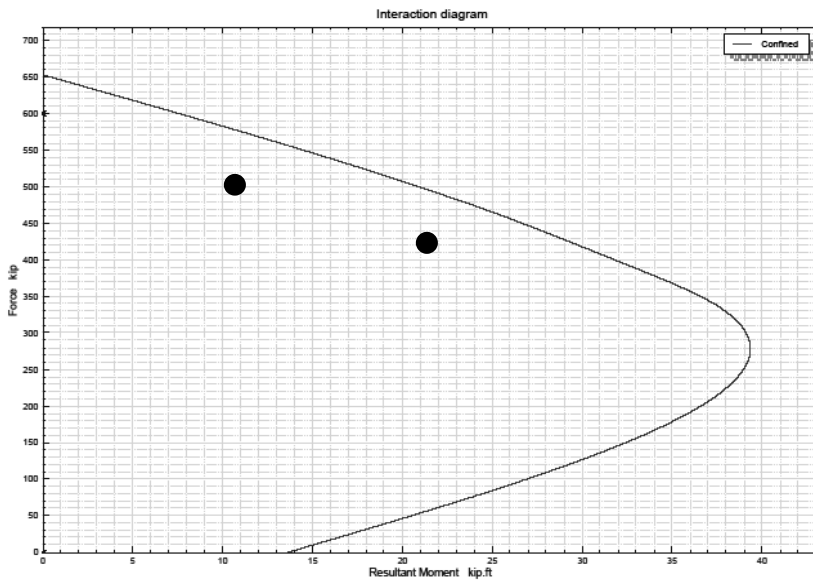
Figure 4-27: KDOT Column Expert Comparison with CFST case 3
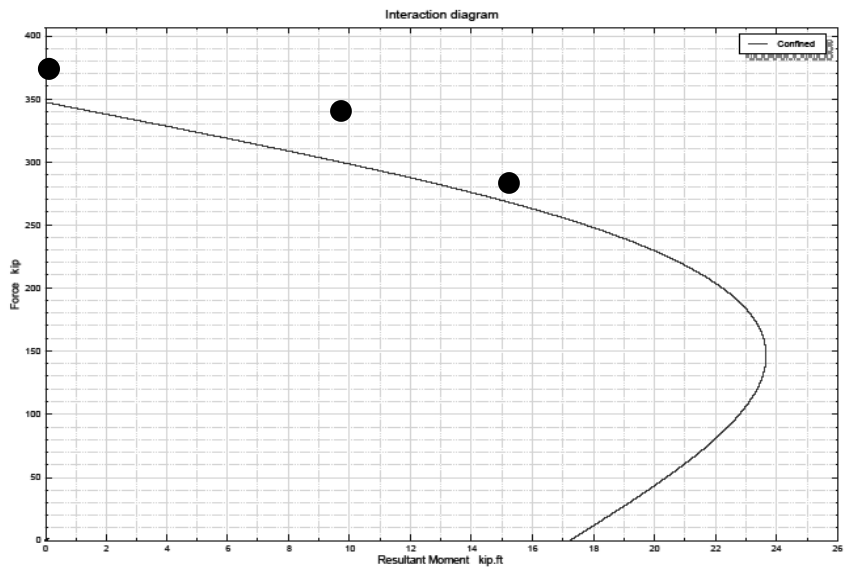
Figure 4-28; KDOT Column Expert Comparison with CFST case 4
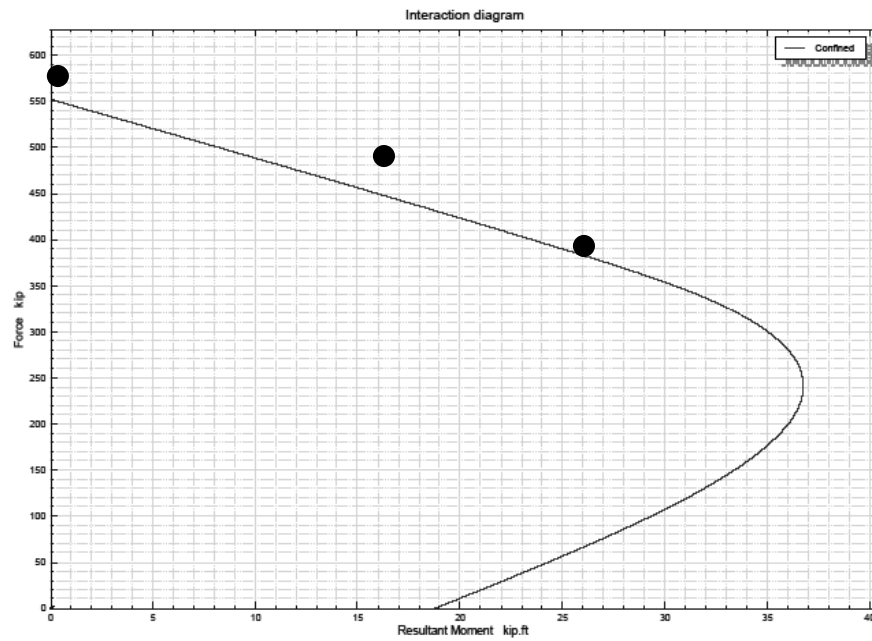
Figure 4-29: KDOT Column Expert Comparison with CFST case 5
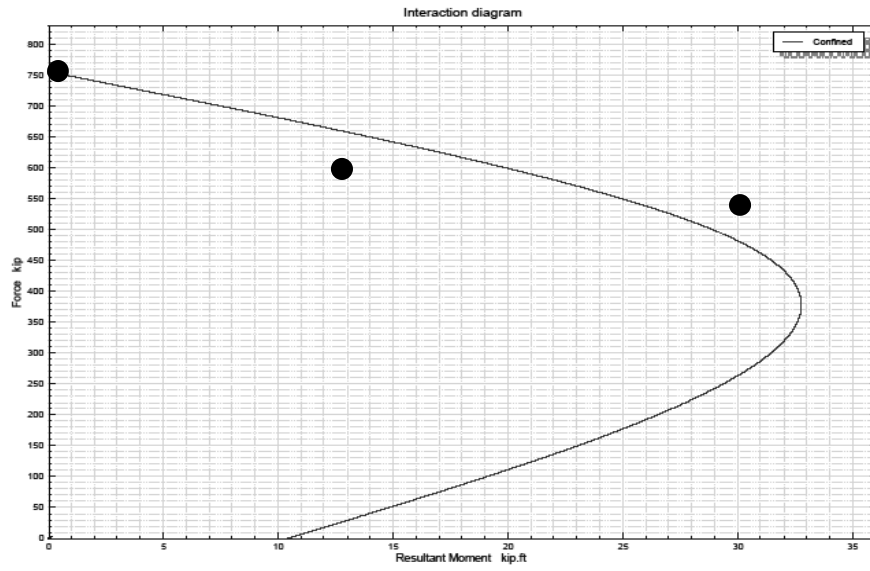
Figure 4-30: KDOT Column Expert Comparison with CFST case 6
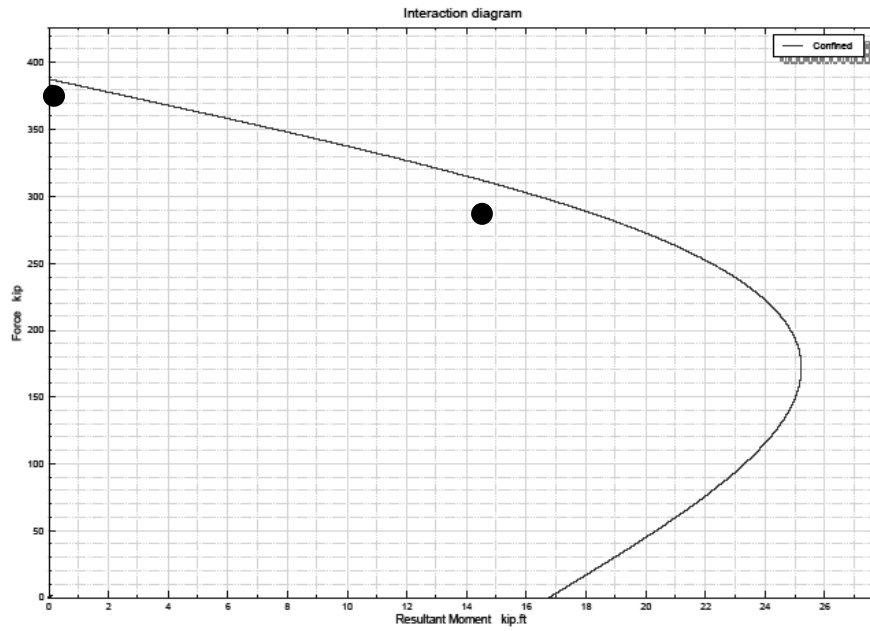
Figure 4-31: KDOT Column Expert Comparison with CFST case 7
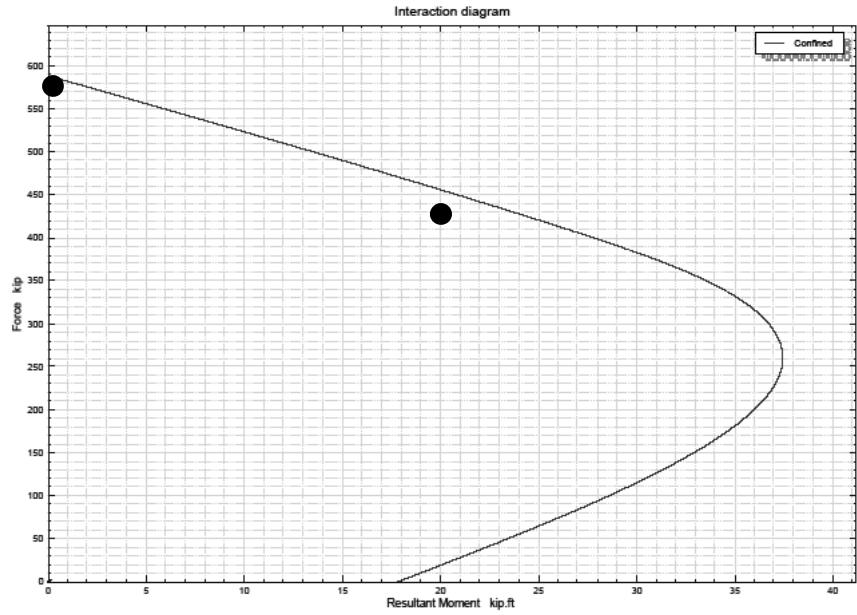
Figure 4-32: KDOT Column Expert Comparison with CFST case 8
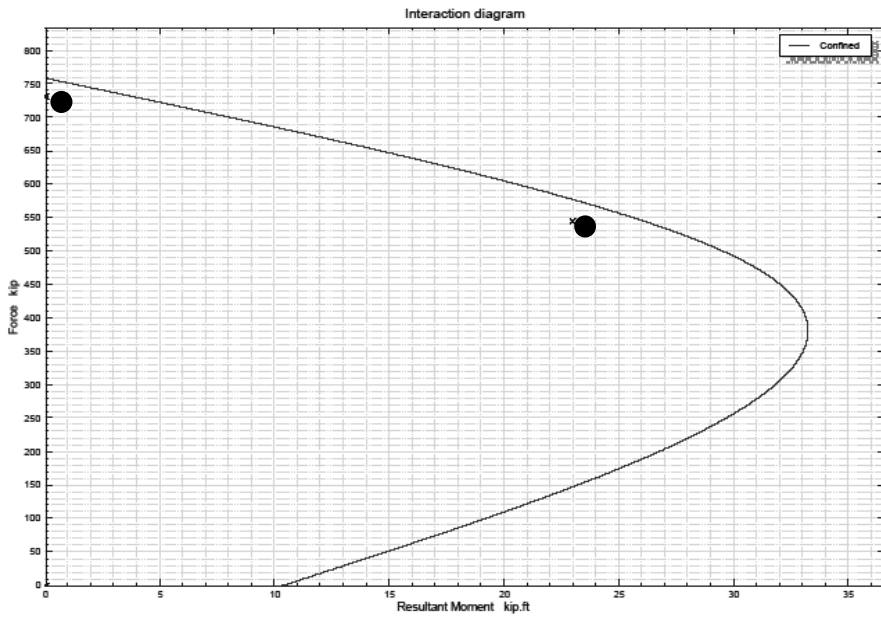
Figure 4-33: KDOT Column Expert Comparison with CFST case 9
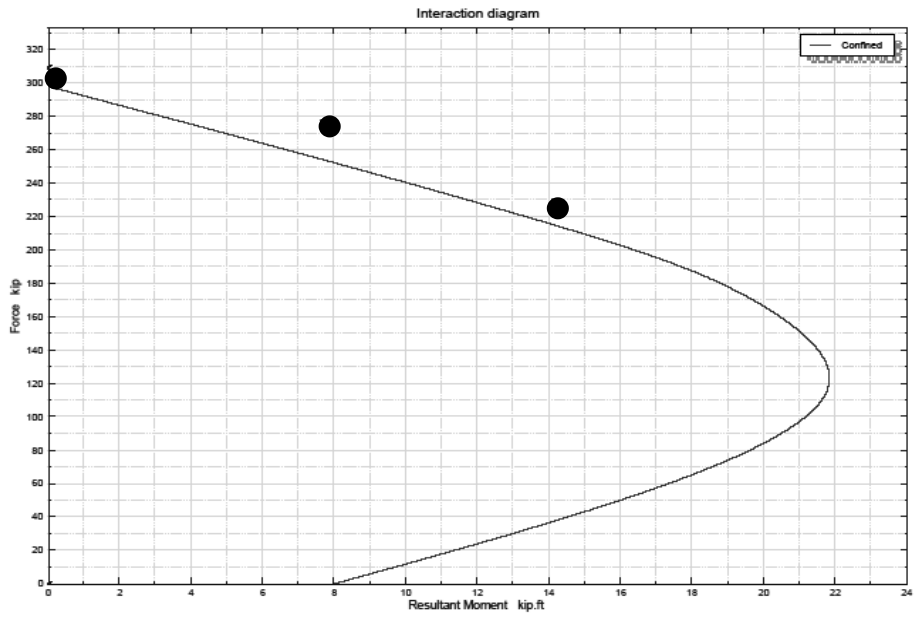
Figure 4-34: KDOT Column Expert Comparison with CFST case 10
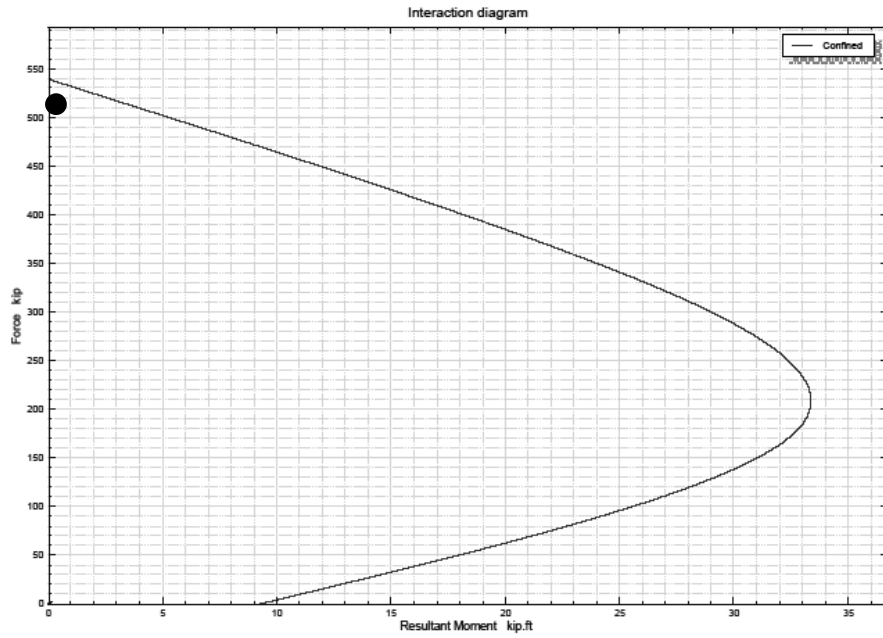
Figure 4-35: KDOT Column Expert Comparison with CFST case 11

286
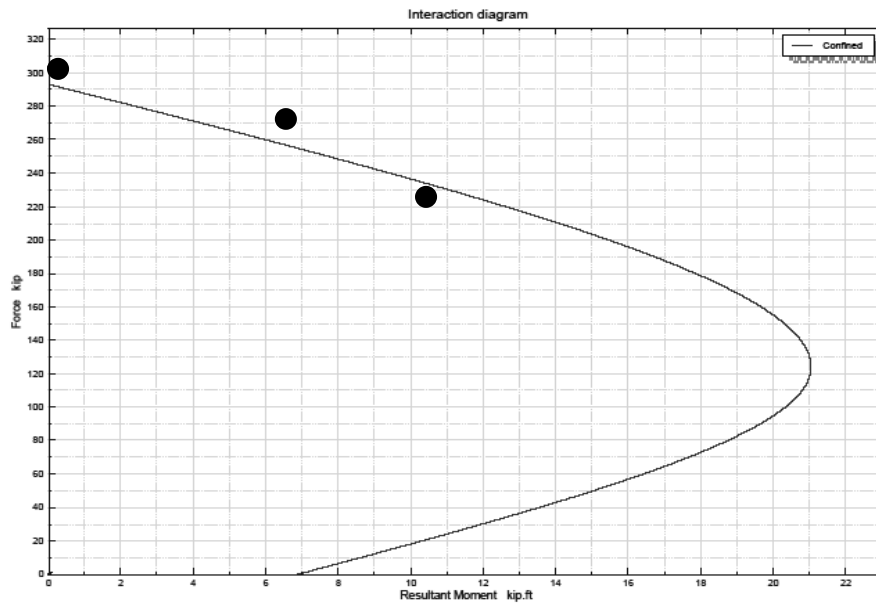
Figure 4-36: KDOT Column Expert Comparison with CFST case 12
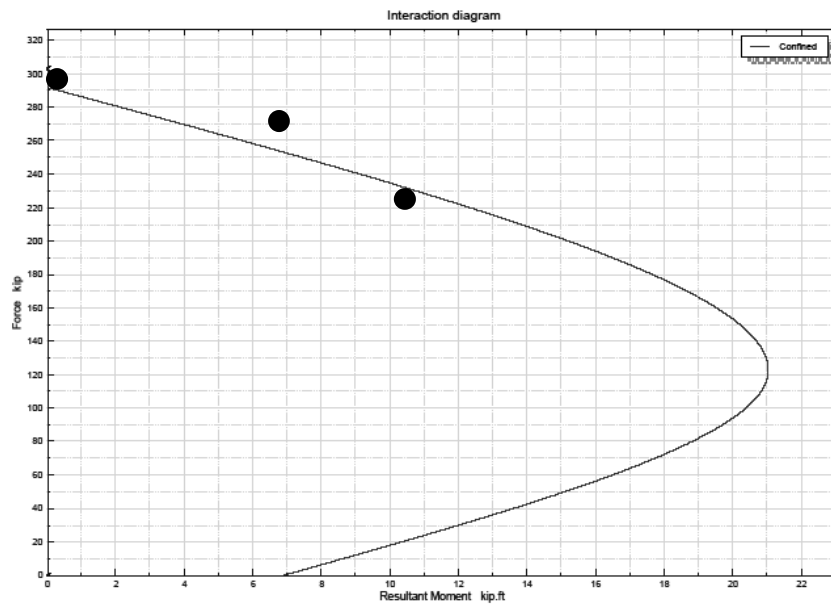
Figure 4-37: KDOT Column Expert Comparison with CFST case 13
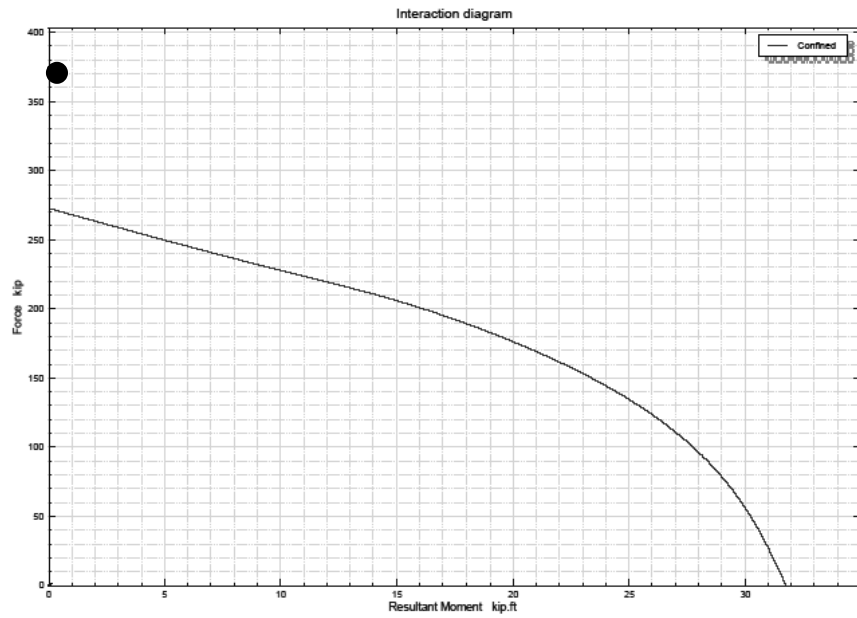
Figure 4-38: KDOT Column Expert Comparison with CFST case 14
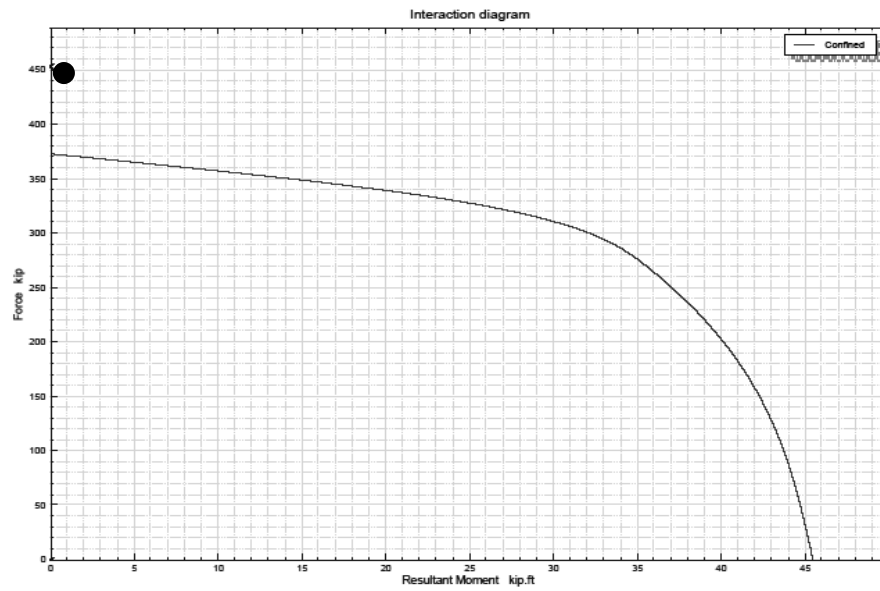
Figure 4-39: KDOT Column Expert Comparison with CFST case 15
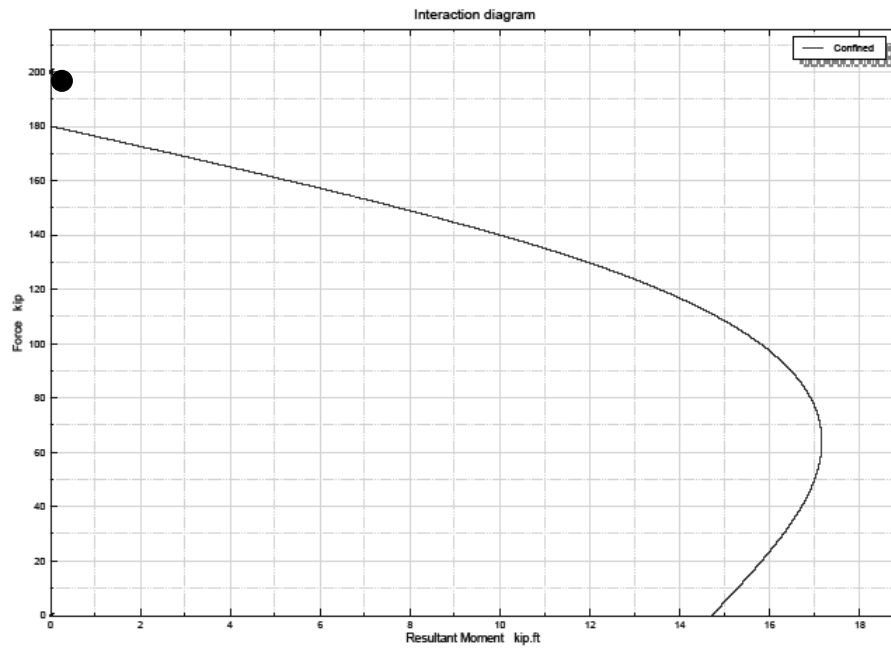
Figure 4-40: KDOT Column Expert Comparison with CFST case 16
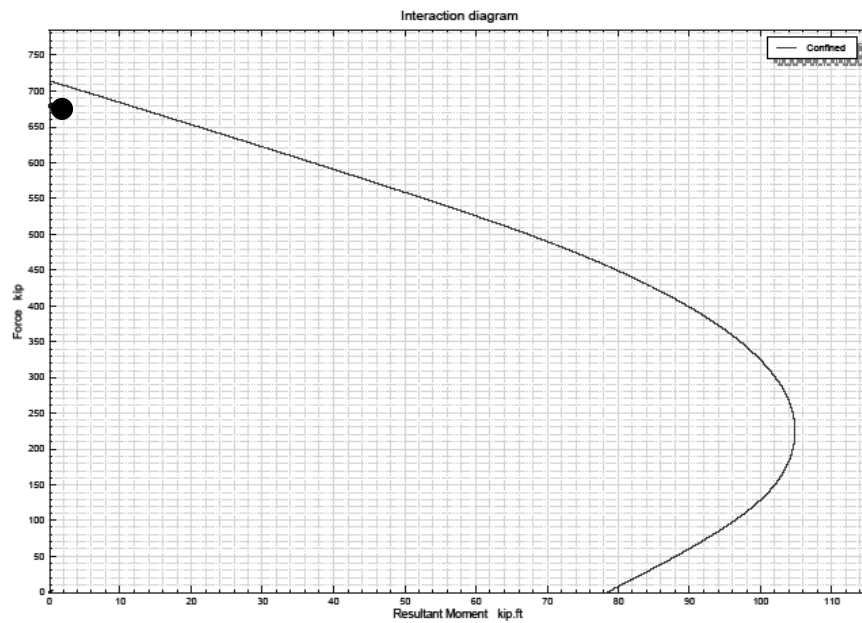
Figure 4-41: KDOT Column Expert Comparison with CFST case 17

289
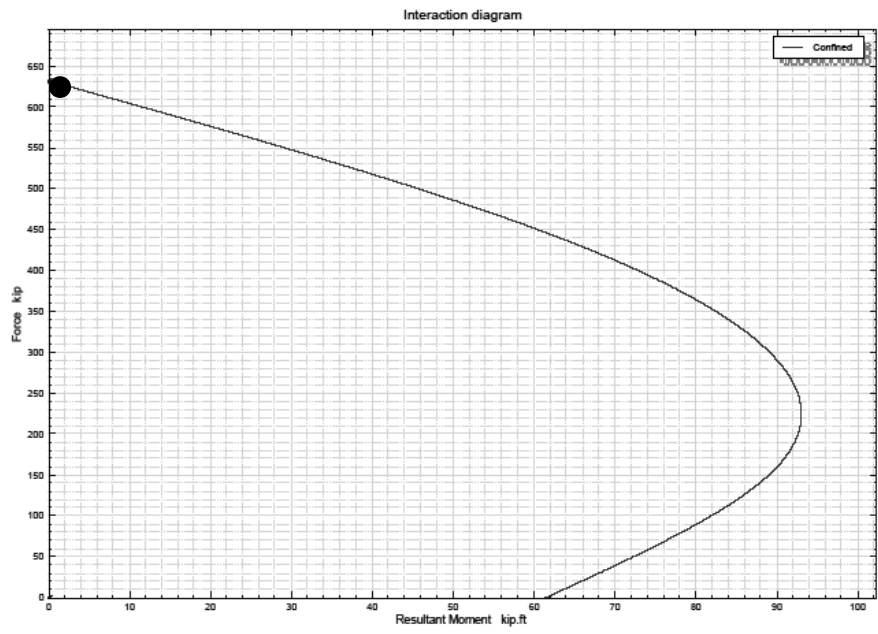
Figure 4-42: KDOT Column Expert Comparison with CFST case 18
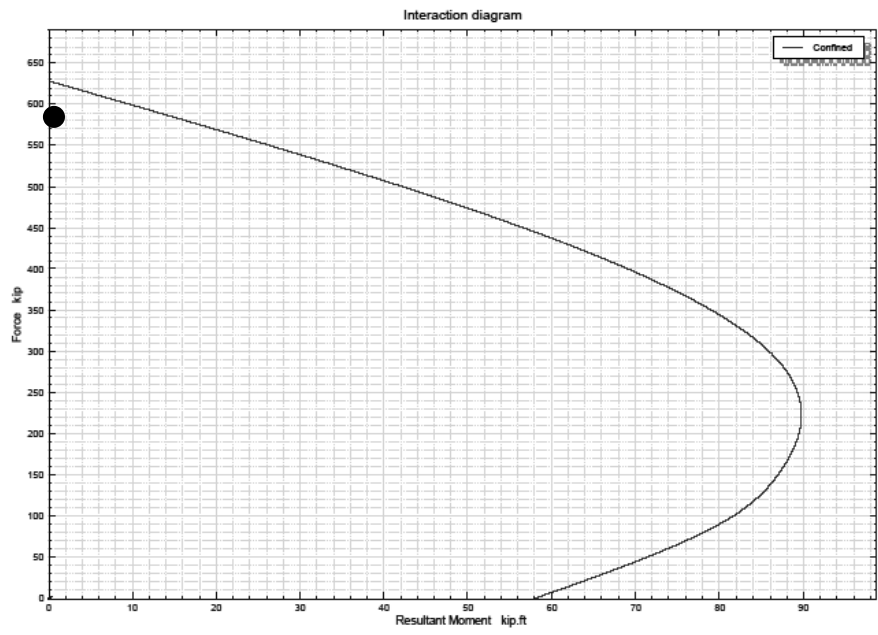
Figure 4-43: KDOT Column Expert Comparison with CFST case 19

Figures (4-25) to (4-43) show the interaction diagrams for the nineteen cases in table 4-2 with comparison to the corresponding experimental points. The interaction diagrams are plotted using KDOT Column Expert software that was implemented using the numerical analysis described in section 4-3-2. Several observations can be drawn:

- In general there is good agreement between the theoretical interaction diagrams and the corresponding experimental data.

- Some experimental points lie inside the envelope of the interaction diagram which represents slightly un-conservative cases. This can be justified due to the following reasons:

1- Local buckling occurance that is not addressed by the model.

2- The effect of the biaxial stress on the steel. For the above cases, the steel is subjected to compression axial stress and tension lateral stress. The steel lateral strain needs to be monitored, and the analysis should account for the yield strength in the lateral direction. A rough calculation is made to case one to test the steel lateral strain. Some values are assumed since they are missing from their source:

$$f_{cc} = f_c^{'} + f_l = 7 + 1.83 = 8.83 ksi$$

It should be noted that the peak strength equation used herein is conservative with respect to Mander and Richart equations. The axial strain at the peak confined stress is calculated based on Mander and Richart equation as follow:

$$\varepsilon_{cc} = \varepsilon_{co}\left[1 + 5\left(\frac{f_{cc}}{f_c^{'}} - 1\right)\right] = 0.002\left[1 + 5\left(\frac{8.83}{7} - 1\right)\right] = 0.0046$$

291

ε_{co} is assumed conservatively equal to 0.002. Poisson's ratio for concrete in non-linear zone is equal to 0.5 (Mazzotti and Savoia 2002), so the lateral strain is equal to 0.0023, and this is the same lateral strain in steel approximately. The yield strain for the steel is calculated from the tube properties given by the author as follow:

$$\varepsilon_y = \frac{f_y}{E_s} = \frac{363.3}{200588} = 0.0018$$

From the previous calculations, it is seen that the steel strain at the peak stress is exceeding the yielding steel strain in the lateral direction. Hence, considering the lateral steel strain to exceed yielding allowing for free expansion of concrete is one of the ways that may improve the results (Shams and Saadeghavaziri 1997).

- For heavy steel cross sections, such as case 14 and 15, the interaction diagram shape looks like the steel cross section's W shape and the interaction diagram is conservative.

Overall there is good agreement between the theoretical model and the experimental data.

Chapter 5 - Rectangular Columns subjected to biaxial bending and Axial Compression

5-1 Introduction

Rectangular reinforced concrete columns can be subjected to biaxial bending moments plus axial force. When the load acts directly on one of the cross section bending axes the problem becomes of uniaxial bending and axial force. However when the load is applied eccentrically on a point that is not along any of the bending axes the case is generally biaxial bending and axial force. The biaxial bending case can be found in many structures nowadays. This case is visited extensively in the literature aside from the confinement effect. The failure surface of rectangular columns is 3D surface consisted of many adjacent 2D interaction diagrams. Each of the 2D interaction diagrams represents one angle between the bending moment about x-axis and the resultant moment. Many simplifications are introduced to justify the compressive trapezoidal shape of the concrete compression zone, due to the existence of the two bending axes. Approximations also were presented to depict the 3D failure shape from the principal interaction diagrams, in the two axes of symmetry. The most effective procedure found in the literature is the predefined ultimate strain profile that determines a certain position of the neutral axis and assigns crushing ultimate strain (typically 0.003) in one of the column corners. With the advance in technology and the enormous speed of computations, analysis is needed to plot a more accurate failure interaction diagram for both the unconfined and confined cases.

The methodology in this study is based on two different approaches;the adjusted predefined ultimate strain profile and the moment of area generalization approaches

described below. The two methods are compared to benchmark the moment of area generalization method that will be used in the actual capacity analysis (Confined analysis). This analysis is compared to experimental data from the literature.

5-2 Unconfined Rectangular Columns Analysis

5-2-1 Formulations

5-2-1-1 Finite Layer Approach (Fiber Method)

The column cross section is divided into finite small-area filaments (Figure 5-1 a). The force and moment of each filament is calculated and stored. The rebars are treated as discrete objects in their actual locations. The advantage of that is to avoid inaccuracy generated from using the approximation of the stress block method, as a representative of the compression zone and to well treat cases that have compressive trapezoidal or triangular shapes generated from the neutral axis inclination (Figure 5-1 b).

a)   b)
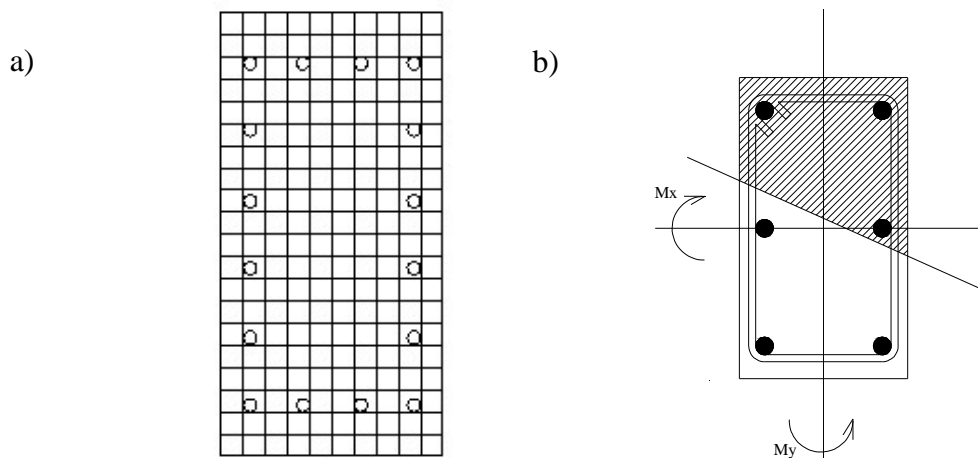
Figure 5-1:a) Using finite filaments in analysis   b)Trapezoidal shape of Compression zone

5-2-1-2 Concrete Model

Concrete is analyzed using the model proposed by Hognestad that was adopted from Ritter's Parabola 1899 (Hognestad 1951). Hognestad model is used extensively in numerous papers as it well explains concrete stress-strain behavior in compression. In addition, it was utilized by widely used concrete models such as Kent and Park model (1971). The stress-strain model is expressed using the following equation (Figure 5-2 a)

$$f_c = f_c' \left(2\frac{\varepsilon_c}{\varepsilon_o} - \left(\frac{\varepsilon_c}{\varepsilon_o}\right)^2 \right) \qquad \qquad 5\text{-}1$$

f_c = stress in concrete in compression.

f_c' = maximum compressive strength of the concrete.

ε_c = strain at f_c

ε_o = strain at f_c'

As shown in Figure (5-2 a) concrete carries tension up to cracking strength, then it is neglected in calculation beyond that.
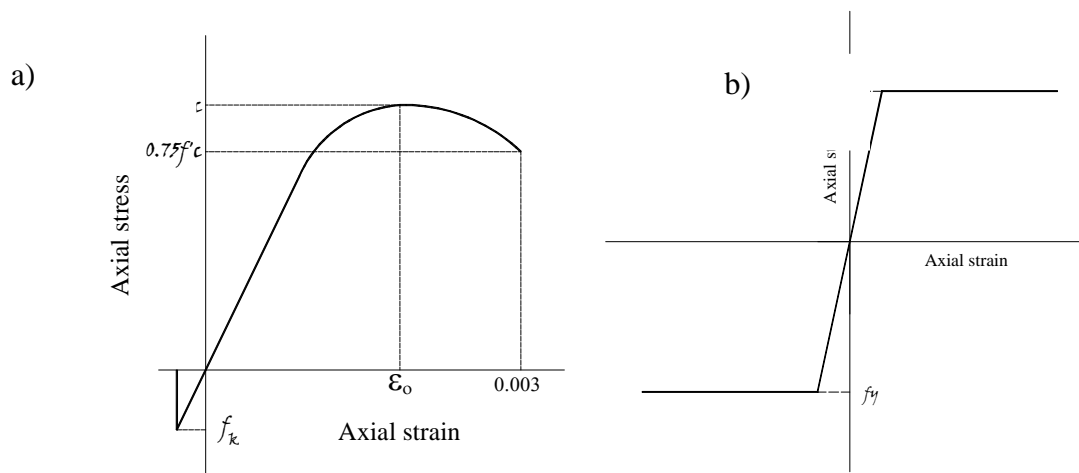
Figure 5-2: a) Stress- strain Model for concrete by Hognestad   b) Steel stress-strain Model

5-2-1-3 Steel Model

Steel is assumed to be elastic up to the yield stress then perfectly plastic as shown in Figure (5.2 b). It is assumed that there is perfect bond between the longitudinal steel bars and the concrete. According to Bernoulli's Hypothesis, strains along the depth of the column are assumed to be distributed linearly.

5-2-2 Analysis Approaches

The process of generalization of the moment-force interaction diagram is developed using two different approaches; the adjusted predefined ultimate strain profile and the generalized moment of area methods. The common features of the two approaches are described as follow:

5-2-2-1 Approach One: Adjusted Predefined Ultimate Strain Profile

The first approach is the well known method that was used by many researchers and practicing engineers. The procedure is to assign compressive failure strain at one of the column corners (0.003) and to vary the position and the inclination angle of the neutral axis that ranges from zero degree, parallel to the width of the column, to ninety degrees parallel to the height as shown in Figure (5-3).
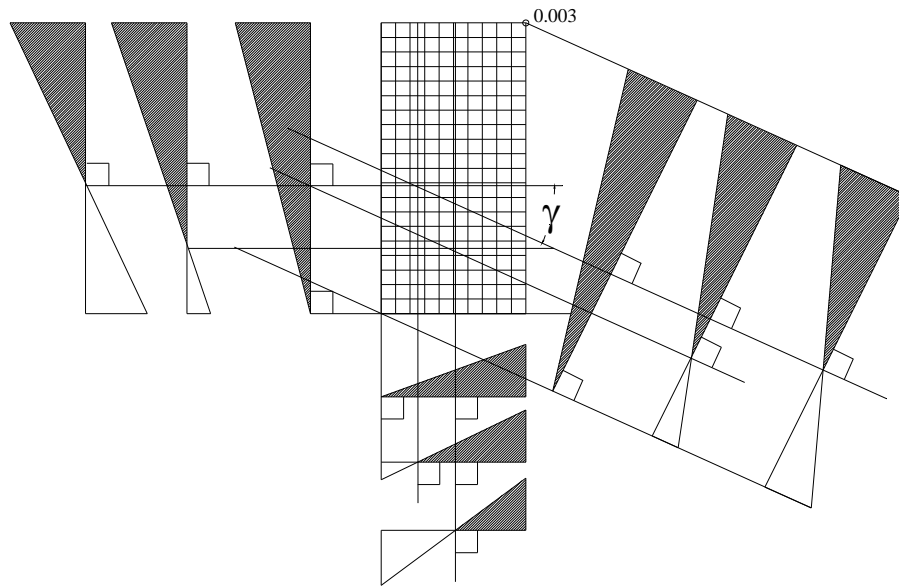
Figure 5-3: Different strain profiles due to different neutral axis positions.

Each set of the parallel neutral axes of a certain orientation represents approximately one 2D interaction diagram, and all of the sets from zero to ninety degrees represent the 3D failure surface in one quadrant, which is identical to the other three quadrants due to the existence of two axis of symmetry with respect of concrete and steel. The procedure is described in the following steps:

1- Defining the strain profile for each neutral axis position and corner ultimate strain applied.

2- Calculating strain and the corresponding stress in each filament of concrete and doing the same for each steel bar (Figure 5-4).
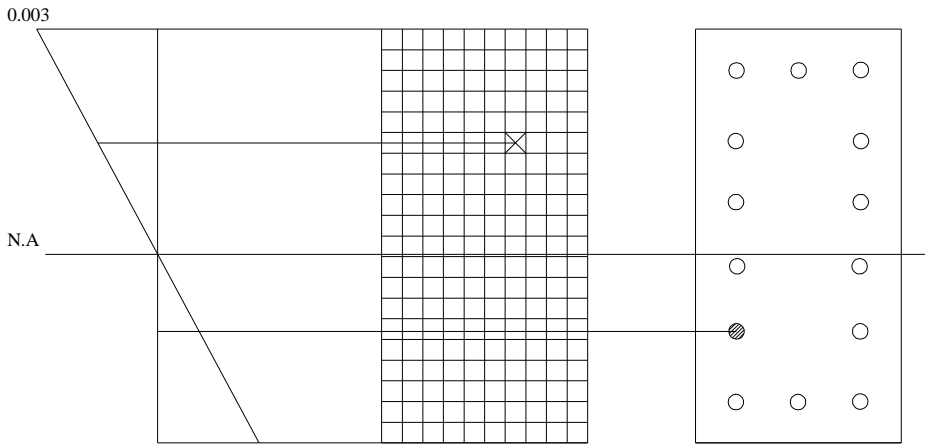
Figure 5-4: Defining strain for concrete filaments and steel rebars from strain profile

3- Calculating the force and the moment about the geometric centroid for each filament and steel bar (Figure 5-5)

for concrete: for steel

$$P_{ci} = f_{ci} w_i t_i \qquad\qquad P_{si} = f_{si} A_{si} \qquad\qquad 5\text{-}2$$

$$Mx_{ci} = P_{ci} * Y\_i \qquad\qquad Mx_{si} = P_{si} * Y\_si \qquad\qquad 5\text{-}3$$

$$My_{ci} = P_{ci} * X\_i \qquad\qquad My_{si} = P_{si} * X\_si \qquad\qquad 5\text{-}4$$
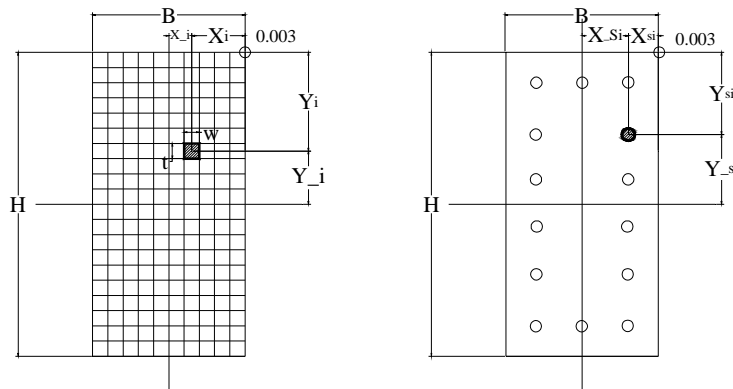
Figure 5-5: Filaments and steel rebars geometric properties with respect to crushing strain point

and geometric centroid

298

4- Summing up the forces and moments, from steel bars and concrete filaments, to get the internal force and moment about x-axis and y-axis. The resultant force and moments represent one point on the unconfined interaction diagram. (Figure 5-6).

```
                    ┌──────────┐
                    │  Start   │
                    └──────────┘
                         │
                    ┌──────────────┐
            ┌──────▶│   Define     │
            │       │ Neutral axis │
            │       │ position &   │
            │       │ orientation  │
            │       └──────────────┘
            │              │
            │       ┌──────────────┐
            │       │ Determine    │
            │       │ strain       │
            │       │ profile based│
            │       │ on 0.003 at  │
            │       │ a corner     │
            │       └──────────────┘
            │              │
            │       ┌──────────────┐
            │       │  Calculate   │
            │       │ εc,εs,fc,fs  │
            │       └──────────────┘
            │              │
            │       ┌──────────────┐
            │       │ Sum up       │
        ┌───◇───┐   │ internal     │
        │ New   │◀──│ forces and   │
        │ Point │   │ moments      │
        └───◇───┘   │ Fz,GMox,GMoy,│
            │       │ GMR          │
            │       └──────────────┘
            │       ┌──────────┐
            └──────▶│   End    │
                    └──────────┘
```
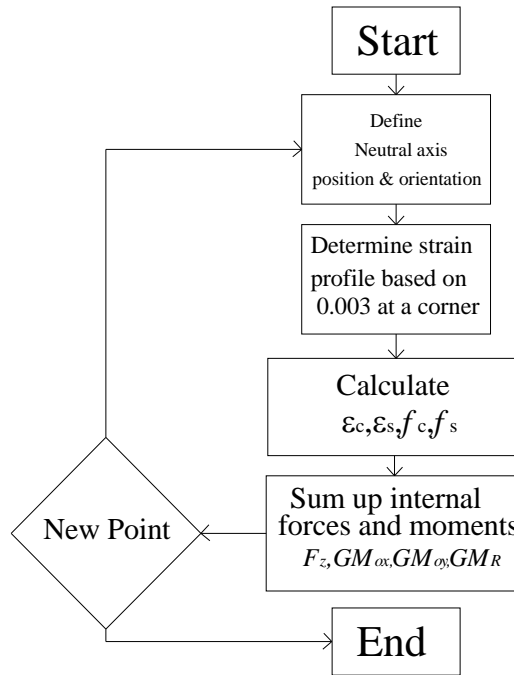
Figure 5-6: Method one Flowchart for the predefined ultimate strain profile method

The problem arising from this procedure is that the points developed from one set of parallel neutral axes are close to but not lined up in one plane. However, they are scattered tightly near that plane (Figure 5-7). To correct for that, an average angle of $\bar{\alpha} = \cos^{-1}(M_x / M_R)$ is calculated and another run is established by slightly changing the inclination angle γ of the neutral axis of the section with respect to the y-axis and iterating till the angle determined for each point converges to the average angle $\bar{\alpha}$. The average angle $\bar{\alpha}$ is taken as the average of all α angles obtained for a certain γ angle orientation of the neutral axis (Figure 5-3 and Figure 5-7).
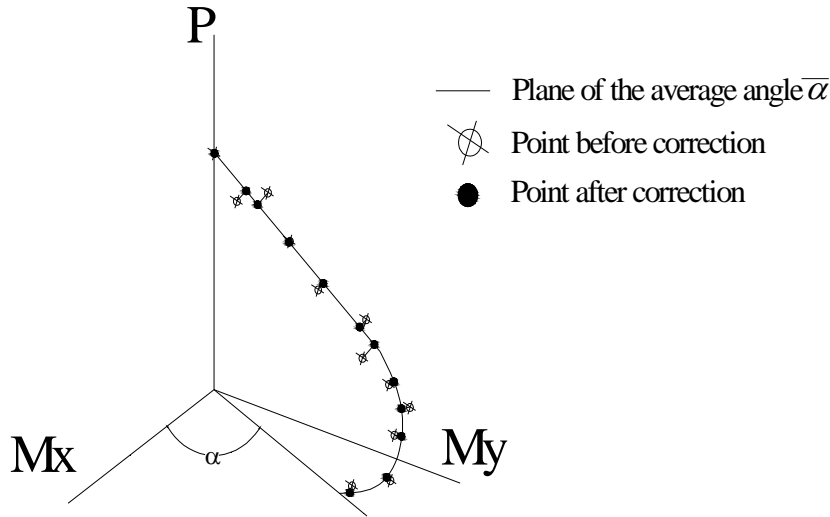
Figure 5-7: 2D Interaction Diagram from Approach One Before and After Correction

The iterations mentioned above converge fast in all cases. This approach yields a very fast computation since it directly evaluates the ultimate unconfined strain profile. However, no moment curvature or load-strain history response is available with this approach

5-2-2-2 Approach Two: Generalized Moment of Area Theorem

5-2-2-2-a Moment of Area Theorem

The very general axial stress equation in an unsymmetrical section subjected to axial force P and biaxial bending M_x and M_y (Hardy Cross 1930):

$$\sigma_z = \frac{P}{A} + \frac{M_x I_y - M_y I_{xy}}{I_x I_y - I_{xy}^2} y + \frac{M_y I_x - M_x I_{xy}}{I_x I_y - I_{xy}^2} x \qquad \text{5-5}$$

σ_z = normal stress at any point (a) in cross section

P = applied load.

A = cross sectional area.

M_x = bending moment about the geometric x-axis

M_y = bending moment about the geometric y-axis

x = distance between the point (a) and y-axis

y = distance between the point (a) and x-axis

I_x = moment of inertia about the geometric x-axis

I_y = moment of inertia about the geometric y-axis

I_{xy} = product moment of inertia in xy plane

Rewriting Equation (5-5) to determine the strain at any point in the cross section:

$$\varepsilon_z = \frac{P}{EA} + \frac{M_x EI_y - M_y EI_{xy}}{EI_x EI_y - EI_{xy}^2} y + \frac{M_y EI_x - M_x EI_{xy}}{EI_x EI_y - EI_{xy}^2} x \qquad \text{5-6}$$

In case of linear elastic analysis, E in EA or EI expressions is constant ($E=E_c$). However, if the

section has linear strain but nonlinear stress profile, it will amount to variable E profile (per layer

or filament) in nonlinear analysis. Accordingly, the section parameters must include $\sum_i E_i A_i$,

$\sum_i E_i I_i$ for a more generalized theory (Rasheed and Dinno 1994). Note that the linear strain

profile of the section from Equation (5-6) yields two distinct constant curvatures:

$$\phi_x = \frac{M_x EI_y - M_y EI_{xy}}{\beta^2} \qquad \text{5-7}$$

$$\phi_y = \frac{M_y EI_x - M_x EI_{xy}}{\beta^2} \qquad \text{5-8}$$

ϕ_x = curvature about the x-axis

ϕ_y = curvature about the y-axis

$$\beta^2 = EI_x EI_y - EI_{xy}^2$$

To prove Equations (5-7) and (5-8) above, invoke the coupled equations of moments about the actual or current centroid (Bickford 1998).

$$M_x = EI_x \phi_x + EI_{xy} \phi_y \tag{5-9}$$

$$M_y = EI_{xy} \phi_x + EI_y \phi_y \tag{5-10}$$

In a matrix form:

$$\begin{bmatrix} M_x \\ M_y \end{bmatrix} = \begin{bmatrix} EI_x & EI_{xy} \\ EI_{xy} & EI_y \end{bmatrix} \begin{bmatrix} \phi_x \\ \phi_y \end{bmatrix} \tag{5-11}$$

Inverting Equation (5-11)

$$\begin{bmatrix} \phi_x \\ \phi_y \end{bmatrix} = \frac{1}{\beta^2} \begin{bmatrix} EI_y & -EI_{xy} \\ -EI_{xy} & EI_x \end{bmatrix} \begin{bmatrix} M_x \\ M_y \end{bmatrix} \tag{5-12}$$

which reproduces Equations (5-7) and (5-8). Rewriting Equation (5-6) in terms of ϕ_x and ϕ_y

$$\varepsilon_z = \frac{P}{EA} + \phi_x y + \phi_y x \tag{5-13}$$

Finding ε_z at the actual or current centroid, since $x = y = 0$.

$$\varepsilon_o = \frac{P}{EA} \tag{5-14}$$

Finding ε_z at the geometric centroid, $y = \bar{y}$

$$\bar{\varepsilon}_o = \frac{P}{EA} + \phi_x \bar{y} + \phi_y \bar{x}$$

Solving for P at the geometric centroid;

$$P = EA\bar{\varepsilon}_o - EA\bar{y}\phi_x - EA\bar{x}\phi_y \tag{5-15}$$

But

$$EAM_x = EA\overline{y} \qquad \overline{y} = Y_G - Y_c$$

$$EAM_y = EA\overline{x} \qquad \overline{x} = X_G - X_c$$

Y_G is the vertical distance to the geometric centroid measured from bottom, X_G is the distance to the geometric centroid measured from the cross section's left side, Y_c is the vertical distance to the inelastic centroid measured from the bottom and X_c is the horizontal distance to the inelastic centroid measured from the cross section's left side, Figure (5-8).

Thus,

$$P = EA\overline{\varepsilon}_o - EAM_x \phi_x - EAM_y \phi_y \qquad \text{5-16}$$

The general formula of the moments about the geometric x-axis and the geometric y-axis is derived as follows:

when the moment is transferred from the centroid to the geometric centroid ,Figure (5-8 a)

$$\overline{M}_x = M_x - P\overline{y} \qquad \text{5-17}$$

Substituting Equations (5-9) and (5-16) in (5-17) yields:

$$\overline{M}_x = EI_x \phi_x + EI_{xy}\phi_y - EA\overline{\varepsilon}_o \overline{y} + EAM_x \phi_x \overline{y} + EAM_y \phi_y \overline{y} \qquad \text{5-18}$$

$$\overline{M}_x = -EAM_x \overline{\varepsilon}_o + \left(EI_x + EAM_x \overline{y}\right)\phi_x + \left(EI_{xy} + EAM_y \overline{y}\right)\phi_y \qquad \text{5-19}$$

Similarly, (Figure 5-8 b):

Figure 5-8: Transfering moment from centroid to the geometric centroid

303

$$\overline{M}_y = M_y - P\overline{x}$$

$$\overline{M}_y = EI_{xy}\phi_x + EI_y\phi_y - EA\overline{\varepsilon}_o\overline{x} + EAM_x\phi_x\overline{x} + EAM_y\phi_y\overline{x}$$

$$\overline{M}_y = -EAM_y\overline{\varepsilon}_o + \left(EI_{xy} + EAM_x\overline{x}\right)\phi_x + \left(EI_y + EAM_y\overline{x}\right)\phi_y$$

The terms $EI_x + EAM_x\overline{y}$ and $EI_y + EAM_y\overline{x}$ represent the $\overline{EI}_x$ and $\overline{EI}_y$ about the geometric

centroid respectively using the parallel axis theorem. And the terms $EI_{xy} + EAM_x\overline{x}$ and

$EI_{xy} + EAM_y\overline{y}$ are equal given that: $EAM_x\overline{x} = EA\overline{y}\,\overline{x}$ and $EAM_y\overline{y} = EA\overline{y}\,\overline{x}$. Using Equations (5-

16), (5-19) and (5-22) yields the extended generalized moment of area equation:

$$\begin{bmatrix} P \\ \overline{Mx} \\ \overline{M}_y \end{bmatrix} = \begin{bmatrix} EA & -EAM_x & -EAM_y \\ -EAM_x & \overline{EI}_x & \overline{EI}_{xy} \\ -EAM_y & \overline{EI}_{xy} & \overline{EI}_y \end{bmatrix} \begin{bmatrix} \overline{\varepsilon}_o \\ \phi_x \\ \phi_y \end{bmatrix}$$

Since the moment of area about the inelastic centroid vanishes (Rasheed and Dinno

1994), Equation (5-23) reduces to a partially uncoupled set when it is applied back at inelastic

the centroid since EAM_x and EAM_y vanish about that centroid.

$$\begin{bmatrix} P \\ M_x \\ M_y \end{bmatrix} = \begin{bmatrix} EA & 0 & 0 \\ 0 & EI_x & EI_{xy} \\ 0 & EI_{xy} & EI_y \end{bmatrix} \begin{bmatrix} \varepsilon_o \\ \phi_x \\ \phi_y \end{bmatrix}$$

which is simply Equations (5-9), (5-10) and (5-14)

5-2-2-2-b Method Two

This approach simulates the radial loading of the force and moments by keeping the

relative proportion between them constant during the loading. Accordingly, all the points

comprising an interaction diagram of angle α will be exactly on that 2D interaction diagram. In addition to the ultimate points, the complete load deformation response is generated. The cross section analyzed is loaded incrementally by maintaining a certain eccentricity between the axial force P and the resultant moment M_R. Since M_R is generated as the resultant of M_x and M_y, the angle $\alpha = \tan^{-1}(M_y/M_x)$ is kept constant for a certain 2D interaction diagram. And since increasing the load and resultant moment proportionally causes the neutral axis to vary unpredictably, the generalized moment of area theorem is devised. This method is based on the general response of rectangular unsymmetrical section subjected to biaxial bending and axial compression. The asymmetry stems from the different behavior of concrete in compression and tension.

The method is developed using incremental iterative analysis algorithm, secant stiffness approach and proportional or radial loading. It is explained in the following steps. (Figure 5-12 presents a flowchart of the outlined procedure):

   1- Calculating the initial section properties:

- Elastic axial rigidity EA:

$$EA = \sum_i E_c w_i t_i + \sum_i (E_s - E_c) A_{si}$$

                                                                             5-25

E_c = initial modulus of elasticity of the concrete

E_s = initial modulus of elasticity of the steel rebar

- The depth of the elastic centroid position from the bottom fiber of the section Y_c and from the left side of the section X_c

$$Y_c = \frac{\sum_i E_c w_i t_i (H - Y_i) + \sum_i (E_s - E_c) A_{si} (H - Y_{si})}{EA}$$

                                                                             5-26

$$X_c = \frac{\sum_i E_c w_i t_i (B - X_i) + \sum_i (E_s - E_c) A_{si} (B - X_{si})}{EA}$$

5-27

where Y_i and Y_{si} are measured to the top extreme fiber, X_i and X_{si} are measured to the right most

extreme fiber, see Figure (5-9)

- Elastic flexural rigidity about the elastic centroid *EI*:

$$EI_x = \sum_i E_c w_i t_i (H - Y_i - Y_c)^2 + \sum_i (E_s - E_c) A_{si} (H - Y_{si} - Y_c)^2$$

5-28

$$EI_y = \sum_i E_c w_i t_i (B - X_i - X_c)^2 + \sum_i (E_s - E_c) A_{si} (B - X_{si} - X_c)^2$$

5-29

$$EI_{xy} = \sum_i E_c w_i t_i (H - Y_i - Y_c)(B - X_i - X_c) + \sum_i (E_s - E_c) A_{si} (H - Y_{si} - Y_c)(B - X_{si} - X_c)$$

5-30

Typically the initial elastic $Y_c = H/2$, $X_c = B/2$ and $EI_{xy} = 0$
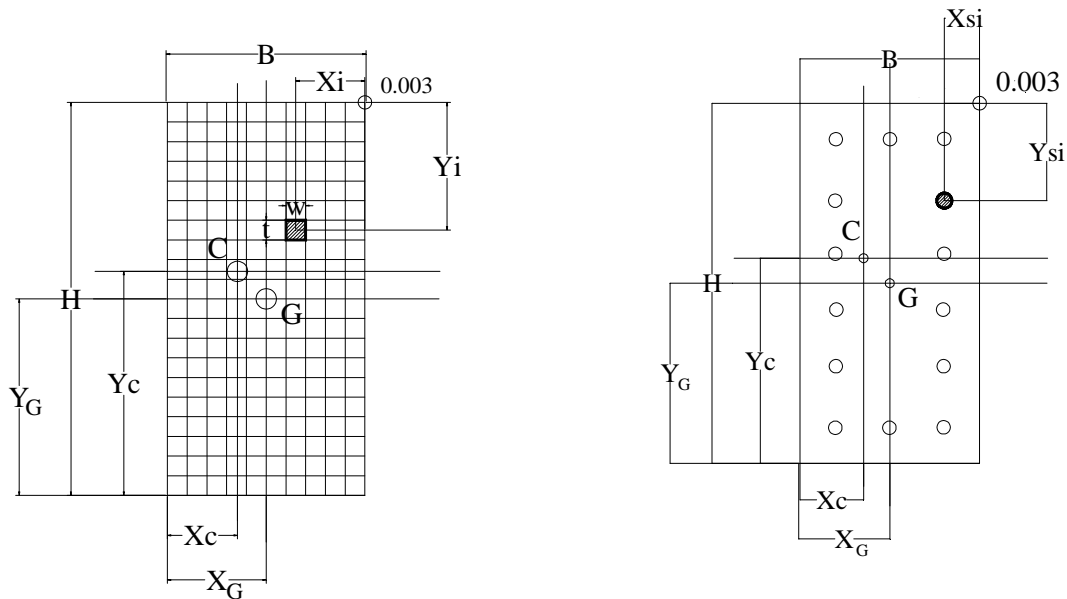
Figure 5-9: geometric properties of concrete filaments and steel rebars with respect to, geometric

centroid and inelastic centroid.

The depth of the geometric section centroid position from the bottom and left fibers of the section Y_G, $X_{G:}$

$$Y_G = \frac{H}{2} \qquad\qquad\qquad\qquad 5\text{-}31$$

$$X_G = \frac{B}{2} \qquad\qquad\qquad\qquad 5\text{-}32$$

2- Defining the eccentricity e, which specifies the radial path of loading on the interaction diagram. Also, defining the angle α in between the resultant moment GM_R and GM_X
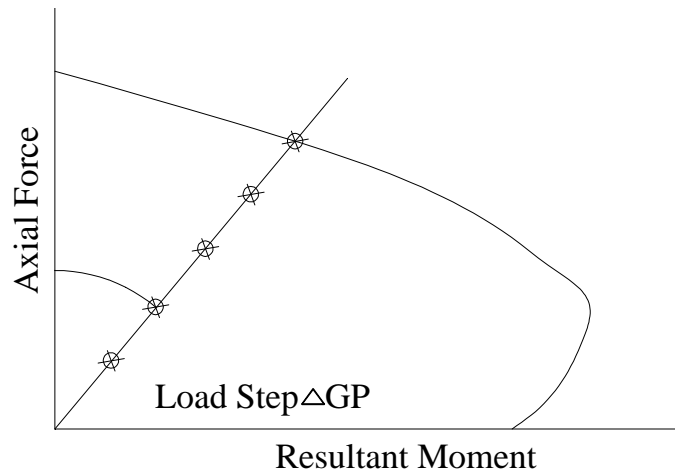
Figure 5-10: Radial loading concept

3- Defining the loading step ΔGP as a small portion of the maximum load, and computing the axial force at the geometric centroid.

$$GP_{new} = GP_{old} + \Delta GP \qquad\qquad\qquad\qquad 5\text{-}33$$

4- Calculating the moment GM_R about the geometric centroid.

$$e = \frac{GM_R}{GP} \qquad\qquad GM_R = e * GP \qquad\qquad 5\text{-}34$$

$$GM_X = GM_R \cos\alpha \qquad\qquad\qquad\qquad 5\text{-}35$$

$$GM_Y = GM_X \tan\alpha \qquad\qquad\qquad\qquad 5\text{-}36$$

5- Transferring the moments to the inelastic centroid and calculating the new transferred moments TM_X and TM_Y :

$$TM_X = GM_X + GP(Y_G - Y_c)$$
$$\text{5-37}$$

$$TM_Y = GM_Y + GP(X_G - X_c)$$
$$\text{5-38}$$

The advantage of transferring the moment to the position of the inelastic centroid is to eliminate the coupling effect between the force and the two moments, since $EAM_x = EAM_y = 0$ about the inelastic centroid

$$\begin{bmatrix} P \\ TM_x \\ TM_y \end{bmatrix} = \begin{bmatrix} EA & 0 & 0 \\ 0 & EI_x & EI_{xy} \\ 0 & EI_{xy} & EI_y \end{bmatrix} \begin{bmatrix} \varepsilon_o \\ \phi_x \\ \phi_y \end{bmatrix}$$
$$\text{5-39}$$
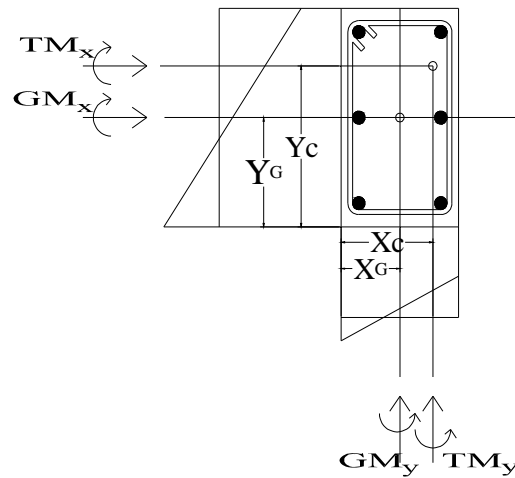
Figure 5-11 Moment transferring from geometric centroid to inelastic centroid

6- Finding: Curvatures ϕ_X and ϕ_Y

$$\phi_X = \frac{TM_X}{\beta^2} * EI_Y - \frac{TM_Y}{\beta^2} * EI_{XY}$$
$$\text{5-40}$$

$$\phi_Y = \frac{TM_Y}{\beta^2} * EI_X - \frac{TM_X}{\beta^2} * EI_{XY}$$
$$\text{5-41}$$

$$\beta^2 = EI_X EI_Y - EI_{xy}^2 \qquad\qquad 5\text{-}42$$

Strain at the inelastic centroid ε_o, the extreme compression fiber strain ε_{ec}, and strain at the extreme level of steel in tension ε_{es} are found as follow:

$$\varepsilon_o = \frac{GP}{EA} \qquad\qquad 5\text{-}43$$

$$\varepsilon_{ec} = \varepsilon_o + \phi_x (H - Y_c) + \phi_y (B - X_c) \qquad\qquad 5\text{-}44$$

$$\varepsilon_{es} = \varepsilon_o - \phi_x (Y_c - Cover) - \phi_y (X_c - Cover) \qquad\qquad 5\text{-}45$$

Where cover is up to center of bars

7- Calculating strain ε_{ci} and corresponding stress f_{ci} in each filament of concrete section by using Hognestad's model (equation 5-1) in case of unconfined analysis

$$\varepsilon_{ci} = \frac{GP}{EA} + \frac{TM_x (H - Y_c - Y_i)}{\beta^2} EI_y + \frac{TM_y (B - X_c - X_i)}{\beta^2} EI_x - \frac{TM_x (B - X_c - X_i)}{\beta^2} EI_{xy}$$
$$- \frac{TM_y (H - Y_c - Y_i)}{\beta^2} EI_{xy} \qquad\qquad 5\text{-}46$$

8- Calculating strain ε_{si} and corresponding stress f_{si} in each bar in the given section by using the steel model shown in Figure (5-2b).

$$\varepsilon_{si} = \frac{GP}{EA} + \frac{TM_x (H - Y_c - Y_{si})}{\beta^2} EI_y + \frac{TM_y (B - X_c - X_{si})}{\beta^2} EI_x - \frac{TM_x (B - X_c - X_{si})}{\beta^2} EI_{xy}$$
$$- \frac{TM_y (H - Y_c - Y_{si})}{\beta^2} EI_{xy} \qquad\qquad 5\text{-}47$$

9- Calculating the new section properties: axial rigidity EA, flexural rigidities about the inelastic centroid EI_x, EI_y, EI_{xy} moment of axial rigidity about inelastic centroid EAM_x, EAM_y, internal axial force F_z, internal bending moments about the inelastic centroid M_{ox}, M_{oy}:

$$EA = \sum_i E_{ci} w_i t_i + \sum_i (E_{si} - E_{ci}) A_{si}$$

5-48

$$EAM_x = \sum_i E_{ci} w_i t_i (H - Y_c - Y_i) + \sum_i (E_{si} - E_{ci}) A_{si} (H - Y_c - Y_{si})$$

5-49

$$EAM_y = \sum_i E_{ci} w_i t_i (B - X_c - X_i) + \sum_i (E_{si} - E_{ci}) A_{si} (B - X_c - X_{si})$$

5-50

$$F_z = \sum f_{ci} w_i t_i + \sum (f_{si} - f_{ci}) A_{si}$$

5-51

$$EI_x = \sum_i E_{ci} w_i t_i (H - Y_c - Y_i)^2 + \sum_i (E_{si} - E_{ci}) A_{si} (H - Y_c - Y_{si})^2$$

5-52

$$EI_y = \sum_i E_{ci} w_i t_i (B - X_c - X_i)^2 + \sum_i (E_{si} - E_{ci}) A_{si} (H - X_c - X_{si})^2$$

5-53

$$EI_{xy} = \sum_i E_{ci} w_i t_i (H - Y_c - Y_i)(B - X_c - X_i)$$
$$+ \sum_i (E_{si} - E_{ci}) A_{si} (H - Y_c - Y_{si})(B - X_c - X_{si})$$

5-54

$$M_{ox} = \sum_i f_{ci} w_i t_i (H - Y_c - Y_i) + \sum_i (f_{si} - f_{ci}) A_{si} (H - Y_c - Y_{si})$$

5-55

$$M_{oy} = \sum_i f_{ci} w_i t_i (B - X_c - X_i) + \sum_i (f_{si} - f_{ci}) A_{si} (B - X_c - X_{si})$$

5-56

where E_{ci} = secant modulus of elasticity of the concrete filament.

   E_{si} = secant modulus of elasticity of the steel bar.

   10- Transferring back the internal moment about the geometric centroid

$$GM_{ox} = M_{ox} - GP(Y_G - Y_c)$$

5-57

$$GM_{oy} = M_{oy} - GP(X_G - X_c)$$

5-58

   11- Checking the convergence of the inelastic centroid

$$TOL_x = EAM_x / EA / Y_c$$

5-59

$$TOL_y = EAM_y / EA / X_c$$

5-60

12- Comparing the internal force to applied force, internal moments to applied moments, and making sure the moments are calculated about the geometric centroid :

$$\left| GP - F_z \right| \leq 1*10^{-5}$$

5-61

$$\left| GM_x - GM_{ox} \right| \leq 1*10^{-5} \qquad \left| GM_y - GM_{oy} \right| \leq 1*10^{-5}$$

5-62

$$\left| TOL_x \right| \leq 1*10^{-5} \qquad \left| TOL_y \right| \leq 1*10^{-5}$$

5-63

If Equations (5-61), (5-62) and (5-63) are not satisfied, the location of the inelastic centroid is Uupdated by EAM_x/EA and EAM_y/EA and steps 5 to 12 are repeated till Equations (5-61), (5-62) and (5-63) are satisfied.

$$Y_{c_{new}} = Y_{c_{old}} + \frac{EAM_x}{EA}$$

5-64

$$X_{c_{new}} = X_{c_{old}} + \frac{EAM_y}{EA}$$

5-65

Once equilibrium is reached, the algorithm checks for ultimate strain in concrete ε_{ec} and steel ε_{es} not to exceed 0.003 and 0.05 respectively, then it increases the loading by ΔGP and runs the analysis for the new load level using the latest section properties. Otherwise, if ε_{ec} equals 0.003 or ε_{es} equals 0.05, the target force and resultant moment are reached as a point on the failure surface for the amount of eccentricity and angle α used.

Start

Calculate initial
section properties
EA, EI_x, EI_y, EI_{xy}
Y_c, Y_G, X_c, X_G

Input P,
e & α

Transfer moment
to inelastic centroid
$TM_x = GM_x + P(Y_G - Y_c)$
$TM_y = GM_y + P(X_G - X_c)$

Calculate
$\emptyset_x, \emptyset_y, \varepsilon_o, \varepsilon_{ec}, \varepsilon_{es}$

Calculate
$\varepsilon_{ci}, \varepsilon_{si}, f_{ci}, f_{si}$

Calculate new
section properties
$EA, EI_x, EI_y, EAM_x,$
EAM_y, EI_{xy}

Calculate internal
force and moments
F_z, M_{ox}, M_{oy}

Transfer moment
back to G.C.
$GM_{ox} = M_{ox} - P(Y_G - Y_c)$
$GM_{oy} = M_{oy} - P(X_G - X_c)$

No convergence
achieved. stop

$P += \Delta P$

$\dfrac{EAMx}{EA*Yc} < 10^{-5}$
$\dfrac{EAMy}{EA*Xc} < 10^{-5}$

yes

$|GP - F_z| < 10^{-5}$
$|GM_x - GM_{ox}| < 10^{-5}$
$|GM_y - GM_{oy}| < 10^{-5}$

no

yes

$\varepsilon_{ec} > 0.003$
$\varepsilon_{es} > 0.05$

no

yes

no

$Y_c += EAMx/EA$
$X_c += EAMy/EA$

yes

New eccintricity

no

New a

no

End

yes

yes

P & M achieved
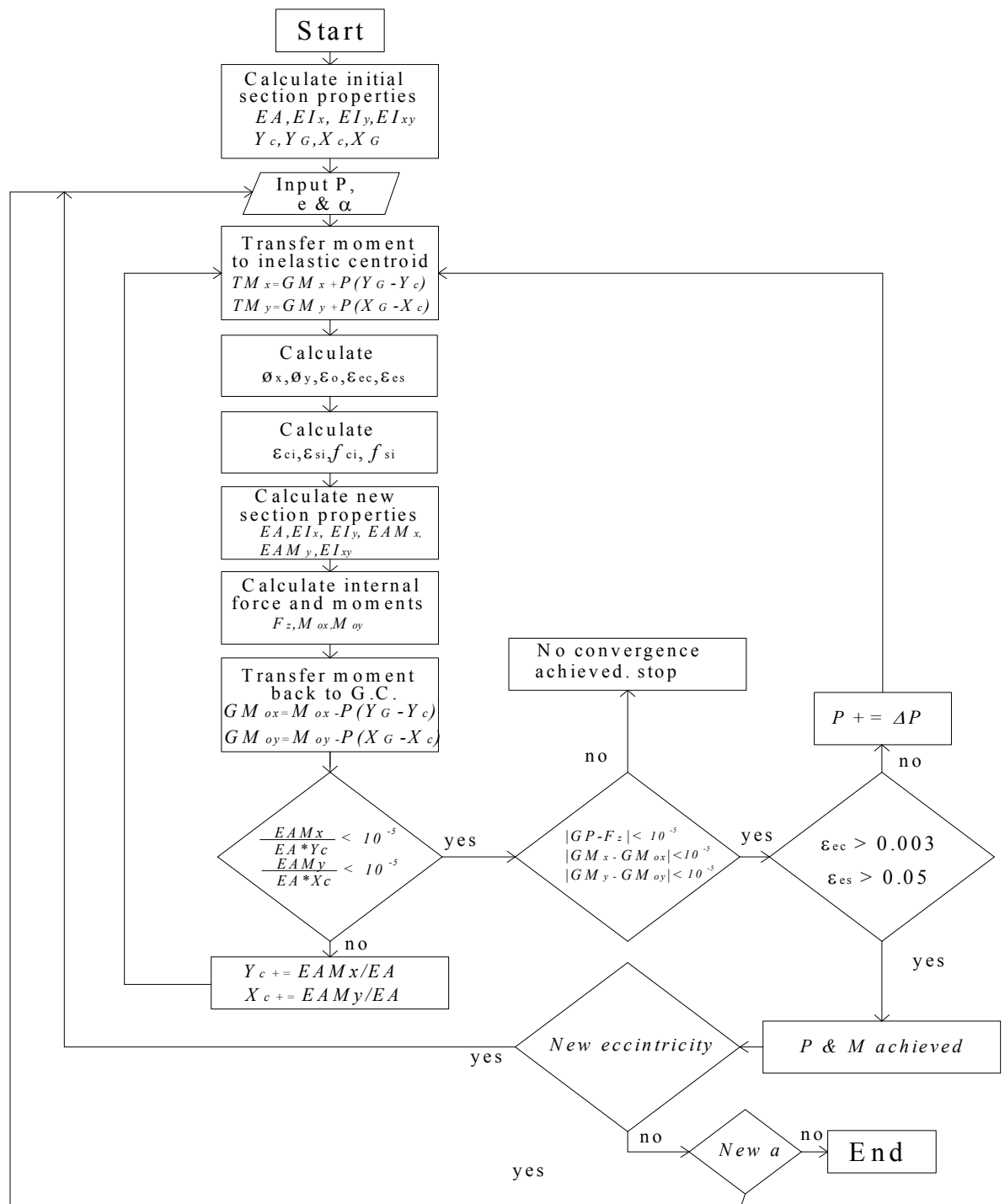
Figure 5-12: Flowchart of Generalized Moment of Area Method used for unconfined analysis

312

5-2-3 Results and Discussion

5-2-3-1 Comparison between the two approaches

The two approaches are compared to each other in the following. The column used in comparison has the following properties:

Section Height = 20 in.

Section Width = 10 in.

Clear Cover   = 2 in

Steel Bars in x direction = 3 # 4

Steel Bars in x direction = 6 # 4

Hoop #3

$f'_c = 4$ ksi

$f_y = 60$ ksi.
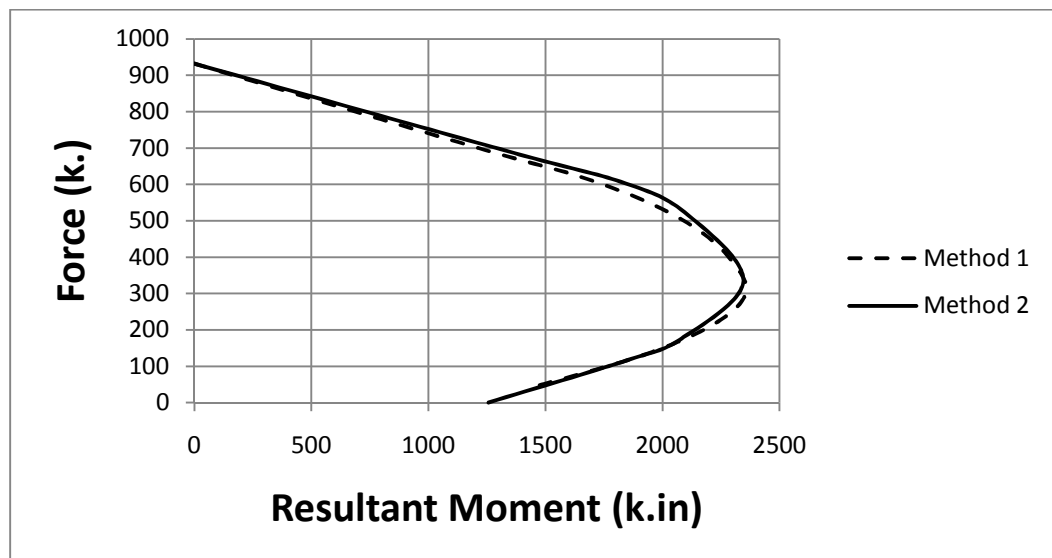
Figure 5-13: Comparison of approach one and two ($\alpha = 0$)
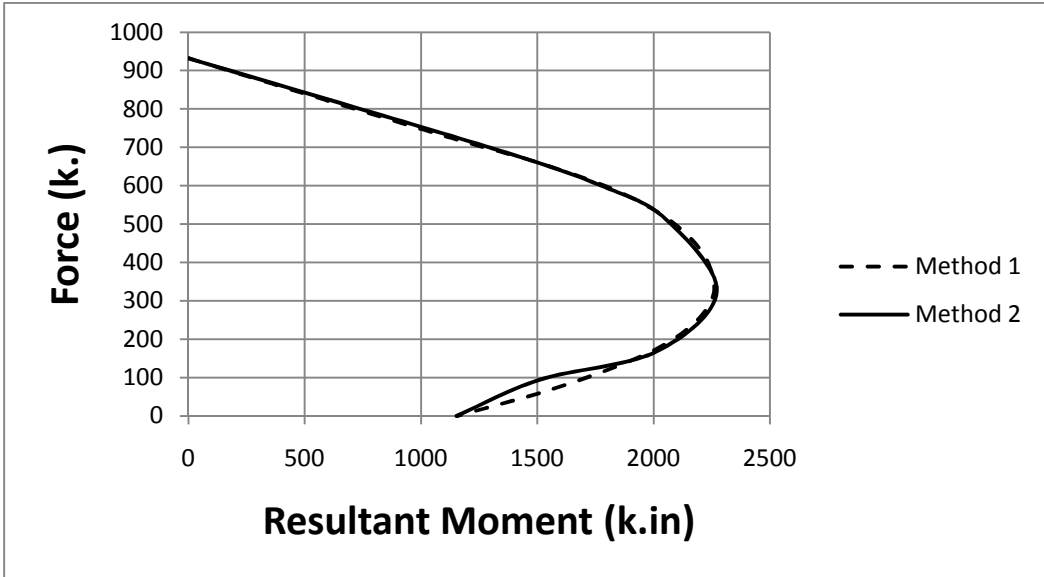
Figure 5-14: Comparison of approach one and two ($\alpha = 4.27$)
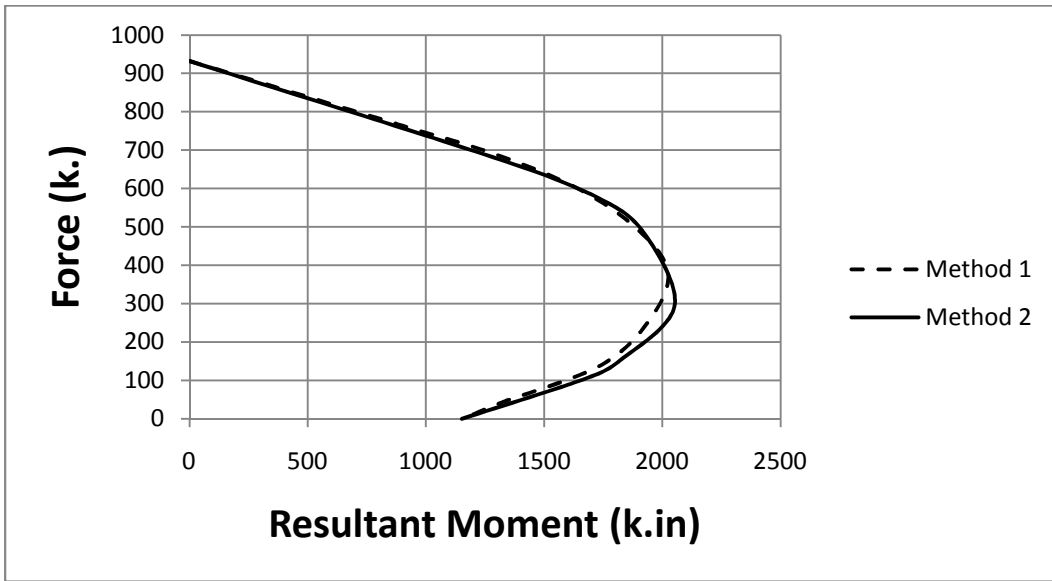
Figure 5-15: Comparison of approach one and two ($\alpha = 10.8$)
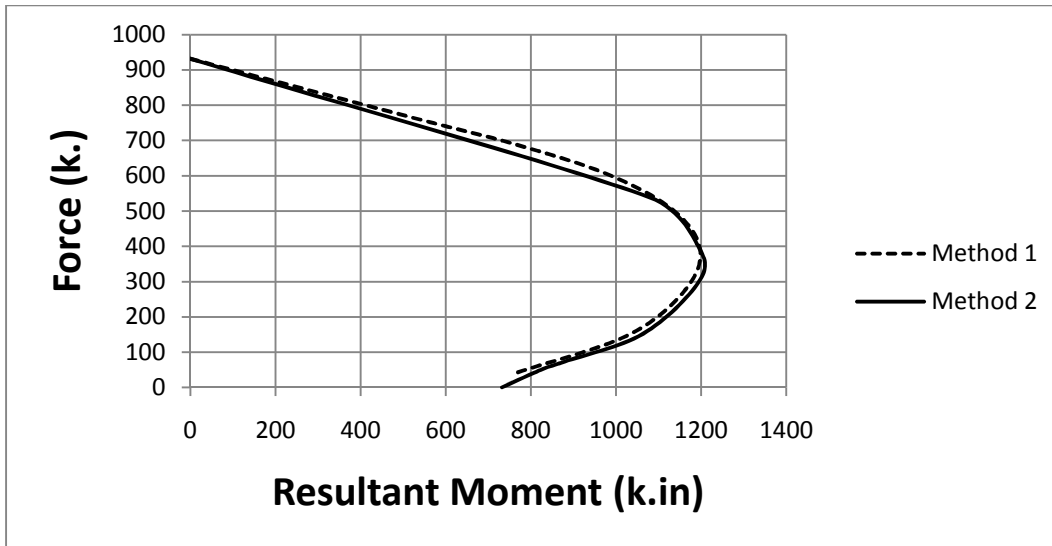
Figure 5-16: Comparison of approach one and two ($\alpha = 52$)

The excellent correlation between the two approaches appears in Figure (5-13) through (5-16). The resultant moment angle is shown below each graph. This is evidence that approach two effectively compared to the well known predefined ultimate strain profile approach. Accordingly, method two can be used in the confined analysis for analyzing the actual capacity of the rectangular columns.

5-2-3-2 Comparison with Existing Commercial Software

KDOT Column Expert is compared with CSI Col 8 of computers and structures Inc. and SP column Software of structure point LLC. The case is selected from Example 11.1 in "Notes on ACI 318-05 Building code Requirements for structural concrete" by PCA. The column details are as follow (Figure 5-17):

Section Height = 24 in.

Section Width = 24 in.

Clear Cover   = 1.5 in

Steel Bars = 16 # 7 evenly distributed

Hoop #3

f'c = 6 ksi

fy = 60 ksi.
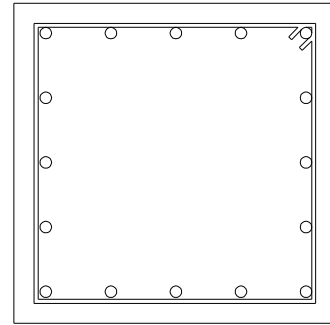
Figure 5-17: column geometry used in software comparison
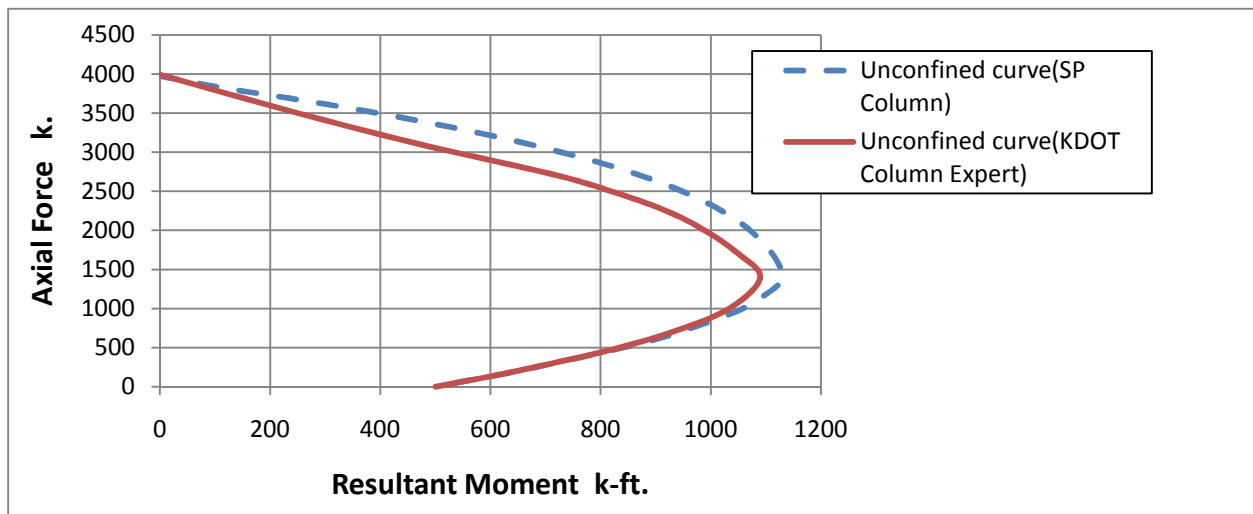
Figure 5-18: Unconfined curve comparison between KDOT Column Expert and SP Column ($\alpha =$

0)

Figure (5-18) shows the match between the two programs in axial compression calculations and in tension controlled zone. However KDOT Column Expert shows to be slightly more conservative in compression controlled zone. This might be due to using finite layer approach in calculations that has the advantage of accuracy over other approximations like Whitney stress block.
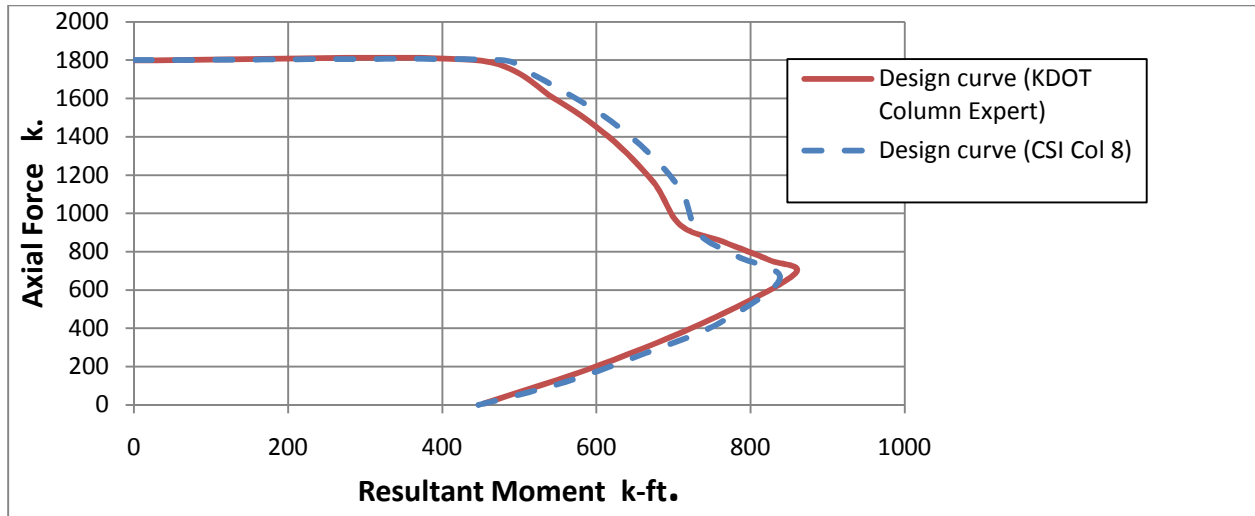
Figure 5-19: Design curve comparison between KDOT Column Expert and CSI Col 8 using ACI Reduction Factors

The design curves in Figure (5-19) and Figure (5-20) were plotted using ACI reduction factors that use a reduction factor of 0.65 in compression controlled zone as opposed to 0.75 used by AASHTO. There is a good correlation between the KDOT Column Expert curve and CSI Col 8 and SP Columns curves as shown in Figure 5-19 and Figure 5-20.
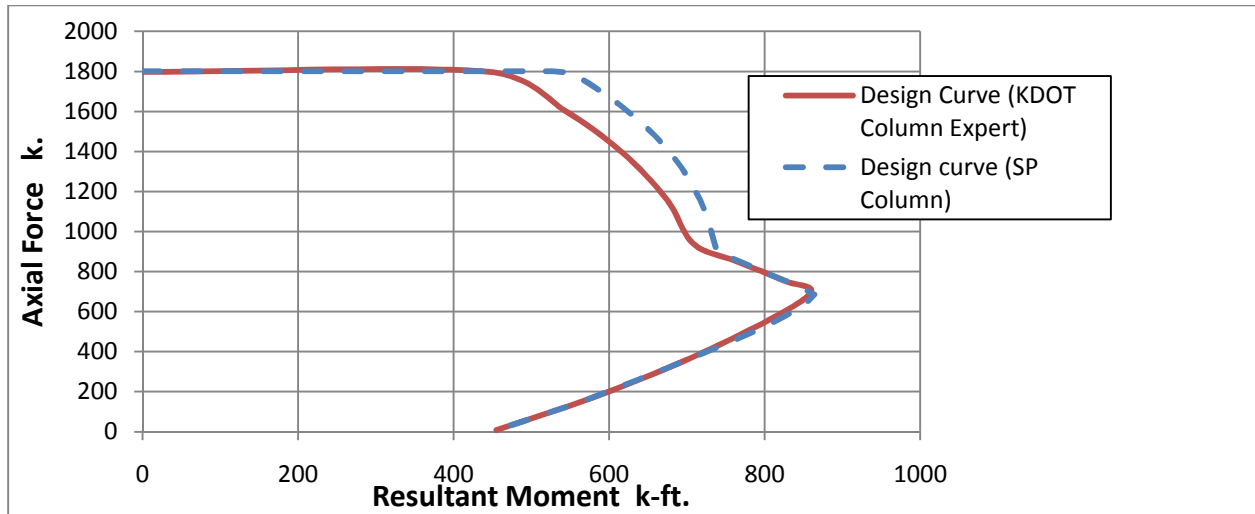
Figure 5-20: Design curve comparison between KDOT Column Expert and SP column using

ACI reduction factors

5-3 Confined Rectangular Columns Analysis

5-3-1 Formulations

5-3-1-1 Finite Layer Approach (Fiber Method)

The column cross section is divided into finite small-area filaments (Figure 5-21 a). The force and moment of each filament is calculated and stored. The rebars are treated as discrete objects in their actual locations. The advantage of that is to avoid inaccuracy generated from using the approximation of the stress block method, as a representative of the compression zone and to well treat cases that have compressive trapezoidal or triangular shapes generated from the neutral axis inclination (Figure 5-21 b).

318

a)   b)
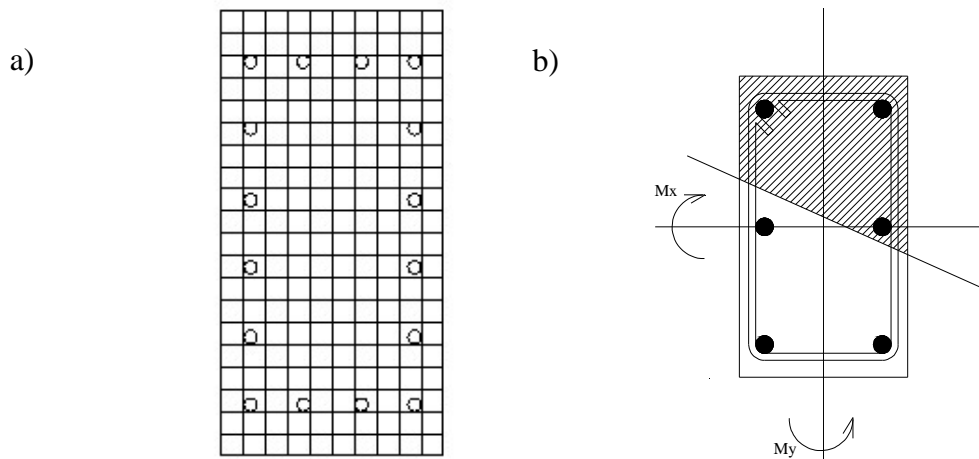
Figure 5-21:a) Using finite filaments in analysis   b)Trapezoidal shape of Compression zone

5-3-1-2 Confinement Model for Concentric Columns

5-3-1-2-a Mander Model for transversely reinforced steel

Mander model (1988) was developed based on the effective lateral confinement pressure, f'_l, and the confinement effective coefficient, k_e which is the same concept found by Sheikh and Uzumeri (1982). The advantage of this procedure is its applicability to any cross section since it defines the lateral pressure based on the section geometry. Mander *et al.* (1988) showed the adaptability of their model to circular or rectangular sections, under static or dynamic loading, either with monotonically or cyclically applied loads. In order to develop a full stress-strain curve and to assess ductility, an energy balance approach is used to predict the maximum longitudinal compressive strain in the concrete.

Mander derived the longitudinal compressive concrete stress-strain equation from Popovics model that was originally developed for unconfined concrete (1973):

319

$$f_c = \frac{f_{cc}\,xr}{r-1+x^r}$$
<div align="right">5-66</div>

$$x = \frac{\varepsilon_c}{\varepsilon_{cc}}$$
<div align="right">5-67</div>

$$r = \frac{E_c}{E_c - E_{sec}}$$
<div align="right">5-68</div>

$$E_c = 4723\sqrt{f_c'} \quad \text{in } MPa$$
<div align="right">5-69</div>

$$E_{sec} = \frac{f_{cc}}{\varepsilon_{cc}}$$
<div align="right">5-70</div>

and as suggested by Richart *et al*. (1928) the strain corresponding to the peak confined compressive strength, f'_{cc}, is:

$$\varepsilon_{cc} = \varepsilon_{co}\left[1 + 5\left(\frac{f_{cc}}{f_c'} - 1\right)\right]$$
<div align="right">5-71</div>

The different parameters of this model are defined in Figure (5-22)
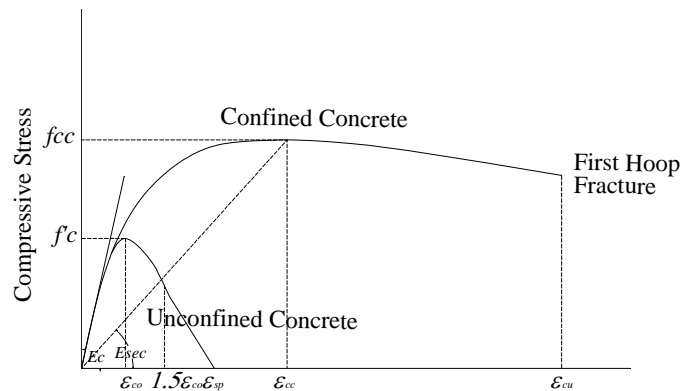
Figure 5-22: Axial Stress-Strain Model proposed by Mander *et al*. (1988) for monotonic loading

As shown in Figure (5-22) Mander *et al*. (1988) model has two curves; one for unconfined concrete (lower curve) and the other for confined concrete (upper one). The upper

one refers to the behavior of confined concrete with concentric loading (no eccentricity). It is shown that it has ascending branch with varying slope starting from E_c decreasing till it reaches the peak confined strength at (f_{cc}, ε_{cc}). Then the slope becomes slightly negative in the descending branch representing ductility till the strain of ε_{cu} where first hoop fractures. The lower curve expresses the unconfined concrete behavior. It has the same ascending branch as the confined concrete curve till it peaks at (f'_c, ε_{co}). Then, the curve descends till 1.5-2ε_{co}. A straight line is assumed after that till zero strength at spalling strain ε_{sp}

Mander *et al.* (1988) utilized an approach similar to that of Sheik and Uzumeri (1982) to determine effective lateral confinement pressure. It was assumed that the area of confined concrete is the area within the centerlines of perimeter of spiral or hoop reinforcement A_{cc} as illustrated in Figure (5-23)

Figure 5-23: Effectively confined core for rectangular hoop reinforcement (Mander Model)

Figure (5-23) shows that effectively confined concrete core A_e is smaller than the area of core within center lines of perimeter spiral or hoops excluding longitudinal steel area, A_{cc}, and to satisfy that condition the effective lateral confinement pressure f'_l should be a percentage of the lateral pressure f_l:

$$f_l^{'} = k_e f_l$$
<div align="right">5-72</div>

and the confinement effectiveness coefficient k_e is defined as the ratio of the effective confined area A_e to the area enclosed by centerlines of hoops execluding the longitudinal bars A_{cc}:

$$k_e = \frac{A_e}{A_{cc}}$$ 5-73

$$A_{cc} = A_c - A_{sl}$$ 5-74

$$\frac{A_{cc}}{A_c} = 1 - \frac{A_{sl}}{A_c}$$ 5-75

$$A_{cc} = A_c \left(1 - \rho_{cc}\right)$$ 5-76

where A_c is the area of the section core enclosed by hoops, A_{sl} is the area of longitudinal steel and ρ_{cc} is the ratio of longitudinal steel to the area of the core.
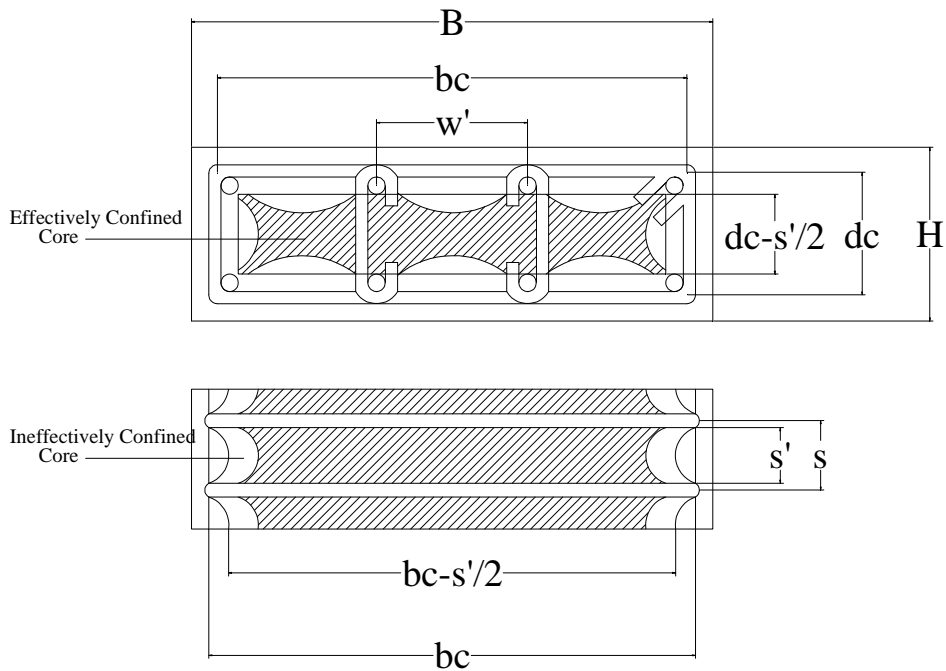
Figure 5-24: Effective lateral confined core for rectangular cross section

The total ineffective confined core area in the level of the hoops when there are n bars:

322

$$A_i = \sum_{i=1}^{n} \frac{\left(w_i^{'}\right)^2}{6}$$

5-77

Given that the arching formed between two adjacent bars (Figure 5-24) is second degree parabola with an initial tangent slope of 45°, the ratio of the area of effectively confined concrete to the core area at the tie level:

$$\lambda = \frac{\left(A_{et} - \sum_{i=1}^{n} \frac{\left(w_i^{'}\right)^2}{6}\right)}{A_{et}}$$

5-78

where $A_c = b_c * d_c$, The area of confined concrete in the midway section between two consecutive ties:

$$A_{emt} = \left(b_c - \frac{s^{'}}{2}\right)\left(d_c - \frac{s^{'}}{2}\right) = b_c d_c \left(1 - \frac{s^{'}}{2b_c}\right)\left(1 - \frac{s^{'}}{2d_c}\right)$$

5-79

Hence, the effective area at midway:

$$A_e = \lambda b_c d_c \left(1 - \frac{s^{'}}{2b_c}\right)\left(1 - \frac{s^{'}}{2d_c}\right) = \frac{1}{b_c d_c}\left(b_c d_c - \sum_{i=1}^{n} \frac{\left(w_i^{'}\right)^2}{6}\right) b_c d_c \left(1 - \frac{s^{'}}{2b_c}\right)\left(1 - \frac{s^{'}}{2d_c}\right)$$

5-80

$$A_e = \left(b_c d_c - \sum_{i=1}^{n} \frac{\left(w_i^{'}\right)^2}{6}\right)\left(1 - \frac{s^{'}}{2b_c}\right)\left(1 - \frac{s^{'}}{2d_c}\right)$$

5-81

Using equation (5-73)

$$k_e = \frac{b_c d_c \left(1 - \sum_{i=1}^{n} \frac{\left(w_i^{'}\right)^2}{6 b_c d_c}\right)\left(1 - \frac{s^{'}}{2b_c}\right)\left(1 - \frac{s^{'}}{2d_c}\right)}{b_c d_c (1 - \rho_{cc})}$$

5-82

$$k_e = \frac{\left(1 - \sum_{i=1}^{n} \frac{\left(w_i^{'}\right)^2}{6 b_c d_c}\right)\left(1 - \frac{s^{'}}{2b_c}\right)\left(1 - \frac{s^{'}}{2d_c}\right)}{(1 - \rho_{cc})}$$

5-83

and the ratio of the volume of transverse steel in x any y directions to the volume of confined core area ρ_x and ρ_y is defined as:

$$\rho_x = \frac{A_{sx}b_c}{sb_cd_c} = \frac{A_{sx}}{sd_c}$$ 5-84

$$\rho_y = \frac{A_{sy}d_c}{sb_cd_c} = \frac{A_{sy}}{sb_c}$$ 5-85

A_{sx}, A_{sy} are the total area of lateral steel in x and y direction respectively. The effective lateral confining pressure in x and y directions are given by:

$$f_{lx}^{'} = k_e\rho_x f_{yh}$$ 5-86

$$f_{ly}^{'} = k_e\rho_y f_{yh}$$ 5-87
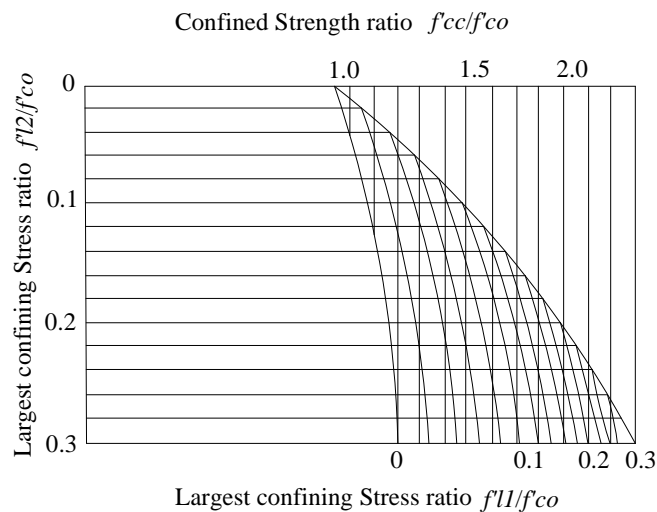
Figure 5-25: Confined Strength Determination

Figure (5-25) was developed numerically using multiaxial stress procedure to calculate ultimate confined strength from two given lateral pressures. The numerical procedure is summarized in the following steps:

1- Determining f'_{lx} and f'_{ly} using equations (5-86) and (5-87)

2- Converting the positive sign of f'_{lx} and f'_{ly} from positive to negative to represent the major and intermediate principal stresses (These values are refered to as σ_1 and σ_2 so that $\sigma_1 > \sigma_2$).

3- Estimating the confined strength f_{cc} (σ_3) as the minor principal stress

4- Calculating the octahedral stress σ_{oct}, octahedral shear stress τ_{oct} and lode angle θ as follows:

$$\sigma_{oct} = \frac{1}{3}\left(\sigma_1 + \sigma_2 + \sigma_3\right) \tag{5-88}$$

$$\tau_{oct} = \frac{1}{3}\left[\left(\sigma_1 - \sigma_2\right)^2 + \left(\sigma_2 - \sigma_3\right)^2 + \left(\sigma_3 - \sigma_1\right)^2\right]^{\frac{1}{2}} \tag{5-89}$$

$$\cos\vartheta = \left[\frac{\sigma_1 - \sigma_{oct}}{\sqrt{2}\tau_{oct}}\right] \tag{5-90}$$

5- Determining the ultimate strength meridian surfaces T,C (for $\theta = 60^o$ and 0° respectively) using the following equations derived by Elwi and Murray (1979) from data by Scickert and Winkler (1977):

$$T = 0.069232 - 0.661091\overline{\sigma}_{oct} - 0.049350\overline{\sigma}_{oct}^{\;2} \tag{5-91}$$

$$C = 0.122965 - 1.150502\overline{\sigma}_{oct} - 0.315545\overline{\sigma}_{oct}^{\;2} \tag{5-92}$$

$$\overline{\sigma}_{oct} = \sigma_{oct} / f_c^{'} \tag{5-93}$$

6- Determinig the octahedral shear stress using the interpolation function found by Willam and Warnke (1975):

$$\overline{\tau_{oct}} = C \frac{0.5D/\cos\theta + (2T-C)[D + 5T^2 - 4TC]^{\frac{1}{2}}}{D + (2T-C)^2}$$

5-94

$$D = 4(C^2 - T^2)\cos^2\theta$$

5-95

$$\tau_{oct} = \overline{\tau_{oct}} f_c'$$

5-96

7- Recalculating f_{cc} using the following equation(same as equation (5-89) but solving for σ_3:

$$\sigma_3 = \frac{\sigma_1 + \sigma_2}{2} - \sqrt{4.5\tau_{oct}^2 - 0.75(\sigma_1 - \sigma_2)^2}$$

5-97

8- If the value from equation (5-97) is close to the initial value then there is convergance. Otherwise, the value from equation (5-97) is reused in steps 4 through 8.

Equations 5-91 and 5-92 that define the tension and compression meredians are compared with different equations for different unconfined compressive strength. The results are shown in section 5-3-3-2

Mander *et al*. (1988) proposed an energy balancing theory to predict the ultimate confined strain, which is determined at the first hoop fracture. They stated that the additional ductility for confined concrete results from the additional strain energy stored in the hoops U_{sh}. Therefore from equilibrium:

$$U_{sh} = U_g - U_{co}$$

5-98

where U_g is the external work done in the concrete to fracture the hoop, and U_{co} is the work done to cause failure to the unconfined concrete. U_{sh} can be represented by the area under the tension stress strain curve for the transverse steel between zero and fracture strain ε_{sf}.

$$U_{sh} = \rho_s A_{cc} \int_0^{\varepsilon_{sf}} f_s d\varepsilon \qquad\qquad 5\text{-}99$$

while *Ug* is equal to the area under the confined stress strain curve plus the area under the longitudinal steel stress strain curve:

$$U_g = \int_0^{\varepsilon_{scu}} f_c A_{cc} d\varepsilon + \int_0^{\varepsilon_{scu}} f_s A_{sl} d\varepsilon \qquad\qquad 5\text{-}100$$

similarly, it was proven experimentally that U_{co} is equal to:

$$U_{co} = A_{cc} \int_0^{\varepsilon_{spall}} f_c d\varepsilon = A_{cc} 0.017\sqrt{f_c'} \ \text{in } MPa \qquad\qquad 5\text{-}101$$

and

$$U_{sh} = \rho_s A_{cc} \int_0^{\varepsilon_{sf}} f_s d\varepsilon = 110 \rho_s A_{cc} \qquad\qquad 5\text{-}102$$

Substituting Equations (5-100), (5-101) and (5-102) into Equation (5-98):

$$110\rho_s = \int_0^{\varepsilon_{cu}} f_c d\varepsilon + \int_0^{\varepsilon_{cu}} f_{sl} d\varepsilon - 0.017\sqrt{f_c'} \qquad\qquad 5\text{-}103$$

where f_{sl} is the stress in the longitudinal steel. Equation (5-103) can be solved numerically for ε_{cu}

5-3-1-3 Confinement Model for Eccentric Columns

Unlike concentric loading, the eccentric loading generates bending moment in addition to axial loading. Columns subjected to eccentric loading behave differently from those concentrically loaded, as the shape of the stress strain curve for fully confined reinforced concrete (concentric loading) shows higher peak strength and more ductility than the unconfined

one (infinite eccentricity). Most of the previous studies were based on the uniform distribution of compressive strain across the column section.
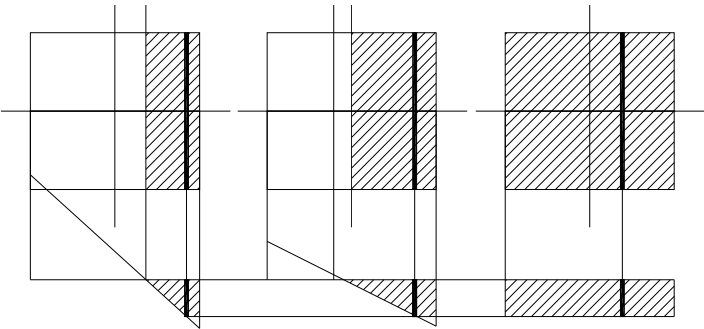
Figure 5-26: Effect of compression zone depth on concrete stress

Figure (5-26) illustrates three different sections under concentric load, combination of axial load and bending moment and pure bending moment, the highlighted fiber in the three cases has the same strain. Anycurrent confinement model yields the same stress for these three fibers. So the depth or size of compression zone does not have any role in predicting the stress. Hence, it is more realistic to relate the strength and ductility in a new model to the level of confinement utilization and compression zone size.
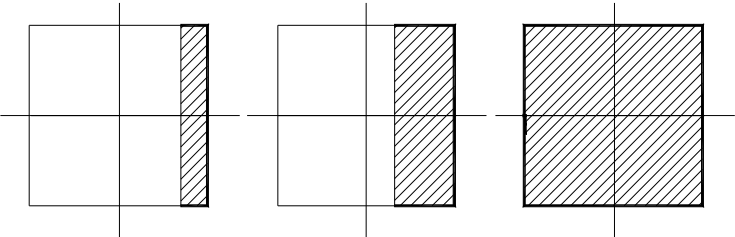
Figure 5-27: Amount of confinement engaged in different cases

By definition, confinement gets engaged only when member is subjected to compression. Compressed members tend to expand in lateral direction, and if confined, confinement will prevent this expansion to different levels based on the degree of compressive force and confinement strength as well. For fully compressed members (Figure 5-27c), confinement

becomes effective 100% as it all acts to prevent the lateral expansion. Whereas members subjected to compression and tension, when the neutral axis lies inside the section perimeter, only confinement adjacent to the compression zone gets engaged. Accordingly, members become partially confined.

In literature, various models were implemented to assess the ultimate confined capacity of columns under concentric axial load. On the other hand the effect of partial confinement in case of eccentric load (combined axial load and bending moments) is not investigated in any proposed model. Therefore, it is pertinent to relate the strength and ductility of reinforced concrete to the degree of confinement utilization in a new model.

The two curves of fully confined and unconfined concrete in any proposed model are used in the eccentricity-based model as upper and lower bounds. The upper curve refers to concentrically loaded confined concrete (zero eccentricity), while the lower one refers to pure bending applied on concrete (infinite eccentricity). In between the two boundaries, infinite numbers of stress-strain curves can be generated based on the eccentricity. The higher the eccentricity the smaller the confined concrete region in compression. Accordingly, the ultimate confined strength is gradually reduced from the fully confined value f_{cc} to the unconfined value f'_c as a function of eccentricity to diameter ratio. In addition, the ultimate strain is gradually reduced from the ultimate strain ε_{cu} for fully confined concrete to the ultimate strain for unconfined concrete $1.5\varepsilon_{co}$.

The relation between the compression area to whole area ratio and normalized eccentricity is complicated in case of rectangular cross sections due to the existence of two bending axes. The force location with respect tothe two axes causes the compression zone to take a trapozidal shape some times if the force applied is not along one of the axes. Hence the relation

329

between the compression area and the load eccentricity needs more investigation as oppose to the case of circular cross section which was shon to be simpler.

The normalized eccentricity is plotted against the compression area to cross sectional area ratio for rectangular cross sections having different aspect ratio (length to width) at the unconfined failure level. The aspect ratios used are 1:1, 2:1, 3:1, 4:1 as shown in Figures (5-28), (5-29),(5-30) and (5-31).Each curve represents specific α angle (tan $\alpha = My/Mx$) ranging from zero to ninty degrees. It is seen from these figures that there is inversely proportional relation between the normalized eccentricity and compression zone ratio regardless of the α angle followed.
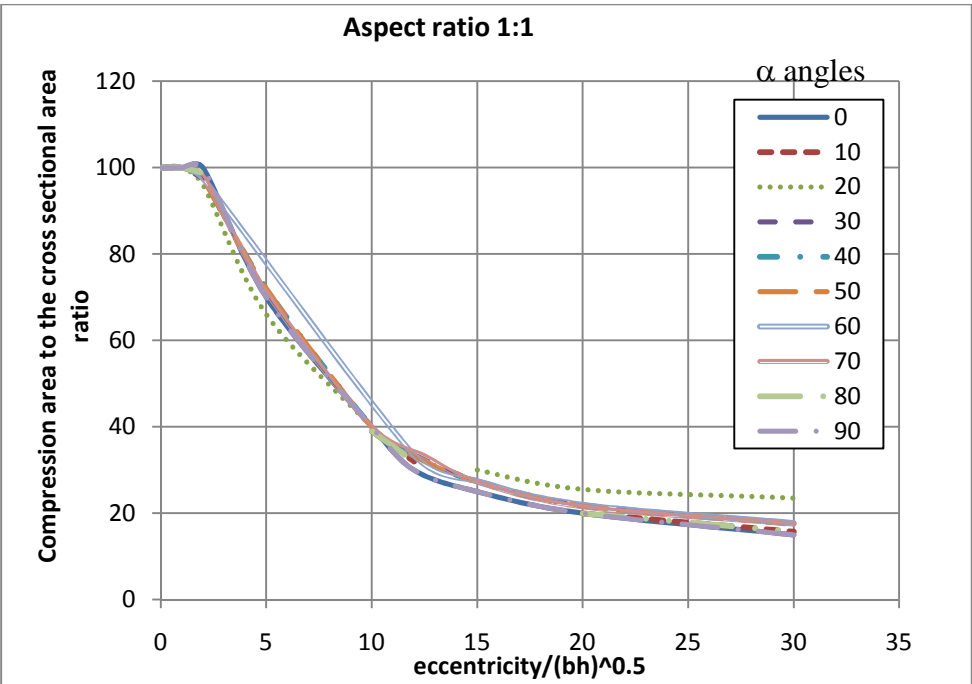
Figure 5-28: Normalized Eccentricity versus Compression Zone to total area ratio (Aspect ratio 1:1)
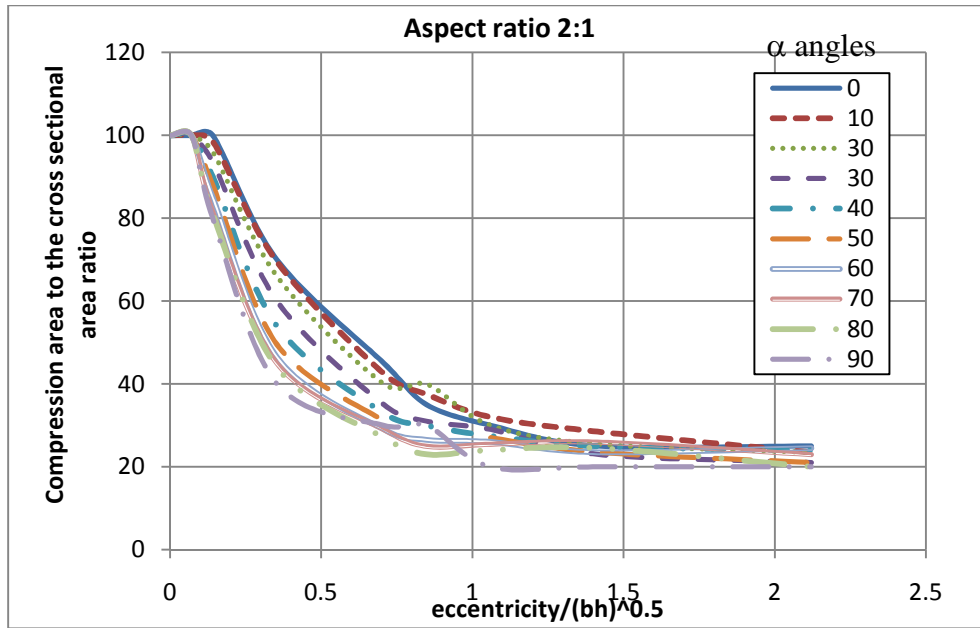
Figure 5-29: Normalized Eccentricity versus Compression Zone to total area ratio (Aspect ratio

2:1)
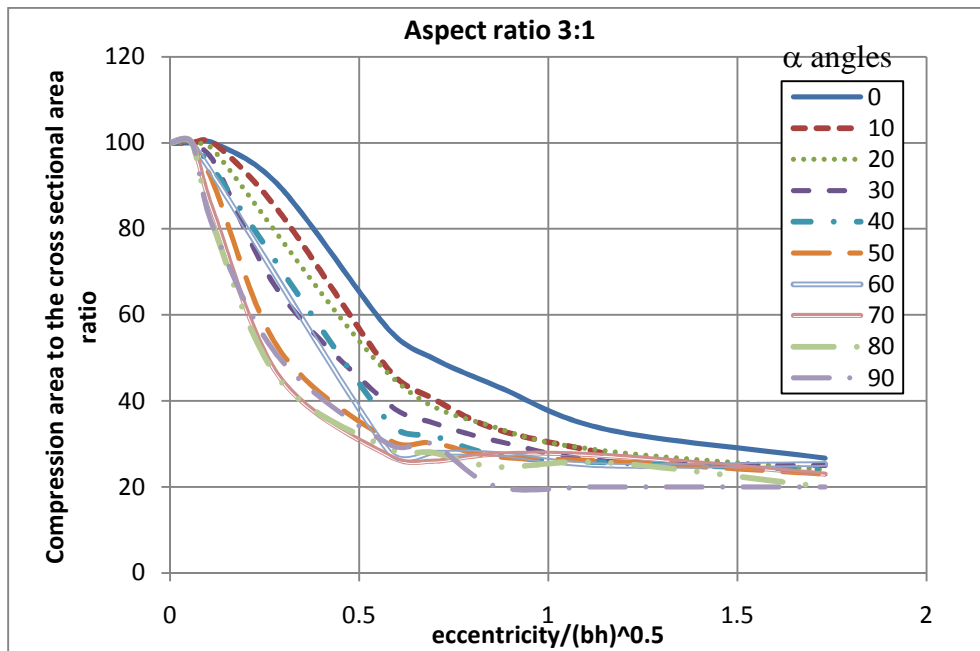
Figure 5-30: Normalized Eccentricity versus Compression Zone to total area ratio (Aspect ratio

3:1)

331
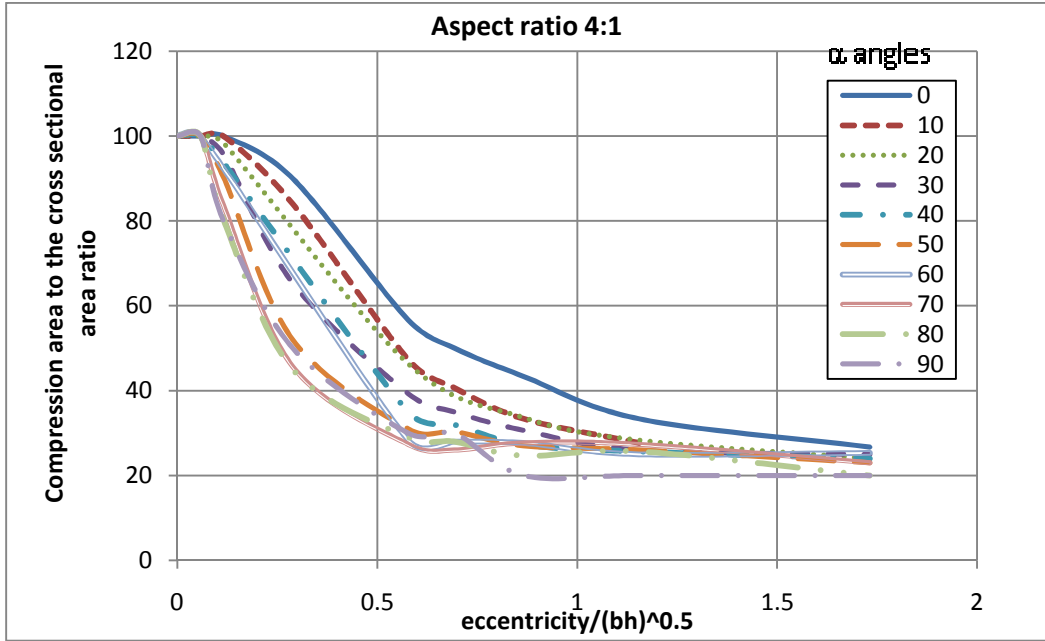
Figure 5-31: Normalized Eccentricity versus Compression Zone to total area ratio (Aspect ratio

4:1)
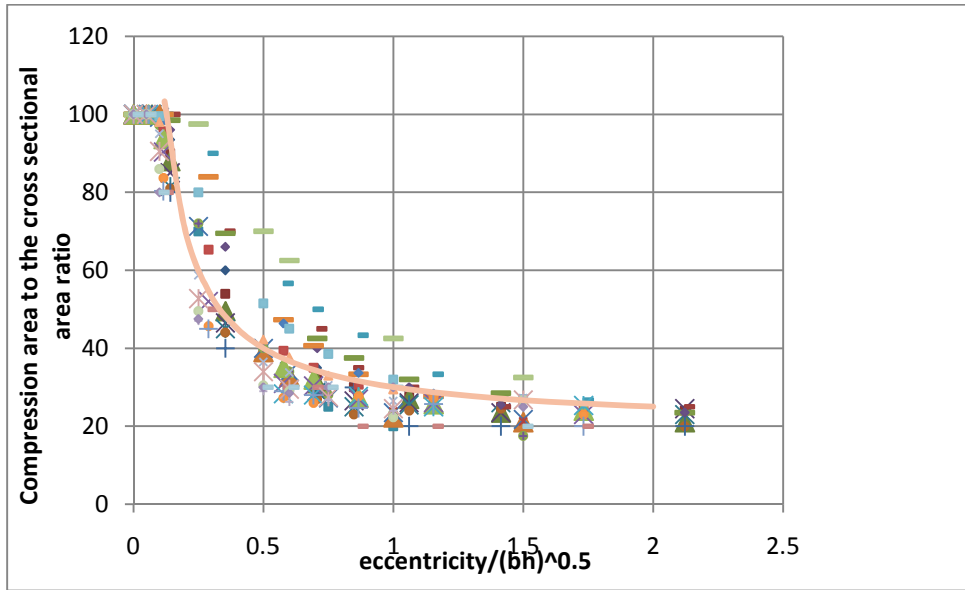
Figure 5-32: Cumulative chart for Normalized Eccentricity against Compression Zone Ratio (All

data points).

In order to find accurate mathematical expression that relates the compression zone to load eccentricity, the data from figures (5-28) throug (5-31) are replotted as scatter points in Figure (5-32).

The best fitting curve of these points based on the least square method has the following equation:

$$C_R = \frac{0.2 * \dfrac{e}{\sqrt{bh}} + 0.1}{\dfrac{e}{\sqrt{bh}}}$$

5-104

where C_R refers to compression area to cross sectional area ratio.

5-3-1-3-a Eccentric Model based on Mander Equations

The equation that defines the peak strength $\overline{f_{cc}}$ according to the eccentricity is:

$$\overline{f_{cc}} = \frac{1}{1 + \dfrac{1}{C_R}} f_{cc} + \frac{1}{1 + C_R} f_c'$$

5-105

Whereas the equation developed for circular cross sections

$$\overline{f_{cc}} = \frac{1}{1 + \dfrac{e}{\sqrt{bh}}} f_{cc} + \frac{1}{1 + \dfrac{\sqrt{bh}}{e}} f_c'$$

5-105 a

where e is the eccentricity, b and h is the column dimensions and $\overline{f_{cc}}$ is the peak strength at the eccentricity (e). The corresponding strain $\overline{\varepsilon_{cc}}$ is given by

$$\overline{\varepsilon_{cc}} = \varepsilon_{co}\left[1 + 5\left(\frac{\overline{f_{cc}}}{f_c'} - 1\right)\right]$$

5-106

333

and the maximum strain corresponding to the required eccentricity will be a linear function of stress corresponding to maximum strain for confined concrete f_{cu} and the maximum unconfined concrete f_{cuo} at $\varepsilon_{cuo} = 0.003$:

$$\overline{\varepsilon_{cu}} = \varepsilon_{cc} \left[\frac{\dfrac{\overline{E_{sec}}}{E_{sec,u}}\overline{r}}{\dfrac{c}{\overline{\varepsilon_{cu}}}+1} - \overline{r} + 1 \right]^{\frac{1}{\overline{r}}} \qquad\qquad E_{sec,u} = \frac{f_{cu}-f_{cuo}}{\varepsilon_{cu}-0.003} \qquad\qquad 5\text{-}107$$

$$c = \frac{f_{cu}-E_{sec,u}*0.003}{E_{sec,u}}$$

$$\overline{E_{sec}} = \frac{\overline{f_{cc}}}{\overline{\varepsilon_{cc}}} \qquad\qquad \overline{r} = \frac{E_c}{E_c - \overline{E_{sec}}}$$

In order to verify the accuracy of the model at the extreme cases, the eccentricity is first set to be zero. The coefficient of f'_c will be zero in Equation (5-105) and Equations (5-105), (5-106) and (5-107) will reduce to be:

$$\overline{f_{cc}} = f_{cc} \qquad\qquad\qquad 5\text{-}108$$

$$\overline{\varepsilon_{cc}} = \varepsilon_{cc} \qquad\qquad\qquad 5\text{-}109$$

$$\overline{\varepsilon_{cu}} = \varepsilon_{cu} \qquad\qquad\qquad 5\text{-}110$$

On the other hand, if the eccentricity is set to be infinity the other coefficient will be zero, and the strength, corresponding strain and ductility equations will be:

$$\overline{f_{cc}} = f'_c \qquad\qquad\qquad 5\text{-}111$$

$$\overline{\varepsilon_{cc}} = \varepsilon_{co} \qquad\qquad\qquad 5\text{-}112$$

$$\overline{\varepsilon_{cu}} = 0.003 \qquad\qquad\qquad 5\text{-}113$$
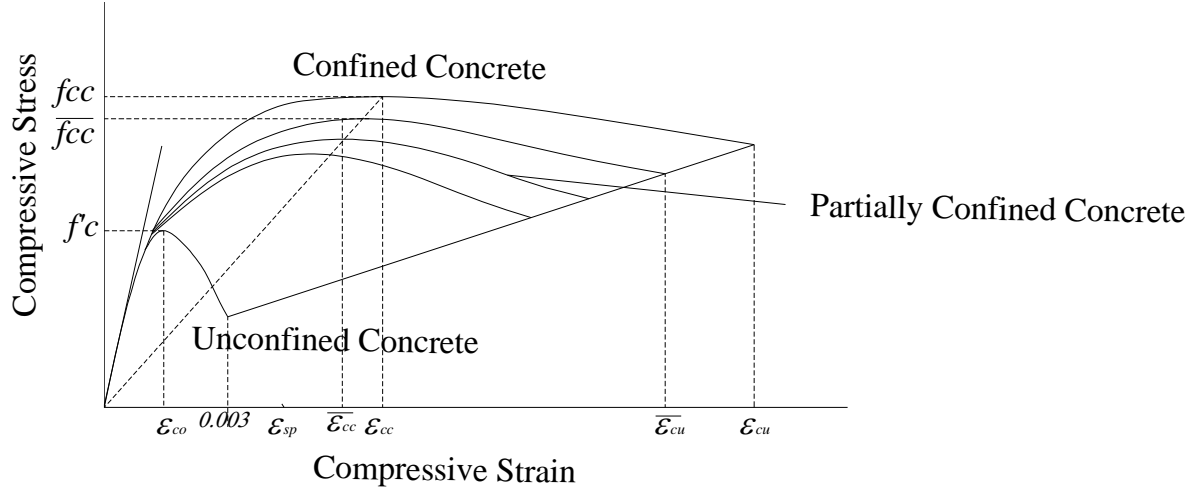
Figure 5-33: Eccentricity Based confined -Mander- Model

Any point on the generated curves the stress-strain function can be calculated using the following equation:

$$f_c = \frac{\overline{f_{cc}}\,\overline{x}\,\overline{r}}{\overline{r} - 1 + \overline{x}^{\overline{r}}}$$

5-114

where:

$$\overline{x} = \frac{\varepsilon_c}{\overline{\varepsilon}_{cc}}$$

5-115

$$\overline{r} = \frac{E_c}{E_c - \overline{E}_{sec}}$$

5-116

$$\overline{E}_{sec} = \frac{\overline{f_{cc}}}{\overline{\varepsilon}_{cc}}$$

5-117

To show the distinction between the Eccentric model designed for rectangular cross sections, Figure (5-34) and that of circular cross sections, Figure (5-35), Equations (5-105) to (5-107) and (5-114) to (5-117) are used in plotting a set of Stress-Strain curves with eccentricity ranging

335

from 0 *in*. to ∞. The column cross sectional properties used to plot these curves is 36 in *36 in., steel bars are 13 #11, spiral bar is # 5, spacing is 4 *in.*, f'_c is equal to 4 *ksi*, f_y is equal to 60 *ksi* and f_{yh} is equal to 60 *ksi*. This case is used in plotting the Eccentric Stress-Strain curve that are developed for rectangular cross sectional concrete columns; Figure (5-34) while the same case is used in plotting the eccentric Strss-Strain curves that are developed for circular cross section, Figure (5-35). The eccentric stress-Strain curves in Figure (5-35) are almost parallel and equidistant to each other. Whereas, the leap from one curve to the next one in Figure (5-34) is varying. This is due to the effect of the coeffiecent C_R, that is used in Equation (5-105), which has non linear impact on the compression zone as oppoased to the linear relation between the eccentricity and compression zone for circular cross sections (Figure (5-35))
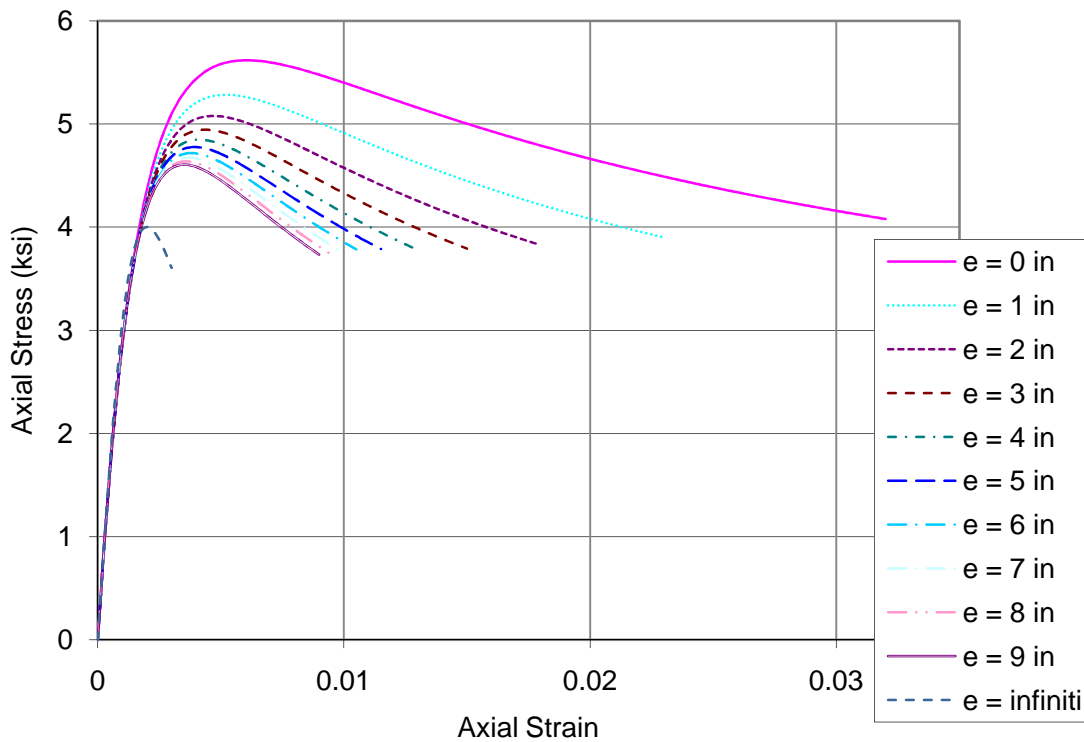
Figure 5-34: Eccentric based Stress-Strain Curves using compression zone area to gross area ratio
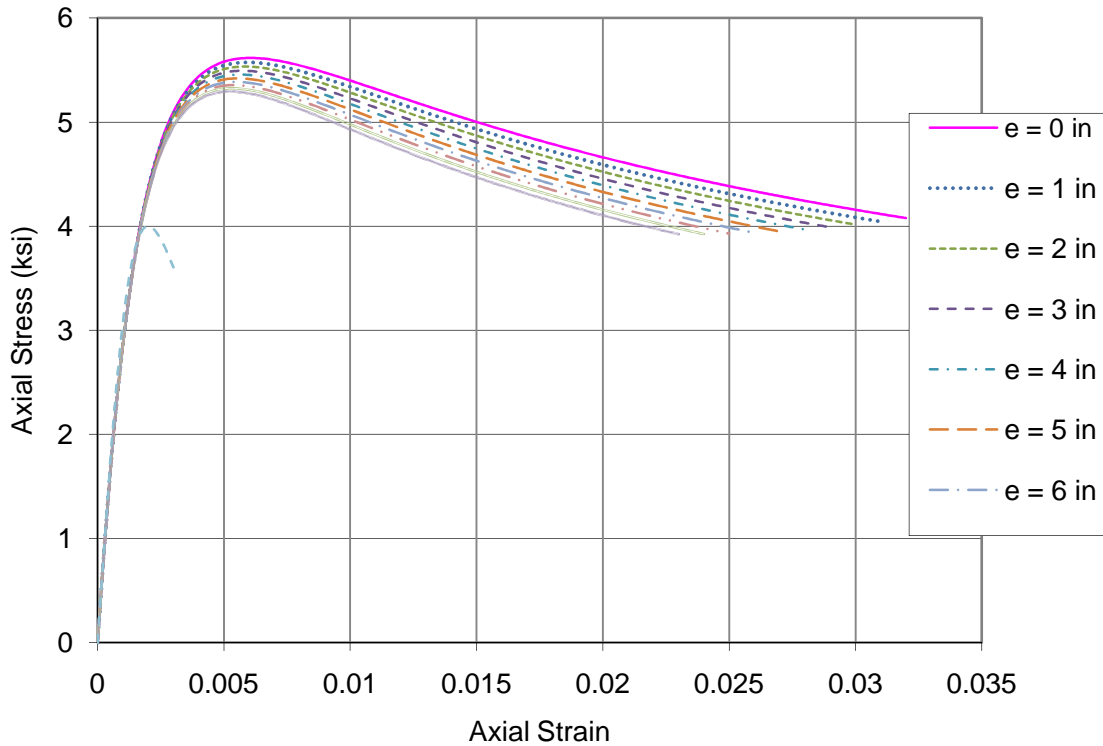
Figure 5-35: Eccentric based Stress-Strain Curves using normalized eccentricity instead of compression zone ratio

5-3-1-4 Generalized Moment of Area Theorem

The very general axial stress equation in an unsymmetric section subjected to axial force P and biaxial bending M_x and M_y (Hardy Cross 1930):

$$\sigma_z = \frac{P}{A} + \frac{M_x I_y - M_y I_{xy}}{I_x I_y - I_{xy}^2} y + \frac{M_y I_x - M_x I_{xy}}{I_x I_y - I_{xy}^2} x \qquad 5\text{-}118$$

σ_z = normal stress at any point (a) in cross section

P = applied load.

A = cross sectional area.

M_x = bending moment about x-axis

337

M_y = bending moment about y-axis

x = distance between the point (a) and y-axis

y = distance between the point (a) and x-axis

I_x = moment of inertia about x-axis

I_y = moment of inertia about y-axis

I_{xy} = product moment of inertia in xy plane

Rewriting Equation (5-118) to determine the strain at any point in the cross section:

$$\varepsilon_z = \frac{P}{EA} + \frac{M_x EI_y - M_y EI_{xy}}{EI_x EI_y - EI_{xy}^2} y + \frac{M_y EI_x - M_x EI_{xy}}{EI_x EI_y - EI_{xy}^2} x \qquad \text{5-119}$$

In case of linear elastic analysis, E in EA or EI expressions is constant ($E=E_c$). However, if the section has linear strain and nonlinear stress profile, it will amount to variable E profile (per filament) in nonlinear analysis. Accordingly, the section parameters must include $\sum_i E_i A_i$, $\sum_i E_i I_i$ for a more generalized theory (Rasheed and Dinno 1994). Note that the linear strain profile of the section from Equation (5-119) yields two distinct constant curvatures:

$$\phi_x = \frac{M_x EI_y - M_y EI_{xy}}{\beta^2} \qquad \text{5-120}$$

$$\phi_y = \frac{M_y EI_x - M_x EI_{xy}}{\beta^2} \qquad \text{5-121}$$

ϕ_x = x- curvature

ϕ_y = y- curvature

$\beta^2 = EI_x EI_y - EI_{xy}^2$

338

To prove Equations (5-120) and (5-121) above, invoke the coupled equations of moments about the centroid (Bickford 1998).

$$M_x = EI_x \phi_x + EI_{xy} \phi_y$$

5-122

$$M_y = EI_{xy} \phi_x + EI_y \phi_y$$

5-123

In a matrix form:

$$\begin{bmatrix} M_x \\ M_y \end{bmatrix} = \begin{bmatrix} EI_x & EI_{xy} \\ EI_{xy} & EI_y \end{bmatrix} \begin{bmatrix} \phi_x \\ \phi_y \end{bmatrix}$$

5-124

Inverting Equation (5-124)

$$\begin{bmatrix} \phi_x \\ \phi_y \end{bmatrix} = \frac{1}{\beta^2} \begin{bmatrix} EI_y & -EI_{xy} \\ -EI_{xy} & EI_x \end{bmatrix} \begin{bmatrix} M_x \\ M_y \end{bmatrix}$$

5-125

which reproduces Equations (5-120) and (5-121). Rewriting Equation (5-119) in terms of ϕ_x and ϕ_y

$$\varepsilon_z = \frac{P}{EA} + \phi_x y + \phi_y x$$

5-126

Finding ε_z at the centroid, since $x = y = 0$.

$$\varepsilon_o = P/EA$$

5-127

Solving for P at the geometric centroid;

$$P = EA\overline{\varepsilon}_o - EA\overline{y}\phi_x - EA\overline{x}\phi_y$$

5-128

$\overline{\varepsilon}_o$ is the axial strain at the geometric centroid

But

$$EAM_x = EA\overline{y} \qquad \overline{y} = Y_G - Y_c$$

$$EAM_y = EA\overline{x} \qquad \overline{x} = X_G - X_c$$

339

Y_G is the vertical distance to the geometric centroid measured from bottom, X_G is the distance to the geometric centroid measured from the cross section's left side, Y_c is the vertical distance to the inelastic centroid measured from the bottom and X_c is the horizontal distance to the inelastic centroid measured from the cross section's left side

Thus,

$$P = EA\overline{\varepsilon}_o - EAM_x\phi_x - EAM_y\phi_y \qquad \text{5-129}$$

The general formula of the moments about the geometric x-axis and the geometric y-axis is derived as follows:

when the moment is transferred from the centroid to the geometric centroid ,Figure (5-36 a)

$$\overline{M}_x = M_x - P\overline{y} \qquad \text{5-130}$$

Substituting Equations (5-122) and (5-129) into (5-130) yields:

$$\overline{M}_x = EI_x\phi_x + EI_{xy}\phi_y - EA\overline{\varepsilon}_o\overline{y} + EAM_x\phi_x\overline{y} + EAM_y\phi_y\overline{y} \qquad \text{5-131}$$

$$\overline{M}_x = -EAM_x\overline{\varepsilon}_o + \left(EI_x + EAM_x\overline{y}\right)\phi_x + \left(EI_{xy} + EAM_y\overline{y}\right)\phi_y \qquad \text{5-132}$$

Similarly, (Figure 5-36 b):
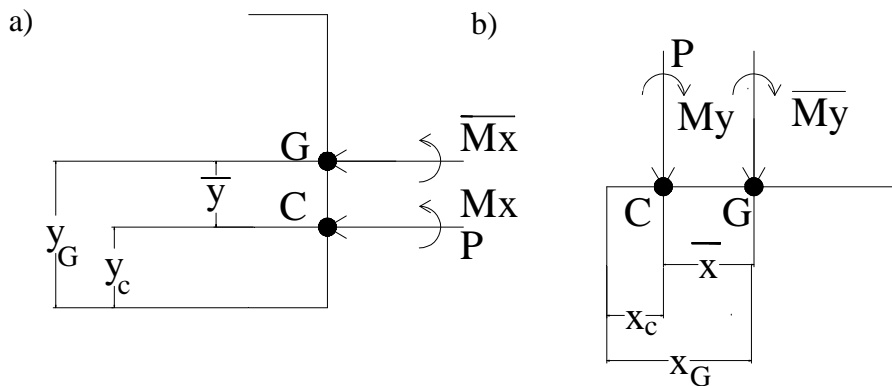
Figure 5-36: Transfering moment from centroid to the geometric centroid

$$\overline{M}_y = M_y - P\overline{x} \tag{5-133}$$

$$\overline{M}_y = EI_{xy}\phi_x + EI_y\phi_y - EA\overline{\varepsilon_o}\,\overline{x} + EAM_x\phi_x\overline{x} + EAM_y\phi_y\overline{x} \tag{5-134}$$

$$\overline{M}_y = -EAM_y\overline{\varepsilon_o} + \left(EI_{xy} + EAM_x\overline{x}\right)\phi_x + \left(EI_y + EAM_y\overline{x}\right)\phi_y \tag{5-135}$$

The terms $EI_x + EAM_x\overline{y}$ and $EI_y + EAM_y\overline{x}$ represent the $\overline{EI}_x$ and $\overline{EI}_y$ about the geometric centroid respectively using the parallel axis theorem. And the terms $EI_{xy} + EAM_x\overline{x}$ and $EI_{xy} + EAM_y\overline{y}$ are equal given that: $EAM_x\overline{x} = EA\overline{y}\,\overline{x}$ and $EAM_y\overline{y} = EA\overline{y}\,\overline{x}$. Using Equations (5-129), (5-132) and (5-135) yields the extended general moment of Area equation:

$$\begin{bmatrix} P \\ \overline{Mx} \\ \overline{M}_y \end{bmatrix} = \begin{bmatrix} EA & -EAM_x & -EAM_y \\ -EAM_x & \overline{EI}_x & \overline{EI}_{xy} \\ -EAM_y & \overline{EI}_{xy} & \overline{EI}_y \end{bmatrix} \begin{bmatrix} \varepsilon \\ \phi_x \\ \phi_y \end{bmatrix} \tag{5-136}$$

Since the moment of area about the centroid vanishes (Rasheed and Dinno 1994), Equation (5-136) reduces to a partially uncoupled set when it is applied back at the centroid since EAM_x and EAM_y vanish about the centroid.

$$\begin{bmatrix} P \\ M_x \\ M_y \end{bmatrix} = \begin{bmatrix} EA & 0 & 0 \\ 0 & EI_x & EI_{xy} \\ 0 & EI_{xy} & EI_y \end{bmatrix} \begin{bmatrix} \varepsilon_o \\ \phi_x \\ \phi_y \end{bmatrix} \tag{5-137}$$

which is simply Equations (5-122), (5-123) and (5-127)

5-3-2 Numerical Formulation

This approach simulates the radial loading of the force and moments by keeping the relative proportion between them constant during the loading. Accordingly, all the points will be

exactly on the 2D interaction diagram. In addition to the ultimate points, the complete load deformation response is generated. The cross section analyzed is loaded incrementally by maintaining a certain eccentricity between the axial force P and the resultant moment M_R. Since M_R is generated as the resultant of M_x and M_y, the angle $\alpha = \tan^{-1}(M_y/M_x)$ is kept constant for a certain 2D interaction diagram. Since increasing the load and resultant moment cause the neutral axis to vary nonlinearly, the generalized moment of area theorem is devised. This method is based on the general response of rectangular unsymmetrical section subjected to biaxial bending and axial compression. The asymmetry stems from the different behavior of concrete in compression and tension.

The method is developed using the incremental iterative analysis algorithm, secant stiffness approach and proportional or radial loading. It is explained in the following steps (Figure 5-40):

1- Calculating the initial section properties:

▪ Elastic axial rigidity EA:

$$EA = \sum_i E_c w_i t_i + \sum_i (E_s - E_c) A_{si}$$
5-138

E_c = initial secant modulus of elasticity of the concrete

E_s = initial modulus of elasticity of the steel rebar

▪ The depth of the elastic centroid position from the bottom fiber of the section Y_c and from the left side of the section X_c, Figur (5-37)

$$Y_c = \frac{\sum_i E_c w_i t_i (H - Y_i) + \sum_i (E_s - E_c) A_{si} (H - Y_{si})}{EA}$$
5-139

342

$$X_c = \frac{\sum_i E_c w_i t_i (B - X_i) + \sum_i (E_s - E_c) A_{si} (B - X_{si})}{EA}$$

<div align="right">5-140</div>

- Elastic flexural rigidity about the elastic centroid *EI*:

$$EI_x = \sum_i E_c w_i t_i (H - Y_i - Y_c)^2 + \sum_i (E_s - E_c) A_{si} (H - Y_{si} - Y_c)^2$$

<div align="right">5-141</div>

$$EI_y = \sum_i E_c w_i t_i (B - X_i - X_c)^2 + \sum_i (E_s - E_c) A_{si} (H - X_{si} - X_c)^2$$

<div align="right">5-142</div>

$$EI_{xy} = \sum_i E_c w_i t_i (H - Y_i - Y_c)(B - X_i - X_c) + \sum_i (E_s - E_c) A_{si} (H - Y_{si} - Y_c)(B - X_i - X_c)$$

<div align="right">5-143</div>

Typically the initial elastic $Y_c = H/2$, $X_c = B/2$ and $EI_{xy} = 0$
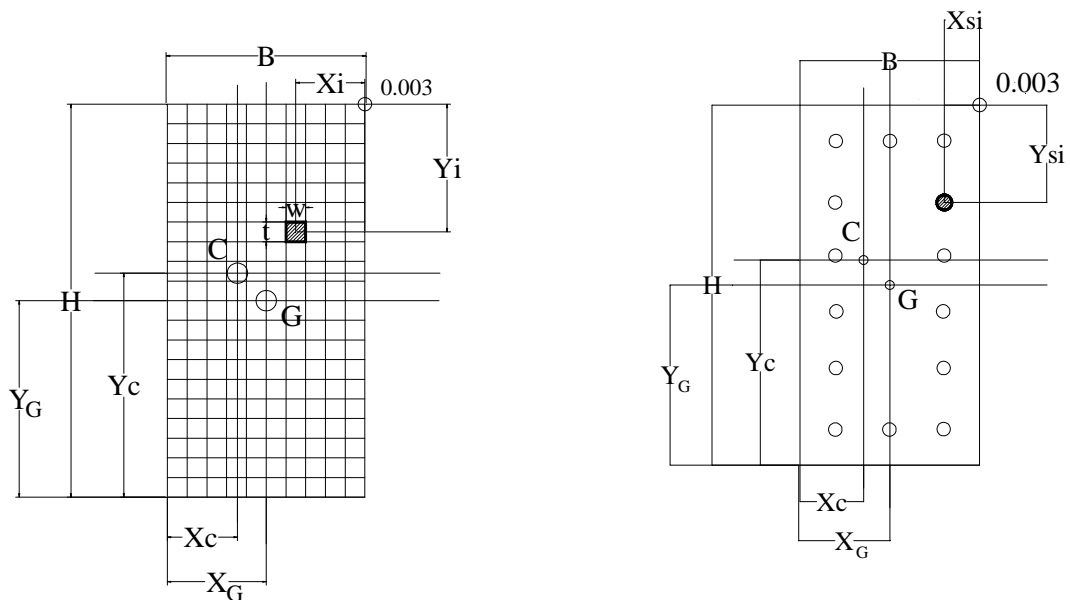
Figure 5-37: geometric properties of concrete filaments and steel rebars with respect to crushing strain point, geometric centroid and inelastic centroid.

The depth of the geometric section centroid position from the bottom and left fibers of the section Y_G, X_G, Figure (5-37):

$$Y_G = \frac{H}{2}$$
<div align="right">5-144</div>

$$X_G = \frac{B}{2}$$
<div align="right">5-145</div>

2- Defining eccentricity *e*, which specifies the radial path of loading on the interaction diagram. Also, defining the angle α in between the resultant moment GM_R and GM_X
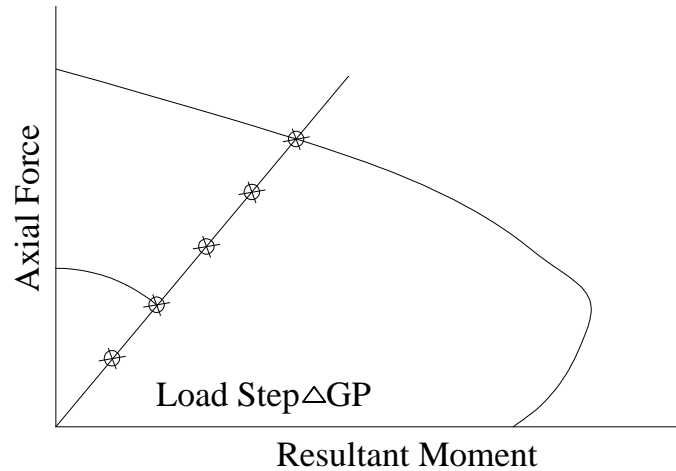
Figure 5-38: Radial loading concept

3- Defining loading step ΔGP as a small portion of the maximum load, and computing the axial force at the geometric centroid.

$$GP_{new} = GP_{old} + \Delta GP$$
<div align="right">5-146</div>

4- Calculating moment *GM* about the geometric centroid.

$$e = \frac{GM_R}{GP} \qquad GM_R = e * GP$$
<div align="right">5-147</div>

$$GM_X = GM_R \cos\alpha$$
<div align="right">5-148</div>

$$GM_Y = GM_X \tan\alpha$$
<div align="right">5-149</div>

5- Transferring moment to the current inelastic centroid and calculating the new transferred moment TM_X and TM_Y :

$$TM_X = GM_X + GP(Y_G - Y_c)$$
<div align="right">5-150</div>

$$TM_Y = GM_Y + GP(X_G - X_c)$$

<div align="right">5-151</div>

The advantage of transferring the moment to the position of the inelastic centroid is to eliminate the coupling effect between the force and moments, since $EAM_x = EAM_y = 0$ about the inelastic centroid

$$\begin{bmatrix} P \\ TM_x \\ TM_y \end{bmatrix} = \begin{bmatrix} EA & 0 & 0 \\ 0 & EI_x & EI_{xy} \\ 0 & EI_{xy} & EI_y \end{bmatrix} \begin{bmatrix} \varepsilon_o \\ \phi_x \\ \phi_y \end{bmatrix}$$

<div align="right">5-152</div>
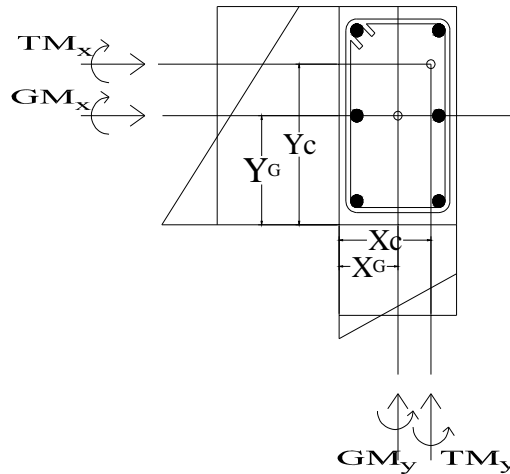
Figure 5-39 Moment Transferring from geometric centroid to inelastic centroid

6- Finding: Curvatures ϕ_X and ϕ_Y

$$\phi_X = \frac{TM_X}{\beta^2} * EI_Y - \frac{TM_Y}{\beta^2} * EI_{XY}$$

<div align="right">5-153</div>

$$\phi_Y = \frac{TM_Y}{\beta^2} * EI_X - \frac{TM_X}{\beta^2} * EI_{XY}$$

<div align="right">5-154</div>

$$\beta^2 = EI_X EI_Y - EI_{xy}^2$$

<div align="right">5-155</div>

Strain at the inelastic centroid ε_o, the extreme compression fiber strain ε_{ec}, and strain at the extreme level of steel in tension ε_{es} are found as follow:

<div align="center">345</div>

$$\varepsilon_o = \frac{GP}{EA}$$

5-156

$$\varepsilon_{ec} = \varepsilon_o + \phi_x(H - Y_c) + \phi_y(B - X_c)$$

5-157

$$\varepsilon_{es} = \varepsilon_o - \phi_x(Y_c - Cover) - \phi_y(X_c - Cover)$$

5-158

where cover is up to the centers of bars

7- Calculating strain ε_{ci} and corresponding stress f_{ci} in each filament of concrete section by using Eccetric Based Model (Mander Equations)

$$\varepsilon_{ci} = \frac{GP}{EA} + \frac{TM_x(H - Y_c - Y_i)}{\beta^2}EI_y + \frac{TM_y(B - X_c - X_i)}{\beta^2}EI_x$$
$$- \frac{TM_x(B - X_c - X_i)}{\beta^2}EI_{xy} - \frac{TM_y(H - Y_c - Y_i)}{\beta^2}EI_{xy}$$

5-159

8- Calculating strain ε_{si} and corresponding stress f_{si} in each bar in the given section by using the steel model shown in Figure (5-2b).

$$\varepsilon_{si} = \frac{GP}{EA} + \frac{TM_x(H - Y_c - Y_{si})}{\beta^2}EI_y + \frac{TM_y(B - X_c - X_{si})}{\beta^2}EI_x$$
$$- \frac{TM_x(B - X_c - X_{si})}{\beta^2}EI_{xy} - \frac{TM_y(H - Y_c - Y_{si})}{\beta^2}EI_{xy}$$

5-160

9- Calculating the new section properties: axial rigidity EA, flexural rigidities about the inelastic centroid EI_x, EI_y, EI_{xy} moment of axial rigidity about inelastic centroid EAM_x, EAM_y, internal axial force F_z, internal bending moments about the inelastic centroid M_{ox}, M_{oy}:

$$EA = \sum_i E_{ci}w_i t_i + \sum_i (E_{si} - E_{ci})A_{si}$$

5-161

$$EAM_x = \sum_i E_{ci}w_i t_i(H - Y_c - Y_i) + \sum_i (E_{si} - E_{ci})A_{si}(H - Y_c - Y_{si})$$

5-162

$$EAM_y = \sum_i E_{ci} w_i t_i (B - X_c - X_i) + \sum_i (E_{si} - E_{ci}) A_{si} (B - X_c - X_{si})$$

5-163

$$F_z = \sum f_{ci} w_i t_i + \sum (f_{si} - f_{ci}) A_{si}$$

5-164

$$EI_x = \sum_i E_{ci} w_i t_i (H - Y_c - Y_i)^2 + \sum_i (E_{si} - E_{ci}) A_{si} (H - Y_c - Y_{si})^2$$

5-165

$$EI_y = \sum_i E_{ci} w_i t_i (B - X_c - X_i)^2 + \sum_i (E_{si} - E_{ci}) A_{si} (H - X_c - X_{si})^2$$

5-166

$$EI_{xy} = \sum_i E_{ci} w_i t_i (H - Y_c - Y_i)(B - X_c - X_i) + \sum_i (E_{si} - E_{ci}) A_{si} (H - Y_c - Y_{si})(B - X_c - X_{si})$$

5-167

$$M_{ox} = \sum f_{ci} w_i t_i (H - Y_c - Y_i) + \sum (f_{si} - f_{ci}) A_{si} (H - Y_c - Y_{si})$$

5-168

$$M_{oy} = \sum f_{ci} w_i t_i (B - X_c - X_i) + \sum (f_{si} - f_{ci}) A_{si} (B - X_c - X_{si})$$

5-169

where E_{ci} = secant modulus of elasticity of the concrete filament = $\frac{f_{ci}}{\varepsilon_{ci}}$.

E_{si} = secant modulus of elasticity of the steel bar = $\frac{f_{si}}{\varepsilon_{si}}$.

10- Transferring back the internal moments about the geometric centroid

$$GM_{ox} = M_{ox} - GP(Y_G - Y_c)$$

5-170

$$GM_{oy} = M_{oy} - GP(Y_G - X_c)$$

5-171

11- Checking the convergence of the inelastic centroid

$$TOL_x = EAM_x / EA / Y_c$$

5-172

$$TOL_y = EAM_y / EA / X_c$$

5-173

12- Comparing the internal force to applied force, internal moments to applied moments, and making sure the moments are calculated about the geometric centroid :

$$|GP - F_z| \leq 1*10^{-5}$$

5-174

347

$$\left|GM_x - GM_{ox}\right| \leq 1*10^{-5} \qquad\qquad \left|GM_y - GM_{oy}\right| \leq 1*10^{-5}$$

5-175

$$\left|TOL_x\right| \leq 1*10^{-5} \qquad\qquad \left|TOL_y\right| \leq 1*10^{-5}$$

5-176

If Equations (5-174), (5-175) and (5-176) are not satisfied, the location of the inelastic centroid is updated by EAM_x/EA and EAM_y/EA and steps 5 to 11 are repeated till equations (5-174), (5-175) and (5-176) are satisfied.

$$Y_{c_{new}} = Y_{c_{old}} + \frac{EAM_x}{EA}$$

5-177

$$X_{c_{new}} = X_{c_{old}} + \frac{EAM_y}{EA}$$

5-178

Once equilibrium is reached, the algorithm checks for ultimate strain in concrete ε_{ec} and steel ε_{es} not to exceed $\overline{\varepsilon_{cu}}$ and 0.05 respectively. Then it increases the loading by ΔGP and runs the analysis for the new load level using the latest section properties. Otherwise, if ε_{ec} equals $\overline{\varepsilon_{cu}}$ or ε_{es} equals 0.05, the target force and resultant moment are reached as a point on the failure surface for the amount of eccentricity and angle α used.

This method can be used combined with Approach One in the unconfined analysis, section (5-2-2-1): Predefined Ultimate Strain Profile, for processing time optimization. Initially unconfined analysis is utilized. The sectional properties, EA, EI_x, EI_y, EI_{xy}, EAM_x, EAM_y,Y_c,X_c F_z, M_{ox} and M_{oy} are calculated from the unconfined failure point and used as section properties for the following step. So instead of loading the section from the beginning, The equilibrium is sought at unconfined failure point, Then, knowing the internal force capacity of the section, ΔP is added and the cross section is analyzed using the proposed numerical formulation of this section until failure of the confined section.

Start

Calculate initial section properties
EA, EI_x, EI_y, EI_{xy}
Y_c, Y_G, X_c, X_G

Input P, e & α

Transfer moment to inelastic centroid
$TM_x = GM_x + P(Y_G - Y_c)$
$TM_y = GM_y + P(X_G - X_c)$

Calculate
$\varnothing_x, \varnothing_y, \varepsilon_o, \varepsilon_{ec}, \varepsilon_{es}$

Calculate
$\varepsilon_{ci}, \varepsilon_{si}, f_{ci}, f_{si}$

Calculate new section properties
$EA, EI_x, EI_y, EAM_x, EAM_y, EI_{xy}$

Calculate internal force and moments
F_z, M_{ox}, M_{oy}

Transfer moment back to G.C.
$GM_{ox} = M_{ox} - P(Y_G - Y_c)$
$GM_{oy} = M_{oy} - P(X_G - X_c)$

$\dfrac{EAMx}{EA*Yc} < 10^{-5}$
$\dfrac{EAMy}{EA*Xc} < 10^{-5}$

yes

$Y_c += EAMx/EA$
$X_c += EAMy/EA$

no

No convergence achieved. stop

$|GP - F_z| < 10^{-5}$
$|GM_x - GM_{ox}| < 10^{-5}$
$|GM_y - GM_{oy}| < 10^{-5}$

no

yes

$P += \Delta P$

$\varepsilon_{ec} >= \overline{\varepsilon}_{cu}$
$\varepsilon_{es} >= 0.05$

no

yes

P & M achieved

New eccintricity

yes

no

New a

yes

no

End

Figure 5-40: Flowchart of Generalized Moment of Area Method

349

5-3-3 Results and Discussion

Interaction diagrams generated by KDOT Column Expert Software are plotted and compared to the corresponding experimental work found in the literature. Interaction diagrams are generated using the numerical formulation described in section 5-3-2.

5-3-3-1 Comparison with Experimental Work

Case 1

A Study of combined bending and axial load in reinforced concrete members (Eivind Hogenstad)

Section Height = 10 in.

Section Width = 10 in.

Clear Cover   = 0.8575 in

Steel Bars in x direction = 2

Steel Bars in y direction = 4

Steel Diameter = 0.785 in.

Tie Diameter = 0.25 in.

$f'c$ = 5.1 ksi fy = 60 ksi. f_{yh} = 61.6 ksi.   Spacing = 8 in.
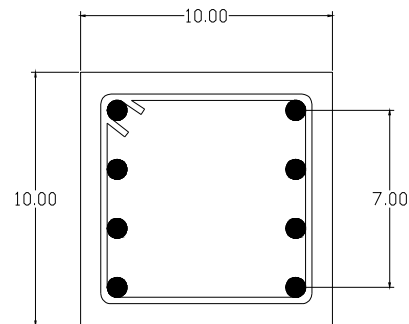
Figure 5-41:Hognestad column
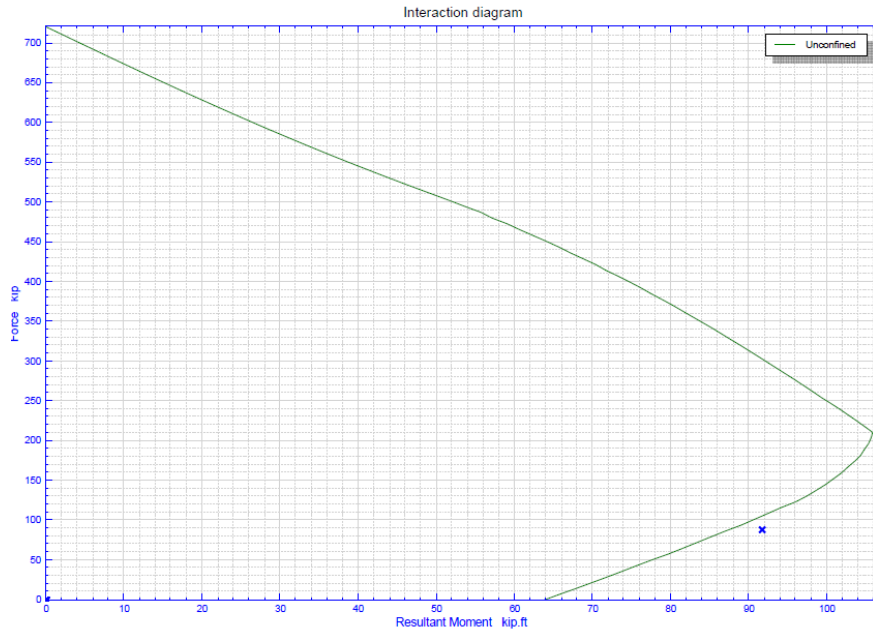
Figure 5-42: Comparison between KDOT Column Expert with Hognestad experiment ($\alpha = 0$)

Case 2

Design criteria for reinforced columns under axial load and biaxial bending (Boris Bresler)

Section Height = 8 in.

SectionWidth = 6 in.

Clear Cover   = 1.1875 in

Steel Bars in x direction = 2#5

Steel Bars in y direction = 2#5

Tie Diameter = 0.25 in.
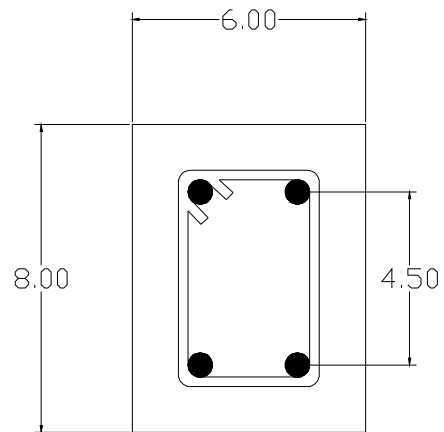
Figure 5-43: Bresler Column

$f'c = 3.7$ ksi $fy = 53.5$ ksi. $f_{yh} = 53.5$ ksi.   Spacing = 4 in

351
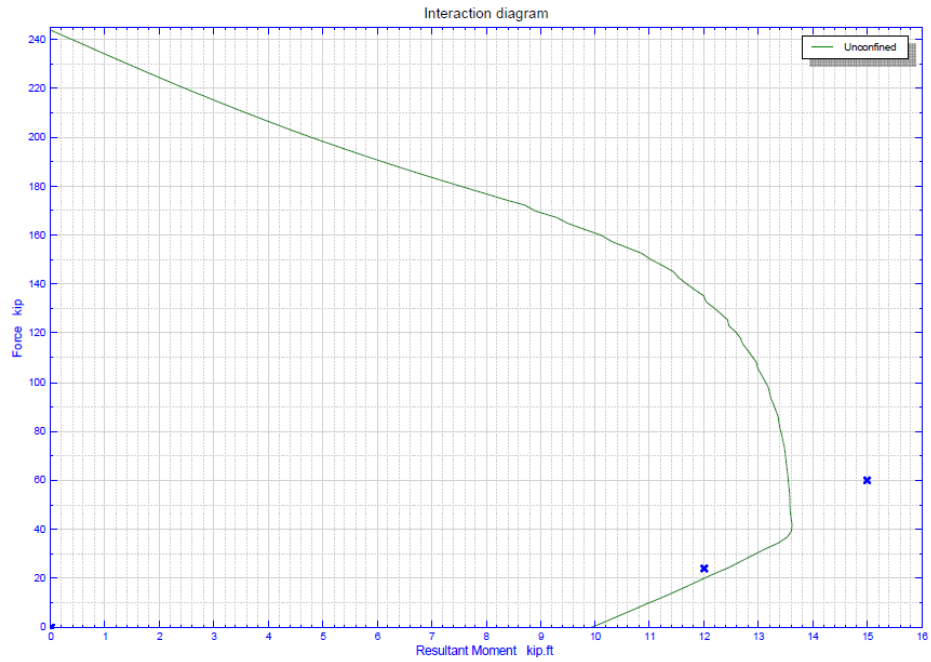
Figure 5-44: Comparison between KDOT Column Expert with Bresler experiment ($\alpha = 90$)
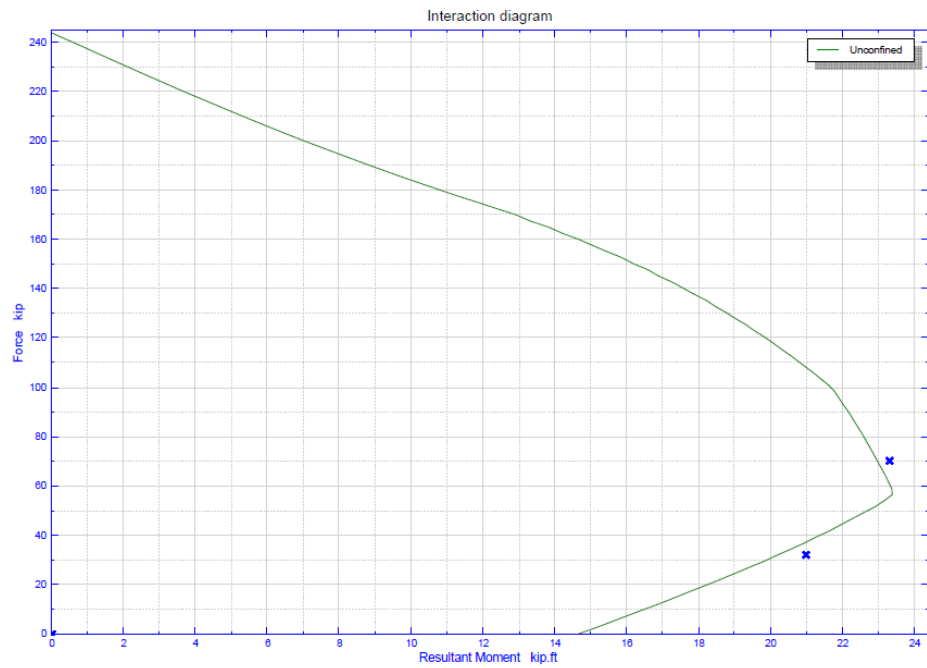
Figure 5-45: Comparison between KDOT Column Expert with Bresler experiment ($\alpha = 0$)

Case 3

Investigation of the ultimate strength of square and rectangular columns under biaxially eccentric loads (L.N. Ramamurthy)

Section Height = 12 in.

Section Width = 6 in.

Clear Cover = 1.2375 in

Steel Bars in x direction = 3#5

Steel Bars in y direction =3#5

Tie Diameter = 0.25 in.

$f'c$ = 3.8 ksi fy = 46.79 ksi f_{yh} = 46.79 ksi.   Spacing = 6 in
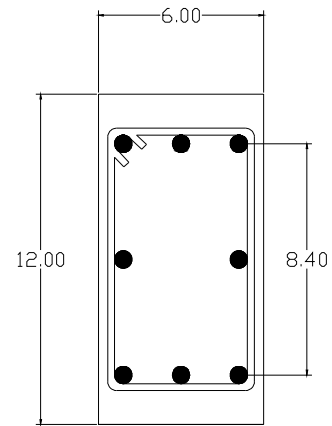
Figure 5-46 : Ramamurthy Column
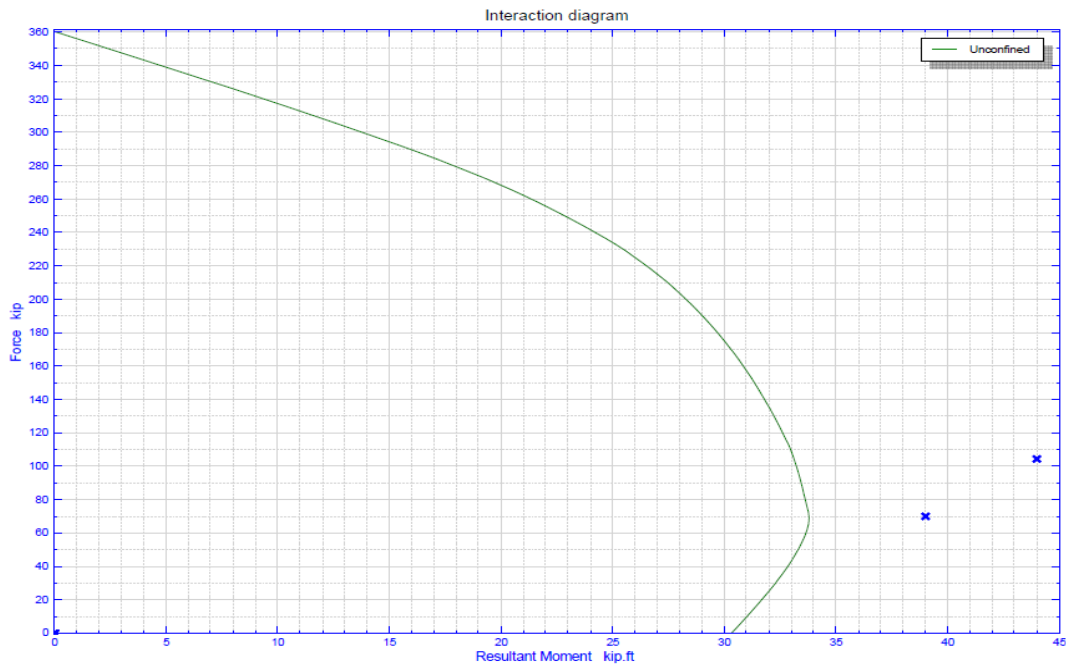
Figure 5-47: Comparison between KDOT Column Expert with Ramamurthy experiment (α = 26.5)

353

case 4

Confined columns under eccentric loading

(Murat Saatcioglu. Amir Salamat amd Salim Razvi)

Section Height = 8.27 in.

SectionWidth =8 .27 in.

Clear Cover   = 0. 5 in

Steel Bars in x direction = 3

Steel Bars in y direction = 3

Steel Area = 0.155 in^2.

Tie Diameter = 0.364 in.

$f'c$ = 5.1 ksi f_y = 75 ksi. f_{yh} = 59.45 ksi.   Spacing = 1.97 in.
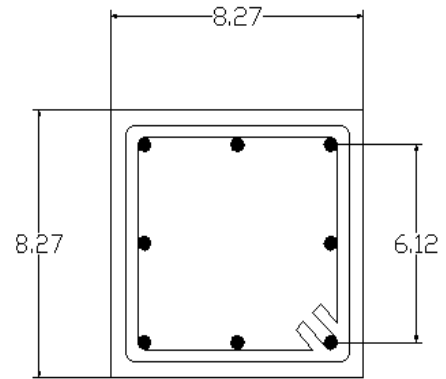
Figure 5-48 : Saatcioglu Column
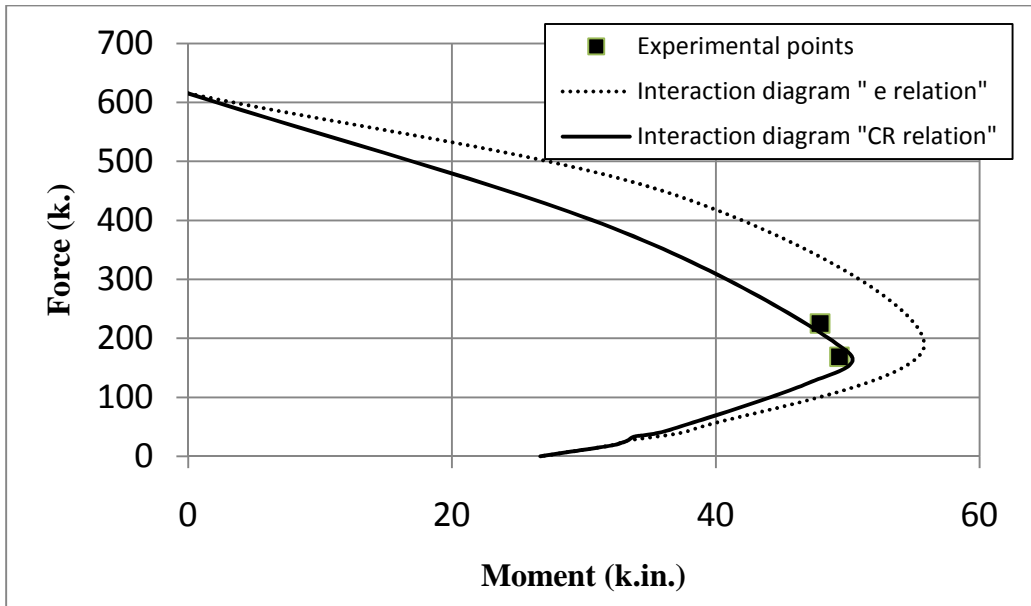
Figure 5-49: Comparison between KDOT Column Expert with Saatcioglu *et al* experiment (α =

0)

case 5

Confined columns under eccentric loading

(Mural Saatcioglu. Amir Salamat amd Salim Razvi)

Section Height = 8.27 in.

SectionWidth =8 .27 in.

Clear Cover   = 0. 5 in

Steel Bars in x direction = 4

Steel Bars in y direction = 4

Steel Area = 0.155 in^2.

Tie Diameter = 0.364 in.

$f'c$ = 5.1 ksi f_y = 75 ksi. f_{yh} = 59.45 ksi.   Spacing = 1.97 in.
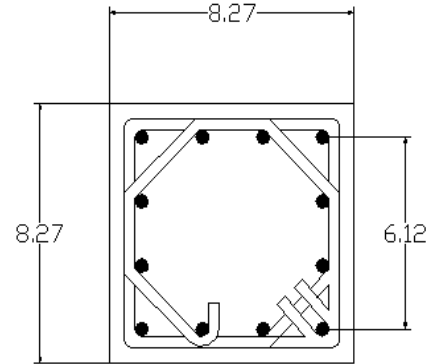
Figure 5-50 : Saatcioglu Column
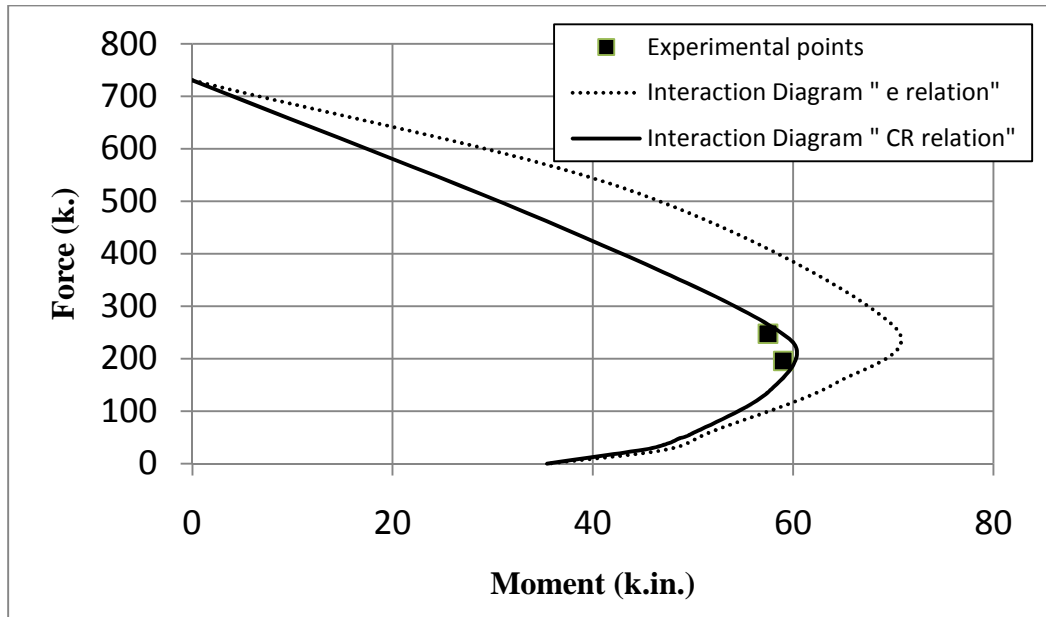
Figure 5-51: Comparison between KDOT Column Expert with Saatcioglu *et al* experiment 1 (α

= 0)

355

case 6

Stress strain behavior of concrete confined by overlapping

hoops at low and high strain rate

(B. Scott, R Park and M. Priestly)

Section Height = 17.7 in.

Section Width =17 .7 in.

Clear Cover   = 0. 787 in

Steel Bars in x direction = 4

Steel Bars in y direction = 4

Steel Area = 0.49 in^2.

Tie Diameter = 0.394 in.

$f'c$ = 3.67 ksi f_y = 63 ksi. f_{yh} = 44.8 ksi.   Spacing = 2.83 in.
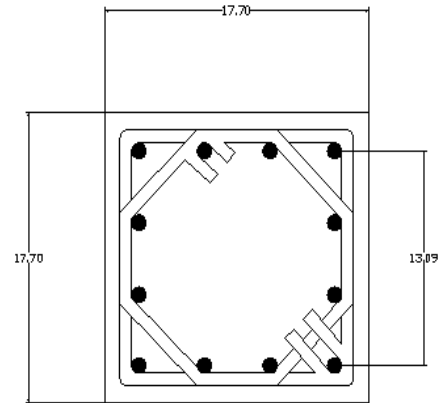
Figure 5-52 : Scott Column
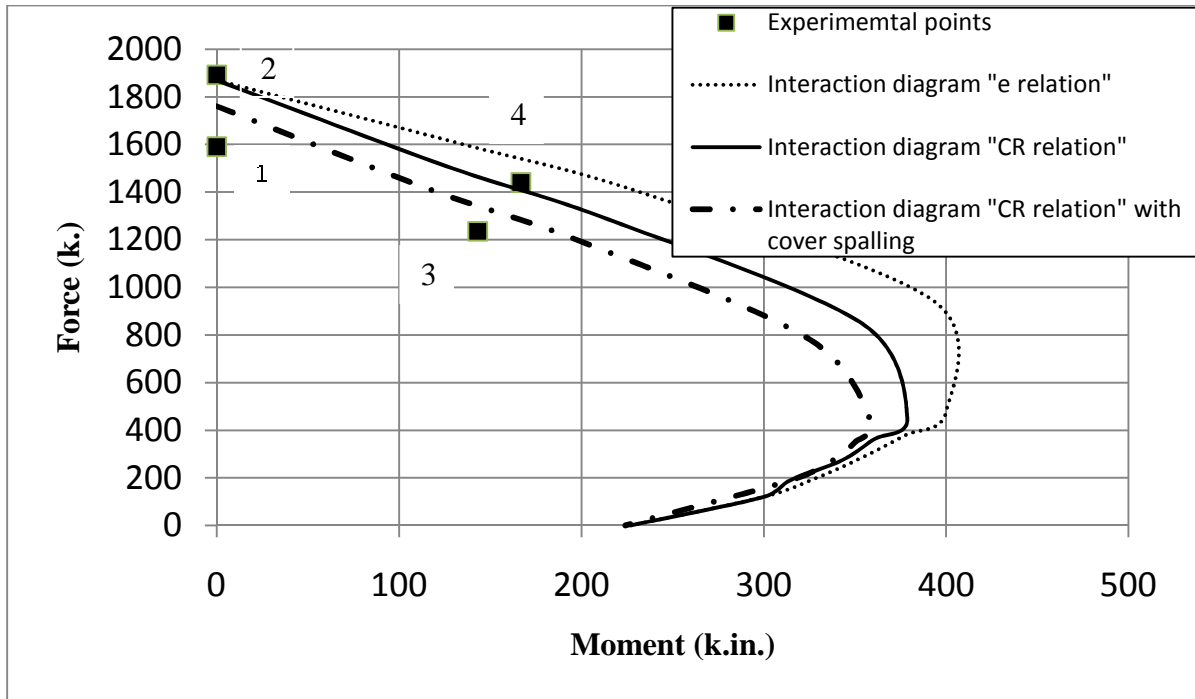
Figure 5-53: Comparison between KDOT Column Expert with Scott *et al* experiment ($\alpha = 0$)

356

case 7

Stress strain behavior of concrete confined by overlapping hoops at low and high strain rate

(B. Scott, R Park and M. Priestly)

Section Height = 17.7 in.

Section Width =17 .7 in.

Clear Cover = 0. 787 in

Steel Bars in x direction = 3

Steel Bars in y direction = 3

Steel Area = 0.7 in^2.

Spiral Diameter = 0.394 in.
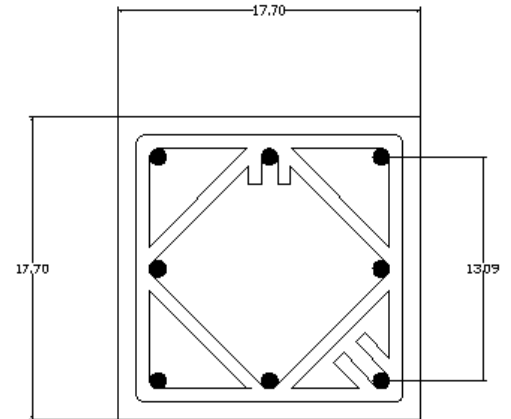
Figure 5-54 : Scott Column

$f'c$ = 3.67 ksi f_y = 57.13 ksi. f_{yh} = 44.8 ksi.   Spacing = 2.83 in.
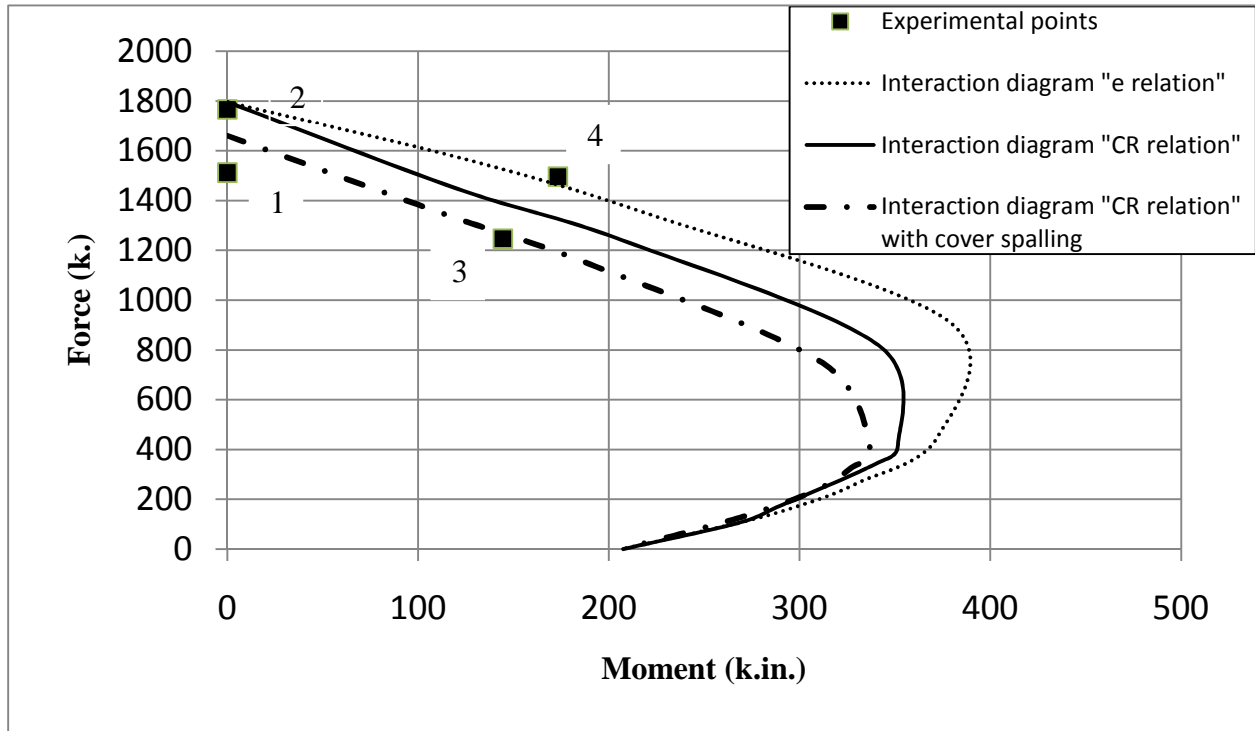
Figure 5-55: Comparison between KDOT Column Expert with Scott *et al* experiment ($\alpha = 0$)

357

The analyzed seven cases cover the three Interaction diagram zones of; compression controlled, tension controlled and balanced zones. There is good agreement between the theoretical interaction diagram and the corresponding experimental data as shown in Figures (5-42), (5-44), (5-45), (5-47), (5-49), (5-51), (5-53) and (5-55).

It is shown from Figures (5-49), (5-51), (5-53) and (5-55) that interaction diagrams plotted using Equation (5-105) that is representative of the compression zone area are more accurate compared to those plotted using Equation (5-105 a) that is a function of eccentricity. Also the experimental data correlate well to its associated interaction diagrams.

Figure (5-53) and (5-55) show more accuracy and conservative interaction diagram when the analysis account for the cover spalling when the unconfined crushing strain is considered. This is represented by the most inner curve in Figures (5-53) and (5-55). Also in Figure (5-53) and (5-55) the experimental points 1 and 2 are having the same eccentricity but the loading strain rate is different. The loading strain rate for point 1 is 0.0000033, whereas it is 0.0167 for point 2. Points 3 and 4 also have the same loading strain rate. It is seen that the loading strain rate for points 1 and 3 are extremely small. Hence points 2 and 4 are more realistic and they are captured well by the theoretical interaction diagram. In conclusion, the strain rate is a parameter that needs further invistigation.

5-3-3-2 Comparison between the surface meridians T & C used in Mander model and Experimental Work

The ultimate strength surface meridians equations for compression C and tension T derived by Elwi and Murray (1979) from the data of Scickert and Winkler (1977), that are utilized by Mander *et al* (1988) to predict the ultimate confined axial strength using the two

lateral confined pressures, are compared herein to some experimental data found from Mills and Zimmerman (1970). The equations used by mander are developed originally for concrete that has unconfined strength of 4.4 ksi. They have the following formulas

$$T = 0.069232 - 0.661091\overline{\sigma_{oct}} - 0.049350\overline{\sigma_{oct}}^2 \qquad \text{5-179}$$

$$C = 0.122965 - 1.150502\overline{\sigma_{oct}} - 0.315545\overline{\sigma_{oct}}^2 \qquad \text{5-180}$$
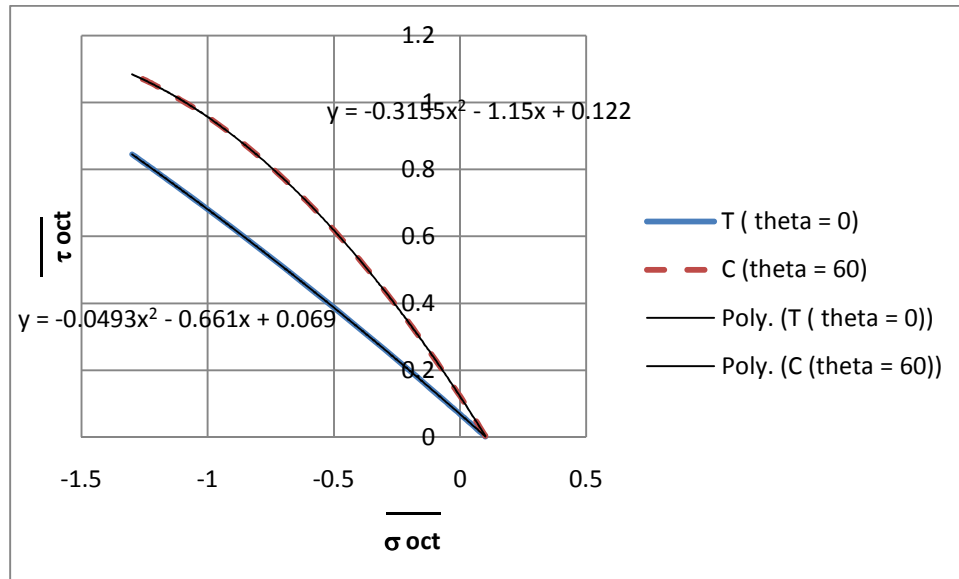
Figure 5-56: T and C meridians using equations (5-179) and (5-180) used in Mander Model for

$$f'_c = 4.4 \text{ ksi}$$

The T and C meridians adopted by Mander from Elwi and Murray (1979) work are reported on in Figure (5-56). Mills and Zimmerman (1970) developed three sets of multiaxial tests for concrete with unconfined strength of 3.34, 3.9 and 5.2 ksi. For each set, the values of $\overline{\sigma_{oct}}$ and $\overline{\tau_{oct}}$ are extracted at unconfined strength f'_c, the cracking tensile strength f'_t, equibiaxial compressive strength f''_{cb} and two extra points; one on each of the meridians. These five points are used to plot the T and C, Tables () meridians as shown in Figures (5-57), (5-58) and (5-59)
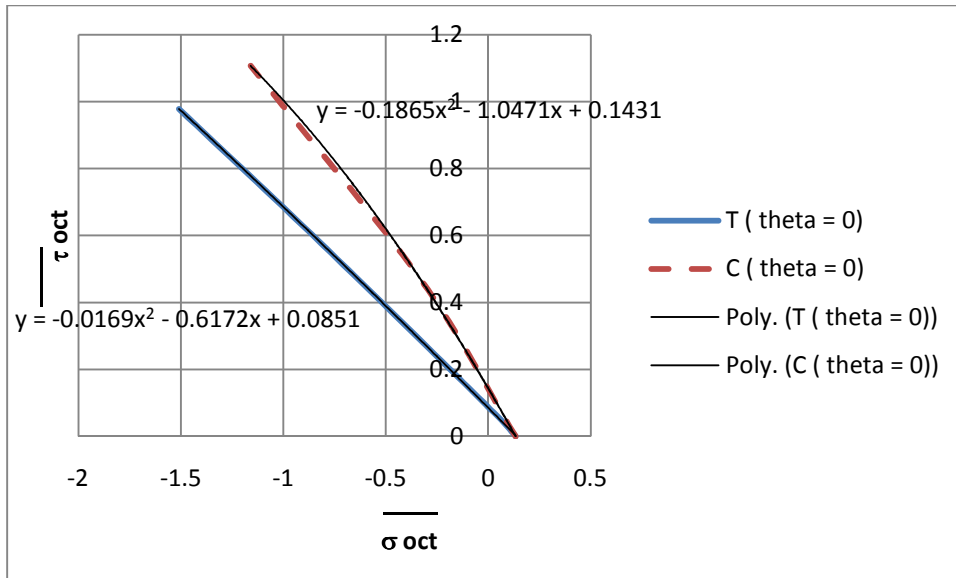
Figure 5-57: T and C meridians for $f'_c = 3.34$ ksi

In the figure: $y = -0.1865x^2 - 1.0471x + 0.1431$ and $y = -0.0169x^2 - 0.6172x + 0.0851$. Legend: T (theta = 0), C (theta = 0), Poly. (T (theta = 0)), Poly. (C (theta = 0)).
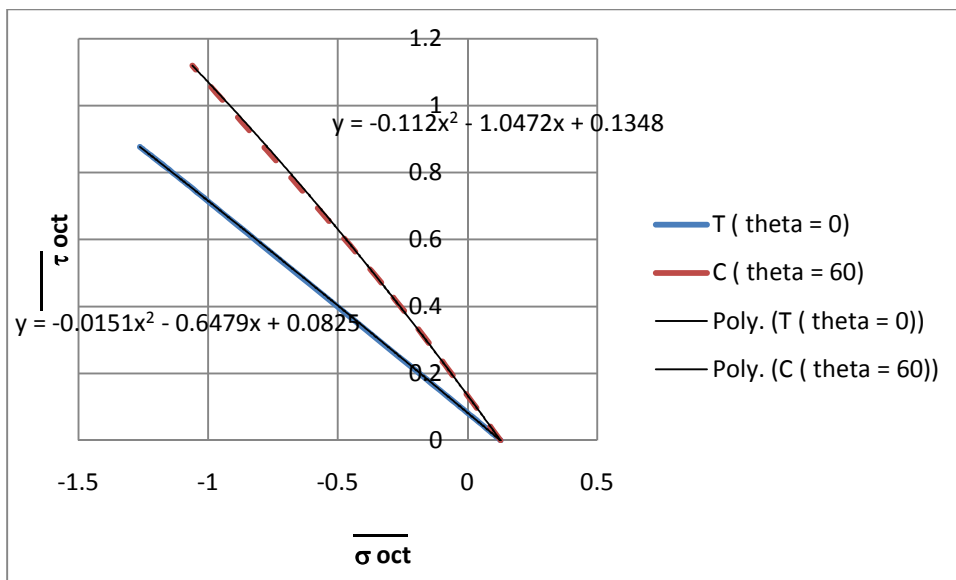
Figure 5-58: T and C meridians for $f'_c = 3.9$ ksi

In the figure: $y = -0.112x^2 - 1.0472x + 0.1348$ and $y = -0.0151x^2 - 0.6479x + 0.0825$. Legend: T (theta = 0), C (theta = 60), Poly. (T (theta = 0)), Poly. (C (theta = 60)).
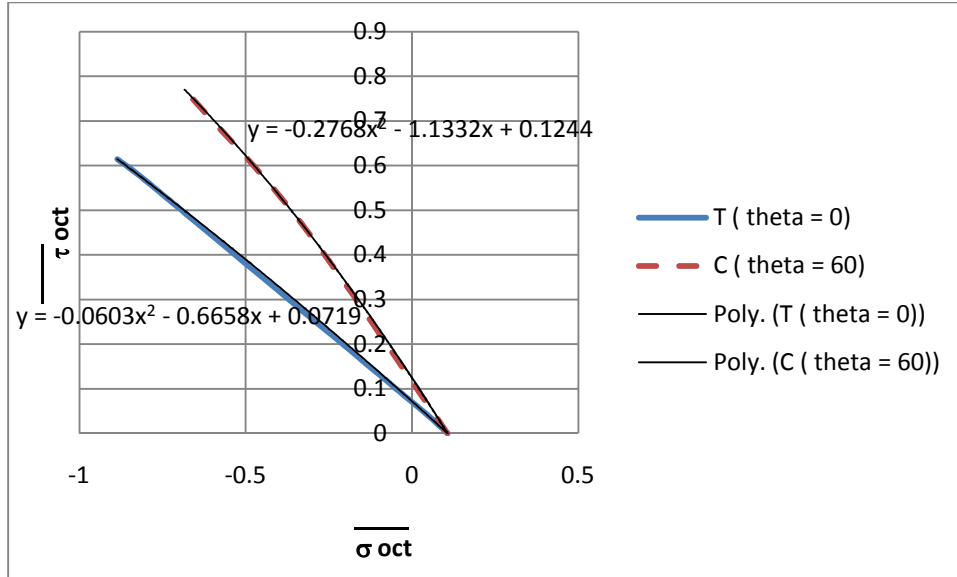
Figure 5-59: T and C meridians for $f'_c = 5.2$ ksi

The T and C equations for Figures (5-57) through (5-59) are as follow:

for $f'_c = 3.34$ ksi:

$$T = 0.0851 - 0.6172\overline{\sigma}_{oct} - 0.0169\overline{\sigma}_{oct}^{2}$$
5-181

$$C = 0.1431 - 1.0471\overline{\sigma}_{oct} - 0.1865\overline{\sigma}_{oct}^{2}$$
5-182

for $f'_c = 3.9$ ksi:

$$T = 0.0825 - 0.6479\overline{\sigma}_{oct} - 0.0151\overline{\sigma}_{oct}^{2}$$
5-183

$$C = 0.1348 - 1.0472\overline{\sigma}_{oct} - 0.112\overline{\sigma}_{oct}^{2}$$
5-184

for $f'_c = 5.2$ ksi:

$$T = 0.0719 - 0.6658\overline{\sigma}_{oct} - 0.0603\overline{\sigma}_{oct}^{2}$$
5-185

$$C = 0.1244 - 1.1332\overline{\sigma}_{oct} - 0.2768\overline{\sigma}_{oct}^{2}$$
5-186

361

Equations (5-181) through (5-186) are used in generating confined strength values for different lateral pressures as shown in Appendix A. Equations (5-179) and (5-180) are used also in developing confined strength values for the same lateral pressure values. It is seen from the tables that equations (5-179) and (5-180) give conservative values compared to equations (5-181) through (5-186). Accordingly, Equations (5-179) and (5-180) are used herin to predict the ultimate confined axial strength values for any given unconfined strength (f'_c) value.

Table 5-1: Data for constructing T and C meridian Curves for f'_c equal to 3.34 ksi

control parameter	σ oct	τ oct
$f'c$= 3.34 *ksi*	-0.33333	0.471405
f't	0.043258	0.061176
f'cb	-0.81497	0.576271
triaxial on C	-1.15968	1.10653
triaxial on T	-1.50898	0.978094

Table 5-2: Data for constructing T and C meridian Curves for f'_c equal to 3.9 ksi

control parameter	σ oct	τ oct
$f'c$= 3.9 *ksi*	-0.33333	0.471405
f't	0.040006	0.056578
f'cb	-1.0904	0.771027
triaxial on C	-1.06018	1.119058
triaxial on T	-1.26248	0.876414

Table 5-3: Data for constructing T and C meridian Curves for f'_c equal to 5.2 ksi

control parameter	σ oct	τ oct
$f'c$= 5.2 *ksi*	-0.33333	0.471405
f't	0.034553	0.048865
f'cb	-0.80229	0.567306
triaxial on C	-0.68386	0.76993
triaxial on T	-0.88634	0.614725

Chapter 6 - Software Development

6-1 Introduction

The software, KDOT Column Expert, is prepared using the object oriented programming "OOP", within the framework of the visual C# language. The OOP is useful tool that breaks the bulky codes into different classes; the components of each class are related to each other. Each class generates objects that have its class characteristics and can be used in other classes. This procedure is adaptable to simulate the real process, as well as it is flexible enough for modification and addition to the program

As shown in Figure (6-1), the main three classes are material, which has concrete, steel and FRP inherited from it, shape that classifies the cross section to Circular or Rectangular, and finally Model that inherites the material models used in the program. Any combination of shapes and material elements forms reinforced concrete cross section. This section is lent, beside the models, to the numerical analysis, and the calculations are implemented to yield the final product.
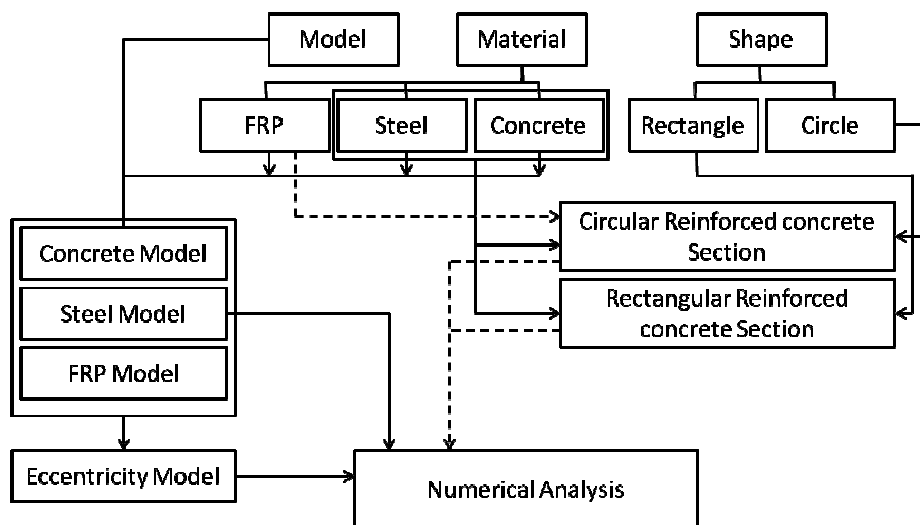
Figure 6-1: KDOT Column Expert classes

363

6-2 Interface Design

The interface was generated using the graphical user interface "GUI" which is a convenient communication tool between the user and the program. The initial form has links to circular columns and rectangular columns.
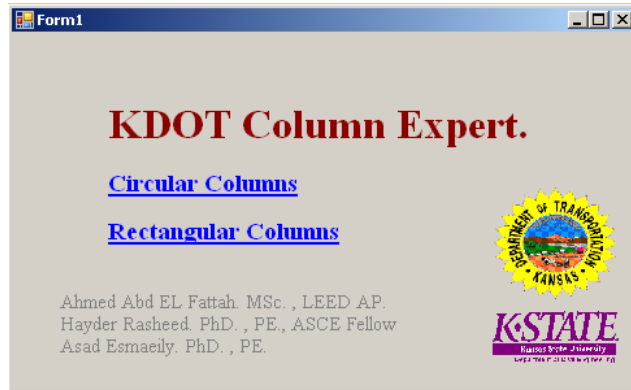
Figure 6-2: KDOT Column Expert Initial form

6-2-1 Circular Columns Interface
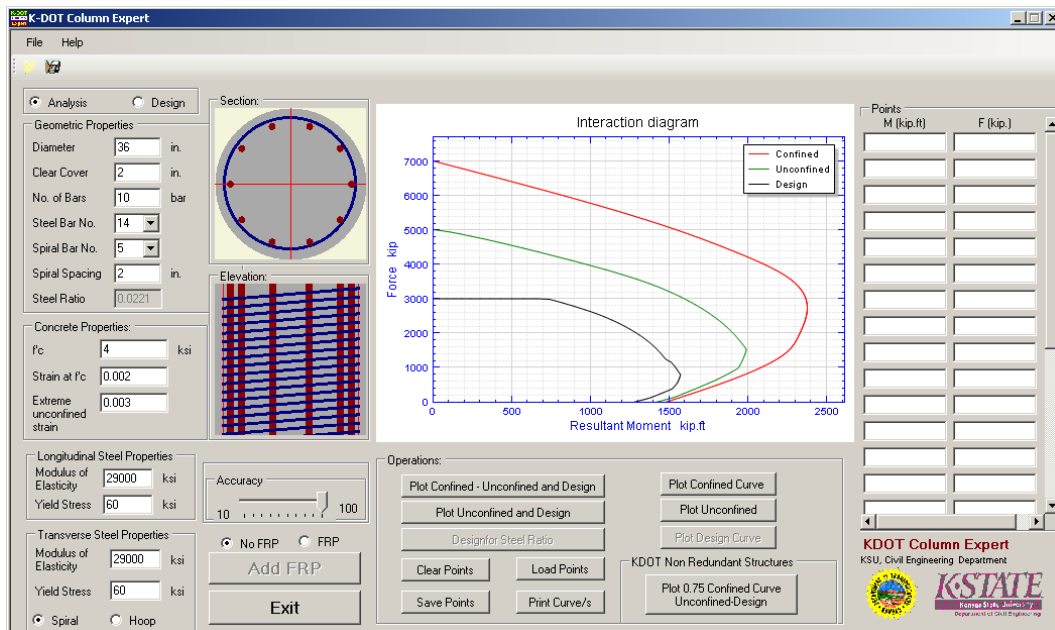
Figure 6-3: Circular Column GUI

364

The interface is divided into five sections as shown in Figure (6-4):

1- Data Input

Data Input section is divided into five sub-sections; Geometric properties, concrete properties, longitudinal steel properties, transverse steel properties and FRP properties

2- Graphics Input representation

This section automatically generates sectional plan view and elevation view of the cross section. It shows the scaled proportional location of each element in the cross section in order to avoid unrealistic overlapping.

3- Selection tools

This section has different buttons which controls plotting the interaction diagram curve/s:

Plotting the three curves; confined concrete, unconfined concrete and design curves

Plotting any one of the previous curves separately.

Plotting a series of design curves for the full range of reinforcement ratio.

Plotting curve for the non-redundent structures. This curve is limited to 75% of the distance between the design curve and the confined curve

It has also buttons for optionally save or load cases defined in the "Data Input" section and print the "plotting area" section view

4- Plotting area

The plotting area section shows the requested curve/s.

5- Projection points input

This section enables the user to input any numbers of moment-force points up to 25 points, which show up immediately on the plotting area with the existing curve/s.
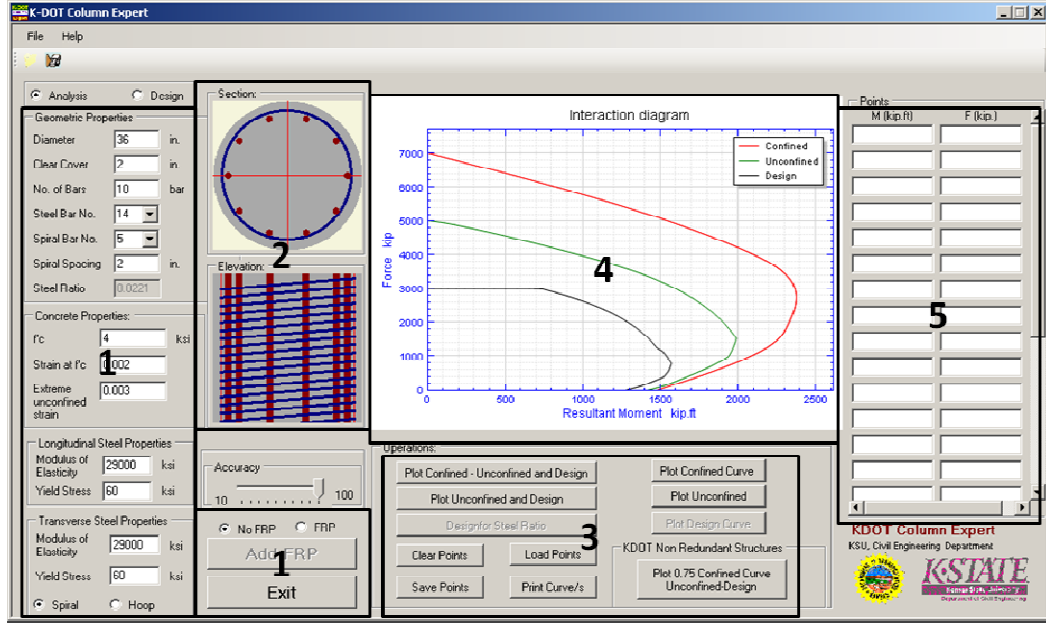
Figure 6-4: Circular Column Interface main sections
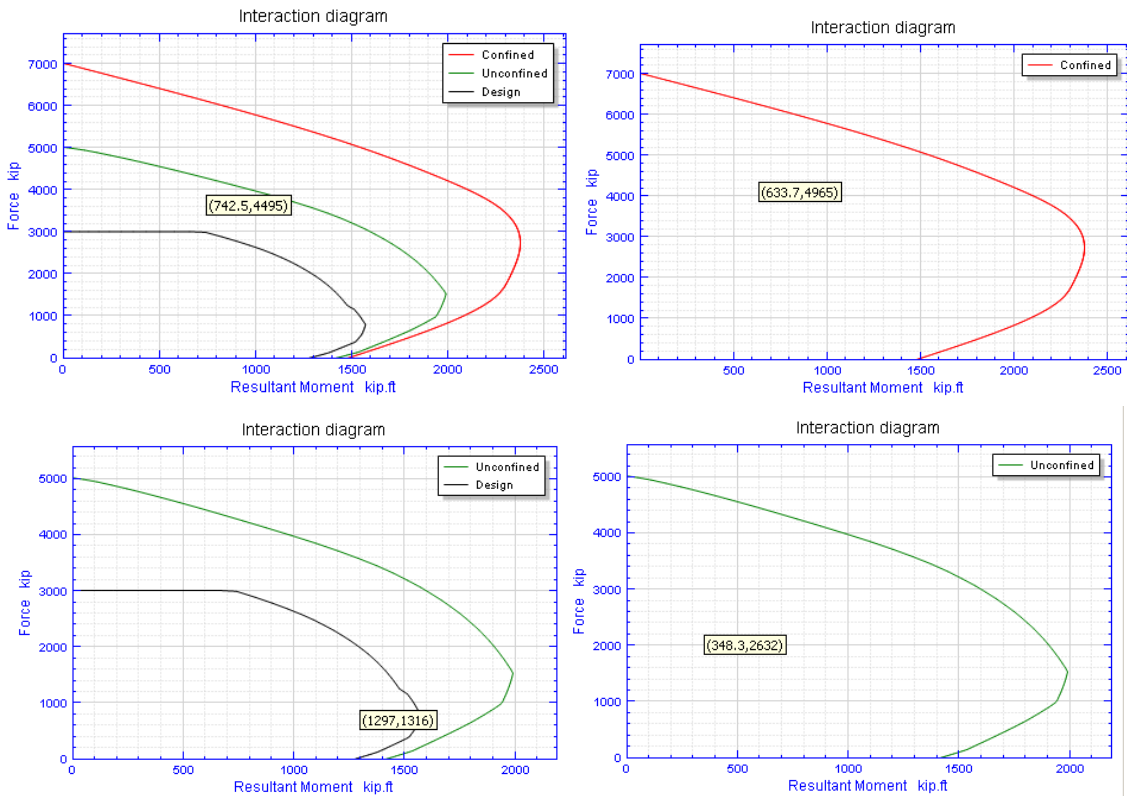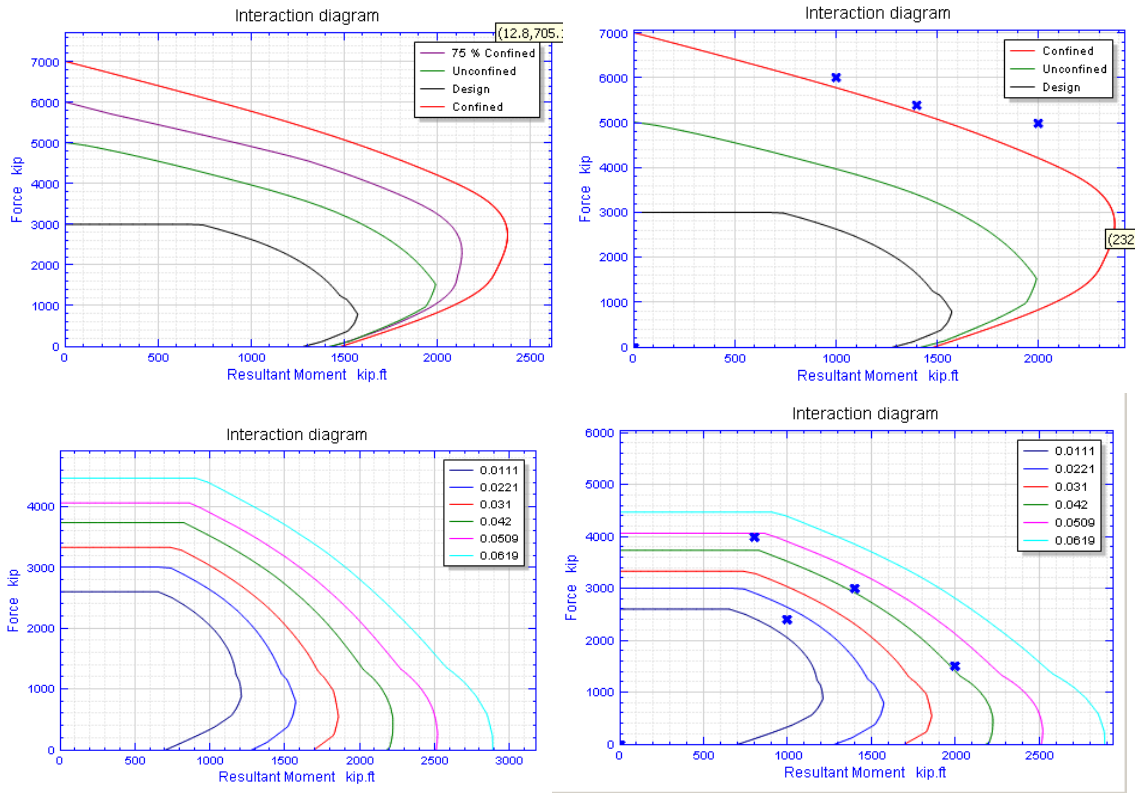
Figure 6-5: Different Interaction Diagrams plot in the Plotting area-Circular Section-
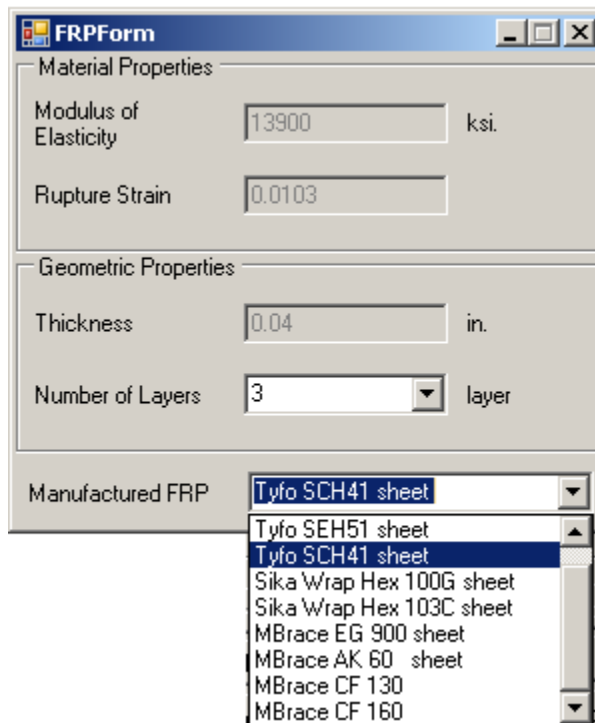
Figure 6-6: FRP form-Manufactured FRP-

367
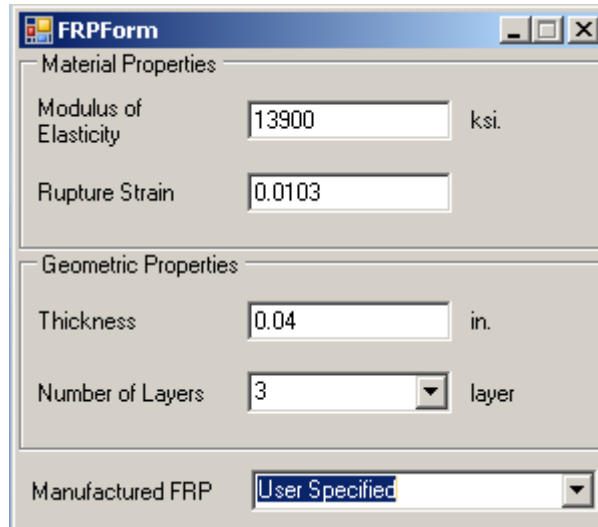
Figure 6-7: FRP form-user defined-

6-2-2 Rectangular Columns Interface
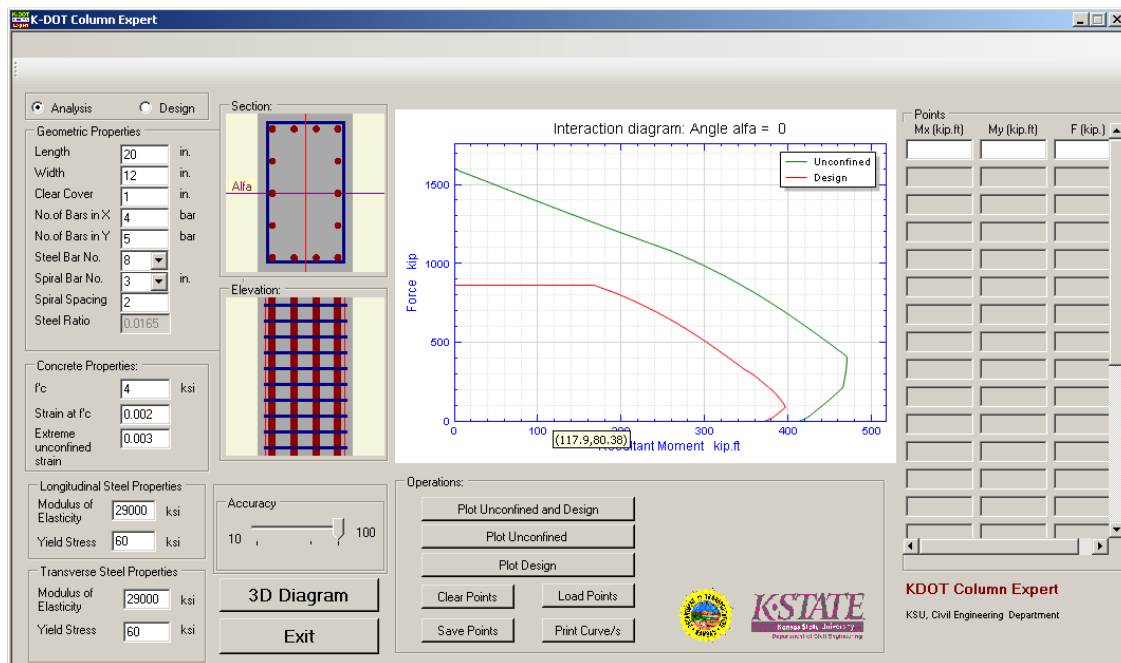
Figure 6-8: Rectangular Column GUI

The interface is divided into five sections as shown in Figure (6-9):

1- Data Input

   Data Input section is divided into four sub-sections; Geometric properties, concrete properties, longitudinal steel properties and transverse steel properties.

2- Graphics Input representation

   This section automatically generates sectional plan view and elevation view of the cross section. It shows the scaled proportional location of each element in the cross section in order to avoid unrealistic overlapping.

3- Selection tools

   This section has different buttons which controls plotting the interaction diagram curve/s:

   Plotting the three curves; confined concrete, unconfined concrete and design curves

   Plotting any one of the previous curves separately.

   Plotting a series of design curves for the full range of reinforcement ratio.

   It has also buttons for optionally save or load cases defined in the "Data Input" section and print the "plotting area" section view

4- Plotting area

   The plotting area section shows the requested curve/s.

5- Projection points input

This section enables the user to input any numbers of moment-force points up to 25 points, which show up immediately on the plotting area with the existing curve/s. The interaction diagram is updated according to the α angle input that is determind from the two moments about

x and y axes. The α angle is plotted on the sectional plan to show the load position and the two

moments' ratio with respect to the cross section.
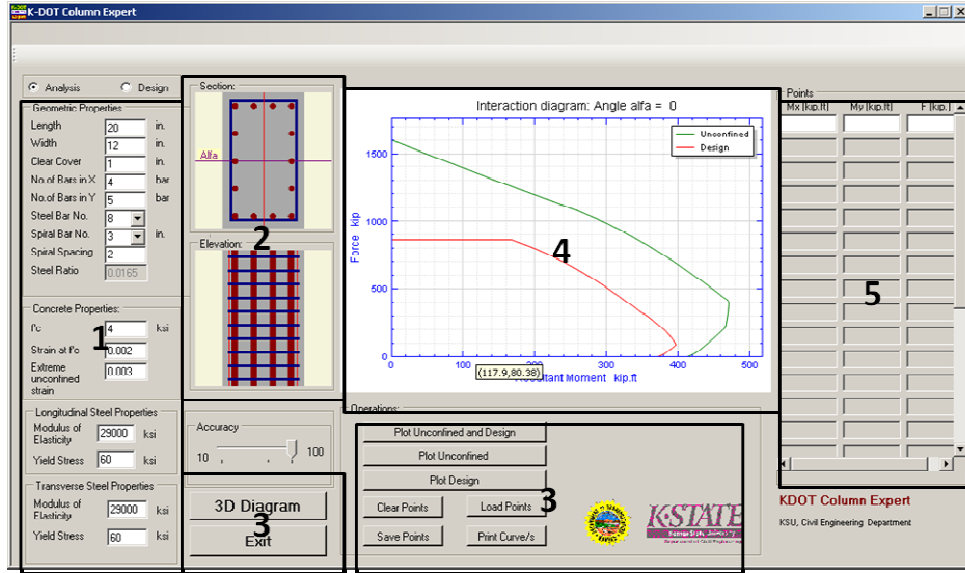
Figure 6-9: Rectangular Column Interface main sections

Figure 6-10: α angle form

The program is able to plot 3D interaction Diagram surface as shown in Figure (6-12).
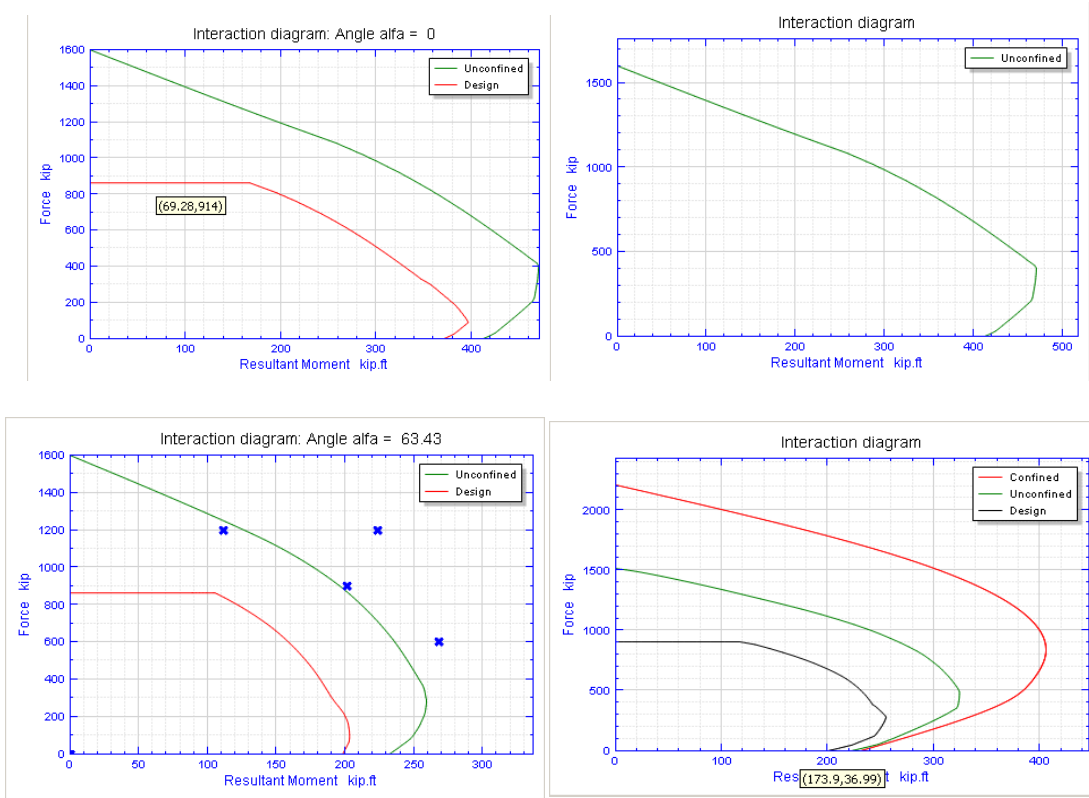
Figure 6-11: Different Interaction Diagrams plot in the Plotting area- Rectangular Section
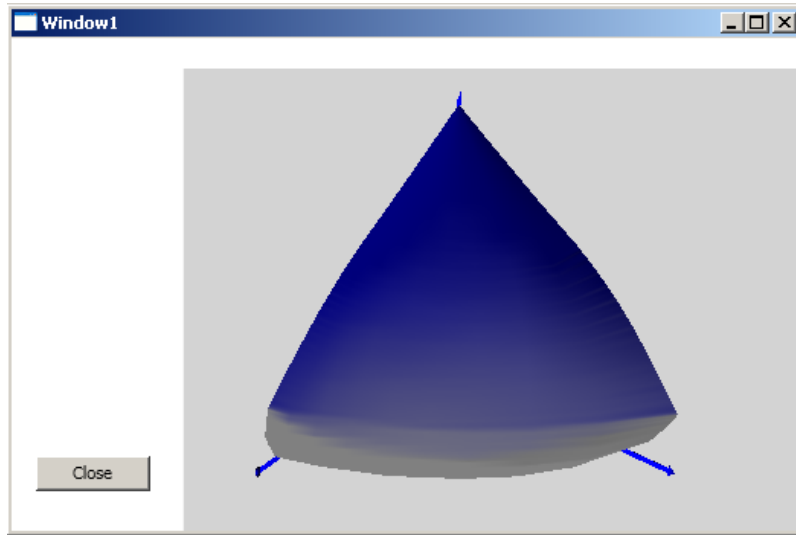
Figure 6-12: 3D Interaction Diagram

Chapter 7 - Conclusions and Recommendations

7-1 Conclusions

This dissertation accomplished several objectives at the analysis, material modeling, design implications and software development levels. It may be concluded that:

1- Based on the extensive review of the confined model available in the literature, Mander Model is found to be the most suitable concentric loading model expressing the stress-strain behavior of circular and rectangular columns confined with convenient lateral steel and steel tubes as well. In addition Lam and Teng model is found to be the suitable for predicting the stress-strain behavior of circular columns confined with FRP in case of concentric loading

2- The eccentric based stress-strain model developed in this study provides more accuracy compared to the available concentric confined models in the literature as it is shown through comparison with experimental data for all of the three cases of different confinements.

3- The stress-strain curve developed for circular columns confined with FRP and steel together compares very well with experimental ones. The amount of FRP provided in strengthening the columns is very essential in determining the shape of the stress-strain curve. It should be a value that causes the ratio of f_{lf}/f'_c to be at least 0.08 in order to have an ascending branch beyond the unconfined peak strength.

4- Columns confined with steel tubes have to have f_l/f'_c ratio equal to or more than 0.4 in order to have an ascending branch beyond the unconfined peak strength.

5- For rectangular columns, the ratio of the area of compression zone to the sectional gross area is more representative than the normalized alone eccentricity in correlating eccentric behavior. For circular columns, the normalized eccentricity is directly correlated to the ratio of compression zone to gross sectional area.

6- The non-linear numerical procedure introduced, using the eccentric model and the finite layer approach, successfully predicted the ultimate capacity of circular and rectangular reinforced concrete columns confined with different materials. The columns examined are circular columns confined with FRP, circular columns confined with steel tubes and rectangular columns confined with lateral steel.

7- A computer program named "KDOT Column Expert" is developed based on the non-linear approach implemented for analysing and designing circular columns wrapped with FRP and rectangular columns confined with lateral steel hoops.

8- The unconfined concrete analysis carried out by KDOT Column Expert is benchmarked successfully against well-established commercial software for a range of design parameters

9- The confined concrete analysis implemented by KDOT Column Expert is well correlated to experimental data for the column types with three different confinements mentioned above.

7-2 Recommendations

This work should be extended to address the following areas:

1- Model the effect of FRP wrapping on confinement for rectangular columns.

2- Model corrosion of longitudinal and transverse steel for circular and rectangular columns

3- Refine CFST modeling by considering the biaxial stress on the steel and accounting for the premature failure of steel.

4- Refine the modeling of concrete wrapped with FRP by determining the Δp that represents the lateral pressure difference developed due to transferring the confinemnet stress from FRP position to lateral steel position

5- Model CFST for rectangular columns

6- Expand the software application to include the CFST columns.

References

Aas-Jakobsen A. (1964). "Biaxial eccentricities in ultimate load design." ACI J., 61(3), 293–316.

Abdel-Salam, M N | Abdel-Ghaffar, M | Zaki, M A. "Axial Load Capacity of Short Circular Concrete Filled Steel Tubes - An Analytical Model" Journal of Engineering and Applied Science (Egypt). Vol. 48, no. 3, pp. 473-490. June 2001

ACI-ASCE Committee 327, "Ultimate Strength Design," ACI Journal, January, 1956; Proceedings, Vol. 52.p 505-524

ACI Committee 440.2R-02 (2002) "Guide for the Design and Construction of Externally Bonded FRP Systems for Strengthening Concrete Structures". American Concrete Institute, Michigan 76p.

Ahmad SM, Khaloo AR, Irshaid A (1991) "Behavior of concrete spirally confined byfiberglass filaments". Mag. Concrete Res., 43(156): 143–148.

Ahmad, S. H., and Shah, S. P. (1982 a). "Complete Triaxial stress-strain curves for concrete." ASCE J., 108(ST4),April 1982, 728-743.

Ahmad, S. H., and Shah, S. P. (1982 b). "Stress-Strain Curves of Concrete Confined by Spiral Reinforcement." ACI J., 79(6), 484-490.

Ahmad, S. H., and Mallare, M. P. (1994). "A Comparative study of models for confinement of concrete by circular spirals." Mag. of Concrete Research 46(166), 49-56.

Aire, C., Gettu, R., Casas, J.R., (2001). "Study of the compressive behaviour of concrete confined by fiber reinforced composites".Proc. of the Int. Conf. "Composites in Constructions",Lisse, NL. Balkema Publishers: 239–243.

Al-Sayed S, Al-Salloum Y, Almussalam T and Ahmed M Z (2001)" A strength model for concrete confined with composite fabrics" Journal of Civil Engineering, The Institution of Engineering, Bangladesh Vol CE29, No. 1, 2001

Amirthanandan, K.and Rangan, B.V. (1991) "Strength of reinforced concrete columns in biaxial bending" Transactions of the Institution of Engineers, Australia. Civil engineering, v CE33, n 2, p 105-110, Apr 1991

Andersen, Paul (1941) "Design Diagrams for Square Concrete Columns Eccentrically Loaded in Two Directions," ACI Journal, November, 1941; Proceedings, Vol. 38, p 149.

Ang, Cho-Lim Charles (1961), "Square Column with Double Eccentricities Solved by Numerical Method," ACI Journal, February, 1961; Proceedings, Vol. 57, p 977.

Assa B., Nishiyama, M., and Watanabe, F. (2001). "New Approach for Modeling Confined Concrete. I: Circular Columns." J. Struct. Eng. ASCE, 127(7), 743-750.

Attard, M. M., and Setunge, S. (1996). "Stress-Strain Relationship of Confined and Unconfined Concrete." ACI Mater. J., 93(5), 432-442.

Au, Tung (1957) "Ultimate Strength Design Charts for Columns Controlled by Tension," ACI Journal, December, 1957; Proceedings, Vol. 54, p 471.

Au, Tung (1958) "Ultimate Strength Design of Rectangular Concrete Members Subjected to Unsymmetrical Bending" ACI Journal, February, 1958; proceedings, Vol. 54, p 657.

Baig, M N, Fan, J and Nie, J (2006). "Strength of Concrete Filled Steel Tubular Columns." Tsinghua Science & Technology 11(6):657- 666.

Bajaj S. and Mendis P.,(2005) "New Method to Evaluate the Biaxial Interaction Exponent for RC Columns", Journal of Structural Engineering, ASCE, 131(12)(2005), pp. 1926–1930.

Bakhoum, Michel (1948) "Analysis of Normal Stresses in Reinforced Concrete Sections under Symmetrical Bending," ACI Journal, February, 1948; Proceedings, Vol. 44, p 457.

Bazant, Z. P., and Bhat, P. D. (1976). "Endochronic Theory of Inelasticity and Failure of Concrete." J. Engrg. Mech. Div., ASCE, 102(4), 701-722.

Bazant, Z. P., and Bhat, P. D. (1977). "Prediction of Hysteresis of Reinforced Concrete Members." J Struct. Div., ASCE, 103(1), 153-167.

Berthet, J.F.; Ferrier, E. and Hamelin, P.(2005); "Compressive behavior of concrete externally confined by composite jackets Part A: Experimental study" Construction and Building Materials, v 19, n 3, April, 2005, p 223-232

Berthet, JF; Ferrier, and E.; Hamelin, P.(2006); "Compressive behavior of concrete externally confined by composite jackets Part B: Modeling" Construction and BuildingMaterials, v 20, n 5, June 2006, p 338-347

Bisby, L.A., Dent, A.J.S, & Green, M.F. (2005). "A comparison of models for FRP-confined concrete", Journal of Composites for Construction, American Society of Civil Engineers, New York, USA, 9 pp.

Binici, B. _2005_. "An analytical model for stress–strain behavior of confined concrete." Eng. Struct., 27_7_, 1040–1051.

Blume, J.A, Newmark, N.M. and Corning L.H. (1961)" Design of multi storey reinforced concrete building for earthquake Motions" Chicago. Portland cement association.

Bonet JL, Barros F M, Romero M L.(2006) "Comparative study of analytical andnumerical algorithms for designing reinforced concrete section under biaxial bending". Comp & Structures 2006;8:31–2.

Bonet, J. L., Miguel, P. F., Fernandez, M. A., & Romero, M. L. 2004. "Analytical Approach to Failure Surfaces in Reinforced Concrete Sections Subjected to Axial Loads and Biaxial Bending." Journal of Structural Engineering, 130(12): 2006-2015.

Building code requirements for reinforced concrete (1956) . ACI 318-56. American Concrete Institute (ACI).Detroit,Michigan.

Bradford, M. A., and Gilbert, R. I. (1992). "Analysis of Circular RC Columns for Short and Long-Term Deformations." J. Struct. Engrg., ASCE, 118(3), 669-683.

Braga F., Gigliotti R., Laterza M. (2006). "Analytical Stress–Strain Relationship for ConcreteConfined by Steel Stirrups and/or FRP Jackets." Journal of Structural Engineering, ASCE,Vol. 132, No. 9: 1402–1416.

Breen, J. E. (1962) , "The Restrained Long Concrete Column as a Part of A Rectangular Frame." Ph. D. Thesis Presented to The University of Texas, Austin, Tex.

Bresler, B. (1960). ''Design, criteria for reinforced columns under axial load bi-axial bending.'' ACI J., Nov., 481–491.

Bresler, B., and Gilberg, P. H. (1961). ''Tie requirements for reinforced concrete columns.'' ACI J., 58(5), 555–570.

Brettle H J; Taylor J M (1969) "Comparison of experimental results with ultimate strength theory for reinforced concrete columns in biaxial bending" Instn Engrs Australia-Civ Eng Trans, v CE 11, n 1, p 63-74, Apr 1969

Campione G., Miraglia N. (2003). "Strength and Strain Capacities of Concrete CompressionMembers Reinforced with FRP." Cement & Concrete Composites, Elsevier, 25 (1), 31-41.Comite Eurointernational du Beton (1993). CEB-FIP Model Code 90. T. Telford, London.

Candappa, D. (2000). "The Constitutive Behavior of High Strength Concrete under Lateral Confinement." PhD Thesis, Monash Univ., Clayton, VIC, Australia.

Candappa, D. P., Sanjayan, J. G., and Setunge, S. (2001). "Complete Triaxial Stress-Strain Curves of High-Strength Concrete." J. Mater. Civ. Eng., 13(3), 209-215.

Candappa, D. P., Setunge, S., and Sanjayan, J. G. (1999). "Stress versus Strain Relationship of High Strength Concrete under High Lateral Confinement." Cem. Concr. Res., 29(12), 1977-1982.

Carreira, D J., and Chu, K. H. (1985). "Stress-Strain Relationship for Plain Concrete in Compression." ACI J., 83(6), 797-804.

Carey S A, Harries K A. (2005) "Axial behavior and modeling of confined small-medium and large-scale circular section with carbon fiberreinforced polymer jackets". ACI Struct J 2005;102(4):596–604.

Cedolin, L.; Cusatis, G.; Eccheli, S.; Roveda, M. (2006) "Biaxial bending of concrete columns: an analytical solution". Studies and Researches v.26. http://www.inti.gov.ar/cirsoc/

Cedolin L, Cusatis G, Ecchelli S, Roveda M.(2008)" Capacity of rectangular crosssections under biaxially eccentric loads". ACI Struct J 2008;105(2):215–24.

Cervin, D. R. (1948), "Design of Rectangular Tied Columns Subjected to Bending with Steel in all Faces," ACI Vol. 19, No. 401-412.

Chan, W. W. L. (2002). "The Ultimate Strength and Deformation of Plastic Hinges in Reinforcement Concrete Frameworks" Magazine of Concrete Research (London), V. 128, No. 12 p. 1551-1564, December 2002.

Cheng, H.L., Sotelino, E.D., Chen, W.F., 2002. Strength estimation for FRP wrapped reinforced concrete columns. Steel and Composite Structures, 2(1):1-20.

Chu, Kuang-Han and Pabarcius, A. "Biaxially Loaded Reinforced Concrete Columns," ASCE Proceedings, Vol. 84, No. ST 8, Paper 1865, December, 1958.

Chun, S.S. and Park H.C. (2002). "Load Carrying Capacity and Ductility of RC Columns Confined by Carbon Fiber Reinforced Polymer", In: Proceedings, Third International Conference on Composites in Infrastructure, in CD-Rom format.

Ciupala, Pilakoutas and Taranu (2003) "Confinement of Concrete Cylinders with Fibre Reinforced Composite Jackets" Ovidius University Annals Series: Civil Engineering 5, 133- 138 (2003)

Cross, H. (1930)" The Column Analogy: Analysis of Elastic Arches and Frames". Urbana, IL: University of Illinois, 1930.

Csuka B and Kollár L. P.,(2010) "FRP confined circular concrete columns subjected to concentric loading", J. of Reinforced Plastics and Composites, 29(23): 3504-3520 (2010).

Cusson, D. and Paultre, P. (1995). "Stress-Strain Model for Confined High-Strength Concrete" ASCE Journal of Structural Engineering, Vol. 121, No.3, p. 468-477.

Czerniak. E., (1962)."Analytical approach to biaxial eccentricity". Proc. ASCE, J. Struct. Div. 88. 105-158 (1962).

Davister, M. D. (1986). "A Computer Program for Exact Analysis," Concrete International: Design and Construction, V. 8, No. 7, July 1986, pp. 56-61.

De Lorenzis L, Tepfers R. (2003). "Comparative Study of Models on Confinement of ConcreteCylinders with Fiber-Reinforced Polymer Composites." ASCE Journal of Composites forConstruction, 7(3), 219-234.

Demagh, K. Chabil, H.; Hamzaoui, L.(2005) "Analysis of reinforced concrete columns subjected to biaxial loads" Proceedings of the International Conference on Concrete for Transportation Infrastructure, p 433-440, 2005

Demers, M., Neale, WK., 1999. Confinement of reinforcedconcrete columns with fibre-reinforced composite sheets—an expemental study. Can. J. Civ Eng;26:226–41.

Dodd, L. L., and Cooke, N. (2000). "Capacity of circular bridge columns subjected to base excitation." ACI J., 97(2), 297-308.

Domingo A. Moran1 and Chris P. Pantelides (2002) "FRP Confined Concrete Stress-Strain Model Utilizing a variable strain ductility ratio" Journal of Composites for Construction, 2002 http://web.arizona.edu/~az-icci/papers/023.pdf

Ehsani, Mohammad R. (1986). "CAD for Columns," Concrete International: Design and Construction, V. 8, No. 9, Step. 1986, pp. 43-47.

Eid, R. and Dancygier A. N. (2005) "Partially confined circular members subjected to axial compression: Analysis of concrete confined by steel ties" Structural engineering and Mechanics, Vol. 21, No. 6 p 737-765.

Eid, R., Roy, N., Paultre, P. (2006). "Behaviour of Circular Reinforced Concrete ColumnsConfined with Transverse Steel Reinforcement and Fiber-Reinforced Composite Sheets."Proceedings of the 2nd International Congress, June 5-8, 2006 – Naples, Italy

Elchalakani M, Zhao XL, Grzebieta RH. Concrete-filled circular steel tubes subjected to pure bending. Journal of Constructional Steel Research 2001;57(11):1141–68. Axial load capacity of short circular concrete filled steel tubes - an analytical model

El-Dash, K. M., and Ahmad, S. H. (1995). "A Model for Stress- Strain Relationship of Spirally Confined Normal and High-Strength Concrete Columns." Mag. Concrete Res., 47(171), 177-184.

Elremaily A., Azizinamini A (2002)., Behavior and strength of circular concrete-filled tube columns, Journal of Constructional Steel Research, Volume 58, Issue 12, December 2002, Pages 1567-1591 "

Ellobody E., Young B., Lam D. (2006), "Behaviour of normal and high strength concrete-filled compact steel tube circular stub columns", Journal of Constructional Steel Research, Volume 62, Issue 7, July 2006, Pages 706-715

Elwi A and. Murray D. W (1979), "A 3D hypoelastic concrete constitutive relationship", J. Eng. Mech., 105, 623±641 (1979)

Esmaily, A. and Xiao, Y. (2004). "Behavior of Reinforced Concrete Columns under Variable Axial Load" ACI Structural Journal, V.101, Issue 1, p.124-132, January 2004.

Everand, Noel J., and Cohen, Edward. (1964). "Ultimate Strength Design of Reinforced Concrete Columns" ACI Special Publication, SP-7, 182 p, Detroit.

Everand, Noel J., (1997). "Axial load moment interaction for cross sections having longitudinal reinforcement arranged in a circle" ACI J, V. 94, No. 6, December 1997.

Fam, A. Z., Flisak, B., and Rizkalla, S. H., (2003). "Experimental and Analytical Modeling of Concrete-Filled Fiber-Reinforcement Polymer Tubes Subjected to combined Bending and Axial Loads". ACI Structural Journal, V.100, Issue 4, p.499-509, August 2003.

Fam, A., and Rizkalla, S.,(2006) "Structural Performance of Laminated and Unlaminated Tempered Glass under Monotonic Transverse Loading," Construction and Building Materials, Elseu· ier 20(9):761- 768 (2006).

Fam A. Rizkalla S. (2001). "Confinement Model for Axially Loaded Concrete Confined byCircular Fiber-Reinforced Polymer Tubes." ACI Struct. J., 98(4), 451-461.

Fafitis A., and Shah, S.P. (1985). "Lateral Reinforcement for High-Strength Concrete Columns" ACI Special Publication, SP 87-12, p.213-232.

Fardis, M.N. and Khalili, H.H. 1981. "Concrete encased in fiberglass-reinforced plastic". ACI Journal, Vol. 78, No. 6, pp. 440-446.

Fardis M N, Khalili H (1982) "FRP-encased concrete as a structural material". Mag. Concrete Res., 34(121): 191–202.

Fleming, J. F., and Werner, S. D., (1965), "Design of Columns Subjected to Biaxial Bending." ACI JOURNAL, Proceedings V. 62, No. 3, Mar. 1965, pp. 327-342

Fujimoto T., Mukai A., Nishiyama I, Sakino K., "Behavior of Eccentrically Loaded Concrete-Filled Steel Tubular Columns", Journal of Structural Engineering 2004, Volume 130, Issue 2, February 2004, Pages 203-212

Fujii, M., Kobayashi, K., Miyagawa, T., Inoue, S. and Matsumoto, T. (1988). "A study on the application of a stress-strain relation of confined concrete," Proc., JCA Cement and Concrete, Vol. 42, Japan Cement

Furlong. R. W. (1961), "Ultimate strength of square columns under biaxially eccentric loads", Journal of the American Concrete Institute, No 57-53, P1129-1140

Furlong R.W., "Strength of steel encased concrete beam-columns", Journal of the Structural Division 1967; Volume 93, Issue 5, Pages115–30

Furlong RW, Hsu CTT, Mirza SA.(2004) "Analysis and design of concrete columns for biaxial bending- overview". ACI Structural Journal 2004;101(3):413–23.

Gardner, N. J., and Jocobson, E. R. ~1967!. ''Structural behavior of concrete-filled steel tubes.'' ACI J., 64~7!, 404–412.

Giakoumelis G., Lam D.(2004), "Axial capacity of circular concrete-filled tube columns", Journal of Constructional Steel Research, Volume 60, Issue 7, July 2004, Pages 1049-1068

Gupta S. R. Davalath and Murthy K. S. Madugula,(1988) "Analyses/design of reinforced concrete circular cross section", ACI Structural Journal, Vol. 85, No. 6, Tital No. 85-s55, Nov-Dec 1988.

Goode, C. D. (2008). "Composite columns – 1819 tests on concre-te-filled steel tube columns compared with Eurocode 4", The Structural Engineer 86(16): 33–38.

Gouwens, Albert J., (1975), "Biaxial Bending Simplified," Reinforced Concrete Columns , SP-50, American Concrete Institute, Detroit, 1975, pp. 233-261.

Gunnin, B. L., Rad, F. N., and Furlong, R. W. (1979). "A General Nonlinear Analysis of Concrete Structures and Comparison With Frame Tests," Computers and Structures, V. 105, No. 2, Apr. 1979, pp. 297-315.

Harmon, T., Salttery, K., and Ramarkrishnan, S. (1995) ''The effect of confinement effectiveness of confined concrete.'' Non-Metallic (FRP) Reinforcement for Concrete Structures, Proc., 2nd Int. Symposium, L.

Helgason V (2010) "Development of a computer program to design concrete columns for biaxial moments and normal force" Ms Thesis. Lunds Institute of Technology Lund University, Lund, Sweden

Harajli MH (2006) Axial stress–strain relationship for FRP confined circular andrectangular concrete columns. Cement & Concrete Composites 28 (2006): 938–948.

Harries, K.A., Kharel, G., (2002). Experimental investigation ofthe behavior of variably confined concrete. J. Cement andconcrete research 2267 (2002) 1-8.

Hartley, G.A.,(1985) "Radial Contour Methods of Biaxial Short Column Design",ACI, Journal, Title No. 82-62, Sept-Oct. 1985, pp 693-700.

Hognestad, E. (1930) "A study of combined bending and axial load in reinforced concrete members", University of Illinois, Urbana.

Hong, H. P. (2000). ''Short RC column capacity under biaxial bending and axial load.'' Can. J. Civ. Eng., 27~6!, 1173–1182.

Hoppel, C.P.R., Bogetti, T.A., Gillespie, J.W. Jr. , Howie, I., Karbhari, V.M.(1994) .Analysis of a Concrete Cylinder with a Composite Hoop Wrap. Proceedings of the ASCE Materials Engineering Conference, San Diego, CA, November 1994, pp 191- 198.

Horowitz. B,(1989) "Design of columns subjected to biaxial bending", ACI Struct. Journal, 86, (6), 717-722 (1989).

Hoshikuma, J., Kawashima, K., Nagaya, K., and Taylor, A. W. (1997). "Stress-Strain Model for Confined Reinforced Concrete in Bridge Piers." J. Struct. Eng., 123(5), 624-633.

Hosotani, M Kawashirna, V. M.,. and Hoshikuma, J.(1997), "A model for confinement effect for concrete cyfinders confined by carbon fiber sheets", NCEER-INCEDE Workshop on Earthquake Engrg. Frontiers of Transp. Fac., NCEER, State University of New York, Buffalo, N.Y., (1997).

Hosotani, M., Kawashima, K. and Hoshikuma, J. (1997). "A study on confinement effect of concrete cylinders by carbon fiber sheets". In: Non-Metallic (FRP) Reinforcement for Concrete Structures (Vol 1). Japan Concrete Institute, pp. 209-216.

Howie, I., and Karbhari, V. M. (1994). ''Effect of materials architecture on strengthening efficiency of composite wraps for deteriorating columns in the North-East.'' Infrastructure: New Materials and Methods of Repair, Proc., 3rd Materials Engineering Conf., K. D. Basham, ed., Material Engineering Division, ASCE, 199–206.

Hsu, C. T. T.,(1988) "Analysis and Design of Square and Rectangular Columnsn by Equation of Failure Surface," ACI Structural Journal, V. 85, No. 2, Mar.-Apr. 1988, pp. 167-179.

Hsu, L. S., and Hsu, C. T. T. (1994). "Complete Stress-Strain Behavior of High-Strength Concrete under Compression." Mag. Concrete Res., 46(169), 301-312.

Hu, Lu-Shien (1955)"Eccentric Bending in Tow Directions of Rectangular Concrete Columns," ACI Journal, May, 1955; Proceedings Vol. 51, p 921.

Hu H.T., Huang C.S., Chen Z.L., (2005) "Finite element analysis of CFT columns subjected to an axial compressive force and bending moment in combination", Journal of Constructional Steel Research, Volume 61, Issue 12, December 2005, Pages 1692-1712

Hu H.T., Huang C.S., Wu,M.H., Wu Y.M.,(2003) "Nonlinear Analysis of Axially Loaded Concrete-Filled Tube Columns with Confinement Effect", Journal of Structural. Engeneering. 129, 1322 (2003)

Huang C.S., Yeh Y.K., Liu G.Y., Hu H.T., Tsai K.C., Weng Y.T., Wang S.H., Wu M.H.,(2002) "Axial Load Behavior of Stiffened Concrete-Filled Steel Columns", Journal of Structural Engineering 2002, Volume 128, Issue 9, September 2002, Pages 1222-1230

Inai, E., Mukai, A., Kai, M., Tokinoya, H., Fukumoto, T., and Mori, K. _(2004)_. "Behavior of concrete-filled tube beam-columns." J. Struct. Eng., 130_2_, 189–202.

Jarquio R V.(2004) "Analytical method of predicting the ultimate strength of CFT columns". In: Proceedings of Structures Congress, ASCE. Nashville, Tennessee, USA, 2004: 1-10

Johansson, M., _AAkesson, M., (2002). "Finite element study on concrete-filled steel tubes using a new confinement sensitive concrete compression model". Nordic Concrete Research 27, 43–62.

Johansson M., Gylltoft K.,(2002) "Mechanical Behavior of Circular Steel-Concrete Composite Stub Columns", Journal of structural engineering, Volume 128, Issue 8, 2002, pages 1073-1081

Karbhari, V. M., and Gao, Y., (1997). "Composite jacketed concreteunder uniaxial compression—verification of simpledesign equations". Journal of Materials in Civil Engineering;ASCE; 9(4):185–193

Karabinis, A. I., and Kiousis P. D. (1994). "Effects of confinement on concrete columns: Plasticity approach: J. SDtruct. Engrg. ASCE, 12099), 2747-2767.

Karabinis AI, Rousakis TC. (2002) "Concrete confined by FRP material: A plasticity approach". Engineering Structures 2002;24:923–32.

Kent, D. and Park, R. (1971). "Flexural Members with Confined Concrete" Journal of Structural Division. Proceedings of the American Society of Civil Engineers. V.97, No.ST7, p 1969-1990, July 1971.

Kono S, Inazumi M, Kaku T. (1998) "Evaluation of confining effects of CFRP sheets on reinforced concrete members". In: Proceedings of the second international conference on composites in infrastructure ICCI'98, Tucson, Arizona, 5–7 January 1998. p. 343–55.

Kroenke, W. C., Gutzwiller, M. J., and Lee, R. H. (1973). "Finite Element for Reinforced Concrete Frame Study." Journal of Structural Division, ASCE, V. 99, No. ST7, July 1973, pp. 1371-1390.

Lam, L. and Teng, J.G. (2001). "A new stress-strain model for FRP-confined concrete". In: Proceedings of International Conference on FRP Composites in Civil Engineering, Hong Kong, pp. 283-292

Lam L, Teng JG (2002) "Strength models for fiber-reinforced plastic-confined concrete".Journal of Structural Engineering, ASCE;128(5):612–23.

Lam, L., Teng, J.G., (2003). "Design-oriented stress-strain modelfor FRP-confined concrete". Journal of Construction andBuilding Materials; ELSEVIER: 17; 471-489.

Lam, L., Teng, J.G., (2004). "Ultimate condition of Fiber ReinforcedPolymer-confined concrete". Journal of Compositesfor Construction, ASCE; 8(6): 539-548.

Lazaro, A. L., and Richards, Jr., r. (1974). "Full Range Analysis of Concrete Frames." Journal of Structural Division, ASCE, V. 100, No. ST12, Dec. 1974, pp. 2419-2432.

Lejano B., A.(2007) "Investigation of biaxial bending of reinforced concrete columns through fiber method modeling. J Res Sci Comput Eng" 2007;4(3):61–73.

Leea S H, Uya B, Kimb S, Choib Y, Choi S (2010) "Behavior of high-strength circular concrete-filled steel tubular (CFST) column under eccentric loading Journal of Constructional Steel Research 67 (2011) 1_13

Li, G., (2006). "Experimental study of FRP confined concrete cylinders".J Engineering Structures ELSEVIER:28; 1001-1008.

Liang Q.Q., Fragomeni S., (2010) "Nonlinear analysis of circular concrete-filled steel tubular short columns under eccentric loading", Journal of Constructional Steel Research, Volume 66, Issue 2, February 2010, Pages 159-169

Liu L. L., Tu Y Q,, Ye Y H. (2010) "The Constitutive Relationship of Concrete Core in Circular Concrete-Filled Steel Tubular Columns Advanced Materials Research Vols. 163-167 (2011) pp 2063-2067

Lokuge W. P. , Sanjayan J. G. and Setunge S. (2005) "Stress strain model for laterally confined concrete". Journal of materials in civil engineering,ASCE, Vol. 17, No. 6 p607-616, December 2005

Lucio, K. (2004) "Analytical performance of reinforced concrete sections using various confinement models" , master thesis, Kansas State University 119 p.

Mander, J.B., Priestley, M.J.N., and Park, R. (1988). "Theoretical Stress-Strain Model for Confined Concrete" Journal of Structural Engineering, ASCE, V.114, No. 8, p. 1827-1849, August 1988.

Mander, J.B., Priestley, M.J.N., and Park, R. (1988). "Observed stress strain behavior of confined concrete" Journal of Structural Engineering, ASCE, V.114, No. 8, p. 1804-1825, August 1988.

Mander, J. B. (1983). "Seismic design of bridge piers" PhD. thesis. University of Canterbury, New Zealand, 442 p.

Mansur, M.A., Chin, M. S., and Wee, T. H. (1997). "Stress-strain relationship of confined high strength plain and fiber reinforcement" Journal of Materials in civil engineering, V.9, No. 4, p. 171-179, November 1997.

Matthys S, Taerwe L, Audenaert K (1999) "Tests on axially loaded concrete columns confined by fiber reinforced polymer sheet wrapping." In: Dolan CW, Rizkalla S, Nanni A, editors. Proceedings of the 4th International Symposium on Fiber Reinforced Polymer Reinforcement for Reinforced Concrete Structures, SP-188, American Concrete Institute, 1999. p. 243±53.

Mattock, Allan H. and Kritz, Ladislav B(1961). "Rectangular Concrete Stress Distribution in Ultimate Strength Design," ACI Journal, February, 1961, Proceedings, Vol. 57, p 875. Discussion by P. W. Abeles, Homer M. Hadley, K. Hanjnal-Konyi, J. L. Meek, Luis Saenz, Ignacio Martin, Rafael Tamargo, ACI Journal, September, 1961, p 1763.

Marques, S. P. C., Marques, D. C., and Silva, J. L. (2004). "Model for analysis of short columns of concrete confined by fiber-reinforced polymer." J. Compos. Contr., 8(4), 332-340.

Martinez, S., Nilson, A. H., and Slate, F. O. (1984). "Spirally reinforced High-Strength Concrete Columns." ACI J., 81(5), 431-442.

Matthys, S., Toutanji, H., and Taerwe, L. (2006). "Stress-strain behavior of large-scale circular columns confined with FRP composites." J. Struct. Eng., ASCE, 132(1): 123-133.

Mazzotti, C. und M. Savoia (2002). "Nonlinear creep, possion's ratio and creep-damage interaction of concrete in compression". ACI Materials Journal 99 (5), 450{457.

Medland, I. C., and Taylor, D. A. (1971). "Flexural Rigidity of Concrete Column Sections." Journal of Structural Division, ASCE, V. 97, No. ST2, Feb. 1971, pp. 573-586.

Meek, J. M. (1963). "Ultimate strength of columns with biaxially eccentric loads." ACI J., 60 (August), 1053–1064.

Mendis P., Pendyala R. and Setunge S. (2000) "Stress strain model to predict the full range moment curvature behavior of high strength concrete section" Mag. Conc. Res. 52(4) 227-234

Mikhalkin. B (1952), "The Strength of Reinforced Concrete Members Subjected to Compression and Unsymmetrical Bending," Ms Thesis, University of California. California.

Mills LL and Zimmerman RM (1970), "Compressive Strength ofplain concrete under multiaxial loading conditions", ACI Mater. J.,67~101, 802–807.

Mirmiran A,(1996) "Analytical and experimental investigation of reinforced concrete columns encased in fibreglass tubular jackets and use of fiber jacket for pile splicing'" Final Report, WPI 0510700, Contract No. B-9135, Florida Department of Transportation, Tallahassee, FL, 1996.

Mirmiran, A., and Shahawy, M. (1995). "A novel FRP-concrete composite construction for the infrastructure." Proc., 13th Structures Congress, ASCE, New York, 1663–166

Mirmiran A, Shahawy M.(1997) "Behavior of concrete columns confined by fiber composites". J Struct Engng, ASCE 1997;123(5):583±90.

Mirmiran A, Shahawy M.(1997) "Dilation characteristics of confined concrete." Int J Mech Cohesive-Frictional Materials 1997;2(3):237± 49.

Miyauchi K, Nishibayashi S, Inoue S (1997) Estimation of strengthening effects withcarbon fiber sheet for concrete column. Proc., FRPRCS-3, Sapporo, Japan, Vol. 1: 217–224.

Monti, G. Alessandri, S.(2005), "Design equations for FRP-Strengthening of Columns", 7th InternationalSymposium on Fiber Reinforced Polymer Reinforcement for Reinforced Concrete Structures (FRPRCS-7), Kansas City, November 7-10, 2005.

Monti, G., Nistico, N. and Santini, S. (2001). "Design of FRP jackets for upgrade of circular bridge piers". Journal of Composites for Construction (ASCE), Vol. 5, No. 2, pp. 94-101.

Montoya E, Vecchio F J, Sheikh S A (2004) "Numerical evaluation of the behaviour of steelandFRP-confined concrete columns using compression field modeling". Elsevier, Engineering Structures, Vol. 26, No. 11, pp: 1535-1545.

Moran DA, Pantelides CP (2002). "Stress–strain model for fiber-reinforced 665 polymer-confined concrete". J Comp Constr, ASCE 2002;6(4):233–40.

Moran DA, Pantelides CP. (2005) "Damage-based stress–strain model forfiber-reinforced polymer-confined concrete". ACI Struct J2005;102(1):54–61.

Muguruma, H., Watanabe, S., Katsuta, S. and Tanaka, S. (1980). "A stress-strain model of confined concrete," Proc., JCA Cement and Concrete, Vol. 34, Japan Cement Assn., Tokyo, Japan, pp. 429–432.

Mylonas, G. A. (1967), "Working Stress Column Design Using Interaction Diagrams," V 64, August 1, 1967.

Najami, A., and Tayem, A. (1996). "Design of round reinforced concrete columns." J. Struct. Engrg., ASCE, 122(9), 1062-1071.

Nanni A and Bradford M. N., (1995) "FRP jacketed concrete under uniaxial compression", Constr. & Bldg. Materials, 9, 115±124 (1995).

Neogi P.K., Sen H.K., Chapman J.C.,(1969) "Concrete-filled tubular steel columns under eccentric loading", The Structural Engineer 1969; Volume 47, Issue 5, Pages 187–195.

O'Shea M.D., Bridge R.Q.,(1997) "Design of thin-walled concrete filled steel tubes", University of Sydney, Department of Civil Engineering, Centre for Geotechnical Research, 1997

O'Shea M.D., Bridge R.Q.,(1997) "Tests on circular thin-walled steel tubes filled with medium and high strength concrete", University of Sydney, Department of Civil Engineering, 1997

O'Shea M.D., Bridge R.Q.,(2000) "Design of Circular Thin-Walled Concrete Filled Steel Tubes", Journal of Structural Engineering 2000, Volume 126, Issue 11, November 2000, Pages 1295-1303

Pantazopoulou SJ, Mills RH (1995) "Microstructural aspects of the mechanical response of plain concrete". ACI Material Journal, V. 92, No. 6, pp. 605-616.

Pannel, F. N., (1963), "Failure Surfaces for Members in Compression and Biaxial Bending," ACI JOURNAL, Proceedings V. 60, No. 1, Jan. 1963, pp. 129-140.

Park, R., Priestley, M.J.N. and Gill,W.D.,(1982) "Ductility of square confined concrete columns", Pro& ASCE 108 (ST4) (1982) 929- 950.

Parker, L. G. and Scanton, J. J.(1940) "A Simple Analysis for Eccentrically Loaded Concrete Sections," Civil Engineering, Vol. 10, No. 10, October, 1940, p 656.

Parme, A. L., Nieves, J. M., and Gouwens, A. (1966). "Capacity of reinforced rectangular columns subject to biaxial bending." J. Am. Concr. Inst., 63(9), 911–923.

Pessiki S, Harries KA, Kestner JT, Sause R, Ricles JM.(2001) "Axial behavior of reinforced concrete columns confined with FRP jackets". ASCE Journal of Composites for Construction 2001;5(4):237–45.

Popovics, S. (1973). "A Numerical Approach to the Complete Stress-Strain Curves of Concrete." Cem. Concr. Res., 3(5), 583-59.

Ramamurthy L. N., (1966) "Investigation of the ultimate strength of square and rectangular columns under biaxially eccentric loads". Symposium on Reinforced Concrete Columns, Detroit, ACI-SP-13, Paper No. 12, 263-298 (1966).

Rasheed, H. A. and Dinno, K. S. (1994) "An efficient nonlinear analysis of RC sections"., Computers and structures Vol 53, No. 3 P613-623

Razvi, S., and Saatcioglu, M. (1999). "Confinement Model for High-Strength Concrete." J. Struct. Eng., 125(3), 281-289.

Richart. F. E., Brandtzaeg, A., and Brown R.L. (1929). "The failure of plain and spirally reinforced concrete in compression." Bulletin No. 190, Engineering Station, University of Illinois, Urbana.

Rocca, S., Galati, N., & Nanni, A. (2009). "Interaction diagrammethodology for design of FRP-confined reinforced concretecolumns." Construction and Building Materials, 23(4): 1508-1520.

Rodriguez JA, Ochoa (1999)" JDA. "Biaxial interaction diagrams for short RC columns of any cross section". Journal Structural Engineering ASCE 1999;125(6):672–83.

Row, D. G., and Paulay, T. E., (1973) "Biaxial Flexure and Axial Load Interaction in Short Rectangular Columns," Bulletin of the New Zealand Society for Earthquake Engineering, Vol. 6, No. 3, Sept., 1973, pp. 110-12

Roy, H. E. H. and Sozen, M. A. (1965). "Ductility of Concrete" Flexural Mechanics of Reinforced Concrete, SP-12, American Concrete Institute/American Society of Civil Engineers, Detroit, pp. 213-224.

Saatcioglu, M., and Razvi, S. R. (1992). "Strength and Ductility of Confined Concrete." J. Struct. Eng., 118(6), 1590-1607.

Saatcioglu, M., Salamt, A. H. and Razvi, S. R. (1995). "Confined columns under eccentric loading." J. Struct. Eng., 121(11), 1547-1556.

Sacks R, Buyukozturk O, (1987) "Expert interactive design of R\C columns under biaxial bending", ASCE J. Comput. Civ. Eng.1 _2. _1987. April.

Saadatmanesh H, Ehsani M R, Li MW (1994) Strength and ductility of concrete columnsexternally reinforced with fiber composite straps. ACI Struct. J., 91(4): 434–447.

Saenz, N Pantelides, C P. (2007) "Strain-based confinement model for FRP-confined concrete" Journal of Structural Engineering, v 133, n 6, p 825-833, 2007

Sakino K., Nakahara H., Morino S., Nishiyama A.,(2004) "Behavior of centrally loaded concrete-filled steel-tube short columns", Journal of Structural Engineering 2004, Volume 130, Issue 2, February 2004, Pages 180-188

Sakino, K., Tomii, M., and Watanabe, K. (1985) ''Substaining load capacity of plain concrete stub columns by circular steel tubes.'' Proc., International Special Conf. on Concrete-filled Steel Tubular Structure, Technology Exchange Center in Heilongjiang Province, Harbin, China, 112–118.

Schneider S.P., (1998) "Axially loaded concrete-filled steel tubes", Journal of Structural Engineering, Volume 124, Issue 10, October 1998, Pages 1125-1138

Shams M., Saadeghvaziri M.A.,(1997) "State of the art of concrete-filled steel tubular columns", ACI Structural Journal 1997, Volume 94, Issue 5, Pages 558–571

Shanmugam N.E., Lakshmi B.,(2001) "State of the art report on steel-concrete composite columns", Journal of Constructional Steel Research, Volume 57, Issue 10, October 2001, Pages 1041-1080

Saenz L.P.,(1964) "Equation for the stress-strain curve of concrete", ACI journal, Volume 61, Issue 9, Pages 1229-1235, 1964

Sallah, A. Y., (1983), "Analysis of Short Rectangular Reinforced Concrete Columns Subjected to Biaxial Moments," M.Eng. thesis, Department of Civil Engineering, Carleton University, Ottawa, Jan. 1983, 124 pp.

Samaan, M., Mirmiran, A., and Shahawy, M. (1998). „„"Model of concrete confined by fiber composite". J. Struct. Eng., 124(9), 1025–1031.

Samra R. M., Deeb,N. A. and Madi, U. R. (1996), "Transverse steel content in spiral concrete columns subject to eccentric loading", ACI j. v93, No. 4, August 1996.

Sargin, M. (1971). "Stress-Strain Relationships for Concrete and the Analysis of Structural Concrete Sections" Solid Mechanics Division, University of Waterloo, Study No. 4.

Scott, B. D., Park, R., and Priestley, N. (1982). "Stress-Strain Behavior of Concrete Confined by Overlapping Hoops at Law and High Strain Rates." ACI J., 79(1), 13-27.

Shams, M., and Saadeghvaziri, M. A. (1999). ''Nonlinear response of CFT columns under axial load.'' ACI Struct. J., 96~S112!, 1009–1017.

Shams, M., and Saadeghvaziri, M. A. (1997). ''State of the art of concrete-filled steel tubular columns.'' ACI Struct. J., 94~S51 558– 571.

Shanmugam NE, Lakshmi B.(2001) "State of the art report on steel–concrete composite columns".Journal of Constructional Steel Research 2001;57:1041–80.

Sheikh S. A.(1982) "A comparative study of confinement models" (1982). ACI Journal, 79(4), 296-306.

Sheikh, S. A., and Uzumeri, S. M. (1982). "Analytical Model for Concrete Confinement in Tied Columns" Journal of Structural Engineering, ASCE, V.108, No.ST12, P.2703-2722, December 1982.

Sheikh, S. A., and Toklucu, M. T. (1993). "Reinforced concrete columns confined by circular spirals and hoops" ACI J., 90(5), 542-553.

Silva, M. A.G., Rodrigues, C.C., (2006). "Size and relative stiffnesseffects on compressive failure of concrete columns wrapped with glass FRP". Journal of Materials in Civil Engineering,ASCE; 18(3): 334-342.

Soliman, M. T. M. and Yu, C. W. (1967). "The Flexural Stress-Strain Relationship of Concrete Confined by Rectangular Transverse Reinforcement" Magazine of Concrete Research (London), V.19, No.61, pp. 223-28, Dec. 1967.

Spoelstra M.R., Monti G. (1999). "FRP-Confined Concrete Model." J. Compos. Constr., ASCE,1999, 3(3), 143-150.

Taerwe, E., Harries, K. A., Kestner, J., Pessiki, S., Sause, R., and Ricles, J. (1998). ''Axial behavior of reinforced concrete columns retrofit with FRPC jackets.'' Proc., 2nd Int. Conf. on Composites in Infrastructures (ICCI), H. Saadatmanesh and M. R. Ehsani, eds., Tucson, Ariz., 411–425

Taniguchi, H. Mutsuyoshi, H., Kita, T., and Machida, A., (1993). " Ductile Behavior of Beams Using FRP as Tendons and Transverse Reinforcement," FRP Reinforcement for Concrete Structures, ACI SP-138, American Concrete Institute, Detroit, pp.651-670.

Taylor. M. A. and Ho, S.W.(1984) "Design contour charts for biaxial bending of rectangular reinforced concrete columns using bresler method" Structural Engineering Practice, 2(4), 301-317 (1983-84)

Teng, J. G., Jiang, T., Lam, L., and Luo, Y.Z., (2009), "Refinement of a design-oriented stress strain model for FRP-Confined concrete" J. Composites for Construction, ASCE, 13(4), 269-278.

Teng, J.G.; Lam, L.(2004); "Behavior and Modeling of Fiber Reinforced Polymer-Confined Concrete" Journal of Structural Engineering, v 130, n 11, November 2004, p1713-1723

Theriault M, Neale KW (2000). "Design equations for axially loaded reinforced concrete columns" strengthened with fibre reinforced polymers wraps. Can J Civil Eng 2000;27:1011–20

Thériault, M., Neale, K. W., Asce, M., Claude, S., (2004). "Fiberreinforcedpolymer-confined circular concrete columns :investigation of size and slenderness effects". Journal ofComposites for Construction, ASCE; 8(4):323–331.

Tomii, M., Yoshimmra, K., and Morishita, Y. (1977) ''Experimental studies on concrete-filled steel stub columns under concentric loading.'' Proc., International Colloquium on Stability of Structural Under Static and Dynamic Loads, National Science Foundation, Washington,D.C., 718–741.

Toutanji H (1999) "Stress-strain characteristics of concrete columns externally confined with advanced fiber composite sheets." ACI Mater. J., 96(3): 397–404.

Troxel, G. E.(1941) "Reinforced Concrete Columns Subjected to Bending about Both Principal Axes," Civil Engineering, Vol. 11, No. 4, April, 1941,p 237.

Vallenas, J., Bertero, V. and Popov, E. (1977). "Concrete Confined by Rectangular Hoops and Subjected to Axial Loads" Research Center Report UCB/EERC-77-13, University of California at Berkeley, August, 1977.

Wang, W. Hong 2002 H "Reliability of reinforced concrete columns under axial load and biaxial bending "Proceedings, Annual Conference - Canadian Society for Civil Engineering, v 2002, p 2161-2169, 2002,

Wang, G. G., and Hsu, C. T. (1992). "Complete Biaxial Load-Deformation Behavior of RC Columns." J. Struct. Engrg., ASCE, 118(9), 2590-2609.

Wang, P. T., Shah, S. P., and Naaman, A. E. (1978). "Stress-Strain Curves of Normal and Lightweight Concrete in Compression." ACI J., 75(11), 603-611.

Watanabe K, Nakamura H, Honda T, Toyoshima M, Iso M, Fujimaki T,(1997) "Confinement effect of FRP sheet on strength and ductility of concrete cylinders under uniaxial compression". In: Non-Metallic (FRP) Reinforcement for Concrete Structures, Proceedings of the Third International Symposium, vol. 1, Sapporo, Japan: Japan Concrete Institute, 1997:233–240

Weber, D.C. (1966) Ultimate strength design charts for columns with biaxial bending. ACI Journal, 63(11), 1205-1230, (1966).

Wee, T. H., Chin, M. S., and Mansur, M. A. (1996). "Stress-Strain Relationship of High Strength Concrete in Compression." J. Mater. Civ. Eng., 8(2), 70-76.

Wei Y Y, Wu YF.(2012) "Unified stress–strain model of concrete for FRP-confined columns". Constr Build Mater 2012;26(1):381–92.

Wessman, Harold E.(1946) "Reinforced Concrete Columns under Combined Compression and Bendind," ACIJournal, September, 1946; Proceedings, Vol. 43, p 1.

Whitney, C. S. and Cohen, E. (1956). "Guide for the ultimate strength design of reinforced concrete", ACI Journal, Proceedings, Vol. 53, November, pp. 455-475.

Wiesinger, Frederick P. T. "Design of Symmetrical Columns with Small Eccentricities in One or Tow Directions," ACI Journal, August, 1958; Proceedings, Vol. 55, p 273.

Xiao, Y. and Wu, H.,(2000) "Compressive behavior of concrete confined by carbon fiber composite jackets", Journal of Materials in Civil Engineering 12 (2) (May 2000) 139-146. v. 1, (Oct. 1997), 217-224.

Xiao, Y., & Wu, H. (2003a). "Retrofit of reinforced concrete columns using partially stiffened steel jackets". Journal of Structural Engineering, 129(6), 725-732.

Xiao, Y., & Wu, H. (2003b). "Compressive behavior of concrete confined by various types of FRP composite jackets". Journal of Reinforced Plastics and Composites, 22(13), 1187-1201.

Yang Y F, Han L H.(2011) "Behaviour of concrete filled steel tubular (CFST) stub columns under eccentric partial compression". Thin-Walled Structures;49(2):379–95.

Yong, Y-K, Nour, M.G. and Nawy, E.G. (1998). "Behavior of laterally Confined High-Strength Concrete under Axial Loads" Journal of Structural Engineering, V.114, No.2, P.332-351 , February 1998.

Yoo, S.H. Shin, S.W. (2007) "Variation of ultimate concrete strain at RC columns subjected to axial loads with bi-directional eccentricities "Key Engineering Materials, v 348-349, p 617-20, 2007

Yu Z.W., Ding F.X., Cai C.S.,(2007) "Experimental behavior of circular concrete-filled steel tube stub columns", Journal of Constructional Steel Research, Volume 63, Issue 2, February 2007, Pages 165-174

Yu Q, Z. Tao, Y. X. Wu,(2008) "Experimental behaviour of high-performance concrete-filled steel tubular columns", Thin-Walled Structures, Vol. 46, No. 4, 2008, pp. 362-370. ISSN 0263- 8231.

Yuan, X.F., Lam, L., Teng, J.G., Smith, S.T. (2001). "FRP-confined RC columns under combined bending and compression: a comparative study of concrete stress-strain models". FRP Composites in Civil Engineering, Vol. 1: 749-758.

ZAK M. (1993)" Computer analysis of reinforced concrete sections under biaxial bending and longitudinal load". ACI Structural Journal, 90(2):163–169, 1993.

Appendix A - Ultimate Confined Strength Tables

Table A-1 is developed for f'c of 3.3 using equations 5-181 and 5-182. Table A-2 is for f'c of 3.9 using equations 5-183 and 5-184. Table A-3 is developed using Mander procedure that utilizes Scickert and Winkler (1977) formulas. Table A-4 is for f'c of 5.2 using equations 5-185 and 5-186. Tables A-5 through A-7 show the confined values for the same lateral pressure using Scickert and Winkler (1977) equations. Tables A-5 through A-7 give conservative values compared to table A-1, A-2 and A-4. This indicates that equations 5-179 and 5-180 found by Scickert and Winkler (1977) and utilized by Mander et al (1988) are conservative enough to be used in the analysis

$$\sigma_1 *= \frac{f_{lx}}{f_c'}$$

$$\sigma_2 *= \frac{f_{ly}}{f_c'}$$

Table A-1: Ultimate confined strength to unconfined strength ratio for $f'_c = 3.3$ ksi

$\sigma1*$ / $\sigma2*$	0.02	0.04	0.06	0.08	0.1	0.12	0.14	0.16	0.18	0.2	0.22	0.24	0.26	0.28	0.3
0.02	3.7260	3.9001	4.0336	4.1442	4.2396	4.3238	4.3994	4.4680	4.5309	4.5888	4.6424	4.6924	4.7389	4.7825	4.8233
0.04	3.9001	4.1298	4.2988	4.4318	4.5436	4.6408	4.7273	4.8054	4.8768	4.9424	5.0032	5.0598	5.1128	5.1624	5.2091
0.06	4.0336	4.2988	4.5141	4.6779	4.8098	4.9220	5.0205	5.1086	5.1887	5.2621	5.3299	5.3930	5.4520	5.5074	5.5596
0.08	4.1442	4.4318	4.6779	4.8808	5.0396	5.1700	5.2821	5.3812	5.4705	5.5519	5.6269	5.6965	5.7614	5.8223	5.8797
0.1	4.2396	4.5436	4.8098	5.0396	5.2316	5.3855	5.5140	5.6257	5.7250	5.8150	5.8974	5.9736	6.0445	6.1109	6.1734
0.12	4.3238	4.6408	4.9220	5.1700	5.3855	5.5679	5.7172	5.8436	5.9544	6.0537	6.1440	6.2271	6.3041	6.3761	6.4436
0.14	4.3994	4.7273	5.0205	5.2821	5.5140	5.7172	5.8910	6.0358	6.1600	6.2698	6.3687	6.4591	6.5425	6.6201	6.6928
0.16	4.4680	4.8054	5.1086	5.3812	5.6257	5.8436	6.0358	6.2019	6.3424	6.4643	6.5728	6.6712	6.7614	6.8450	6.9230
0.18	4.5309	4.8768	5.1887	5.4705	5.7250	5.9544	6.1600	6.3424	6.5015	6.6380	6.7575	6.8647	6.9623	7.0522	7.1357
0.2	4.5888	4.9424	5.2621	5.5519	5.8150	6.0537	6.2698	6.4643	6.6380	6.7907	6.9233	7.0405	7.1462	7.2428	7.3322
0.22	4.6424	5.0032	5.3299	5.6269	5.8974	6.1440	6.3687	6.5728	6.7575	6.9233	7.0703	7.1991	7.3139	7.4180	7.5137
0.24	4.6924	5.0598	5.3930	5.6965	5.9736	6.2271	6.4591	6.6712	6.8647	7.0405	7.1991	7.3407	7.4660	7.5784	7.6810
0.26	4.7389	5.1128	5.4520	5.7614	6.0445	6.3041	6.5425	6.7614	6.9623	7.1462	7.3139	7.4660	7.6026	7.7245	7.8347
0.28	4.7825	5.1624	5.5074	5.8223	6.1109	6.3761	6.6201	6.8450	7.0522	7.2428	7.4180	7.5784	7.7245	7.8566	7.9753
0.3	4.8233	5.2091	5.5596	5.8797	6.1734	6.4436	6.6928	6.9230	7.1357	7.3322	7.5137	7.6810	7.8347	7.9753	8.1031

Table A-2: Ultimate confined strength to unconfined strength ratio for $f'_c = 3.9$ ksi

σ_{1^*} / σ_{2^*}	0.02	0.04	0.06	0.08	0.1	0.12	0.14	0.16	0.18	0.2	0.22	0.24	0.26	0.28	0.3
0.02	4.4819	4.7318	4.9351	5.1101	5.2656	5.4063	5.5355	5.6552	5.7670	5.8721	5.9712	6.0651	6.1544	6.2394	6.3206
0.04	4.7318	5.0412	5.2854	5.4880	5.6642	5.8217	5.9649	6.0969	6.2196	6.3345	6.4427	6.5450	6.6422	6.7347	6.8230
0.06	4.9351	5.2854	5.5802	5.8187	6.0197	6.1962	6.3548	6.4998	6.6337	6.7587	6.8759	6.9865	7.0914	7.1911	7.2862
0.08	5.1101	5.4880	5.8187	6.1005	6.3333	6.5323	6.7083	6.8674	7.0134	7.1488	7.2753	7.3943	7.5068	7.6136	7.7154
0.1	5.2656	5.6642	6.0197	6.3333	6.6037	6.8308	7.0273	7.2024	7.3616	7.5081	7.6443	7.7720	7.8923	8.0062	8.1145
0.12	5.4063	5.8217	6.1962	6.5323	6.8308	7.0908	7.3125	7.5063	7.6802	7.8389	7.9855	8.1222	8.2506	8.3718	8.4868
0.14	5.5355	5.9649	6.3548	6.7083	7.0273	7.3125	7.5631	7.7795	7.9704	8.1427	8.3007	8.4471	8.5840	8.7128	8.8346
0.16	5.6552	6.0969	6.4998	6.8674	7.2024	7.5063	7.7795	8.0215	8.2328	8.4208	8.5913	8.7483	8.8942	9.0310	9.1599
0.18	5.7670	6.2196	6.6337	7.0134	7.3616	7.6802	7.9704	8.2328	8.4670	8.6733	8.8582	9.0269	9.1827	9.3279	9.4644
0.2	5.8721	6.3345	6.7587	7.1488	7.5081	7.8389	8.1427	8.4208	8.6733	8.9002	9.1018	9.2837	9.4503	9.6048	9.7492
0.22	5.9712	6.4427	6.8759	7.2753	7.6443	7.9855	8.3007	8.5913	8.8582	9.1018	9.3219	9.5190	9.6978	9.8624	10.0154
0.24	6.0651	6.5450	6.9865	7.3943	7.7720	8.1222	8.4471	8.7483	9.0269	9.2837	9.5190	9.7328	9.9255	10.1014	10.2638
0.26	6.1544	6.6422	7.0914	7.5068	7.8923	8.2506	8.5840	8.8942	9.1827	9.4503	9.6978	9.9255	10.1334	10.3220	10.4948
0.28	6.2394	6.7347	7.1911	7.6136	8.0062	8.3718	8.7128	9.0310	9.3279	9.6048	9.8624	10.1014	10.3220	10.5243	10.7080
0.3	6.3206	6.8230	7.2862	7.7154	8.1145	8.4868	8.8346	9.1599	9.4644	9.7492	10.0154	10.2638	10.4948	10.7080	10.9060

Table A-3: Ultimate confined strength to unconfined strength ratio for $f'_c = 4.4$ ksi (used by Mander et al. (1988))

$\sigma_{1}*$ / $\sigma_{2}*$	0.02	0.04	0.06	0.08	0.1	0.12	0.14	0.16	0.18	0.2	0.22	0.24	0.26	0.28	0.3
0.02	5.0255	5.2550	5.4259	5.5656	5.6849	5.7895	5.8829	5.9674	6.0444	6.1152	6.1806	6.2412	6.2976	6.3502	6.3993
0.04	5.2550	5.5622	5.7791	5.9460	6.0845	6.2040	6.3096	6.4044	6.4906	6.5695	6.6423	6.7098	6.7728	6.8315	6.8866
0.06	5.4259	5.7791	6.0569	6.2623	6.4247	6.5613	6.6803	6.7860	6.8815	6.9686	7.0487	7.1230	7.1920	7.2566	7.3171
0.08	5.5656	5.9460	6.2623	6.5164	6.7112	6.8688	7.0030	7.1209	7.2263	7.3218	7.4094	7.4903	7.5654	7.6355	7.7012
0.1	5.6849	6.0845	6.4247	6.7112	6.9456	7.1307	7.2834	7.4150	7.5313	7.6359	7.7312	7.8188	7.9000	7.9756	8.0464
0.12	5.7895	6.2040	6.5613	6.8688	7.1307	7.3486	7.5248	7.6726	7.8012	7.9157	8.0193	8.1140	8.2013	8.2825	8.3582
0.14	5.8829	6.3096	6.6803	7.0030	7.2834	7.5248	7.7283	7.8964	8.0394	8.1650	8.2775	8.3797	8.4735	8.5604	8.6413
0.16	5.9674	6.4044	6.7860	7.1209	7.4150	7.6726	7.8964	8.0875	8.2480	8.3864	8.5089	8.6193	8.7200	8.8127	8.8989
0.18	6.0444	6.4906	6.8815	7.2263	7.5313	7.8012	8.0394	8.2480	8.4282	8.5818	8.7156	8.8350	8.9431	9.0422	9.1338
0.2	6.1152	6.5695	6.9686	7.3218	7.6359	7.9157	8.1650	8.3864	8.5818	8.7522	8.8994	9.0289	9.1451	9.2510	9.3483
0.22	6.1806	6.6423	7.0487	7.4094	7.7312	8.0193	8.2775	8.5089	8.7156	8.8994	9.0610	9.2022	9.3276	9.4408	9.5443
0.24	6.2412	6.7098	7.1230	7.4903	7.8188	8.1140	8.3797	8.6193	8.8350	9.0289	9.2022	9.3560	9.4916	9.6130	9.7231
0.26	6.2976	6.7728	7.1920	7.5654	7.9000	8.2013	8.4735	8.7200	8.9431	9.1451	9.3276	9.4916	9.6383	9.7687	9.8861
0.28	6.3502	6.8315	7.2566	7.6355	7.9756	8.2825	8.5604	8.8127	9.0422	9.2510	9.4408	9.6130	9.7687	9.9087	10.0343
0.3	6.3993	6.8866	7.3171	7.7012	8.0464	8.3582	8.6413	8.8989	9.1338	9.3483	9.5443	9.7231	9.8861	10.0343	10.1683

Table A-4: Ultimate confined strength to unconfined strength ratio for $f'_c = 5.2$ ksi

σ_1* / σ_2*	0.02	0.04	0.06	0.08	0.1	0.12	0.14	0.16	0.18	0.2	0.22	0.24	0.26	0.28	0.3
0.02	5.9070	6.1647	6.3409	6.4785	6.5923	6.6891	6.7730	6.8467	6.9120	6.9700	7.0217	7.0679	7.1091	7.1458	7.1783
0.04	6.1647	6.5586	6.8072	6.9847	7.1258	7.2436	7.3448	7.4332	7.5113	7.5810	7.6435	7.6996	7.7502	7.7959	7.8370
0.06	6.3409	6.8072	7.1633	7.4023	7.5789	7.7215	7.8417	7.9458	8.0373	8.1187	8.1917	8.2574	8.3170	8.3710	8.4201
0.08	6.4785	6.9847	7.4023	7.7279	7.9573	8.1317	8.2746	8.3962	8.5020	8.5957	8.6794	8.7548	8.8231	8.8853	8.9420
0.1	6.5923	7.1258	7.5789	7.9573	8.2579	8.4780	8.6495	8.7917	8.9137	9.0206	9.1157	9.2010	9.2782	9.3485	9.4126
0.12	6.6891	7.2436	7.7215	8.1317	8.4780	8.7576	8.9688	9.1369	9.2778	9.3996	9.5070	9.6028	9.6893	9.7678	9.8395
0.14	6.7730	7.3448	7.8417	8.2746	8.6495	8.9688	9.2303	9.4332	9.5975	9.7367	9.8579	9.9652	10.0615	10.1486	10.2280
0.16	6.8467	7.4332	7.9458	8.3962	8.7917	9.1369	9.4332	9.6790	9.8740	10.0344	10.1716	10.2917	10.3987	10.4951	10.5826
0.18	6.9120	7.5113	8.0373	8.5020	8.9137	9.2778	9.5975	9.8740	10.1061	10.2937	10.4501	10.5850	10.7039	10.8102	10.9063
0.2	6.9700	7.5810	8.1187	8.5957	9.0206	9.3996	9.7367	10.0344	10.2937	10.5135	10.6941	10.8465	10.9790	11.0964	11.2019
0.22	7.0217	7.6435	8.1917	8.6794	9.1157	9.5070	9.8579	10.1716	10.4501	10.6941	10.9029	11.0770	11.2255	11.3555	11.4713
0.24	7.0679	7.6996	8.2574	8.7548	9.2010	9.6028	9.9652	10.2917	10.5850	10.8465	11.0770	11.2759	11.4438	11.5885	11.7159
0.26	7.1091	7.7502	8.3170	8.8231	9.2782	9.6893	10.0615	10.3987	10.7039	10.9790	11.2255	11.4438	11.6338	11.7959	11.9367
0.28	7.1458	7.7959	8.3710	8.8853	9.3485	9.7678	10.1486	10.4951	10.8102	11.0964	11.3555	11.5885	11.7959	11.9776	12.1342
0.3	7.1783	7.8370	8.4201	8.9420	9.4126	9.8395	10.2280	10.5826	10.9063	11.2019	11.4713	11.7159	11.9367	12.1342	12.3084

Table A-5: Ultimate confined strength to unconfined strength ratio for $f'_c = 3.3$ ksi (using Scickert and Winkler (1977))

σ_{1*} / σ_{2*}	0.02	0.04	0.06	0.08	0.1	0.12	0.14	0.16	0.18	0.2	0.22	0.24	0.26	0.28	0.3
0.02	3.7369	3.9076	4.0347	4.1385	4.2272	4.3050	4.3745	4.4373	4.4946	4.5472	4.5958	4.6408	4.6827	4.7218	4.7584
0.04	3.9076	4.1360	4.2973	4.4214	4.5244	4.6133	4.6918	4.7623	4.8263	4.8850	4.9391	4.9894	5.0361	5.0799	5.1208
0.06	4.0347	4.2973	4.5039	4.6566	4.7773	4.8789	4.9674	5.0460	5.1170	5.1818	5.2414	5.2966	5.3479	5.3959	5.4410
0.08	4.1385	4.4214	4.6566	4.8456	4.9904	5.1076	5.2074	5.2950	5.3734	5.4445	5.5096	5.5697	5.6255	5.6777	5.7266
0.1	4.2272	4.5244	4.7773	4.9904	5.1647	5.3023	5.4159	5.5137	5.6002	5.6780	5.7489	5.8140	5.8744	5.9306	5.9832
0.12	4.3050	4.6133	4.8789	5.1076	5.3023	5.4643	5.5954	5.7053	5.8009	5.8861	5.9631	6.0335	6.0984	6.1588	6.2151
0.14	4.3745	4.6918	4.9674	5.2074	5.4159	5.5954	5.7467	5.8717	5.9780	6.0714	6.1551	6.2311	6.3009	6.3654	6.4256
0.16	4.4373	4.7623	5.0460	5.2950	5.5137	5.7053	5.8717	6.0138	6.1332	6.2361	6.3271	6.4092	6.4841	6.5531	6.6171
0.18	4.4946	4.8263	5.1170	5.3734	5.6002	5.8009	5.9780	6.1332	6.2671	6.3813	6.4809	6.5696	6.6500	6.7237	6.7918
0.2	4.5472	4.8850	5.1818	5.4445	5.6780	5.8861	6.0714	6.2361	6.3813	6.5081	6.6175	6.7138	6.8003	6.8789	6.9513
0.22	4.5958	4.9391	5.2414	5.5096	5.7489	5.9631	6.1551	6.3271	6.4809	6.6175	6.7377	6.8427	6.9359	7.0201	7.0970
0.24	4.6408	4.9894	5.2966	5.5697	5.8140	6.0335	6.2311	6.4092	6.5696	6.7138	6.8427	6.9571	7.0579	7.1481	7.2300
0.26	4.6827	5.0361	5.3479	5.6255	5.8744	6.0984	6.3009	6.4841	6.6500	6.8003	6.9359	7.0579	7.1669	7.2639	7.3512
0.28	4.7218	5.0799	5.3959	5.6777	5.9306	6.1588	6.3654	6.5531	6.7237	6.8789	7.0201	7.1481	7.2639	7.3681	7.4614
0.3	4.7584	5.1208	5.4410	5.7266	5.9832	6.2151	6.4256	6.6171	6.7918	6.9513	7.0970	7.2300	7.3512	7.4614	7.5611

Table A-6: Ultimate confined strength to unconfined strength ratio for f'_c = 3.9 ksi (using Scickert and Winkler (1977))

σ_{1}* / σ_{2}*	0.02	0.04	0.06	0.08	0.1	0.12	0.14	0.16	0.18	0.2	0.22	0.24	0.26	0.28	0.3
0.02	4.4163	4.6181	4.7683	4.8909	4.9958	5.0877	5.1698	5.2441	5.3118	5.3740	5.4314	5.4846	5.5342	5.5804	5.6236
0.04	4.6181	4.8880	5.0786	5.2253	5.3470	5.4520	5.5448	5.6281	5.7038	5.7732	5.8372	5.8965	5.9518	6.0035	6.0519
0.06	4.7683	5.0786	5.3228	5.5032	5.6460	5.7660	5.8705	5.9635	6.0474	6.1239	6.1944	6.2596	6.3203	6.3770	6.4302
0.08	4.8909	5.2253	5.5032	5.7266	5.8977	6.0362	6.1542	6.2577	6.3504	6.4344	6.5113	6.5824	6.6484	6.7100	6.7677
0.1	4.9958	5.3470	5.6460	5.8977	6.1038	6.2664	6.4006	6.5162	6.6184	6.7104	6.7941	6.8711	6.9424	7.0089	7.0711
0.12	5.0877	5.4520	5.7660	6.0362	6.2664	6.4578	6.6127	6.7426	6.8557	6.9563	7.0473	7.1305	7.2072	7.2785	7.3452
0.14	5.1698	5.5448	5.8705	6.1542	6.4006	6.6127	6.7916	6.9392	7.0650	7.1753	7.2742	7.3640	7.4465	7.5228	7.5939
0.16	5.2441	5.6281	5.9635	6.2577	6.5162	6.7426	6.9392	7.1072	7.2483	7.3699	7.4775	7.5745	7.6630	7.7445	7.8202
0.18	5.3118	5.7038	6.0474	6.3504	6.6184	6.8557	7.0650	7.2483	7.4066	7.5416	7.6592	7.7641	7.8591	7.9462	8.0267
0.2	5.3740	5.7732	6.1239	6.4344	6.7104	6.9563	7.1753	7.3699	7.5416	7.6913	7.8207	7.9345	8.0367	8.1297	8.2152
0.22	5.4314	5.8372	6.1944	6.5113	6.7941	7.0473	7.2742	7.4775	7.6592	7.8207	7.9628	8.0868	8.1970	8.2964	8.3874
0.24	5.4846	5.8965	6.2596	6.5824	6.8711	7.1305	7.3640	7.5745	7.7641	7.9345	8.0868	8.2220	8.3412	8.4478	8.5446
0.26	5.5342	5.9518	6.3203	6.6484	6.9424	7.2072	7.4465	7.6630	7.8591	8.0367	8.1970	8.3412	8.4700	8.5846	8.6878
0.28	5.5804	6.0035	6.3770	6.7100	7.0089	7.2785	7.5228	7.7445	7.9462	8.1297	8.2964	8.4478	8.5846	8.7077	8.8175
0.3	5.6236	6.0519	6.4302	6.7677	7.0711	7.3452	7.5939	7.8202	8.0267	8.2152	8.3874	8.5446	8.6878	8.8175	8.9358

Table A-7: Ultimate confined strength to unconfined strength ratio for f'_c = 5.2 ksi (using Scickert and Winkler (1977))

σ_{2^*} \ σ_{1^*}	0.02	0.04	0.06	0.08	0.1	0.12	0.14	0.16	0.18	0.2	0.22	0.24	0.26	0.28	0.3
0.02	5.8885	6.1574	6.3577	6.5213	6.6610	6.7836	6.8931	6.9921	7.0823	7.1652	7.2418	7.3128	7.3788	7.4405	7.4980
0.04	6.1574	6.5173	6.7715	6.9671	7.1294	7.2694	7.3931	7.5042	7.6051	7.6976	7.7829	7.8620	7.9357	8.0046	8.0692
0.06	6.3577	6.7715	7.0970	7.3376	7.5279	7.6880	7.8274	7.9513	8.0632	8.1652	8.2592	8.3461	8.4270	8.5027	8.5736
0.08	6.5213	6.9671	7.3376	7.6354	7.8636	8.0483	8.2056	8.3437	8.4672	8.5792	8.6818	8.7765	8.8645	8.9467	9.0237
0.1	6.6610	7.1294	7.5279	7.8636	8.1384	8.3552	8.5342	8.6883	8.8246	8.9472	9.0588	9.1615	9.2566	9.3452	9.4281
0.12	6.7836	7.2694	7.6880	8.0483	8.3552	8.6105	8.8169	8.9902	9.1409	9.2750	9.3963	9.5073	9.6096	9.7047	9.7935
0.14	6.8931	7.3931	7.8274	8.2056	8.5342	8.8169	9.0554	9.2523	9.4200	9.5671	9.6989	9.8187	9.9286	10.0304	10.1251
0.16	6.9921	7.5042	7.9513	8.3437	8.6883	8.9902	9.2523	9.4763	9.6644	9.8265	9.9700	10.0994	10.2174	10.3261	10.4270
0.18	7.0823	7.6051	8.0632	8.4672	8.8246	9.1409	9.4200	9.6644	9.8755	10.0554	10.2123	10.3522	10.4789	10.5949	10.7023
0.2	7.1652	7.6976	8.1652	8.5792	8.9472	9.2750	9.5671	9.8265	10.0554	10.2551	10.4276	10.5793	10.7155	10.8396	10.9536
0.22	7.2418	7.7829	8.2592	8.6818	9.0588	9.3963	9.6989	9.9700	10.2123	10.4276	10.6170	10.7824	10.9293	11.0619	11.1832
0.24	7.3128	7.8620	8.3461	8.7765	9.1615	9.5073	9.8187	10.0994	10.3522	10.5793	10.7824	10.9627	11.1216	11.2637	11.3928
0.26	7.3788	7.9357	8.4270	8.8645	9.2566	9.6096	9.9286	10.2174	10.4789	10.7155	10.9293	11.1216	11.2934	11.4462	11.5838
0.28	7.4405	8.0046	8.5027	8.9467	9.3452	9.7047	10.0304	10.3261	10.5949	10.8396	11.0619	11.2637	11.4462	11.6103	11.7574
0.3	7.4980	8.0692	8.5736	9.0237	9.4281	9.7935	10.1251	10.4270	10.7023	10.9536	11.1832	11.3928	11.5838	11.7574	11.9144